



National Library
of Canada

Bibliothèque nationale
du Canada

Canadian Theses Service

Services des thèses canadiennes

Ottawa, Canada
K1A 0N4

CANADIAN THESES

THÈSES CANADIENNES

NOTICE

The quality of this microfiche is heavily dependent upon the quality of the original thesis submitted for microfilming. Every effort has been made to ensure the highest quality of reproduction possible.

If pages are missing, contact the university which granted the degree.

Some pages may have indistinct print especially if the original pages were typed with a poor typewriter ribbon or if the university sent us an inferior photocopy.

Previously copyrighted materials (journal articles, published tests, etc.) are not filmed.

Reproduction in full or in part of this film is governed by the Canadian Copyright Act, R.S.C. 1970, c. C-30. Please read the authorization forms which accompany this thesis.

AVIS

La qualité de cette microfiche dépend grandement de la qualité de la thèse soumise au microfilmage. Nous avons tout fait pour assurer une qualité supérieure de reproduction.

S'il manque des pages, veuillez communiquer avec l'université qui a conféré le grade.

La qualité d'impression de certaines pages peut laisser à désirer, surtout si les pages originales ont été dactylographiées à l'aide d'un ruban usé ou si l'université nous a fait parvenir une photocopie de qualité inférieure.

Les documents qui font déjà l'objet d'un droit d'auteur (articles de revue, examens publiés, etc.) ne sont pas microfilmés.

La reproduction, même partielle, de ce microfilm est soumise à la Loi canadienne sur le droit d'auteur, SRC 1970, c. C-30. Veuillez prendre connaissance des formules d'autorisation qui accompagnent cette thèse.

THIS DISSERTATION
HAS BEEN MICROFILMED
EXACTLY AS RECEIVED

LA THÈSE A ÉTÉ
MICROFILMÉE TELLE QUE
NOUS L'AVONS REÇUE



National Library
of Canada

Bibliothèque nationale
du Canada

Ottawa, Canada
K1A 0N4

TC -

0-315-23270-6

CANADIAN THESES ON MICROFICHE SERVICE - SERVICE DES THÈSES CANADIENNES SUR MICROFICHE

PERMISSION TO MICROFILM - AUTORISATION DE MICROFILMER

• Please print or type - Écrire en lettres moulées ou dactylographier

AUTHOR - AUTEUR

Full Name of Author - Nom complet de l'auteur

Bjorn Ystad

Date of Birth - Date de naissance

JAN. 14 1955

Canadian Citizen - Citoyen canadien

☐ Yes - Oui

☒ No - Non

Country of Birth - Lieu de naissance

NORWAY

Permanent Address - Résidence fixe

BCKFINVEIEN 12
1620 GRESSVIK
NORWAY

THESIS - THÈSE

Title of Thesis - Titre de la thèse

AN EXPERIMENTAL INVESTIGATION OF A CLOSED-LOOP TWO-PHASE
THERMOSYPHON SYSTEM FOR LOW GRADE HEAT RECOVERY FROM
GASEOUS HEAT SOURCES

Degree for which thesis was presented
Grade pour lequel cette thèse fut présentée

M.Sc.

Year this degree conferred
Année d'obtention de ce grade

Fall 1985

University - Université

THE UNIVERSITY OF ALBERTA

Name of Supervisor - Nom du directeur de thèse

Dr. K.C. CHENG

AUTHORIZATION - AUTORISATION

Permission is hereby granted to the NATIONAL LIBRARY OF CANADA to
microfilm this thesis and to lend or sell copies of the film.

The author reserves other publication rights, and neither the thesis nor exten-
sive extracts from it may be printed or otherwise reproduced without the
author's written permission.

L'autorisation est, par la présente, accordée à la BIBLIOTHÈQUE NATIONAL
DU CANADA de microfilmer cette thèse et de prêter ou de vendre des
emplaires du film.

L'auteur se réserve les autres droits de publication; ni la thèse ni de longs ex-
traits de celle-ci ne doivent être imprimés ou autrement reproduits sans
l'autorisation écrite de l'auteur.

ATTACH FORM TO THESIS - VEUILLEZ JOINDRE CE FORMULAIRE À LA THÈSE

Signature

Bjorn Ystad

Date

July 7 - 1985

THE UNIVERSITY OF ALBERTA

An Experimental Investigation of a Closed-Loop Two-Phase
Thermosyphon System for Low Grade Heat Recovery from Gaseous
Heat Sources

by

C

Bjorn Ystad

A THESIS

SUBMITTED TO THE FACULTY OF GRADUATE STUDIES AND RESEARCH
IN PARTIAL FULFILMENT OF THE REQUIREMENTS FOR THE DEGREE
OF Master of Science

Mechanical Engineering

EDMONTON, ALBERTA

25 JUNE 1985

THE UNIVERSITY OF ALBERTA

RELEASE FORM

NAME OF AUTHOR

Bjorn Ystad

TITLE OF THESIS

An Experimental Investigation of a
Closed-Loop Two-Phase Thermosyphon
System for Low Grade Heat Recovery from
Gaseous Heat Sources

DEGREE FOR WHICH THESIS WAS PRESENTED Master of Science

YEAR THIS DEGREE GRANTED 25 JUNE 1985

Permission is hereby granted to THE UNIVERSITY OF
ALBERTA LIBRARY to reproduce single copies of this
thesis and to lend or sell such copies for private,
scholarly or scientific research purposes only.

The author reserves other publication rights, and
neither the thesis nor extensive extracts from it may
be printed or otherwise reproduced without the author's
written permission.

(SIGNED)

PERMANENT ADDRESS:

Bokfinkveien 12

1620 Gressvik

Norway

DATED:

June 25 1985

THE UNIVERSITY OF ALBERTA

FACULTY OF GRADUATE STUDIES AND RESEARCH

The undersigned certify that they have read, and recommend to the Faculty of Graduate Studies and Research, for acceptance, a thesis entitled An Experimental Investigation of a Closed-Loop Two-Phase Thermosyphon System for Low Grade Heat Recovery from Gaseous Heat Sources submitted by Bjorn Ystad in partial fulfilment of the requirements for the degree of Master of Science.

.....K.C. Cheng.....

Supervisor

.....H. Chakrabarti.....

.....S. M. Lee.....

Date: June 25, 1985.....

To

Elizabeth Ann,
Michelle Cecilia and Paul Andreas

Abstract

A two-phase closed-loop thermosyphon was designed and constructed to study the transport of low grade heat from a gaseous heat source to a liquid heat sink, with both water and refrigerant R-11 as the two-phase working fluids. The performance of single phase natural and forced circulation systems with water as the working fluid was also studied. The heating air temperature was below 80°C for the two-phase experiments and less than 100°C for the single phase water tests.

The effect of external operating parameters such as air volume flow rate, air temperature and working fluid charge level were studied.

The two-phase water tests showed agreement with theoretical single phase heat transfer rather than with two-phase empirical predictions as a result of low vapor quality flow. The two-phase R-11 tests gave heat transfer results which were 1 to 5 times higher than values predicted by empirical equations for two-phase flow.

The R-11 charged system was the best performer and transferred heat between the source and sink reservoirs when the temperature difference was as low as 30°C . Due to low evaporator heat transfer coefficients and restrictions in the primary loop, the system thermodynamic efficiency was less than 20%. However, the tests indicate that this type of system has definite application for the recovery of heat from low temperature gaseous sources.

Acknowledgement

The author wishes to express his deep gratitude to Dr. K. C. Cheng for his expert guidance and assistance during his supervision of this work.

The author is grateful to Terry Nord for his assistance with the electronic instrumentation and to technical staff and machinists for their help with system modifications.

Special thanks to Zbigniew Wolanski, Ron Pelot and David Mackay for their help in making this thesis readable.

The companionship and useful discussions with my fellow student Glen Rovang during this work have been invaluable to me.

The financial support was provided by the Natural Sciences and Engineering Research Council (NSERC) of Canada under Strategic Grant #G-0822 and is greatly appreciated.

Finally, I would like to thank my wife; her help and encouragement was a great support to me.

Table of Contents

Chapter	Page
1. INTRODUCTION	1
1.1 Background Information	1
1.2 Scope of the Study	3
2. Heat Recovery Utilizing a Closed-Loop Hydronic System Tested with Natural and Forced Circulation	6
2.1 Introduction	7
2.2 Experimental Apparatus	8
2.2.1 The secondary heating loop	8
2.2.2 The primary working fluid loop	12
2.2.3 The secondary cooling loop	16
2.2.4 The data acquisition system	16
2.2.5 Hydronic system modifications	18
2.3 Instrumentation and Calibration	18
2.3.1 Thermocouples and thermopile	19
2.3.2 Liquid flowmeters	20
2.3.3 Pressure transducers	20
2.3.4 Pressure gauges	21
2.3.5 Wattmeter	22
2.3.6 Pitot tube and air bar	22
2.4 Experimental Procedure	22
2.5 Basic Equations for Data Analysis	27
2.6 Results and Discussion for Single-Phase Thermosyphon System	38
2.6.1 Overall system performance	38
2.6.2 Evaporator results	45
2.6.3 Condenser results	60

2.7	Results and Discussions for Forced Circulation Flow	66
2.7.1	Overall system performance	67
2.7.2	Evaporator results	71
2.7.3	Condenser results	77
2.8	Concluding Remarks	82
3.	A Closed-Loop Two-Phase Thermosyphon System Using Water under Partial Vacuum as Working Fluid	85
3.1	Introduction	86
3.2	Experimental Apparatus, Instrumentation and Calibration	87
3.3	Experimental Procedure	89
3.4	Basic Equations for Data Analysis	92
3.5	Results and Discussion	99
3.5.1	Evaporator results	105
3.5.2	The condenser results	112
3.5.3	Heat transfer correlations	117
3.6	Concluding Remarks	120
4.	A Closed-Loop Two-Phase Thermosyphon System Using Freon R-11 as Working Fluid	126
4.1	Introduction	127
4.2	Experimental Apparatus, Instrumentation and Calibration	127
4.3	Experimental Procedure	128
4.4	Basic Equations for Data Analysis	129
4.5	Results and Discussion	129
4.5.1	The overall system results	130
4.5.2	The evaporator results	137
4.5.3	The condenser results	146

4.5.4 Heat transfer correlation	148
4.6 Concluding Remarks	156
5. Conclusions	158
References	163
Appendix I	167
Appendix II	177
Appendix III	180
Appendix IV	183

List of Tables

Table	Page
2.1 Evaporator dimensions	13
2.2 Condenser dimensions	14
2.3 Heating air flow rate and temperature	27
2.4 Summary of operating characteristics for natural fluid circulation	39
2.5 Overall system efficiency and effectiveness	42
2.6 Heat transfer rates for w.fl. and cooling water in cond. and heat loss across tube and cond. insulation	48
2.7 Evap. tube wall temp. distribution for tube no.4 on evaporator panels 1 and 3	52
2.8 Average recorded air and evap. tube wall temps. and the difference between these two temps.	59
2.9 Overall, inside and outside heat transfer coefficients for the condenser	66
2.10 Summary of operating characteristics for forced fluid circulation	68
2.11 Working fluid and cooling water temps., heat recovery rate and overall heat transfer coefficient for the condenser	82
3.1 Operating working fluid charge levels and air temperatures	93
3.2 Constants used in the Kandlikar correlation for vertical water flow	98
3.3 Summary of operating characteristics for 2-phase water tests	100
4.1 Constants used in the Kandlikar correlation for vertical Freon R-11 flow	130
4.2 A summary of the operating characteristics	131

List of Figures

Figure	Page
2.1 Schematic diagram of the 2-phase closed-loop thermosyphon system used for single phase tests	9
2.2 a) Counter flow evaporator consisting of 4 parallel evap. panels heated by air. b) Evap. panels 1 and 3 with thermocouple locations and cross-sectional cut of the panel	11
2.3 Flow chart showing data recording, storing and computation sequence	17
2.4 Schematic diagram showing the temperature recording positions in the primary loop	30
2.5 Heat recovered by cooling water vs. inlet air minus inlet cooling water temperature	41
2.6 System efficiency vs. average wall heat flux for the working fluid side of the evap.	41
2.7 System effectiveness vs. Reynolds number, Re ,	44
2.8 Total working fluid mass flux, G , vs. density pressure difference of the working fluid in the primary loop	44
2.9 Heat recovered by working fluid in evap. vs. heat released by air in evap.	46
2.10 Heat lost by air to surroundings vs. air volume flow rate	46
2.11 Evaporator efficiency vs. average wall heat flux for the working fluid side of the evap.	47
2.12 Wall tube temperature distribution for evap. tube no.4 of evap. panel 3 with air volume flow rate $0.27\text{m}^3/\text{s}$	51
2.13 Wall tube temperature distribution for evap. tube no. 4 of evap. panel 3 with air volume flow rate $0.72\text{m}^3/\text{s}$	51

2.14	Arithmetic mean overall heat transfer coefficient for evap. vs. average wall heat flux for the working fluid side of the evap.	54
2.15	Logarithmic mean overall heat transfer coefficient for evap. vs. average wall heat flux for the working fluid side of the evap.	54
2.16	Combined convection and radiation heat transfer coefficient for evap. air side vs. average air side wall heat flux	56
2.17	Radiation heat transfer coefficient for evap. air side vs. difference between mean air temp. and mean wall temp.	56
2.18	Working fluid heat transfer coefficient vs. average wall heat flux for working fluid side of evap.	58
2.19	Inlet working fluid mass flux for one evap. tube vs. average wall heat flux for working fluid side of evap.	58
2.20	Nusselt number for evap. working fluid side vs. Reynolds number for one evap. tube	61
2.21	Nusselt number for evap. working fluid side vs. inverse Graetz number	61
2.22	Heat recovered by cooling water vs. heat recovered by working fluid in evap.	63
2.23	Condenser overall heat transfer coefficient vs. wall heat flux for cooling water side of cond.	63
2.24	Condenser overall heat transfer coefficient vs. working fluid mass flow rate through cond.	65
2.25	Outside heat transfer coefficient of cond. coil vs working fluid mass flow rate through cond.	65

2.26	Heat recovered by cooling water vs. inlet air temperature minus inlet cooling water temperature	70
2.27	System efficiency vs. Reynolds number based on total working fluid flow rate	70
2.28	System effectiveness vs. Reynolds number based on the total working fluid mass flow rate	72
2.29	Evap. efficiency vs. Reynolds number based on inlet flow condition for one evap. tube	72
2.30	Wall temp. distribution for evap. tube no. 4 of panel 3 as a function of w.fl. mass flow rate, air flow rate=0.44m ³ /s, air temp.=40°C	74
2.31	Wall temp. distribution for evap. tube no. 4 of panel 3 as a function of w.fl. mass flow rate, air flow rate=0.44m ³ /s, air temp.=60°C	74
2.32	Wall temp. distribution for evap. tube no. 4 of panel 3 as a function of air temp., air flow rate=0.44m ³ /s, w.fl. flow rate=4.5 g/s	75
2.33	Wall temp. distribution for evap. tube no. 4 of panel 3 as a function of air temp, air flow rate=0.44m ³ /s, w.fl. flow rate=10 g/s	75
2.34	Wall heat flux for working fluid side of evaporator vs. inlet mass flux for one evaporator tube	76
2.35	Heat transfer coefficient for working fluid side of evap. vs. mass flux for working fluid flow thru one evap. tube, air flow rate=0.44 m ² /s	78
2.36	Heat transfer coefficient for working fluid side of evap. vs. mass flux for working fluid flow thru one evap. tube, air flow rate=0.72 m ² /s	78

2.37	Nusselt number for evap. working fluid side vs. Reynolds number for one evap. tube	79
2.38	Nusselt number for evap. working fluid side vs. inverse Graetz number for working fluid of evap.	79
2.39	Arithmetic mean overall heat transfer coefficient for cond. vs. wall heat flux for the cooling water	81
2.40	Estimated outside heat transfer coefficient for cond. coil vs. mass flow rate of working fluid flow thru evap.	81
3.1	Schematic diagram of two-phase closed-loop thermosyphon	88
3.2	Schematic diagram defining the six initial working fluid charge levels (dim. in mm)	91
3.3	Heat recovered by cooling water vs. extreme system temperature difference	101
3.4	System efficiency vs. wall heat flux from evap. tube wall to working fluid	103
3.5	System efficiency vs. Reynolds number based on the inlet fluid conditions for one evaporator tube	103
3.6	Downcomer and condensate mass flow rates and system pressure recorded by chart recorders during steady state for Ch.L. 2, 21 kPa abs. pressure and 75°C air temperature	104
3.7	Temperature distribution along the wall of evap. tube #4 on panel 1 at steady state (Ch.L. 4, 21 kPa abs. pressure, open downcomer)	106
3.8	Temperature distribution along the wall of evap. tube #4 on panel 3 at steady state (Ch.L. 4, 21 kPa abs. pressure, open downcomer)	106

Figure	Page
3.9 Overall heat transfer coefficient of the evaporator vs. average wall heat flux from the evap. tube wall to the working fluid	108
3.10 Overall heat transfer coefficient of the evaporator vs. mass flux through one evaporator tube	108
3.11 Combined radiation and convection heat transfer coefficient vs. wall heat flux from air to evap. wall	109
3.12 Radiation heat transfer coefficient vs. difference between mean air and mean wall temperatures	109
3.13 Inside heat transfer coefficient of evaporator vs. inlet working fluid mass flux for one evap. tube	111
3.14 Mass flux of the working fluid per evap. tube vs. average wall heat flux from evap. wall to working fluid	111
3.15 Vapour quality exiting the evap. vs. average wall heat flux from evap. wall to working fluid	113
3.16 Nusselt number for the working fluid vs. inverse Graetz number per evap. tube	113
3.17 Overall heat transfer coefficient of the condenser vs. average wall heat flux from wall to cooling water	115
3.18 Overall heat transfer coefficient of the condenser vs. vapour quality entering the condenser	115
3.19 Estimated heat transfer coefficient of fin side of condenser coil vs. average wall heat flux from working fluid to condenser coil	116
3.20 Estimated heat transfer coefficient of the fin side of the condenser coil vs. entering vapour quality	116

3.21	Ratio of exp. to single phase Dittus-Boelter heat transfer coefficient vs. Boiling number	118
3.22	Ratio of exp. to single phase Dittus-Boelter heat transfer coefficient vs. inverse Lockhart-Martinelli parameter	118
3.23	Ratio of exp. to liquid-only Dittus-Boelter heat transfer coefficient vs. Boiling number	119
3.24	Ratio of experimental heat transfer coefficient to Schrock-Grossman prediction vs. Boiling number	121
3.25	Ratio of experimental heat transfer coefficient to Shah prediction vs. Boiling number	121
3.26	Ratio of experimental heat transfer coefficient to Kandlikar prediction vs. Boiling number	122
3.27	Ratio of experimental heat transfer coefficient to prediction in [30] vs. Boiling number	122
4.1	Heat recovered by cooling water vs. heat recovered by working fluid in evap.	132
4.2	Heat recovered by cooling water vs. heating air temperature minus entrance cooling water temperature	132
4.3	System efficiency vs. average wall heat flux for the working fluid side of the evaporator	135
4.4	Fluctuations of working fluid properties due to flow boiling (air temperature=68°C, Ch.L. 2)	136
4.5	Wall temperature distribution for evaporator tube #4 on panel 3 (air volume flow rate=0.44 m ³ /s, Ch.L. 1)	138
4.6	Wall temperature distribution for evaporator tube #4 on panel 3 (air volume flow rate=0.44 m ³ /s, Ch.L. 3)	138

Figure	Page
4.7 Wall temperature distribution for evaporator tube #4 on panel 3 (air volume flow rate=0.44 m ³ /s, Ch.L. 6)	140
4.8 Overall heat transfer coefficient for evap. vs. wall heat flux for Freon	140
4.9 Combined convection and radiation heat transfer coefficient for air side vs. average air side wall heat flux	141
4.10 Radiation heat transfer coefficient for air vs. difference between mean air and mean evap. wall temperatures	141
4.11 Average mass flux for one evap. tube vs. average inside wall heat flux for evap.	143
4.12 Vapour quality at evap. exit vs. average inside wall heat flux for evap	143
4.13 Heat transfer coefficient for working fluid side of evap. vs. exit vapour quality	145
4.14 Nusselt number for working fluid side of evap. vs. inverse Graetz number for working fluid per evap. tube	145
4.15 Vapour quality at cond. entrance vs. vapour quality at evap. exit	147
4.16 Heat recovered by cooling water vs. vapour quality at cond. entrance	147
4.17 Overall heat transfer coefficient for cond. vs. cooling water wall heat flux	149
4.18 Predicted fin side heat transfer coefficient of cond. vs. fin side wall heat flux of cond.	149
4.19 Ratio of exp. heat transfer coefficient to Dittus-Boelter single phase prediction vs. Boiling number	151
4.20 Ratio of exp. heat transfer coefficient to Dittus-Boelter liquid-only prediction vs. Boiling number	151

Figure

Page

4.21	Ratio of exp. heat transfer coefficient to Dittus-Boelter single phase prediction vs. inverse Lockhart-Martinelli parameter	153
4.22	Ratio of exp. heat transfer coefficient to Dittus-Boelter liquid-only prediction vs. inverse Lockhart-Martinelli parameter	153
4.23	Ratio of experimental heat transfer coefficient to Kandlikar prediction vs. Boiling number	155
4.24	Ratio of experimental heat transfer coefficient to prediction with Ref. [30] vs. Boiling number	155

Nomenclature

A	availability, W
A_F	flow cross-sectional area, m^2
A_s	surface area, m^2
$A_{s,p}$	plane side surface area of individual evaporator panel, m^2
$A_{s,t}$	tube side surface area of individual evaporator panel, m^2
Bo	Boiling number, q_{x1}/G_i
Co	Convection number
C	heat capacity rate of liquid at constant pressure, W/kg K
$c_p, c_{p,l}$	specific heat of liquid at constant pressure, J/kg K
c_p	specific heat of vapor at constant pressure, J/kg K
D1-D4	constants used in Eq. (3.11)
d	inside diameter, m
dh	differential height, m
e	evaporator panel emissivity = 0.6
F_{11}	fluid dependent correction factor used in Eq. (3.11)
G_t	total working fluid mass flux at evaporator entrance, kg/m^2s
G_i	inlet mass flux of evaporator tube, kg/m^2s
Gz	Graetz number, $Pe d/l$
g	gravitational constant, $9.81 m/s^2$
H	height, m
h	average heat transfer coefficient, $W/m^2°C$
h_1	modified Dittus-Boelter turbulent liquid phase heat transfer correlation, $W/m^2°C$
h_2	Dittus-Boelter turbulent liquid phase heat transfer

	correlation, $W/m^2\text{ }^\circ C$
h_2	fin side heat transfer coefficient of condenser, $W/m^2\text{ }^\circ C$
i_g	latent heat of vaporization, J/kg
k	thermal conductivity, $W/m\text{ }^\circ C$
L	heat exchanger tube length, m
m	mass flow rate, kg/s
Nu	Nusselt number, hd/k
Pe	Peclet number, $RePr$
Pr	Prandtl number, $c \mu/k$
Q	total heat transfer rate, W
q	average wall heat flux, W/m^2
R	radius of curvature of condenser coil, m
Re	Reynolds number, Gd/μ
T	absolute temperature, K
T_o	reference temperature, K
t	temperature of working fluid, $^\circ C$
t_{sat}	saturation temperature of working fluid, $^\circ C$
t_w	wall temperature, $^\circ C$
ΔT	characteristic temperature difference, K
U	overall heat transfer coefficient, $W/m^2\text{ }^\circ C$
V	volumetric flow rate, ml/s
W	working fluid pump work, W
X_{11}	Martinelli parameter
x	vapor mass quality
ΔP_p	working fluid density pressure, Pa
ϵ	heat exchanger effectiveness
η	second law thermodynamic efficiency

μ	absolute viscosity, kg/ms
ν	kinematic viscosity, m ² /s
π	constant=3.1416
ρ	density, kg/m ³
σ	Stefan-Boltzman constant=5.67x10 ⁻⁸ , W/m ² K ⁴

Subscripts

a	air stream
al	lost by air stream
am	arithmetic mean
c	cooling stream
con	convection
cr	convection and radiation
f	fluid
h	heating stream
i	inlet
l	liquid only
lm	logarithmic mean
m	mean, average
min	minimum
o	outlet
rad	radiation
s	single phase
sat	saturated liquid
t	total
tl	loss across connecting tubes
tp	two-phase

- v vapour
- w evaporator tube wall
- 1,2 at evaporator and condenser, respectively
- 1,3 entrance fluid properties at evaporator and
condenser, respectively
- 12 between temperature measuring points 1 and 2
- 13 between temperature measuring points 1 and 3
- 21 loss by working fluid across condenser
- 2,4 exit fluid properties at evaporator and condenser,
respectively
- 23 between temperature measuring points 2 and 3

Superscripts

- a dimensionless variable used in Eqs. (2.13) and (2.14)

1. INTRODUCTION

1.1 Background Information

Low temperature heat sources are found all over the world. Pumping power is sometimes used to transfer this energy to a heat sink [1]. Yet, this method has been regarded as mechanically impractical or economically unfeasible in many cases. However, as energy prices increase and conventional resources dwindle, there is renewed interest in alternative methods of recovering low grade heat [1-4]. One such method is based on natural circulation of the fluid transporting the heat and finds application in the system called thermosyphon [5-7].

The fluid (working fluid) in the thermosyphon transfers heat absorbed from the heat source in the lower section to the heat sink in the upper part of the system. Gravitational forces due to local density differences between the heated and the cooled fluid cause pressure differences in the fluid within the thermosyphon. When these forces overcome the friction forces opposing the fluid motion, natural circulation of the working fluid is established.

Two different types of systems are the *closed-tube* [5,6] and *closed-loop* [7] thermosyphons. A closed-tube system is a sealed vertical pipe filled with working fluid. The fluid, heated by the heat source and cooled by the heat sink, establishes preferred flow streams inside the tube. Yet, the warmer and colder regions of the fluid are still in

intimate contact with each other as the working fluid transports heat from the heat source to the heat sink. This restricts the flow and hence, the efficiency of the heat transportation.

The closed-loop thermosyphon consists of two heat exchangers (lower and upper) and their connecting tubes. The working fluid absorbs heat from the heat source in the lower heat exchanger. The heated fluid flows through the *riser tube* to the upper heat exchanger in which the working fluid releases heat to the heat sink. The cooled working fluid flows back to the lower heat exchanger through the *condensate* or *return tube* and thereby completes the working fluid loop (*primary loop*). In this system the warmer and cooler working fluids are never in contact with each other, which makes the closed-loop thermosyphon more efficient than the closed-tube system.

In a *two-phase* thermosyphon the working fluid undergoes a phase change between liquid and vapour in both heat exchangers (evaporator and condenser). Due to this latent heat transfer process, the working fluid at constant temperature transfers heat rates from the heat source to the heat sink, that the would require a working fluid temperature increase of several degrees for a *single phase* thermosyphon to transfer the same heat rate between the two heat reservoirs. This makes the two-phase thermosyphon system interesting for low grade heat transportation.

Closed-loop hydronic systems were used for space heating in Europe prior to the Second World War. Later two-phase thermosyphons were employed in chemical reboilers and used for gas-turbine blade cooling.

Solar collector systems utilizing the closed-loop two-phase thermosyphon principle were commercialized for hot water and space heating in the early 1970's [9,10]. Additional research work has been done to improve the performance of the two-phase closed-loop solar collector system and adapt its use to cold regions into the present [7,11,12]. Simultaneously, investigations of these two-phase systems in other areas of low grade heat transportation and recovery took place. These include the increasing research efforts devoted to the application of two-phase thermosyphons for permafrost and icedam constructions [8], cooling of nuclear reactors, geothermal energy recovery [4] as well as waste heat recovery.

1.2 Scope of the Study

This project investigates low grade heat recovery from air using a closed-loop two-phase thermosyphon system. The heat is recovered by a cooling water loop.

The main objectives of the study are:

- to investigate the heat transfer characteristics of the overall system and the two heat exchangers separately.
- to compare the results with existing heat transfer

correlations.

- to determine how different working fluids influence the two-phase system performance.
- to indicate how the vapour quality affects the system behaviour.
- to compare results for single phase thermosyphon with the two-phase system results
- to establish system limitations.

Single-phase thermosyphon tests are performed with water as the working fluid (Chapter 2). Water is used since it is readily available, inexpensive, easy to handle and non-toxic. Both natural and forced circulation tests are performed and the results are compared. However, the main purpose of these hydronic tests is to obtain some information about the system operation characteristics. This knowledge is applied in the two-phase thermosyphon analyses.

Water is used as the working fluid for the two-phase thermosyphon tests discussed in Chapter 3. This allows comparison of the results from a two-phase and a single-phase system, which both operate with the same working fluid. Moreover, satisfactory results from the two-phase system may encourage the use of this working fluid in future thermosyphon research projects. The system performance is examined for different heating air temperatures, liquid charge levels of the working fluid and the effect of the liquid-vapour separator.

Freon R-11 is used as the working fluid for the closed-loop two-phase thermosyphon system in Chapter 4. The low boiling point of R-11 (23.7°C at atm. pressure) and high latent heat of vapourization makes this fluid suitable as the working medium for low grade heat recovery research. The low toxic level, readily known thermodynamic properties and available results from other R-11 closed-loop two-phase thermosyphon systems made this fluid a practical choice. The overall system performance and the heat transfer characteristics for the two heat exchangers are discussed separately in this chapter.

Each of the three Chapters 2 - 4 includes introduction, problem statement, theory, results and concluding remarks. To avoid unnecessary repetition, the basic system apparatus, testing procedure and employed theory are not discussed in Chapters 3 or 4 unless new methods or concepts are applied.

The final chapter (Chapter 5) ties related experimental observations and results together and gives overall conclusions and recommendations resulting from this study.

2. Heat Recovery Utilizing a Closed-Loop Hydronic System

Tested with Natural and Forced Circulation

Summary

Heat is transported from a warm air heat source to a cold water reservoir utilizing water as the transport medium.

Both natural and forced working fluid circulation tests are conducted. Heat and mass transfer characteristics are studied and results from the two flow conditions are compared.

Depending upon the heating air parameters (volume flow rates $0.27 - 0.72 \text{ m}^3/\text{s}$ and temperatures $75 - 96^\circ\text{C}$) the natural flow tests give heat recovery rates of $650 - 1800 \text{ W}$, exiting cooling water temperatures from 18 to 25.5°C and working fluid mass flow rates between $3.0 - 6.5 \text{ g/s}$.

The controlled fluid circulation experiments are conducted with working fluid flow rates from 4.5 to 20.0 g/s . The heating air temperature ranges from $40 - 70^\circ\text{C}$, while the air flow rates are the same as conducted for natural working fluid circulation. The results show a cooling water exit temperature range of $14.5 - 28.7^\circ\text{C}$ and heat recovery rates between $350 - 2400 \text{ W}$. The experiments reveal system efficiencies between $2 - 6.5\%$ for thermosyphonic flow and $2 - 11\%$ for forced working fluid flow.

2.1 Introduction

The main objective of this project is to study the steady-state operating characteristics of a closed-loop two-phase thermosyphon transporting low grade heat from warm air to cold water. Therefore, the system apparatus is described using two-phase thermosyphon terminology. But since single phase tests results are discussed in this chapter, some terminology will be changed as mentioned later in the chapter.

Experiments are executed with both natural and forced working fluid circulation. Water is chosen as the working fluid due to the practicalities and conveniences mentioned in Chapter 1. The working fluid loop is referred to as the primary loop, while the heating air and the cooling water loops are often called the secondary heating loop and secondary cooling loop respectively.

The tests are performed for different air volume flow rates ($0.27 - 0.72 \text{ m}^3/\text{s}$) and heating air temperatures ($75 - 96^\circ\text{C}$ for natural circulation, $40 - 70^\circ\text{C}$ for forced flow). The controlled working fluid flow rates during forced circulation are between 4.5 and 20.0 g/s .

The heat and mass transfer characteristics of the two heat exchangers are studied for stable system conditions for both natural and forced circulation. These tests are performed to acquire an understanding of the system operation and to obtain operating results which can be used for two-phase thermosyphon analyses. The results for

thermosyphonic and forced flow conditions are discussed in different sections of this chapter.

2.2 Experimental Apparatus

The system used in this work, shown schematically in Fig. 2.1, is a closed-loop two-phase thermosyphon system and will be referenced as such. The description of the system is arranged into different subsections discussing the secondary heating loop, the primary working fluid loop, the secondary cooling loop and the data acquisition system. A final subsection discusses the system changes made to accommodate the hydronic testing conditions.

The system instrumentation (flowmeters, thermocouples, pressure transducers, etc.) will be described in detail in Section 2.3.

2.2.1 The secondary heating loop

The heating air is circulated by a backward inclined centrifugal blower, whose speed is controlled from 0 to 2650 rpm. using a Variac autotransformer controlling a 1.5 hp variable speed motor.

Two pressure taps, a pitot tube and an annubar (air bar), are located in the duct loop 0.45 m downstream and 2.15 m upstream of the blower as shown in Fig. 2.1. The dynamic air pressure obtained from these two pressure taps, was converted to electronic signals using two sensitive Validyne pressure transducers.

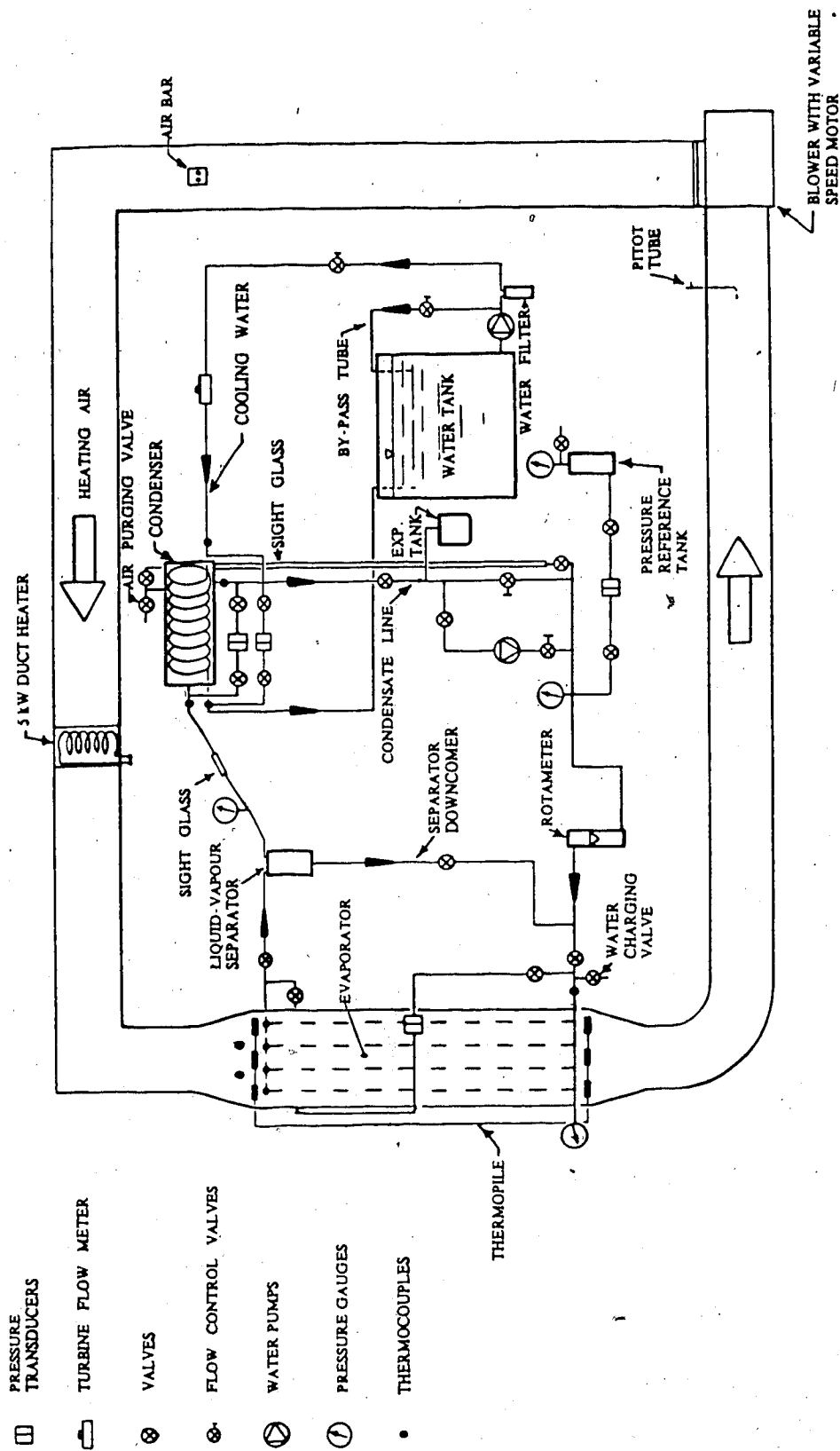


Fig. 2.1 Schematic diagram of the 2-phase-closed-loop thermosyphon system used for single phase tests

A 5 kW electric duct heater heats the air before it enters the evaporator. A thermocouple located 1.0 m downstream of the heater is connected to a Thermo Electric PID temperature controller. This controller regulates the power supply to the heater to maintain a prescribed air temperature (accuracy within $\pm 0.8^{\circ}\text{C}$).

The air temperature entering the evaporator is recorded using two thermocouples, while the air temperature difference across the evaporator is measured with a nine-joint thermopile as shown in Fig. 2.1.

The evaporator is a built-on-site heat exchanger, consisting of four solar collector panels' [9], (1.764 m high x 0.480 m wide) which are mounted 0.07 m apart in a 0.508 m x 0.310 m x 1.764 m section of the air duct as shown in Fig. 2.2a. The air flows parallel to each of the four collector panels, usually referred to as *evaporator panels* or *panels*). Fig. 2.2b shows how the *evaporator tubes* and thermocouples are mounted onto the (1.727 m high, 0.480 m wide and 0.61 mm thick) *evaporator plate*. A cross section of the panel is shown in Section A-A. The tube side of the panel is referred to as *tube-side* and the opposite side is called the *plane-side*. The original black coating was not removed from the evaporator panel. The thermocouples, shown in Fig. 2.2b, are attached only to evaporator panels 1 and 3.

Manufactured by Solar Research, Division of Refrigeration Research, Inc., Michigan.

2.2.2 The primary working fluid loop

The evaporator is designed as a counter flow heat exchanger as indicated in Fig. 2.1. From the lower main evaporator header (0.0156 m i.d.) located outside the air duct, the working fluid is assumed to be equally distributed to the four lower evaporator headers (0.0156 m i.d.). The eight evaporator tubes (0.007747 m i.d.) are equally spaced (0.054 m centre to centre) on the fin-plate as shown in Fig. 2.2b. Further details about the evaporator dimensions are found in Table 2.1.

A liquid-vapour separator is located in the vapour line between the two heat exchangers. Here some of the liquid is separated from the working fluid before it enters the condenser.

The horizontal centre line of the shell and coil condenser² is located 2.13 m above the evaporator inlet. The helically coiled copper tube (0.0127 m i.d.) has 16 continuous low integral fins³ per inch and an outside surface area of 0.952 m². Other physical dimensions for the condenser are given in Table 2.2.

A sight glass mounted in the inclined riser is used for visual flow observation. The vertical sight glass parallel to the *condensate line* is used as a liquid level indicator.

A connecting tube attaches a storage tank to the condensate line of the primary loop as shown in Fig. 2.1.

²Manufactured by Solar Research, Division of Refrigeration Research, Inc., Michigan, condenser model 5835.

³The fin root radius and fin height are approximately 12.7 mm (1/2 in) and 1.6 mm (1/16 in).

TABLE 2.1: EVAPORATOR DIMENSIONS

HEAT EXCHANGER MAKE	ON SITE BUILT 4 SOLAR COLLECTOR PANELS MOUNTED IN PARALLEL
MANUFACTURER OF SOLAR COLLECTOR	SOLAR RESEARCH, DIV. OF REFRIGERATION RESEARCH, INC.
TYPE OF HEAT EXCHANGER	COUNTER FLOW EVAPORATOR (EVAP.)
HEATING FLUID	AIR
WORKING FLUIDS	DISTILLED WATER/FREON R-11
COLLECTOR PLATE DESCRIPTION	EVAPORATOR PANEL
EVAP. PLATE, TUBE AND HEADER MATERIAL	CARBON STEEL FUSED WITH COPPER WITH BLACK CARBON-COATING COVER
MAIN EVAP. HEADER MATERIAL	COPPER
EVAP. SIZE W x B x H [cu.m]	0.508 x 0.310 x 1.764
OPEN CROSS-SEC. AREA FACING THE AIR FLOW THROUGH EVAP. [sq.m]	0.22
DIST. BETWEEN 2 PANELS [m]	0.07
CROSS-SECTIONAL AIR FLOW AREA BETWEEN 2 EVAP.PANELS [sq.m]	0.0336
EVAP. PLATE DIM. w x t x h [cu.m]	0.480 x 0.00061 x 1.727
SURF.AREA PER EVAP.PANEL [sq.m]	1.923
PANEL SURF.AREA, TUBE SIDE [sq.m]	1.094
PANEL SURF.AREA, PLANE SIDE [sq.m]	0.829
MAIN EVAP. HEADERS	2
HEADERS PER EVAP. PANEL	2
TUBES PER EVAP. PANEL	8 EVAP. TUBES
MAIN EVAP. HEADER LENGTH [m]	0.270
EVAP. HEADER LENGTH [m]	0.408
EVAP. TUBE LENGTH [m]	1.764
ID/OD MAIN EVAP.HEADER [m]	0.0156/0.0195
ID/OD EVAP. PANEL HEADER [m]	0.0156/0.0195
ID/OD EVAP.TUBE [m]	0.007747/0.009529
CENTER-CENTER DISTANCE BETWEEN EVAP.TUBES [m]	0.054
EVAP. TUBE LENGTH TO INSIDE DIAMETER RATIO	227.7
INSIDE SURF.AREA PER EVAP.TUBE [sq.m]	0.0429

TABLE 2.2: CONDENSER DIMENSIONS

MANUFACTURER	SOLAR RESEARCH, DIV. OF REFRIGERATION RESEARCH, INC.
TYPE OF CONDENSER	SHELL AND COIL
TYPE OF CONDENSER COIL	HELICALLY COILED CONTINUOUS LOW-FINNED COPPER TUBE
SHELL MATERIAL	STEEL
WORKING FLUIDS	DISTILLED WATER/FREON R-11
COOLING FLUID	WATER
CONDENSER TUBE LENGTH [m]	7.620
NUMBER OF COILS	21
OUTSIDE CONDENSER COIL SURFACE AREA [sq.m]	0.952
INSIDE CONDENSER COIL SURFACE AREA [sq.m]	0.304
INSIDE DIAMETER OF THE COPPER TUBE [m]	0.0127
APPROX. FIN HEIGHT [m]	0.0016
APPROX. FIN ROOT RADIUS [m]	0.0127
TUBE LENGTH TO INSIDE DIAMETER RATIO	600.
RADIUS OF CURVATURE OF THE CONDENSER COIL [m]	0.106
OUTSIDE SHELL DIAMETER [m]	0.1524
INSIDE SHELL DIAMETER [m]	0.1461
SHELL WALL THICKNESS [m]	0.00315

This is used for storing excess working fluid during system operation.

The working fluid flow rate is measured by a rotameter located close to the inlet of the evaporator.

The locations of pressure gauges, pressure transducers and thermocouples in the system are indicated in Fig. 2.1. The pressure reference tank shown in the figure is kept at constant pressure. Hence, the pressure transducer connected to the tank and the condensate line monitors the system pressure at all times. Wire meshes are used to disturb the working fluid upstream of the thermocouples to improve the accuracy of the bulk temperature recordings. The pressure drop of the working fluid across each heat exchanger is measured by pressure transducers as shown in the figure. Pressure gauges record the local working fluid pressures at strategic positions in the loop.

The inside diameter of the connecting tubes are reduced from 0.019 m (3/4 in.) to 0.0127 m (1/2 in.) to fit the flowmeters. The tubes are insulated with Armstrong Armaflex tube insulation. All the tube joints are silver soldered, while Swagelok brass fittings are used to attach instruments and valves to copper and glass tubes. To make system modifications easier, several valves are located in the working fluid loop.

2.2.3 The secondary cooling loop

As shown in Fig. 2.1 the gold water is stored in a storage tank (1110 l capacity), and the water is circulated around the cooling loop by a Jacuzzi water pump with a 370 W (1/2 hp) motor.

Cooling water flow rate, regulated by throttling valves and a tube by-passing the condenser, is measured using a turbine flow meter located in the cooling water supply line.

The water pressure drop across the condenser is registered by a Validyne pressure transducer, attached to both the inlet and the outlet cooling water tubes of the heat exchanger. Wire meshes are used to ensure proper water bulk temperature is recorded. A water filter is mounted between the pump and the turbine flow meter to reduce the amount of sediments entering the flowmeter and the heat exchanger.

2.2.4 The data acquisition system

A flow chart of the data recording and storing procedure is shown schematically in Fig. 2.3. Voltage signals from all the electronic measuring instruments are monitored by a Hewlett Packard* 3497A data acquisition/control unit. This unit is controlled by an HP-85 micro computer which collects, stores and prints all the data. The pressure gauges and rotameter recordings are entered manually into the micro computer. All the collected

*From here on Hewlett Packard will be referred to as HP.

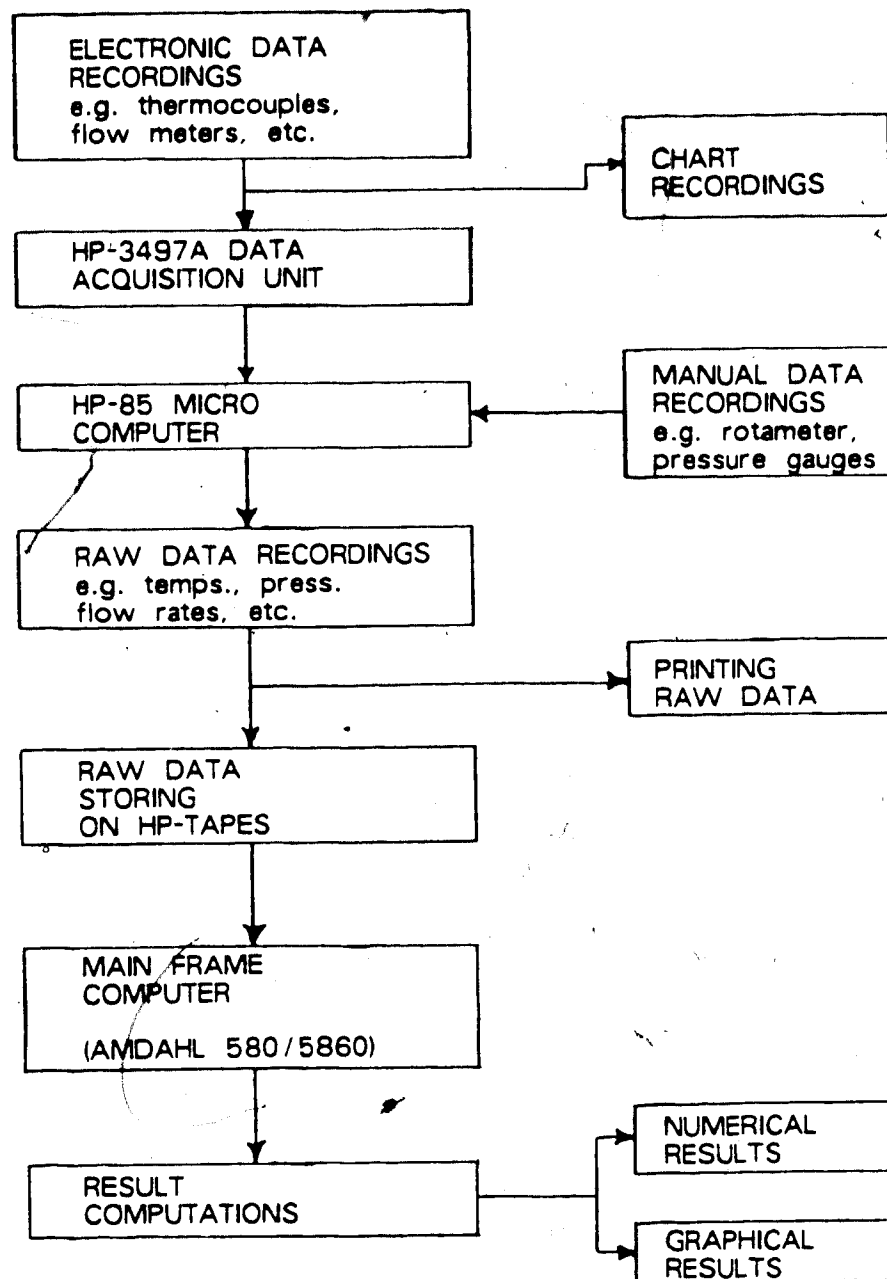


Fig. 2.3 Flow chart showing data recording, storing and computation sequence

data are stored on magnetic tapes and printed out by a Decwriter terminal. The collected data are later transferred to the University of Alberta main frame computer (Amdahl 580/5860) to perform required numerical calculations, data processing and plotting.

2.2.5 Hydronic system modifications

Distilled water was used as the working fluid. The working fluid storage tank used during the two-phase experiments, is replaced by a 510 kPa (75 psi) expansion tank. The sole purpose of this tank is to absorb the expanded liquid volume as the working fluid is heated.

A 1/25 hp Taco water pump is located parallel to the condensate line, as shown in Fig. 2.1, for use during forced working fluid operation. Valves in the tube downstream of the pump and in the parallel thermosyphon line are used to regulate the forced working fluid flow rates.

Although no liquid-vapour phase change takes place for these hydronic tests, the heat exchangers will still be referred to as evaporator and condenser.

2.3 Instrumentation and Calibration

All the electronic data recording instruments were calibrated using the HP-85 micro computer and the HP-4397A data acquisition/control unit. Hence, the recording procedure was the same for both calibration and experiments.

2.3.1 Thermocouples and thermopile

All temperature sensors were made from type J, iron-constantan, thermocouple wires. The working fluid and cooling water temperatures were all measured using 0.7 mm o.d. sheathed thermocouples, while the air stream temperatures and the wall temperatures of the evaporator were recorded with 0.225 mm o.d. thermocouples.

A Rosemount model 910C controlled temperature calibration bath was used to calibrate the thermocouples. A Fluke 2189A thermometry unit with 0.01°C resolution and 0.1°C maximum error was used as the temperature standard.

The thermocouples were calibrated over their operating range. A linear curve fit of recorded voltage versus measured standard temperature gave correlation coefficients of 1.000 for all the thermocouples. The maximum error was $\pm 0.3^\circ\text{C}$.

The nine-joint junction iron-constantan (0.225 mm o.d.) thermopile was calibrated using twelve previously calibrated thermocouples (0.225 mm). Six of them were located in the inlet and six in the outlet air stream of the evaporator. Repeated calibrations for air temperatures ranging from 40 to 90°C and with air temperature differences range of 3 - 11°C gave good repeatability with a maximum deviation of 0.1°C.

2.3.2 Liquid flowmeters

The rotameter (capacity 3 - 23 ml/s) and the turbine flowmeter (capacity 5 - 80 ml/s) were calibrated by averaging their respective readings over the collection time of a certain mass of water. The mass flow rate of the water was assumed constant over the collection period. A calibrated scale was used to record the water mass during calibration. The accuracy of the scale was 0.005 kg and the resolution was 0.0005 kg. The collected water mass varied between 0.5 and 4.0 kg depending upon flow rate. The collection time was recorded with a digital stop watch with a 1/100 sec. resolution.

The water temperature was recorded and the density difference was incorporated into the calibration curves. Repeated calibrations of the same flow rate showed less than 0.5% deviation. Linear curve fits of the results gave correlation coefficients of 0.999 and 1.000 for the rotameter and the turbine flowmeter respectively. The maximum error was 0.3 g/s for both flowmeters.

2.3.3 Pressure transducers

Six Validyne pressure transducers were used in the overall heat transfer system. The working fluid system pressure was recorded by a 68,900 Pa (10 psi) transducer, while the pressure drop of the cooling water across the condenser was measured with a 34,450 Pa (5 psi) pressure transducer. Both these transducers were calibrated over

their operating range using a mercury manometer with a 60 Pa resolution.

The working fluid pressure drops across the two heat exchangers were recorded by two 3,450 Pa (0.5 psi) transducers. A U-tube water manometer (5 Pa resolution) was used to calibrate these pressure transducers over their operating range.

The pressure differences recorded across the pitot tube and the air bar were measured with two 200 Pa (0.8 inH₂O) pressure transducers. A micro-manometer, 0.2 Pa resolution, was used for this calibration.

Linear calibration curves showed a correlation coefficient of 1.000 for all six transducers and the error did not exceed 0.5% of the recorded pressure for any transducer.

2.3.4 Pressure gauges

The three pressure gauges installed in the working fluid loop are all Robinair refrigerant gauges with operating range from 30 inHg vacuum (abs. zero pressure) to 861,300 Pa (120 psi) pressure⁵.

The pressure in the reference tank was recorded by a pressure gauge with an operating range of 0 - 205,000 Pa (0 - 30 psi) pressure and 3450 Pa (0.5 psi) resolution. All the gauges were checked and calibrated against a Budenberg

⁵Atmospheric pressure, 101,325 Pa (14.7 psi) absolute pressure, is used as datum for pressures above this value. Pressures below atmospheric pressure are referred to as partial vacuum or as absolute pressure.

dead weight tester, before installation.

2.3.5 Wattmeter

The Wattmeter in the electric duct-heater control loop was calibrated against the voltage reading of a Fluke multimeter with 1.0 mV resolution. The wattmeter was used to indicate the power supply to the duct heater. It was also used to verify steady state of the operating system.

One volt on the voltmeter corresponded to 1000 W power supply. The maximum error of the wattmeter was 30 W over 800 - 4500 W calibrated range.

2.3.6 Pitot tube and air bar

The air flow rates were obtained from the dynamic pressure recorded from an annubar and a pitot tube. The standard equal area method [13] was used to integrate the dynamic pressure over the cross section of the circular duct. The annubar mounted in the square duct was installed and recorded according to the specifications recommended by the manufacturer.

2.4 Experimental Procedure

The working fluid loop was leak-tested with compressed air (300 kPa) for 48 hours. The voltmeter of the HP-3497A data acquisition/control unit (7.0 Pa resolution) was used as a leak-indicator, and Snoop (liquid leak detector) was

'Air bar model Air-79, manufactured by Dieterich Standard Corporation, Boulder, Colorado.

used to locate the leaks.

When no leaks were detected over the leak-testing period, the primary loop was charged with working fluid, distilled water treated with Zeotec 5900 corrosion inhibitor (0.5% vol/vol). The inhibitor was assumed to have no effect on the system performance. The working fluid had a pH-range of 8.5 - 10.0 and an electric conductivity of 1,000 - 2,000 mmho/cm.

A water pump forced the working fluid through the liquid charging valve located by the evaporator inlet (shown in Fig. 2.1). The system was charged until only liquid came out of the air purging valve at the top of the condenser. Then several test-runs were conducted so air pockets in the working fluid would collect in the condenser shell. This air was purged out of the condenser by the working fluid which was pressurized to 35 kPa (5 psi). Visual observations of the purging process were possible since the air/water mixture was purged through a transparent plastic hose. This procedure was repeated until no air was seen leaving the heat exchanger. After air was purged from the primary loop, additional working fluid was forced into the system. This ensured that the loop was always full of liquid.

Before any experiment was commenced, all the electronic control and recording instruments were allowed minimum 24 hours to warm up. The cooling water was cooled down to the operating temperature of 12 - 13 °C. The water temperature was maintained at this temperature as the water was

continuously replaced by cold tap water throughout the daily testing period. This was done to ensure that constant cooling water temperature entered the condenser.

One data recording set lasted approximately 45 sec. and read each of the 74 data channels on the HP data acquisition unit several times. After all the data signals were recorded, the mean value for each data channel was stored on tape. During a data recording set the thermocouple data channels were read 2 times, the pressure transducer data channels (monitoring the dynamic air pressure) were read 25 times and all the other data channels were read 10 times. This was a compromise between accuracy and recording time, and the recording sequence was chosen after several trial tests.

All the trial tests were performed at steady state for air temperatures 40, 60 and 80°C and air flow rates 0.44 and 0.72 m³/s. At each system condition the thermocouples data channels were recorded 1, 2 and 10 times, the data channels for the dynamic air pressure were read 10, 25 and 50 times, while the other data channels were read 5, 10 and 25 times. Each of the three readings per data channel was averaged, and the mean values were compared. The temperatures were collected using three different reading procedures. The mean values of 1 and 2 thermocouple readings showed 0.7 and 0.3% deviation from the average of 10 readings respectively. For the two pressure transducers monitoring the dynamic air pressure, the mean of 10 and 25 readings gave 25 and 4%

deviation from the average value of the 50 readings respectively. For the other data channels the mean values for 5 readings showed 7% and for 10 readings showed 2% deviation from the average value of the 25 readings. All these results were maximum relative deviations for all the trial tests.

Prior to each test an initial reading was processed and the data were used to eliminate zero-offsets for the electronic instruments.

Experiments were always started with adjusting the heating and cooling fluids to desired flow rates. When the tests were conducted with forced working fluid circulation, the fluid flow rate was set before turning the heater on. This flow rate had to be adjusted occasionally as the flow rate increased with increasing working fluid temperatures until the system reached steady state. This fluid flow searching was mainly caused by gravity acting on the density differences of the working fluid around the primary loop due to different fluid temperatures.

The rotameter was read over the sampling period, while the working fluid pressure gauges were checked immediately before and after this period. The average readings were entered into the HP-85 micro-computer. All the electronic data signals were automatically recorded by the micro computer through the HP-3497A data acquisition/control unit according to the procedure explained in Section 2.2.

Data recording sets were taken every 10 - 15 minutes until the system reached steady state 2.5 to 3 hours after the experiment started. After one steady state condition was reached and a operating parameter was changed, a 1 to 2 hours stabilizing period was required before the system stabilized again. Steady state was assumed when the heat source temperature changed less than 0.1°C and the power supply was nearly constant over a 30-minute period. The steady system data were recorded and stored on magnetic tapes for later analyses.

Experiments were conducted with four air flow rates (0.27, 0.44, 0.57 and $0.72 \text{ m}^3/\text{s}$) and for an air temperature range of $75 - 96^{\circ}\text{C}$ for thermosyphonic flow , while the temperatures used for forced flow were $40, 50, 60$ and 70°C . The air temperatures for the natural circulation tests are shown in Table 2.3. The forced circulation tests were analysed using four different flow rates (4.5, 6.5, 10.0 and 20.0 g/s).

All other system operating parameters, such as cooling water flow rate (40 g/s), cooling water inlet temperature (approximately 13°C) and initial working fluid pressure (10 kPa gauge) were kept constant. The separator downcomer tube and the vertical sight glass indicating the liquid level were always closed for the single phase experiments.

TABLE 2.3: HEATING AIR FLOW RATE AND TEMPERATURE

AIR FLOW RATE [m ³]	HEATING AIR TEMPERATURE [°C]
0.27	78.5
	85.6
	89.6
	94.7
	96.3
0.44	77.6
	83.5
	84.7
	88.4
0.57	76.0
	78.8
	81.9
	83.8
0.72	84.3
	76.1
	78.2
	81.1
	82.2

2.5 Basic Equations for Data Analysis

The heat rate, Q , absorbed by a fluid flowing through a heat exchanger is

$$Q = V \bar{\rho} \bar{c}_p (t_{fo} - t_{fi}) \quad (2.1a)$$

or

$$Q = m \bar{c}_p (t_{fo} - t_{fi}) \quad (2.1b)$$

where V' is the volumetric fluid flow rate, m is the mass flow rate of the fluid, $\bar{\rho}$ is the fluid density and \bar{c}_p is the specific heat of the fluid. All thermodynamic properties are calculated based on the average temperature of the inlet and outlet fluid of the heat exchanger, unless stated otherwise. The thermodynamic properties of water are obtained from empirical formulas [14], given in Appendix II. A negative value of Q obtained from Eq. (2.1a) or Eq. (2.1b) indicates that the fluid has released heat in the heat exchanger.

The wall heat flux, q , is defined as

$$q = \frac{Q}{A_s} \quad (2.2)$$

where A_s is the surface area through which the heat is transferred.

The heat loss from the air in the evaporator to the surroundings, Q_{a1} , is

$$Q_{a1} = Q_a - Q_1 \quad (2.3a)$$

where Q_a is heat released by the air and Q_1 is heat recovered by the working fluid. Similarly, the heat loss from the working fluid in the condenser to the surroundings, Q_{21} , is

$$Q_{21} = Q_2 - Q_c \quad (2.3b)$$

A complete list of notations used in this thesis is given in the Nomenclature.

where Q_2 is the heat released by the working fluid and Q_c is the heat recovered by the cooling water. The heat lost by the single phase working fluid in the connecting tubes, Q_{t1} , is

$$Q_{t1} = m [\bar{c}_p(t_2 - t_3) + \bar{c}_p(t_4 - t_1)] \quad (2.3c)$$

Throughout this thesis the subscript 1 refers to the working fluid in the evaporator and the subscript 2 to the working fluid in the condenser. It should be noted however, that also the properties of the working fluid entering and exiting the evaporator are referenced with the subscripts 1 and 2 respectively. The properties of the working fluid entering the condenser are indicated with the subscript 3 and the properties of the fluid leaving this heat exchanger have 4 as the subscript. The positions in the primary loop corresponding to these subscript notations are shown in the schematic diagram in Fig. 2.4.

The wall heat flux of the air side, q_a , is

$$q_a = \frac{Q_a - Q_{a1}}{A_{sa}} \quad (2.4)$$

where the total surface area of the evaporator panels, A_{sa} , is

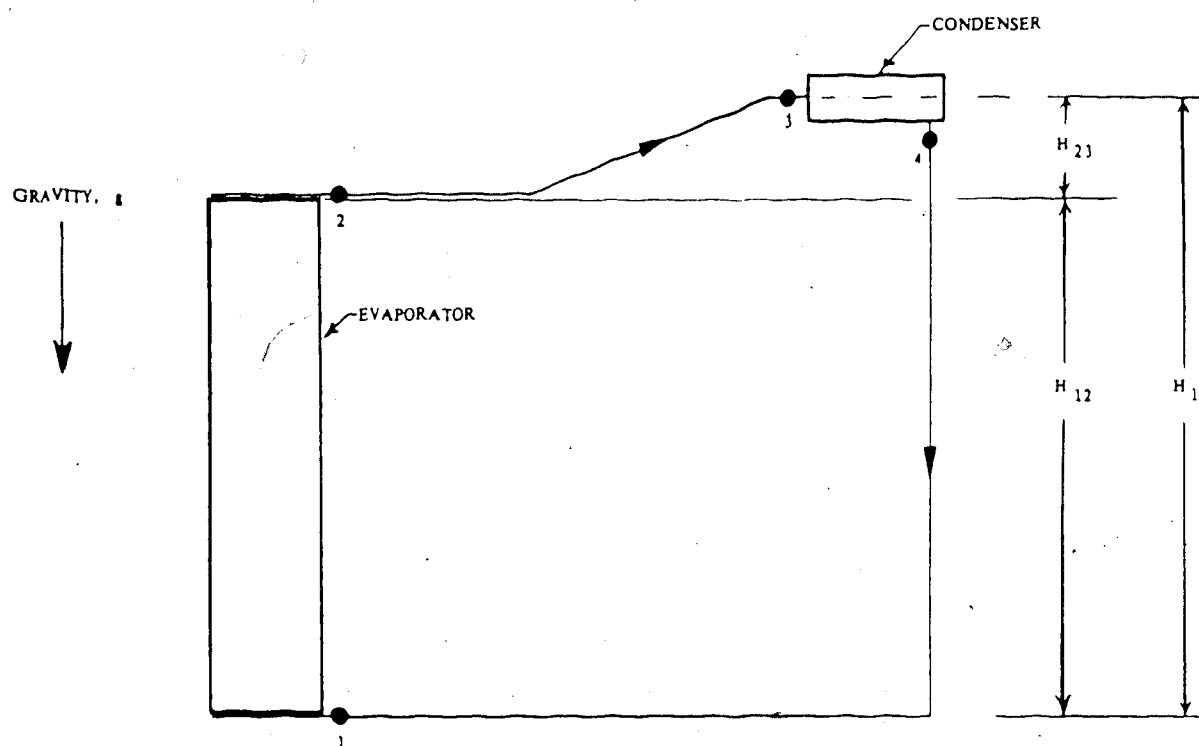


Fig. 2.4 Schematic diagram showing the temperature recording positions in the primary loop

$$A_{sa} = 4 (A_{st} + A_{sp}) \quad (2.5)$$

where A_{st} is the tube-side surface area and A_{sp} is the plane-side surface area of the evaporator panel.

The overall heat transfer coefficient, U , of any heat exchanger is defined as

$$U = \frac{Q}{A_s \Delta T} \quad (2.6)$$

where A_s can be either the inside or the outside surface area through which the heat is being transferred. The inside surface was used for both heat exchangers in this work. The temperature difference, ΔT , is either the logarithmic mean (ΔT_{lm}) or the arithmetic mean (ΔT_{am}) temperature difference between the two fluids. Overall heat transfer coefficients based on both these temperature differences are used in this analysis. For counterflow heat exchangers these temperature differences are defined as

$$\Delta T_{lm} = \frac{(T_{hi} - T_{co}) - (T_{ho} - T_{ci})}{\ln \frac{T_{hi} - T_{co}}{T_{ho} - T_{ci}}} \quad (2.7)$$

and

$$\Delta T_{am} = \frac{1}{2} (T_{hi} + T_{ho}) - \frac{1}{2} (T_{ci} + T_{co}) \quad (2.8)$$

where T_{hi} is the inlet and T_{ho} is the outlet bulk

temperature of the hot fluid stream, while $T_{c,i}$ is the inlet and $T_{c,o}$ is the outlet bulk temperature of the cold fluid stream.

The heat transfer coefficient based on the arithmetic mean temperature difference, h , is

$$h = \frac{q}{\Delta T_m} \quad (2.9)$$

where

$$\Delta T_m = \bar{T}_w - \bar{T}_f \quad (2.10a)$$

or

$$\Delta T_m = \bar{T}_f - \bar{T}_w \quad (2.10b)$$

and \bar{T}_w is the average recorded wall temperature and \bar{T}_f is the mean recorded fluid temperature.

Eq. (2.10a) is used when the wall temperature is higher than the fluid temperature, and Eq. (2.10b) is used when the wall is heated by the fluid.

The combined convection and radiation heat transfer coefficient of the air side of the evaporator, $h_{c,r}$, can either be obtained from Eq. (2.9) or by adding the convective heat transfer coefficient, $h_{c,o,n}$, and the radiation heat transfer coefficient, $h_{r,a,d}$, as done in [15] and below

$$h_{cr} = h_{con} + h_{rad} \quad (2.11)$$

A simplified method described in [16] is used to calculate the radiation heat transfer coefficient

$$h_{rad} = \sigma e \frac{\bar{T}_a^4 - \bar{T}_w^4}{\bar{T}_a - \bar{T}_w} \quad (2.12)$$

where σ is the Stefan-Boltzman constant ($\sigma = 5.67 \times 10^{-8} \text{ W/m}^2 \cdot \text{K}^4$), e is the emissivity of the evaporator plate ($e = 0.6$) [7] and \bar{T}_a is the mean air temperature through the evaporator.

The following assumptions are made when calculating the working fluid heat transfer coefficient through the heat source exchanger:

- the working fluid flow rate is equally distributed to the evaporator tubes.
- the working fluid recovers heat at the same rate in each evaporator tube.
- the bulk temperature of the working fluid entering an evaporator tube is the average of the lower tube wall temperature and the temperature of the working fluid entering the evaporator, t_1 .
- the temperature through the wall of the evaporator

 *This assumption is made since the working fluid is heated somewhat in the lower header of the evaporator panel and the actual temperature is unknown. This assumption is only used for single phase analysis. Similar analyses in Chapters 3 and 4 use the temperature of the working fluid entering the evaporator.

tubes is the same for all the tubes at similar distance from the lower evaporator header.

Since the condenser tube wall temperature is unknown, an empirical equation [17] for helically coiled tubes is used to calculate the cooling water heat transfer coefficient, h_c .

$$h_c = \{ 3.65 + 0.08 [1.0 + 0.08 \left(\frac{d}{2R} \right)^{0.9}] Re^\alpha Pr^{1/3} \} \frac{k}{d} \quad (2.13)$$

where

$$\alpha = 0.5 + 0.2903 \left(\frac{d}{2R} \right)^{0.194} \quad (2.14)$$

where d is the inside diameter the copper tube, R is the radius of curvature of the coil, Re is Reynolds number, Pr is Prandtl number and k is the thermal conductivity of the liquid. Reynolds number is defined as

$$Re = \frac{G d}{\mu} \quad (2.15)$$

where μ is the absolute viscosity of the fluid based on the fluid temperature entering the heat exchanger. The mass flux G is defined as

$$G = \frac{\dot{m}}{A_F} \quad (2.16)$$

where A_f is the inside cross sectional area of the tube. The thermodynamic properties used to calculate Reynolds number are based on the temperature of the entering fluid. This is done because the fluid flow rate is measured at this temperature and an exact value of Reynolds number can be calculated. As it is heated in the evaporator tubes, the temperature becomes unknown at any location and the value of Reynolds number can only be approximated. Prandtl number is defined as

$$Pr = \frac{\mu c_p}{k} \quad (2.17)$$

The outside heat transfer coefficient of the condenser coil, h_2 , is calculated using the overall heat transfer coefficient equation for circular pipes [18]. The heat conduction term is neglected as the temperature through the copper tube wall is assumed constant. In rearranged form, the outside (fin side) heat transfer coefficient can be expressed as

$$h_2 = \left\{ \frac{A_{s2}}{U_c A_{sc}} - \frac{A_{s2}}{h_c A_{sc}} \right\}^{-1} \quad (2.18)$$

where A_{s2} is surface area in contact with the working fluid and A_{sc} is the surface area through which heat is transferred to the cooling water. The applied assumption is justifiable since the thermal conductivity of copper is high, 393 W/m·K [19], and the tube wall is thin.

Nusselt number, Nu , is the dimensionless heat transfer coefficient, and it is defined as

$$Nu = \frac{h d}{k_c} \quad (2.19)$$

Peclet number, Pe , is the product of Reynolds and Prandtl numbers

$$Pe = Re Pr \quad (2.20)$$

and the dimensionless group

$$Gz = Pe \frac{d}{L} \quad (2.21)$$

is called Graetz number, Gz , where L is the total length of one heat exchanger tube.

The working fluid pressure difference, in the primary loop, ΔP_p , caused by the gravitational forces acting on the fluid can be described as

$$\Delta P_p = \int g \rho \, dh \quad (2.22)$$

Assuming that the temperature varies linearly between the measuring points Eq. (2.22) can be simplified as follows:

$$\begin{aligned} \Delta P_p = \frac{g}{2} \{ & -(\rho_1 + \rho_2)H_{12} - (\rho_2 + \rho_3)H_{23} \\ & + (\rho_4 + \rho_1)H_{13} \} \end{aligned} \quad (2.23)$$

where g is the gravitational acceleration and H is the

height difference between temperature measuring points as shown in Fig. 2.3.

The heat exchanger effectiveness, ϵ , is defined [20] as

$$\epsilon = \frac{C_c(t_{co} - t_{ci})}{C_{min}(t_{hi} - t_{ci})} \quad (2.24)$$

and is valid for single phase fluid flow. Since the heat rate capacity of the cold fluid stream, C_c , equals the minimum heat capacity rate, C_{min} , in this study, Eq. (2.24) can be written as

$$\epsilon = \frac{t_{co} - t_{ci}}{t_{hi} - t_{ci}} \quad (2.25)$$

where t_{hi} , t_{ci} and t_{co} are the bulk temperatures of the entering hot fluid, the entering cold fluid and the exiting cold fluid respectively.

The efficiency, η , is in this study based on the second law of thermodynamics and defined as

$$\eta = \frac{A_{cf}}{A_{hf}} \quad (2.26)$$

where A_{cf} is the availability [21,22] of the cold fluid across the heat exchanger and A_{hf} is the maximum obtainable availability for the hot fluid stream in the heat exchanger for the particular system operating condition. The expression for the system efficiency in Eq. (2.27a) below is

valid for thermosyphon systems and is derived from Eq. (2.26) according to [23].

$$\eta = \frac{(m c_p)_{cf} [T_{co} - T_{ci} - T_0 \ln(\frac{T_{co}}{T_{ci}})]}{(m c_p)_{hf} [T_{hi} - T_{ho} - T_0 \ln(\frac{T_{hi}}{T_{ho}})]} \quad (2.27a)$$

where T_0 is the temperature of the reference environment. The system efficiency for forced flow systems are calculated using Eq. (2.27b).

$$\eta = \frac{(m c_p)_{cf} [T_{co} - T_{ci} - T_0 \ln(\frac{T_{co}}{T_{ci}})]}{(m c_p)_{hf} [T_{hi} - T_{ho} - T_0 \ln(\frac{T_{hi}}{T_{ho}})] + W_p} \quad (2.27b)$$

2.6 Results and Discussion for Single-Phase Thermosyphon System

In this section the overall system, evaporator and condenser performances are discussed individually in separate subsections. A summary of the operating characteristics of the thermosyphon is shown in Table 2.4.

2.6.1 Overall system performance

The total heat rate recovered by the system, Q_c , as a function of the temperature difference between the heat source and the heat sink is shown in Fig. 2.4. An apparent

TABLE 2.4: SUMMARY OF OPERATING CHARACTERISTICS
FOR NATURAL FLUID CIRCULATION

VARIABLES	EVAPORATOR	CONDENSER ¹
Air volume flow rate [m^3/s]	0.27-0.72	
Air temperature [$^{\circ}\text{C}$]	75-96	
Liquid mass flow rate [g/s]	3.1-6.6	40
Inlet minus outlet water temp. [K]		4-11
Maximum outlet water temp. [$^{\circ}\text{C}$]		25.5
Heat supply (air) [W]	1050-2500	
Heat recovery [W]		700-1810
Wall heat flux [W/m^2]	560-1360 ²	2260-6000
Heat transfer coefficient [$\text{W}/(\text{m}^2\text{K})$]	28-120 ²	28-65
Overall heat transfer coefficient ΔT_m [$\text{W}/(\text{m}^2\text{K})$]	24-55	160-273
Overall heat transfer coefficient ΔT_m [$\text{W}/(\text{m}^2\text{K})$]	18-38	86-183
Nusselt number	0.3-1.5 ^{2, 3}	
Reynolds number	19-38 ⁴ 200-425 ⁵	3500
Dean number		1200
Graetz number	0.5-1.0	47
Efficiency:	2-6.5% ⁶	
Effectiveness:	6-14% ⁶	

Notes:

- ¹ Cooling water
- ² Working fluid
- ³ Based on AMTD
- ⁴ W.fl. flow (1 evap.tube)
- ⁵ Total w.fl. flow
- ⁶ Overall system

linear relationship is seen between Q_c and $(T_{a,i} - T_{c,i})$. The heat recovery is increased with higher air flow rate (or higher air velocity) through the evaporator. The increased air velocity causes more air disturbance which improves the heat transfer coefficient (discussed later) between the air and the wall of the evaporator panel.

The system efficiency is obtained by regarding the primary loop, including evaporator and condenser, as the system heat exchanger. Hence, the heating air is the hot and the cooling water is the cold fluid stream used in Eq. (2.27). The inlet cooling water temperature is chosen as the reference since it is the lowest temperature in the global system'. The system efficiency results are shown in Figure 2.6 and tabulated in Table 2.5. Figure 2.6 is a graph of system efficiency versus average wall heat flux for the working fluid side of the evaporator. The system efficiency increased with higher wall heat flux. However, the low efficiencies (2 - 6.5%) indicate the need for improved system design. Since the heat exchangers are designed for heat transfer by boiling or condensation, the liquid-phase fluid could cause lower system efficiency than a two-phase thermosyphon system.

The system effectiveness is calculated, Eq. (2.25), by regarding the working fluid loop as one heat exchanger. The heat source represents the hot fluid and the heat sink represents the cold fluid flowing through this assumed heat

'The thermosyphon system and the immediate surroundings.

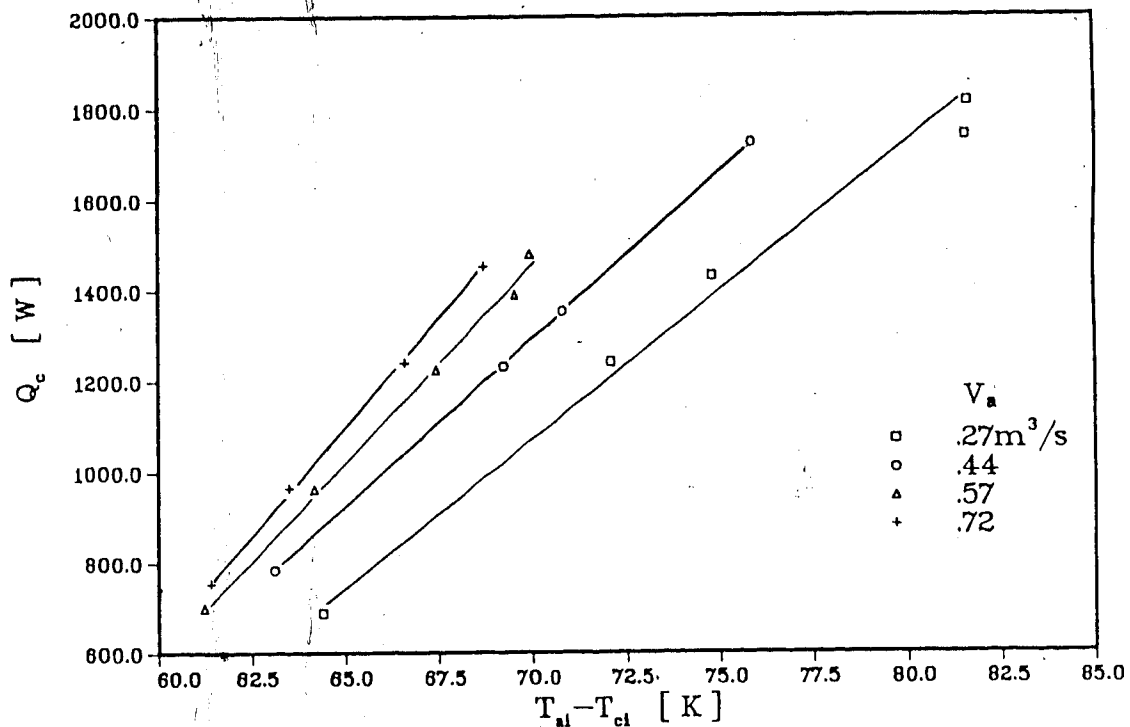


Fig. 2.5 Heat recovered by cooling water vs. inlet air minus inlet cooling water temperature

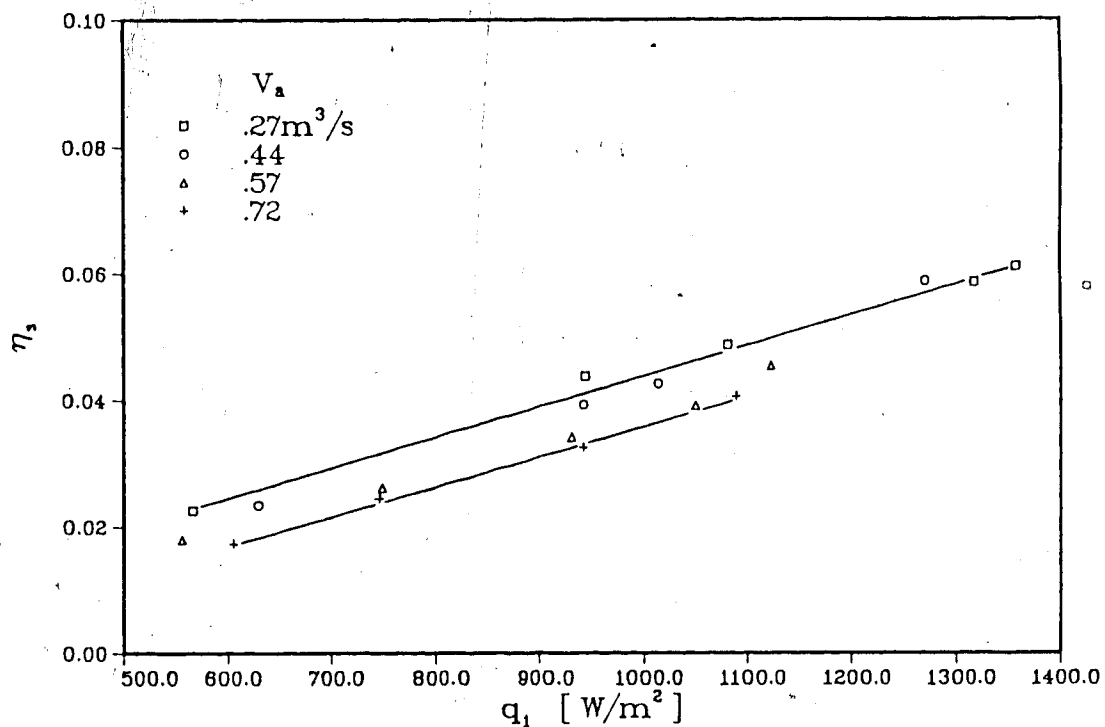


Fig. 2.6 System efficiency vs. average wall heat flux for the working fluid side of the evap.

TABLE 2.5: OVERALL SYSTEM EFFICIENCY AND EFFECTIVENESS

AIR VOLUME FLOW RATE [m ³ /s]	AIR VEL.. THRU EVAP. [m/s]	HEATING AIR TEMPERATURE [°C]	SYSTEM EFFICIENCY [%]	SYSTEM EFFECTIVENESS [%]
0.27	1.8	78.5	2.3	6.3
		85.6	4.4	10.3
		89.6	4.9	11.2
		94.7	5.9	12.8
		96.3	6.1	13.2
0.44	3.0	77.6	2.4	7.3
		83.5	3.9	10.6
		84.7	4.3	11.4
		88.4	5.9	13.6
0.57	3.8	76.0	1.8	6.9
		78.8	2.6	8.9
		81.9	3.4	10.9
		83.8	3.9	12.0
		84.3	4.5	12.7
0.72	4.8	76.1	1.7	7.3
		78.2	2.5	9.1
		81.1	3.3	11.1
		82.2	4.1	12.6

exchanger. System effectiveness, ϵ_s , is shown as a function of Reynolds number, Re_s , in Fig. 2.7. This Reynolds number is based on inside diameter of the main evaporator header shown in Fig. 2.2b, and the thermodynamic properties are based on the recorded inlet working fluid temperature, t_i . Apparently, the effectiveness is dependent on working fluid Reynolds number and appears to be unaffected by different heat source flow rate (0.27 - 0.72 m³/s). However, table 2.5 shows system efficiency and system effectiveness for different air temperatures, velocites and flow rates, and

the the system effectiveness improves with increased air volume flow rate (from 6.3 to 9.1% as the air flow rate, with air at approximately 78°C, is increased from 0.27 to 0.72 m³/s). But the table shows that the system effectiveness is more dependent on the heating air temperature than the heating air flow rate.

Total working fluid mass flux (based on total mass flow rate and inside cross sectional area of the main evaporator header) is linearly related to the density pressure difference of the working fluid in primary loop, $\Delta P\rho$, as shown in Fig. 2.7. The figure shows clearly that the mass flux increased with increasing air flow rate. According to experimental observations, increasing density pressure difference corresponded to increased air temperature.

However, variations of density pressure difference, Eq. 2.23, are caused only by working fluid density changes, which are solely a function of working fluid temperature. Hence, the results in Fig. 2.8 obviate that the mass flux (therefore mass flow rate) must be dependent on another variable as well as the forces caused by density pressure difference. As mentioned earlier, the bouyancy forces do have a contribution to the working fluid driving forces during thermosyphonic flow. It could be the effect of the local bouyancy forces which caused the increased mass flux shown for the higher air flow rates in Fig. 2.8.

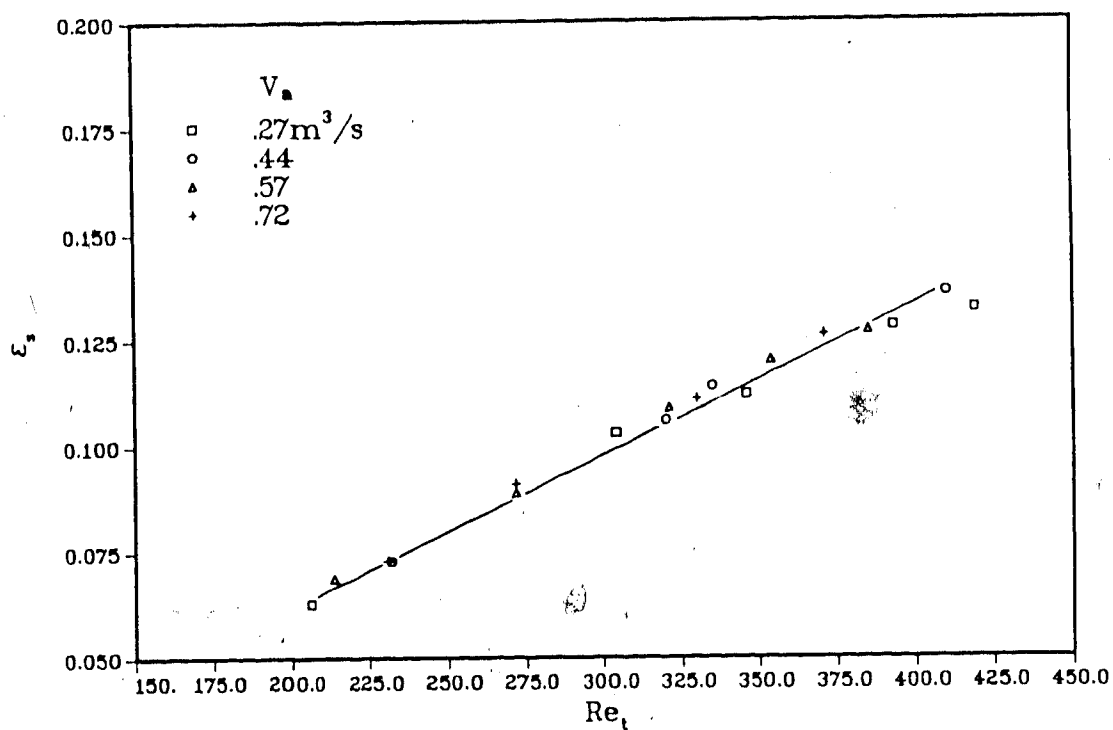


Fig. 2.7 System effectiveness vs. Reynolds number, Re_t .

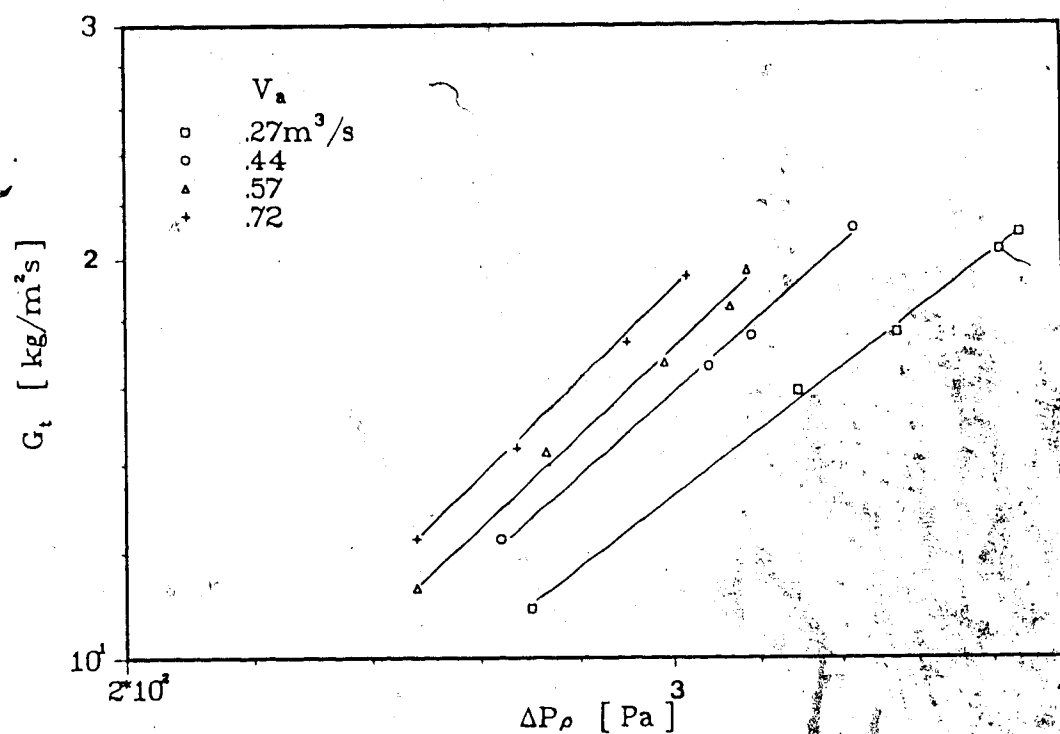


Fig. 2.8 Total working fluid mass flux, G_t , vs. density pressure difference of the working fluid in the primary loop.

2.6.2 Evaporator results

The heat loss from the evaporator to the surroundings increased with increasing heating air temperature and air flow rate. This is shown in both Figs. 2.9 and 2.10. The heat rate released by the heating air in the evaporator is shown higher than the heat rates recovered by the working fluid in the evaporator for corresponding data points in Fig. 2.9. The heat rate lost by the air to the surroundings across the evaporator is shown as a function of both air volume flow rate and air temperature in Fig. 2.10.

The evaporator efficiency is shown as a function of the average working fluid wall heat flux in Fig. 2.11. The higher efficiencies obtained with lower air flow rates are mainly caused by the lower heat losses from the air to the surroundings, as discussed above. The efficiency calculation is based on the surrounding air temperature, T_0 , as datum. The relatively high efficiencies (18 to 35%) compared with the overall system efficiency (1.7 to 6.1%) suggest that the energy losses around the rest of the working fluid loop are responsible in part for the low overall system efficiencies (shown in Fig. 2.6). These losses, tabulated in Table 2.6, may be caused by flow obstructions (i.e. installed measuring instruments or inefficient system design) and heat losses across the connecting tubes and condenser to the surroundings. Heat loss across the tube insulation varies from 21 to 74 W, while the heat loss across the condenser is in the range of 0 to 65 W as seen in Table 2.6. The sum of

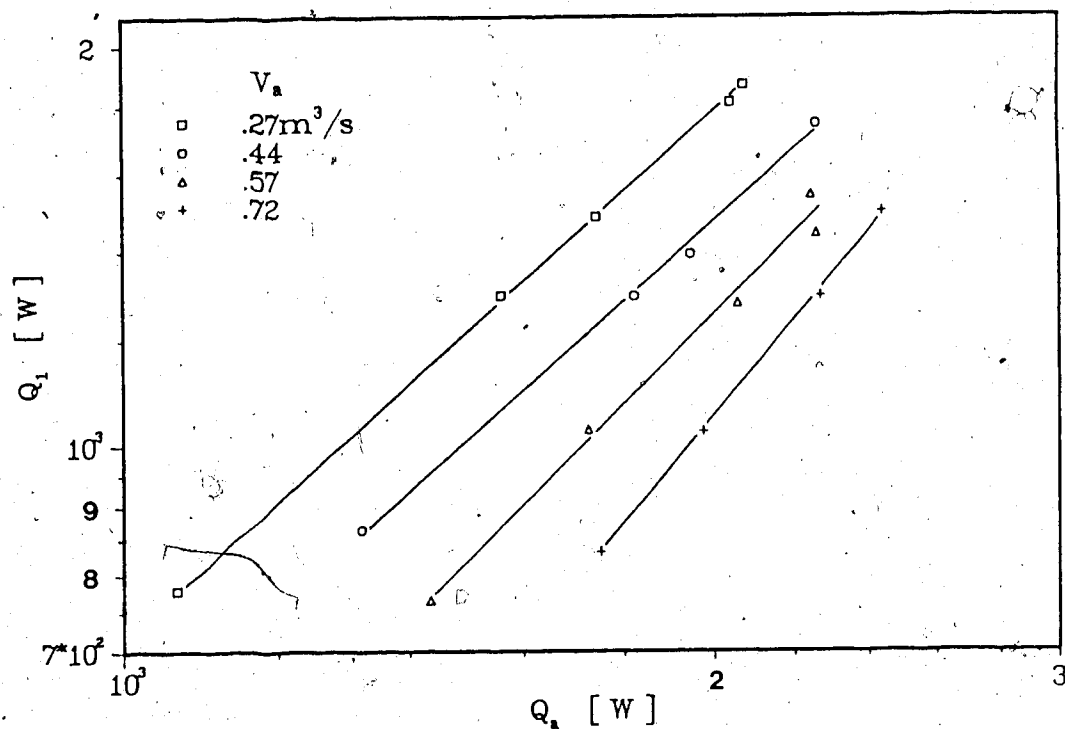


Fig. 2.9. Heat recovered by working fluid in evap. vs. heat released by air in evap.

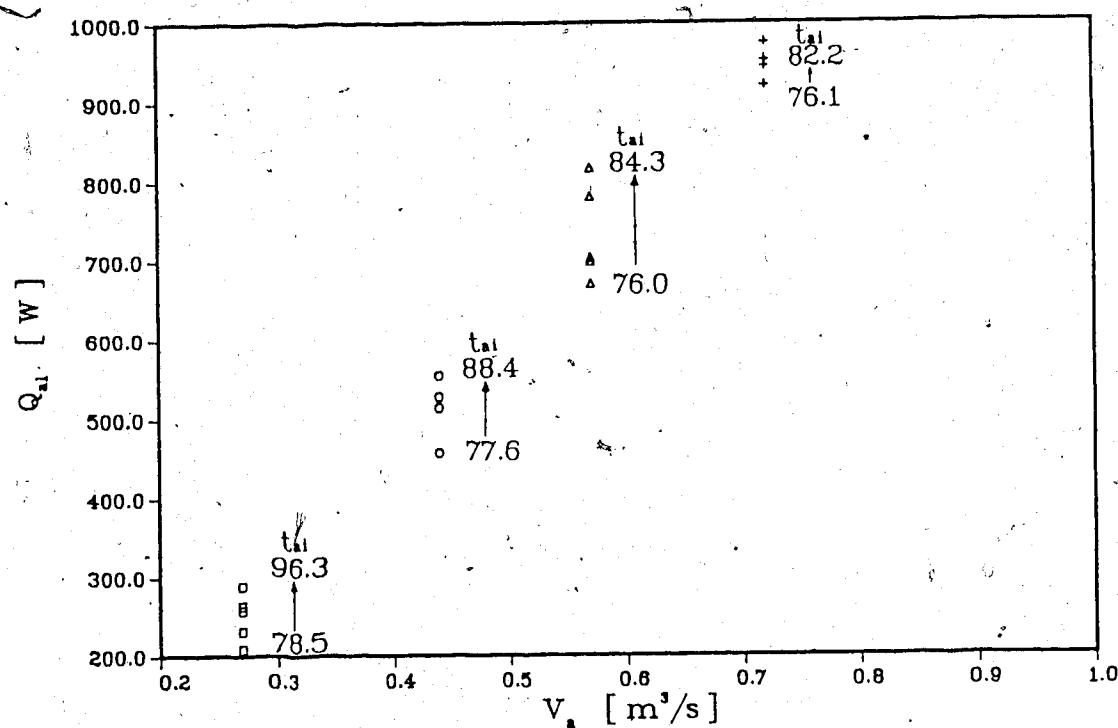


Fig. 2.10 Heat lost by air to surroundings vs. air volume flow rate

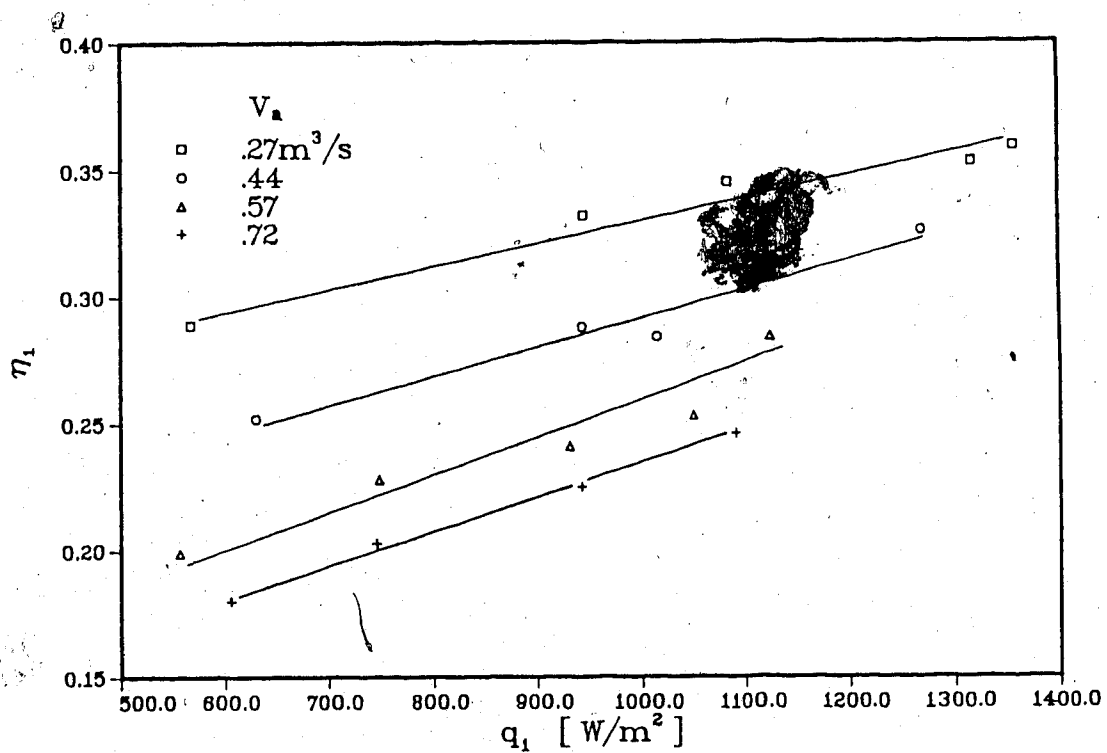


Fig. 2.11 Evaporator efficiency vs. average wall heat flux for the working fluid side of the evap.

TABLE 2.6: HEAT TRANSFER RATES FOR W.FL. AND COOLING WATER
IN
COND. AND HEAT LOSS ACROSS TUBE AND COND. INSULATION

AIR VOL. FLOW RATE	AIR TEMP.	HEAT RELEASED BY W.FL.	HEAT ABSORBED BY WATER	HEAT LOSS ACROSS COND.	HEAT LOSS ACROSS CONNECT. TUBES	TOTAL HEAT LOSS EXCL. EVAP.
[m ³ /s]	[°C]	[W]	[W]	[W]	[W]	[W]
0.27	78.5	754.	689.	65.	26.	91.
	85.6	1248.	1240.	8.	50.	58.
	89.6	1443.	1430.	13.	43.	56.
	94.7	1761.	1739.	22.	50.	72.
	96.3	1810.	1810.	0.	74.	74.
0.44	77.6	844.	785.	59.	21.	80.
	83.5	1259.	1232.	27.	36.	63.
	84.7	1359.	1354.	5.	35.	40.
	88.4	1721.	1721.	0.	25.	25.
0.57	76.0	745.	701.	44.	21.	65.
	78.8	1001.	962.	39.	28.	67.
	81.9	1230.	1224.	6.	50.	56.
	83.8	1389.	1389.	0.	56.	56.
	84.3	1505.	1478.	27.	38.	65.
0.72	76.1	811.	754.	57.	22.	79.
	78.2	999.	965.	34.	26.	60.
	81.1	1261.	1240.	21.	34.	55.
	82.2	1464.	1451.	13.	35.	48.

these two heat losses, 25 - 91 W, normally between 5 - 15% of the heat lost from the air to the surroundings in the evaporator. However, for the lower heat recovery rates, this heat loss gets as high as 45% of the heat lost by the air across the evaporator. This indicates that the heat loss around the primary loop excluding the evaporator is another factor which affects the overall system efficiency. Even though the evaporator efficiency results, η_1 , (18 - 35%) are several times larger than the values obtained for the overall system efficiency, η_s , (1.8 - 6.1%), evaporator efficiencies less than 35% indicates the obvious need for an improved evaporator design for single phase water as a working fluid.

The wall temperature distributions along evaporator tube no. 4 of evaporator panels 1 and 3 (acquired from the same data set) are shown in Table 2.7. The locations of the temperature measuring points along the tube are indicated on the schematic diagram shown in Fig. 2.2b. Some differences are seen between the two wall temperature distributions in Table 2.7. The temperature differences could be caused by an uneven working fluid flow distribution through the evaporator tubes. According to isothermal flow distribution tests which were done with the evaporator without the upper main header, the flow was very unevenly distributed between the four panels. The results from these tests are shown in Appendix III. However, care must be taken when making any assumption about the working fluid flow distribution through

the evaporator based on these isothermal flow distribution tests. These tests were done to an open system, while the experimental system was a closed system. Moreover, the evaporator had no upper header during these flow distribution tests and this might change the distribution through the evaporator significantly. Hence, it has to be implied that the assumed uniform flow rate and average heat transfer distribution across the 32 evaporator tubes (discussed in Section 2.5) are not strictly correct.

Nevertheless, they are the best assumptions which can be made with this particular apparatus and are used for the data analyses.

Heat transfer calculations based on the evaporator wall temperature are using the wall temperatures recorded for tube no. 4 on evaporator panel 3. The tube wall temperature distribution for this evaporator tube is shown for air flow rates 0.27 and 0.72 m³/s in Figs. 2.12 and 2.13 respectively.

The tube wall temperature is higher for lower air temperatures when the distance from the lower evaporator header is less than approximately 900 mm. Above this distance the tube wall temperatures are highest for the highest air temperature as seen in Figs. 2.12 and 2.13. This is a result of the lower air temperatures creating smaller driving forces in the primary loop. Lower working fluid driving force makes the working fluid travel slower through the evaporator tubes. Hence, the tube wall temperatures are

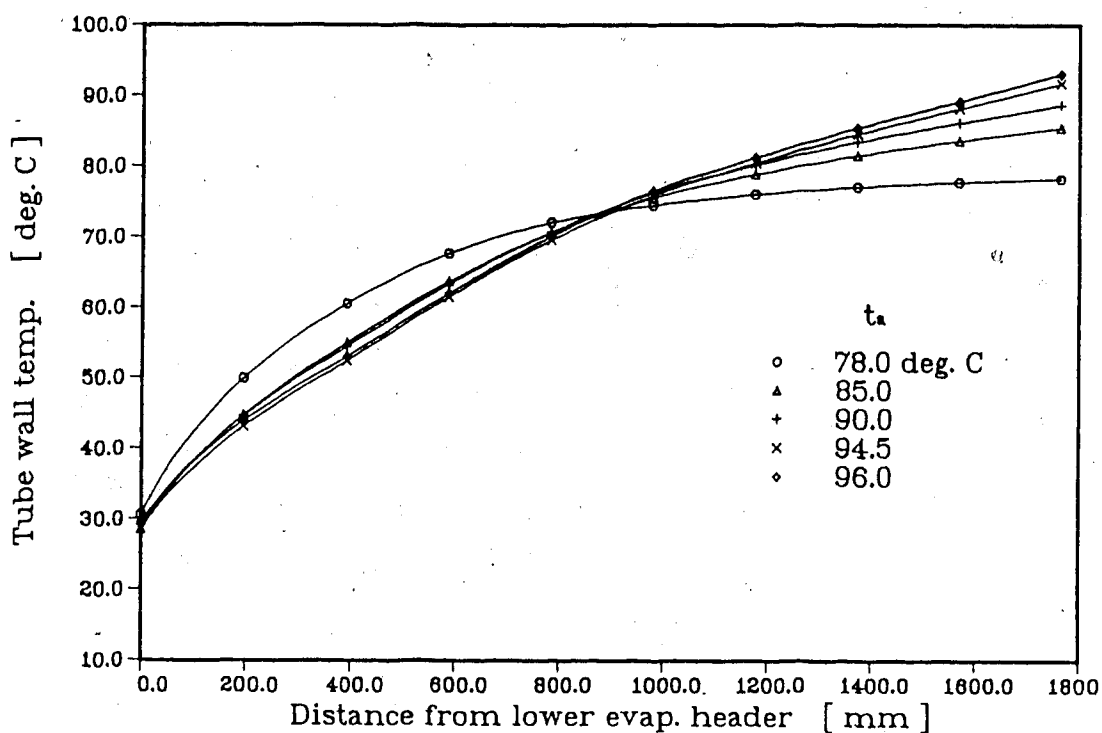


Fig. 2.12 Wall tube temperature distribution for evap. tube no.4 of evap. panel 3 with air volume flow rate 0.27 m³/s

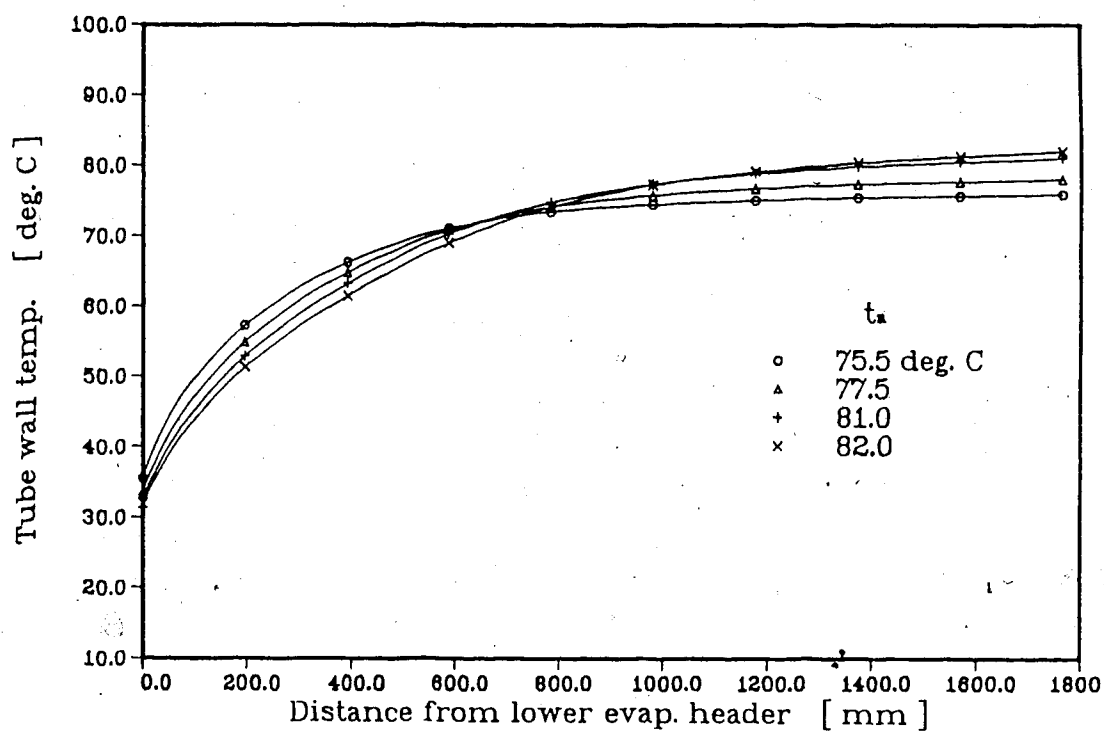


Fig. 2.13 Wall tube temperature distribution for evap. tube no. 4 of evap. panel 3 with air volume flow rate 0.72 m³/s

TABLE 2.7: EVAP. TUBE WALL TEMP. DISTRIBUTION FOR
TUBE No.4 ON EVAPORATOR PANELS 1 AND 3

DISTANCE FROM THERMOCOUPLE TO LOWER EVAP.HEADER [mm]	EVAP.TUBE WALL TEMP. PANEL No.1 [°C]	EVAP.TUBE WALL TEMP. PANEL No.3 [°C]
0	31.7	31.8
196	52.6	52.1
392	63.8	62.5
588	69.7	69.0
784	72.9	72.8
980	74.8	74.7
1176	75.8	75.9
1372	76.5	76.6
1568	76.9	77.1
1764	77.4	77.5

higher for lower air temperatures in the lower section of the evaporator, as there is more time for the air to heat the working fluid and evaporator wall. At higher air flow rates, the evaporator tube wall temperature approaches the air temperature a shorter distance from the lower evaporator header as seen when Figs. 2.12 and 2.13 are compared. This is due to the improved air side heat transfer coefficient at higher air flow rates, this is discussed later in this subsection.

The overall heat transfer coefficient for the evaporator based on the arithmetic mean temperature difference is plotted versus the average wall heat flux for the working fluid side of the evaporator in Fig. 2.14. The overall heat transfer coefficient for the evaporator based

on the logarithmic mean temperature difference is plotted versus the same wall heat flux in Fig. 2.15. The overall heat transfer coefficient based on the logarithmic mean temperature difference gives the higher results of the two heat transfer coefficients. This is because the arithmetic temperature difference is larger than the logarithmic mean temperature difference, which is according to the heat transfer theory [24]. The overall heat transfer coefficients are seen to be strictly dependent on the wall heat flux which is as expected according to Eq. (2.6).

The combined convection and radiation heat transfer coefficient is seen to be highly dependent upon the heat source flow rate in Fig. 2.16. This is expected, because higher air flow rate (air velocity) through the evaporator would cause more air flow disturbance, hence the heat transfer coefficient would increase. For the three highest air flow rates, the heat transfer coefficient are highest when the wall heat flux is lowest as shown in Fig. 2.16. This is because the mean evaporator wall temperature, \bar{T}_w , was relatively constant (66.4 - 69.2°C) over the operating range of the tests, while the mean air temperature changed significantly (73 - 85°C). The difference between these two temperatures was used to calculate the heat transfer coefficient, Eqs. (2.9) and (2.10b). The operating values of the average wall temperature, the average heating air temperature and the difference between these two temperatures are tabulated in Table 2.8. Regardless of the

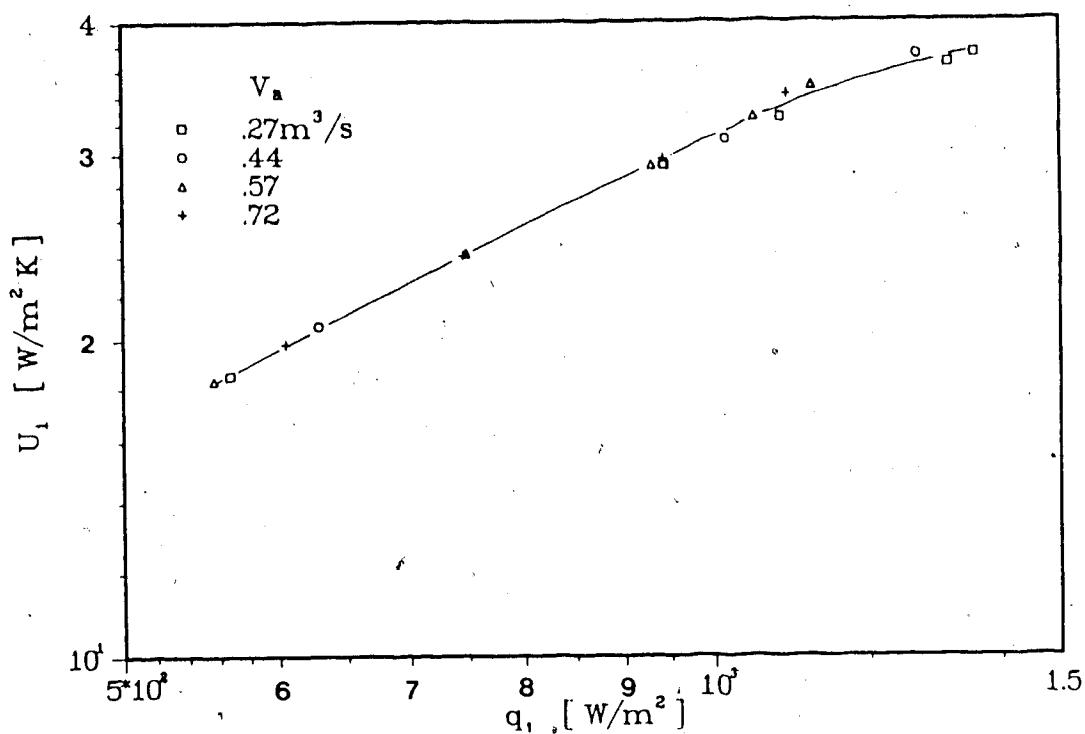


Fig. 2.14 Arithmetic mean overall heat transfer coefficient for evap. vs. average wall heat flux for the working fluid side of the evap.

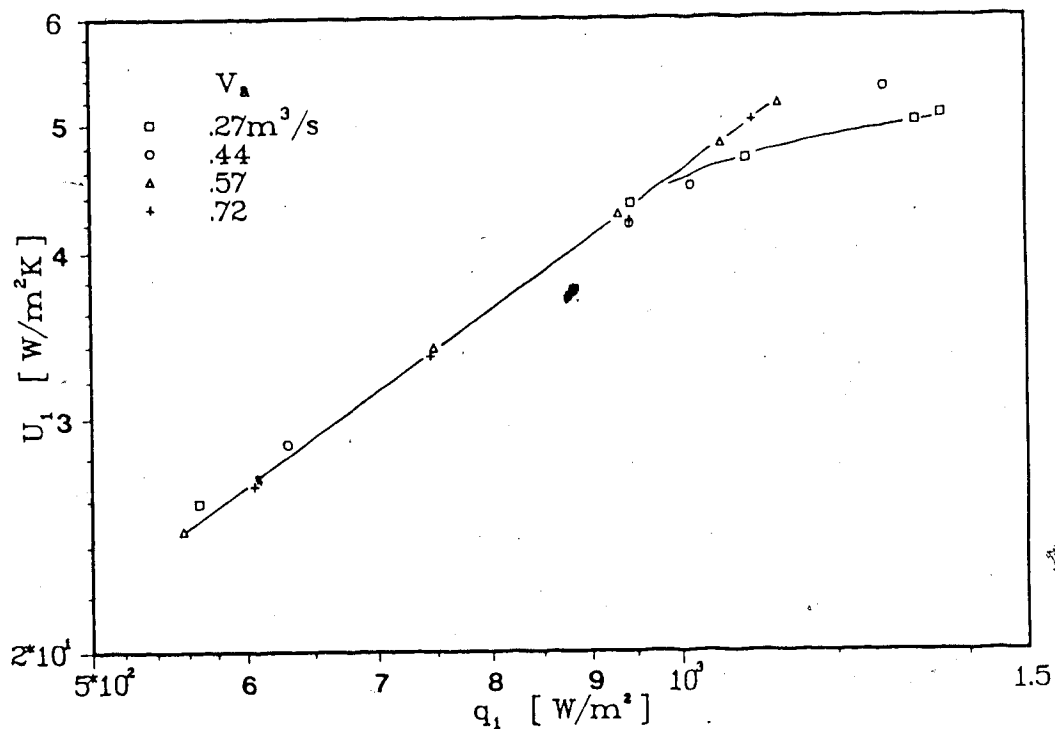


Fig. 2.15 Logarithmic mean overall heat transfer coefficient for evap. vs. average wall heat flux for the working fluid side of the evap.

increasing wall heat flux, the heat transfer coefficient decreased, as seen in Fig. 2.16, because of the relatively higher increasing temperature difference, ΔT_m . However, the differences between the heat transfer coefficient values for the same air flow rate are small (maximum $1.0 \text{ W/(m}^2\text{K)}$)). This air side heat transfer coefficient is calculated based on the outside heat transfer area of the evaporator while the overall heat transfer coefficient is calculated based on the almost six times smaller inside surface area. This causes the air side combined convection and radiation heat transfer coefficient to be smaller than the overall heat transfer coefficient for the evaporator. The radiation heat transfer coefficient shows small, but obvious, increasing values as the difference between the average air and the average wall temperature increases in Fig. 2.17. These increasing heat transfer coefficients are as expected according to Eq. (2.12). The relatively small temperature differences, from 5.6 to 22.5°C as shown in Table 2.8, caused the minimal difference between the lowest, $5.5 \text{ W/m}^2\text{K}$, and the highest radiation heat transfer coefficient, $5.7 \text{ W/m}^2\text{K}$.

The heat transfer coefficient for the working fluid side of the evaporator, h_1 , is shown versus the average wall heat flux for the working fluid side of the evaporator, G_1 , in Fig. 2.18. It is apparent for a given wall heat flux the heat transfer coefficient decreased with increasing air flow rate. This is mainly caused by the fact that the heat loss

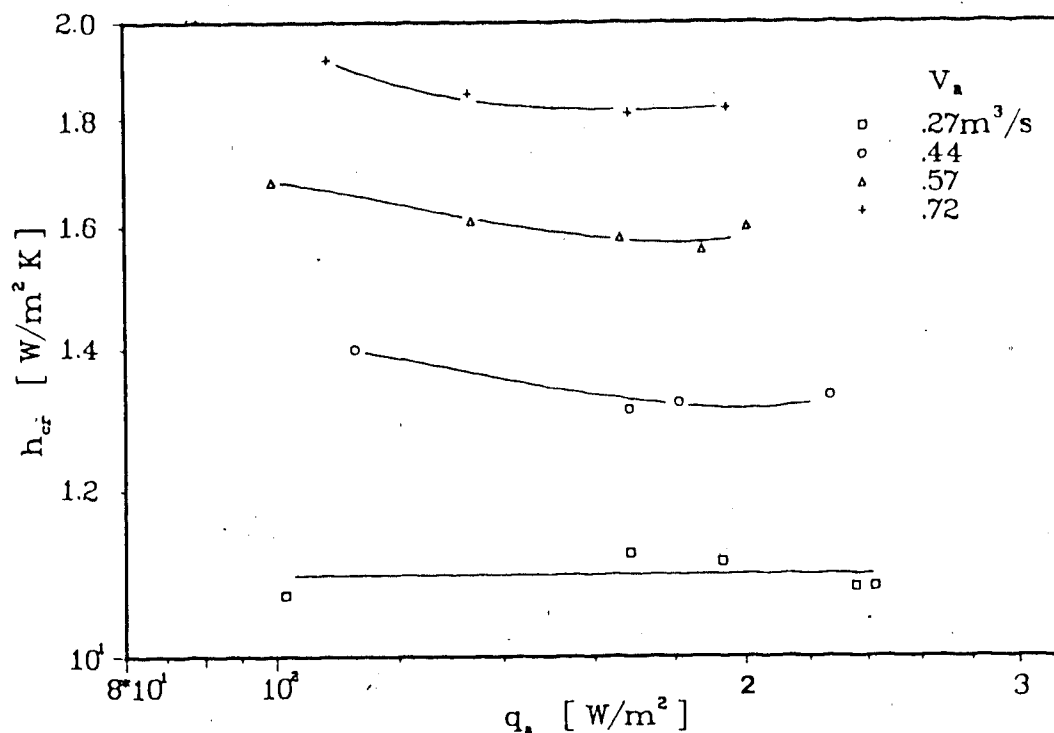


Fig. 2.16 Combined convection and radiation heat transfer coefficient for evap. air side vs. average air side wall heat flux

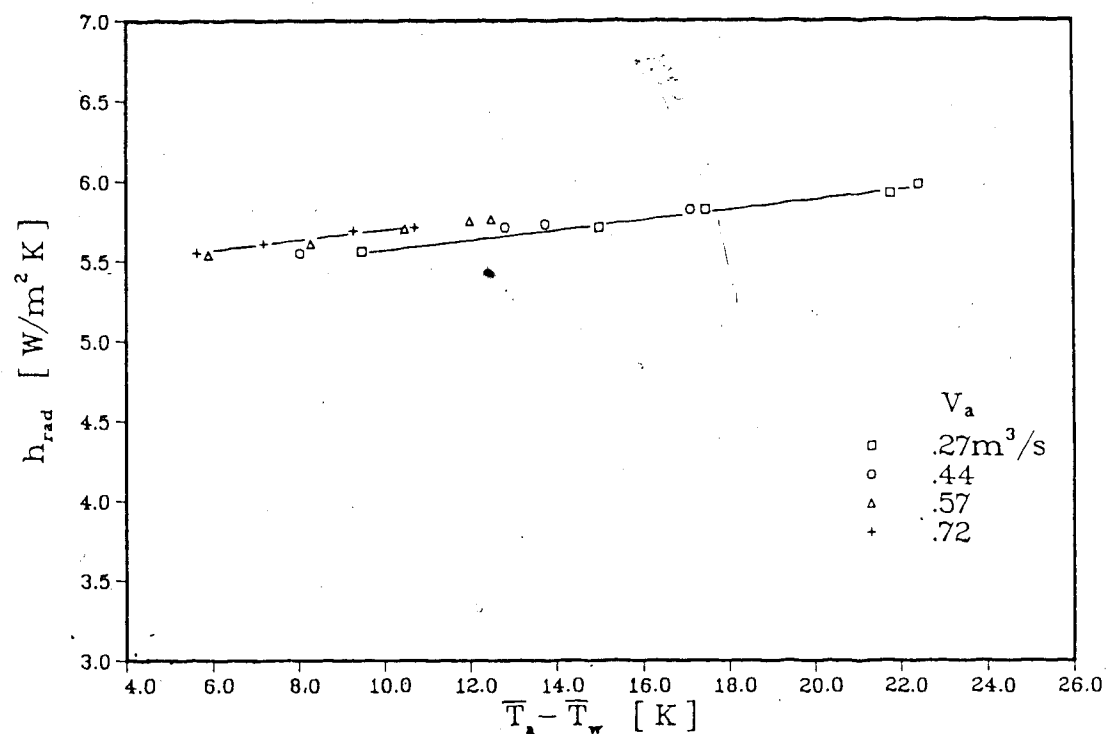


Fig. 2.17 Radiation heat transfer coefficient for evap. air side vs. difference between mean air temp. and mean wall temp.

from the heating air to the surroundings increases with increasing air flow rate. This is discussed with Fig. 2.10 earlier in this section.

The relationship between the same heat transfer coefficient, h_1 , and the average working fluid mass flux for one evaporator tube, G_1 , is shown in Fig. 2.19. As the heating air flow rate increased, the same heat transfer coefficient resulted in increased mass flux.

The evaporator and the condenser wall heat fluxes caused the temperature differences around the working fluid loop. These temperature differences created the natural working fluid circulation due to the action of the buoyancy and gravitational forces on the working fluid. The average working fluid mass flux based on the inside cross sectional area of one evaporator tube is plotted as a function of the average evaporator working fluid wall heat flux in Fig. 2.19. It is clearly seen how the mass flux is functionally dependant on the wall heat flux.

Nusselt number for the working fluid in the evaporator is plotted versus the evaporator tube Reynolds number, Re_1 , in Fig. 2.20. The Reynolds number is based on the mass flow rate through one evaporator tube. Nusselt number results observed in the figure are surprisingly low. This is believed to be caused by the working fluid flow being unevenly distributed to the 32 evaporator tubes, as mentioned in Appendix III and in the discussion referring to Table 2.7. Hence, the heat transferred from the air to the

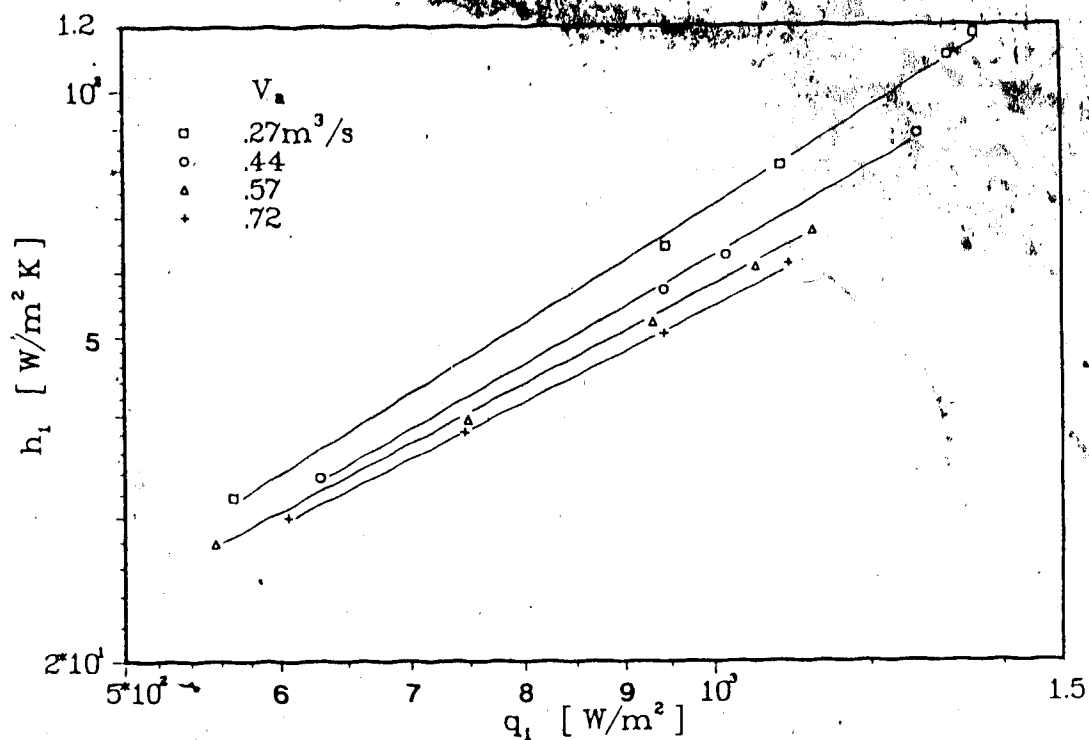


Fig. 2.18 Working fluid heat transfer coefficient vs. average wall heat flux for working fluid side of evap.

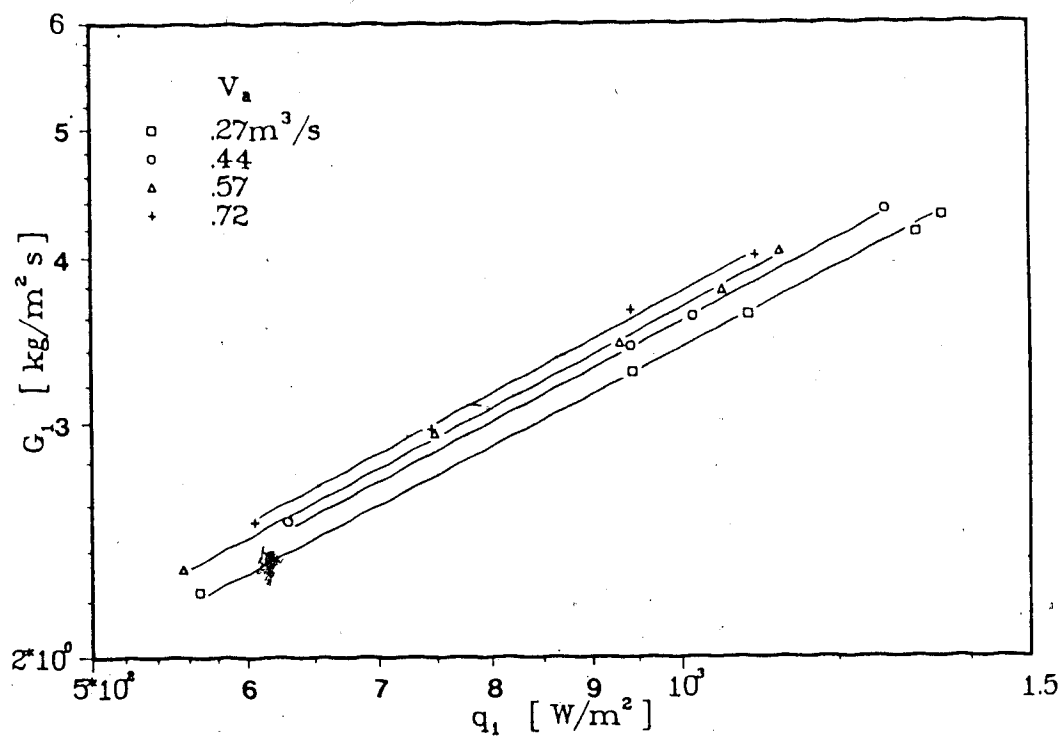


Fig. 2.19 Inlet working fluid mass flux for one evap. tube vs. average wall heat flux for working fluid side of evap.

TABLE 2.8: AVERAGE RECORDED AIR AND EVAP. TUBE WALL TEMPS.
AND THE DIFFERENCE BETWEEN THESE TWO TEMPS.

V_a [m ³ /s]	$t_{a,i}$ [°C]	\bar{t}_a [°C]	\bar{t}_w [°C]	$\bar{t}_a - \bar{t}_w$ [°C]
0.27	78.5	76.0	66.4	9.6
	85.6	81.8	66.8	15.0
	89.6	85.2	67.7	17.5
	94.7	89.4	67.6	21.8
	96.3	90.9	68.4	22.5
0.44	77.6	75.0	67.0	8.0
	83.5	80.6	67.8	12.8
	84.7	81.6	67.9	13.7
	88.4	84.9	67.9	17.0
0.57	76.0	73.6	67.7	5.9
	78.8	76.4	68.1	8.3
	81.9	79.2	68.7	10.5
	83.8	81.2	69.2	12.0
	84.3	81.7	69.2	12.5
0.72	76.1	73.7	68.1	5.6
	78.2	75.7	68.5	7.2
	81.1	78.5	69.2	9.3
	82.2	79.6	68.9	10.7

working fluid is incorrectly assumed to be averaged across the evaporator. Nevertheless, this is the best assumption which can be made under the circumstances, as mentioned earlier. The low working fluid flow rates ($Re_1 = 19 - 38$) could be another factor causing the low Nusselt number results. Experimental observations have shown that Nusselt number has a lower limit of 4.36 when the heating source wall heat flux is constant, and 3.66 when the heat transfer surface has constant wall temperature [25]. The experiments conducted for this work, were conducted with neither

constant wall heat flux nor constant wall temperature condition. However, McAdams [26] has showed

$$Nu = \frac{2}{\pi} Gz \quad (2.28)$$

as a limiting empirical value applicable to forced flow and natural convection through vertical circular tubes. The experimental values are comparable to this limit, as shown in Fig. 2.21, where Nusselt number is plotted versus the inverse Graetz number. Graetz number is based on one evaporator tube and its inside diameter. The relatively high inverse Graetz number [27], seen in Fig. 2.21, is due to the extremely low Reynolds numbers (19 - 38), observed in Fig. 2.20, and the large L/d-ratio shown in Table 2.1.

2.6.3 Condenser results

The heat losses from the working fluid to the surroundings across the condenser did never exceeded 65 W as shown in Table 2.6. Cooling water heat recovery rates larger than 1.0 kW showed less than 2% of the heat rate recovered by the cooling water was lost across the condenser, while the heat loss increased to 9.5% of heat recovery when this recovery rate was less than 1.0 kW. It is uncertain why the heat losses were higher (44 - 65 W) for heat recovery rates below 1.0 kW than the heat losses (0 - 39 W) resulted from heat recovery rates above 1.0 kW. However, the low working fluid flow rates encountered with these recovery rates could be one reason. The slower travelling fluid allows more time

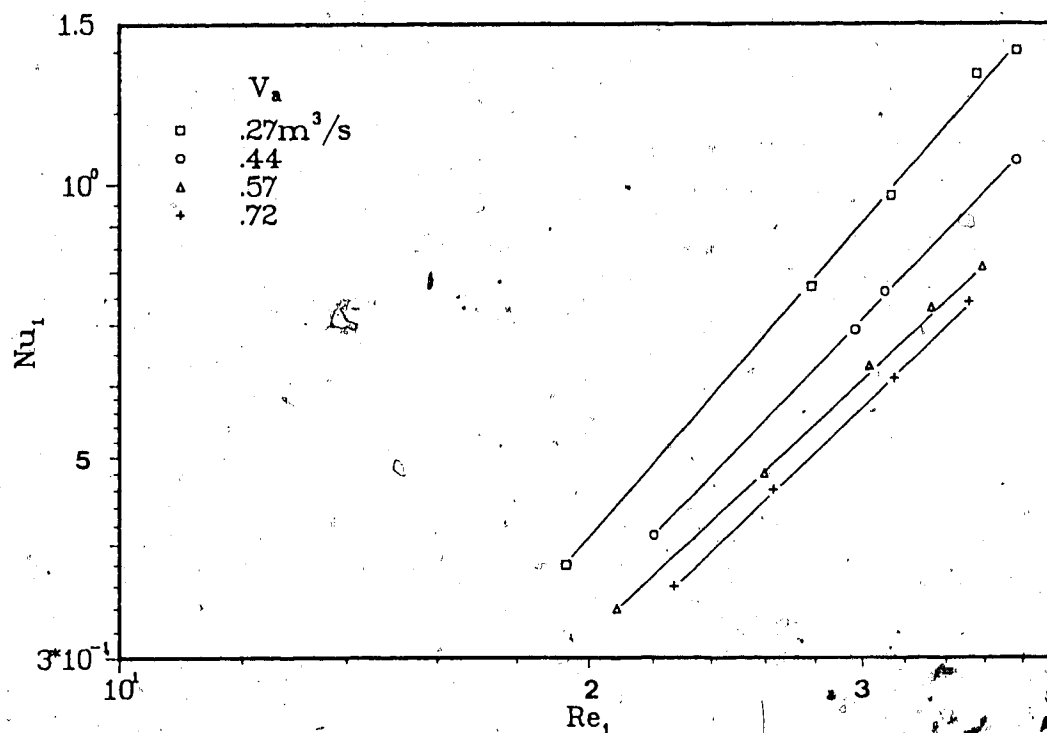


Fig. 2.20 Nusselt number for evap. working fluid side vs. Reynolds number for one evap. tube

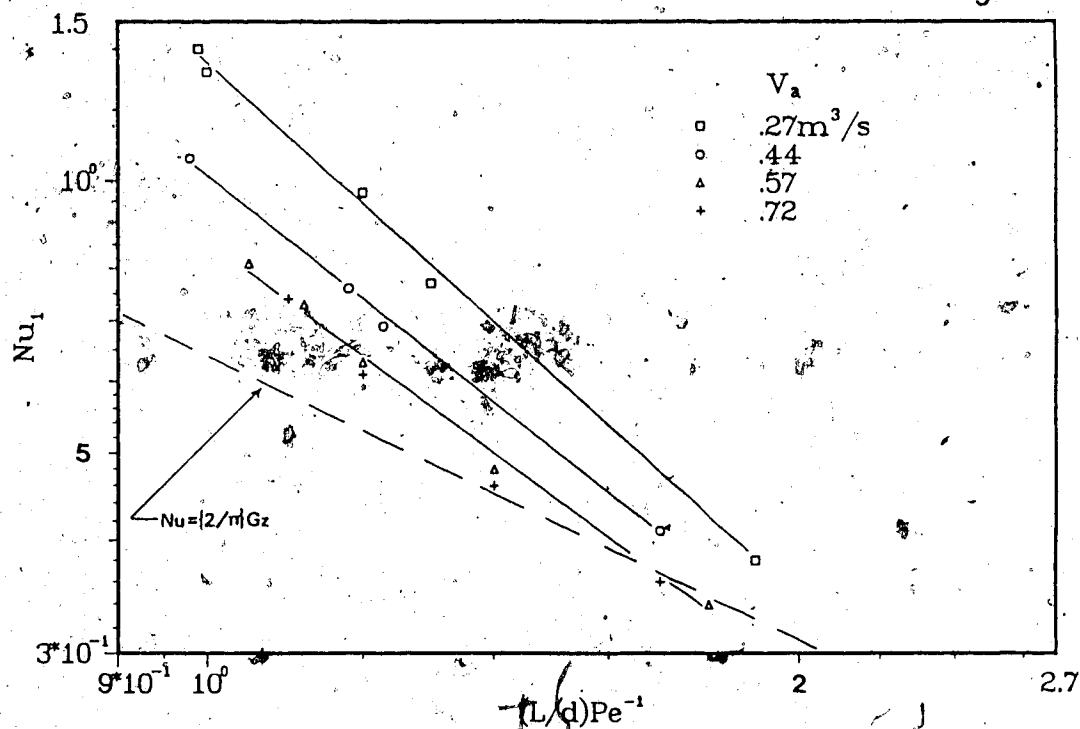


Fig. 2.21 Nusselt number for evap. working fluid side vs. inverse Graetz number

for heat loss from the working fluid to the surroundings. As well, the low fluid velocities might not allow complete working fluid mixing after the wire meshes, hence, the measured temperature would not be indicative of the true bulk temperature.

The relationship between the working fluid heat recovery rate in the evaporator and the cooling water heat recovery rate in the condenser is shown in Fig. 2.22. The linear relationship indicates basically constant heat loss from the thermosyphon loop to the surroundings. This heat loss, shown in Table 2.6, was always between 25 and 91 W (1.5 - 13% of the cooling water heat recovery rate), and normally, it was between 40 and 80 W (3 - 10% of the cooling water heat recovery rate).

The overall heat transfer coefficient for the condenser is based on the arithmetic mean temperature difference and inside surface area of the condenser coil. This overall heat transfer coefficient is plotted versus the wall heat flux for the cooling water side of the condenser in Fig. 2.23.

The apparent functional relationship between the overall heat transfer coefficient and the wall heat flux is as expected according to the definition of the overall heat transfer coefficient based on the arithmetic temperature difference, Eqs. (2.6) and (2.8).

The overall heat transfer coefficient of the condenser based on the arithmetic temperature difference and the working fluid mass flow rate through the condenser are shown

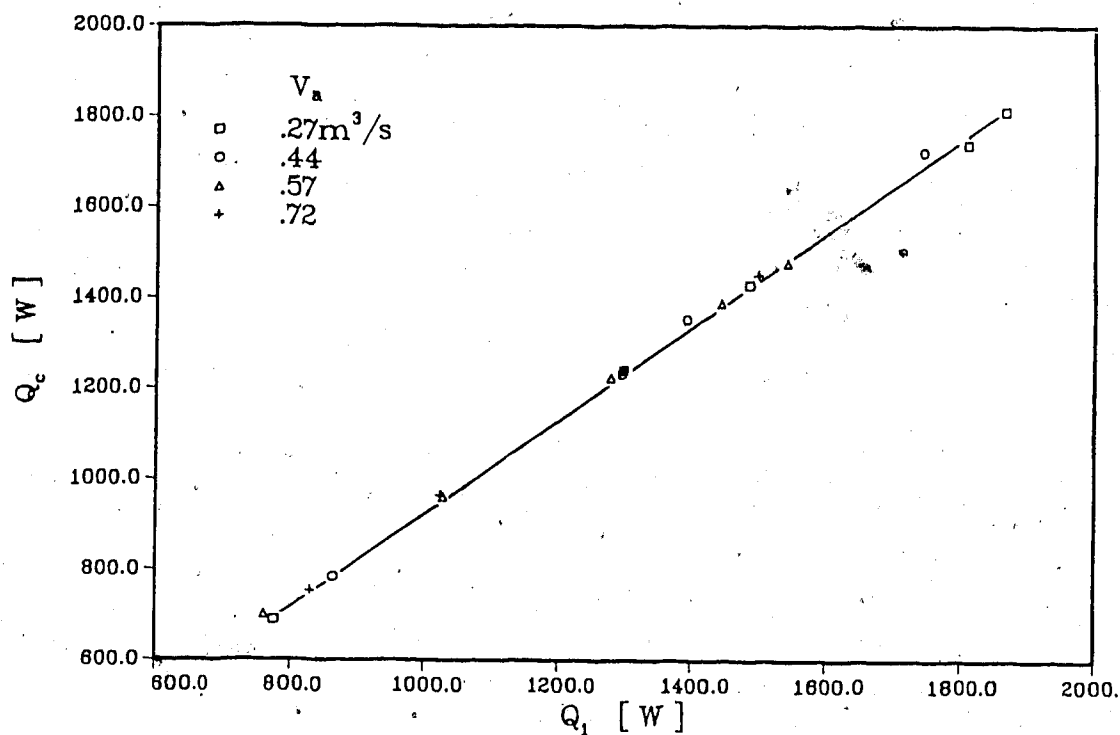


Fig. 2.22 Heat recovered by cooling water vs. heat recovered by working fluid in evap.

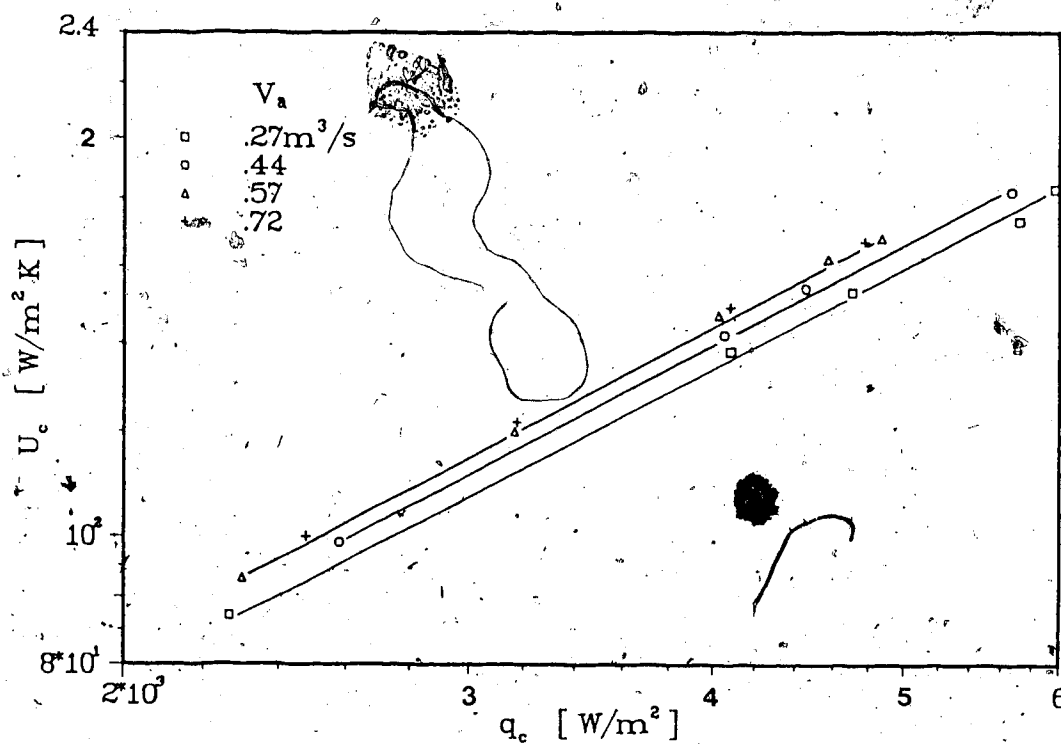


Fig. 2.23 Condenser overall heat transfer coefficient vs. wall heat flux for cooling water side of cond.

as axes for the graph in Fig. 2.24.

The estimated outside heat transfer coefficient of the condenser coil, Eq. (2.18), is shown versus the working fluid mass flow rate through the condenser in Fig. 2.25. The results for the overall and the outside heat transfer coefficients of the condenser show a similar relationship with the working fluid mass flow rate through the condenser, as seen in Figs. 2.24 and 2.25. This is logical when knowing that the calculated inside heat transfer coefficient of the coil is high relative to the overall heat transfer coefficient, as shown in Table 2.9 which tabulates the overall, the inside and the outside heat transfer coefficients for the condenser. The inside, cooling water side, heat transfer coefficient for the condenser is much more than an order of magnitude higher than the overall heat transfer coefficient of the condenser. The resistance to heat transfer through the condenser tube wall is assumed negligible (as discussed in Section 2.5). Therefore, the low overall heat transfer coefficient which were calculated from the test data has to be caused by low values for the outside heat transfer coefficient of the condenser coil. The outside heat transfer coefficient for the coil is seen to be of similar magnitude as the the overall heat transfer coefficient when the results in Figs. 2.24 and 2.25 are compared. The overall heat transfer coefficient is based on the inside surface area which is three times smaller than the outside surface area; hence, the overall heat transfer

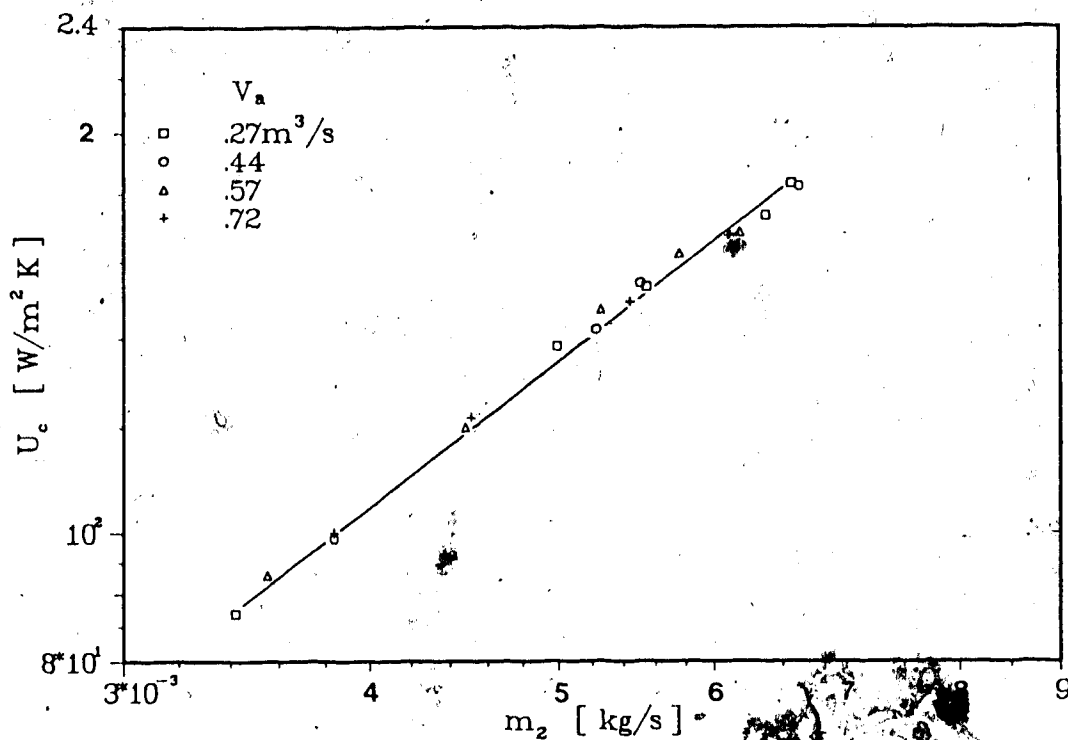


Fig. 2.24 Condenser overall heat transfer coefficient vs. working fluid mass flow rate through cond.

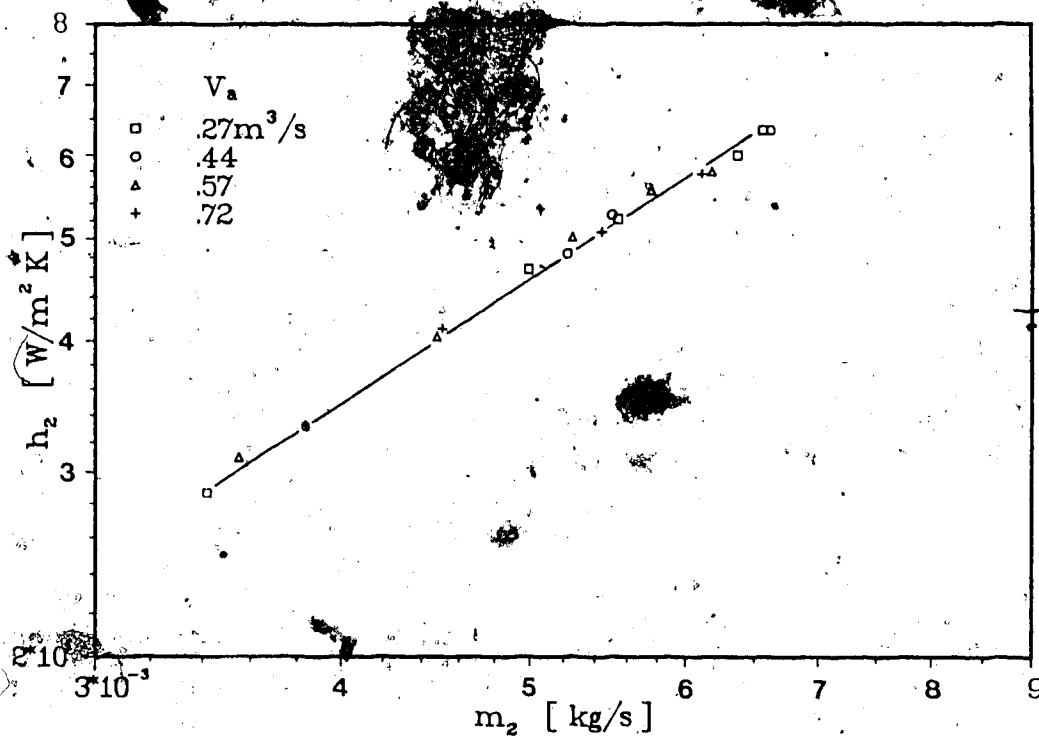


Fig. 2.25 Outside heat transfer coefficient of cond. coil vs. working fluid mass flow rate through cond.

TABLE 2.9: OVERALL, INSIDE AND OUTSIDE HEAT TRANSFER COEFFICIENTS FOR THE CONDENSER

V_a [m ³ /s]	$t_{a,i}$ [°C]	U_c [W/(m ² K)]	h_c [W/(m ² K)]	h_2 [W/(m ² K)]
0.27	78.5	87.	2310	29.
	85.6	138.	2260	47.
	89.6	153.	2310	52.
	94.7	173.	2230	60.
	96.3	183.	2270	63.
0.44	77.6	99.	2310	33.
	83.5	142.	2280	48.
	84.7	154.	2270	53.
	88.4	182.	2220	63.
0.57	76.0	99.	2290	31.
	78.8	120.	2300	40.
	81.9	147.	2270	50.
	83.8	162.	2270	56.
	84.3	168.	2260	58.
0.72	76.1	100.	2290	33.
	78.2	122.	2280	41.
	81.1	149.	2280	51.
	82.2	167.	2240	58.

coefficient is larger than the outside heat transfer coefficient.

2.7 Results and Discussions for Forced Circulation Flow

The experiments were conducted using the same heating air flow rates (0.27 - 0.72 m³/s) as used for the thermosyphon tests discussed in the previous Section 2.6. However, to limit the number of displayed figures and to avoid overcrowded figures, mainly the results obtained with air flow rate 0.44 m³/s are shown in this section. Short

comments are occasionally made where different heat source flow rates alter the results significantly. Only air volume flow rate, $0.44 \text{ m}^3/\text{s}$, is being analysed during two-phase thermosyphon tests, which is the reason for discussing the particular flow rate in this section.

A summary of the operating characteristics for the forced working fluid circulation tests are shown in Table 2.10.

2.7.1 Overall system performance

The inlet cooling water temperature, $t_{c,i}$, is kept nearly constant ($13 \pm 0.5^\circ\text{C}$) for all these tests. Therefore, the difference between the inlet air temperature, $t_{a,i}$, and the inlet cooling water temperature, $t_{c,i}$, seen in Fig. 2.26, is basically caused by the increase of air temperature, which is increased from 40 to 70°C in increments of 10°C . This temperature difference is plotted as abscissa in the figure where the heat rate recovered by the cooling water is the ordinate. Increased air temperature increased as expected the heat recovery rate since more energy was transferred with the air at higher temperatures. An increase of the air flow rate from 0.27 to $0.72 \text{ m}^3/\text{s}$ increased the heat recovery rate more than 100% for all four air temperatures. This is caused by more air disturbance through the evaporator, hence an increased heat transfer coefficient from the air to the evaporator heat transfer surface, as discussed in Section 2.6 for Fig. 2.16.

TABLE 2.10: SUMMARY OF OPERATING CHARACTERISTICS
FOR FORCED FLUID CIRCULATION

VARIABLES	EVAPORATOR	CONDENSER ¹
Air volume flow rate [m ³ /s]	0.27-0.72	
Air temperature [°C]	40-70	
Liquid mass flow rate [g/s]	4.5-20.0	40
Inlet minus outlet water temp. [K]		2-14
Maximum outlet water temp. [°C]		27.2
Heat supply (air) [W]	500-2600	
Heat recovery [W]		400-2400
Wall heat flux [W/m ²]	240-1700 ²	1300-7440
Heat transfer coefficient [W/(m ² K)]	40-500 ²	36-180
Overall heat transfer coefficient [W/(m ² K)]	24-63 ³	110-440
Nusselt number	0.5-6.0 ^{2,3}	
Reynolds number	23-120 ⁴ 300-1500 ⁵	3500
Dean number		1200
Gräetz number	0.4-2.7	47
Efficiency:	2-11% ⁴	
Effectiveness:	8-25% ⁴	

Notes:

- ¹ Cooling water
- ² Working fluid
- ³ Based on AMTD
- ⁴ W.fl. flow (1 evap.tube)
- ⁵ Total w.fl. flow
- ⁶ Overall system

The system efficiency is plotted versus total working fluid Reynolds number, Re , in Figure 2.27. The efficiency increases more than three times as Reynolds number is increased from approximately 300 to approximately 1400. However, a maximum system efficiency of 11% is not satisfactory, and the need for different working fluid or system design is confirmed also for forced fluid circulation tests. Higher air temperatures improved the system efficiency as seen in Fig. 2.27. For the same working fluid flow rates 3 to 6.5 g/s the system efficiency has decreased (2 - 5%) for the forced flow conditions compared with the thermosyphon results (2 - 6%) shown in Fig. 2.5 for the same working fluid flow rate range. This is not surprising since the heating temperatures are lower for the forced circulation tests. The system effectiveness is plotted versus the same Reynolds number in Fig. 2.28, and the heating air temperature does not have any apparent effect on the system effectiveness.

The effectiveness (8 - 14%) values are the same as experienced with the natural circulation tests (8 - 14.5% shown in Fig. 2.6) for the same working fluid flow range, Reynolds number between 250 and 450. Hence, it is obvious that the forced circulation system does not perform any more effectively than the natural flow circulation. It is purely the ability to obtain higher working fluid flow rates with forced circulation tests that causes the increased system performance compared to natural circulation tests.

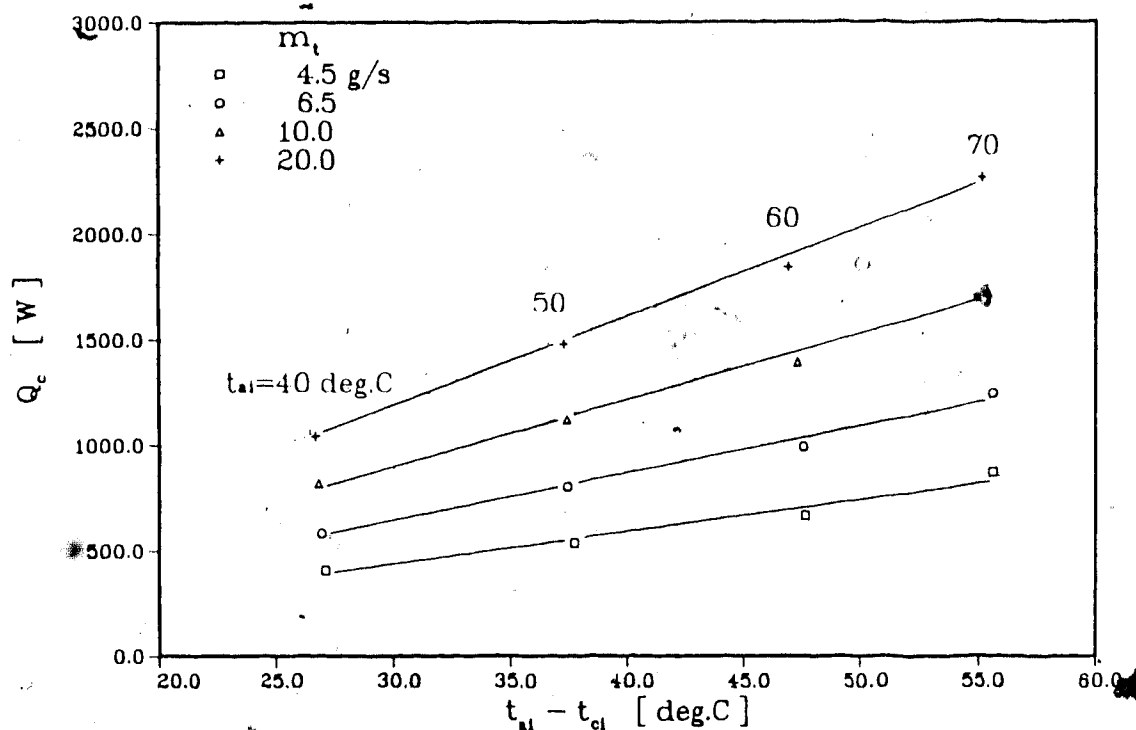


Fig. 2.26 Heat recovered by cooling water vs. inlet air temperature minus inlet cooling water temperature

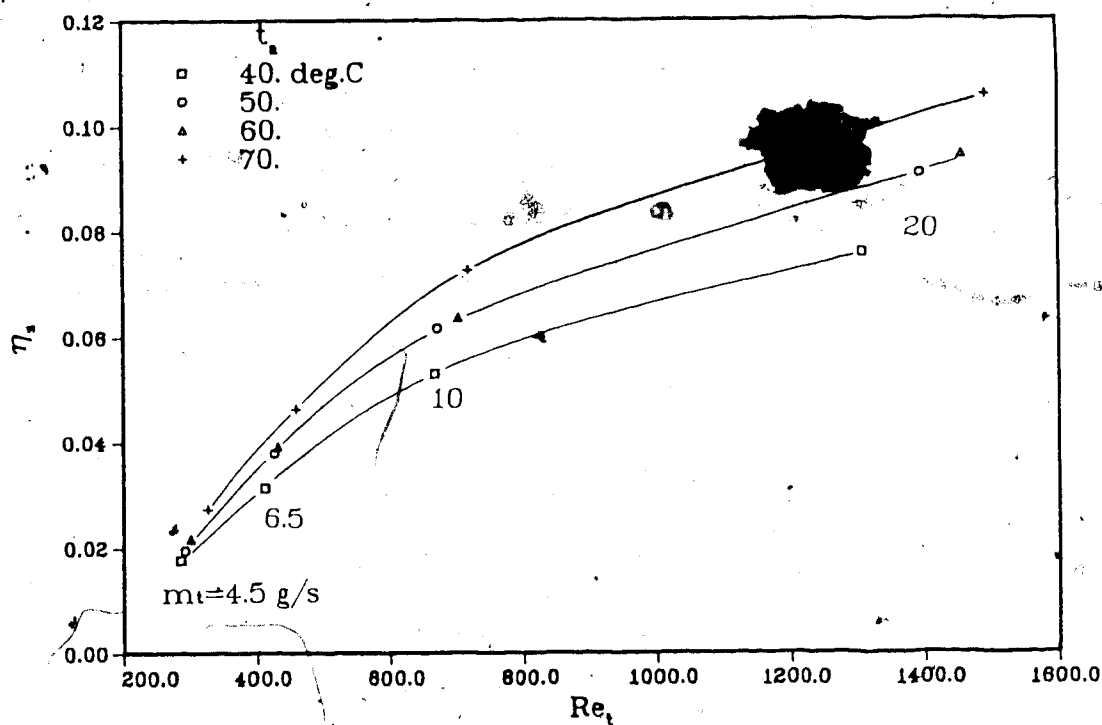


Fig. 2.27 System efficiency vs. Reynolds number based on total working fluid flow rate

2.7.2 Evaporator results

The evaporator efficiency is plotted versus the working fluid Reynolds number in Fig. 2.29. Reynolds number is based on the assumed working fluid flow rate through one evaporator plate, the inside evaporator tube diameter and the assumed working fluid temperature at the tube entrance. The decreasing efficiency observed for constant air temperature as Reynolds number is increased, is a result of the controlled air temperature. For a particular air temperature, the system recovers a certain optimum heat rate before the system efficiency begins to decrease. The Reynolds numbers which resulted in this optimum heat transfer is 40 for $t_{a,i}=50^{\circ}\text{C}$ and approximately 60 for both $t_{a,i}=60^{\circ}\text{C}$ and $t_{a,i}=70^{\circ}\text{C}$. The optimum Reynolds number cannot be determined from Fig. 2.29, since this value appears to be below the lowest Reynolds number value of 23.

Figs. 2.30 - 2.33 show the wall temperature distribution along evaporator tube no. 4 of panel 3 for air flow rate $0.44 \text{ m}^3/\text{s}$. Fig. 2.30 shows the wall temperature distributions as a function of all four working fluid flow rates and $t_{a,i}=40^{\circ}\text{C}$. The same parameters are studied in Fig. 2.31, but for $t_{a,i}=60^{\circ}\text{C}$. The wall temperature approaches the heat source temperature at a distance farther away from the evaporator header the higher the working fluid mass flow rate. For the highest working fluid flow rate (20 g/s), there are several degrees difference between the highest wall temperature and the heating air temperature.

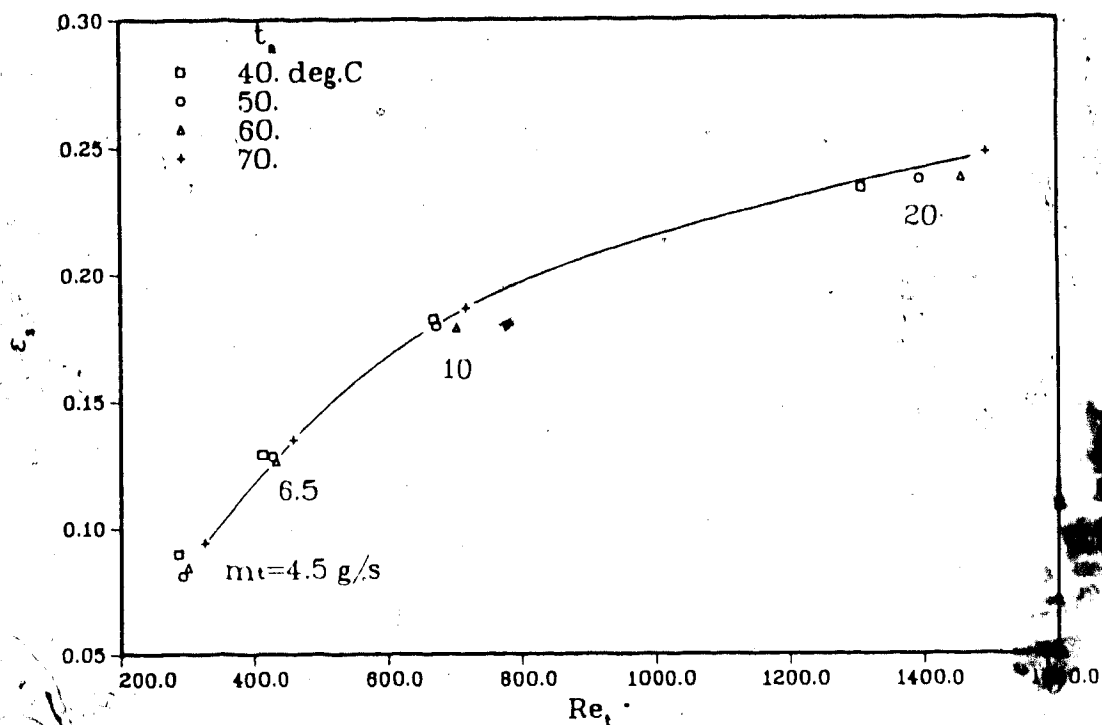


Fig. 2.28 System effectiveness vs. Reynolds number based on the total working fluid mass flow rate

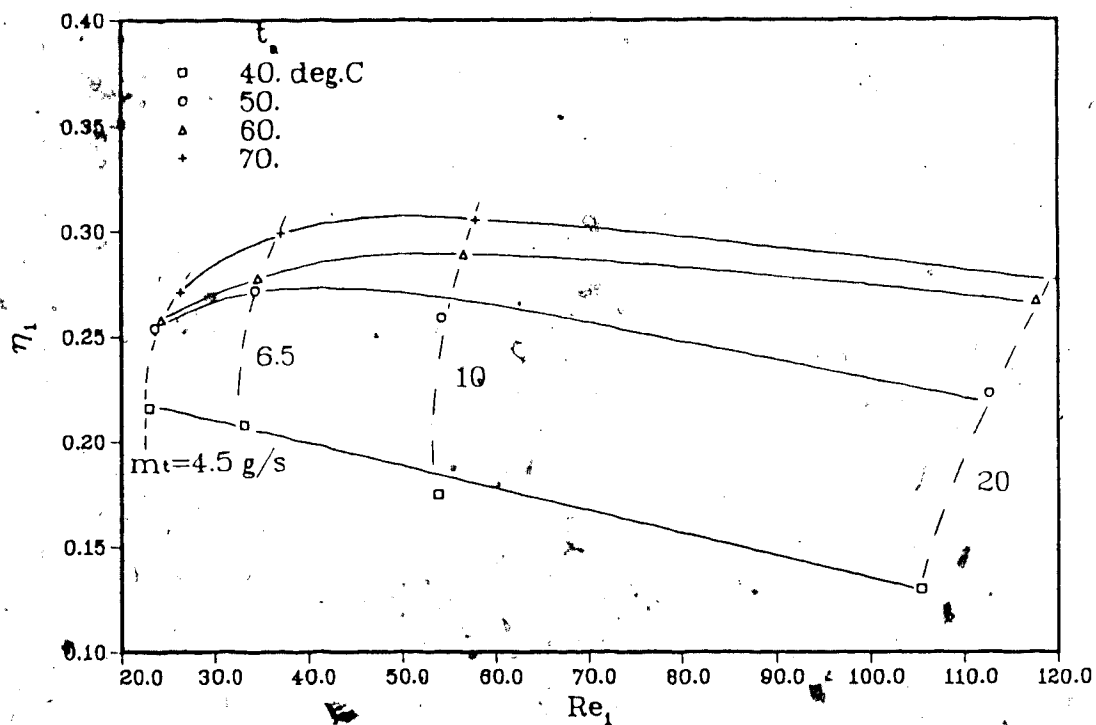


Fig. 2.29 Evap. efficiency vs. Reynolds number based on inlet flow condition for one evap. tube

Fig. 2.32 shows the same wall temperature distribution as a function of the heating air temperatures at constant (4.5 g/s) working fluid flow rate. Similar conditions are revealed in Fig. 2.33, but for higher working fluid flow rate (10.0 g/s). It is seen from these two figures that the maximum wall temperature is reached a shorter distance from the lower evaporator header the lower the heating air temperature.

Average wall heat flux for the working fluid side of the evaporator versus working fluid mass flux, G_1 , for one evaporator tube is plotted in Fig. 2.34. Increased working fluid mass flow and increased heating air temperature both resulted in increased wall heat flux as shown in the figure. Hence, the heat transfer is controlled by heating source temperature and working fluid mass flow rate when the heating source flow rate is constant.

The heat transfer coefficient for the working fluid side of the evaporator is plotted versus working fluid mass flux for the inlet of one evaporator tube in Figs. 2.35 and 2.36. Fig. 2.35 shows results from the tests performed with air flow rate 0.44 m³/s, while the data in Fig. 2.36 resulted from tests conducted with 0.72 m³/s as the air volume flow rate. Different isotherms resulted in minimal changes, normally less than 5%, of the heat transfer coefficient results. Higher working fluid flow rates increased the heat transfer more than an order of magnitude as the working fluid flow rate was increased from 4.5 to

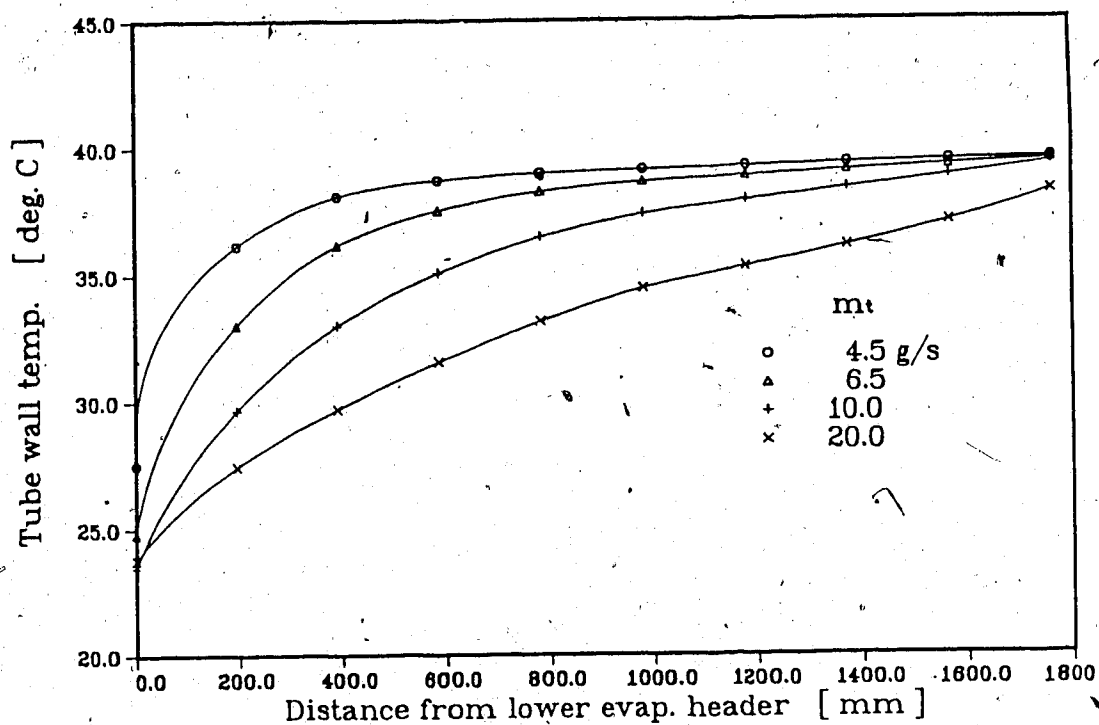


Fig. 2.30 Wall temp. distribution for evap. tube no. 4 of panel 3 as a function of w.fl. mass flow rate, air flow rate=0.44 m³/s, air temp.=40°C

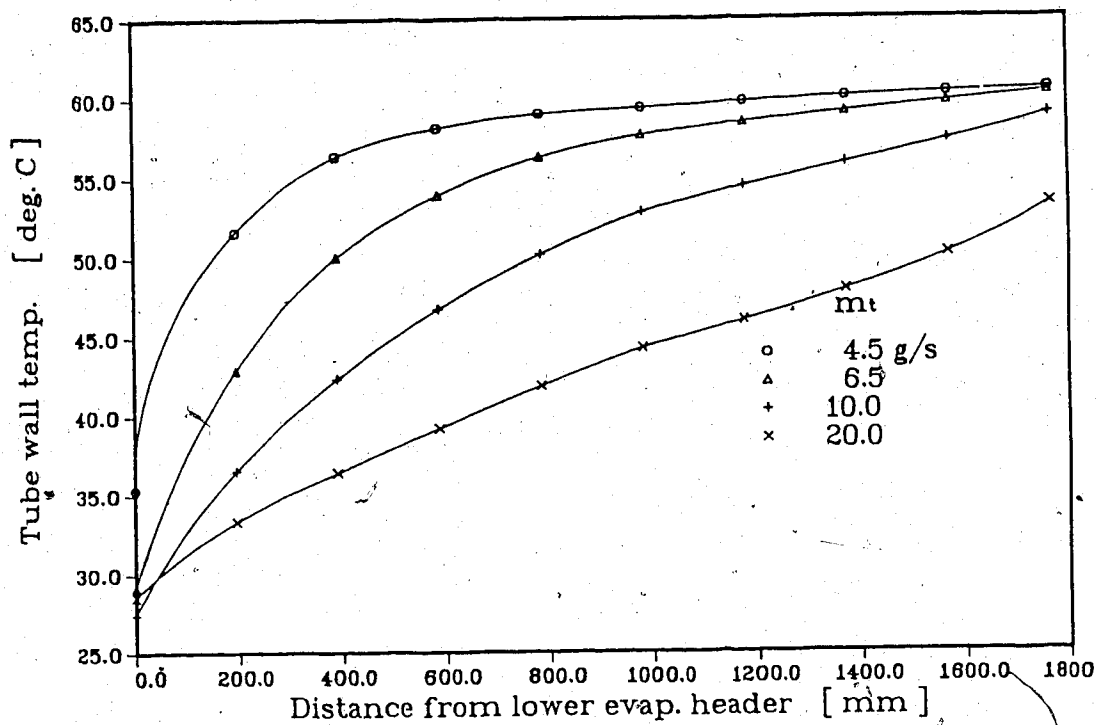


Fig. 2.31 Wall temp. distribution for evap. tube no. 4 of panel 3 as a function of w.fl. mass flow rate, air flow rate=0.44 m³/s, air temp.=60°C

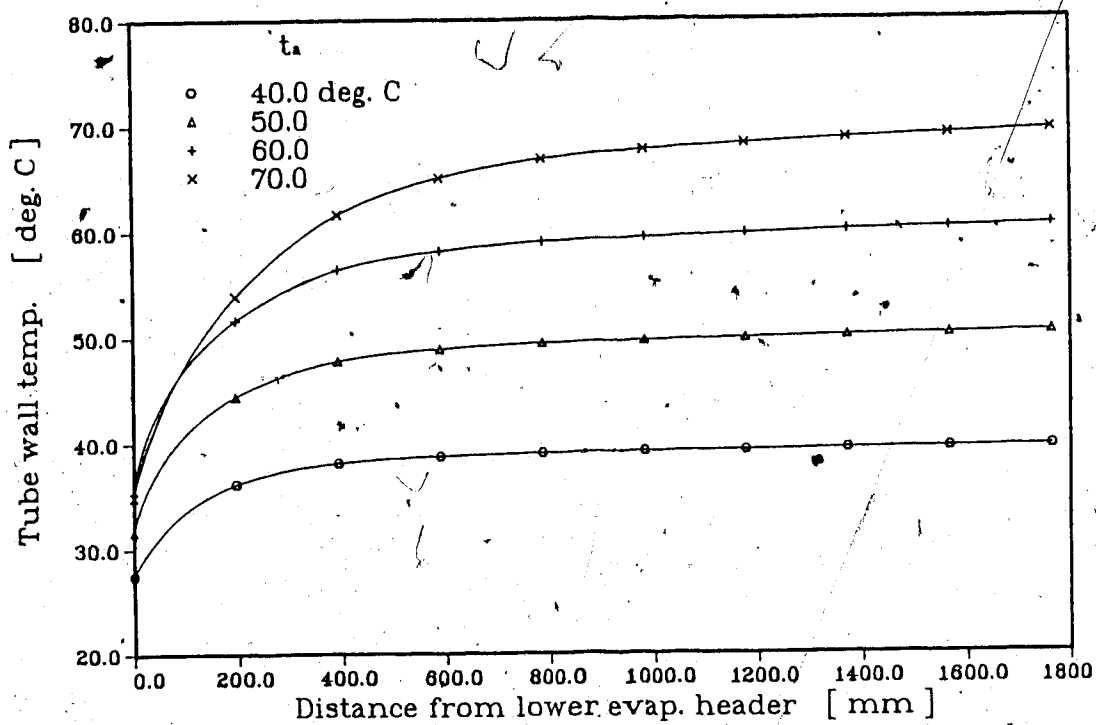


Fig. 2.32 Wall temp. distribution for evap. tube no. 4 of panel 3 as a function of air temp., air flow rate=0.44m³/s, w.fl. flow rate=4.5 g/s

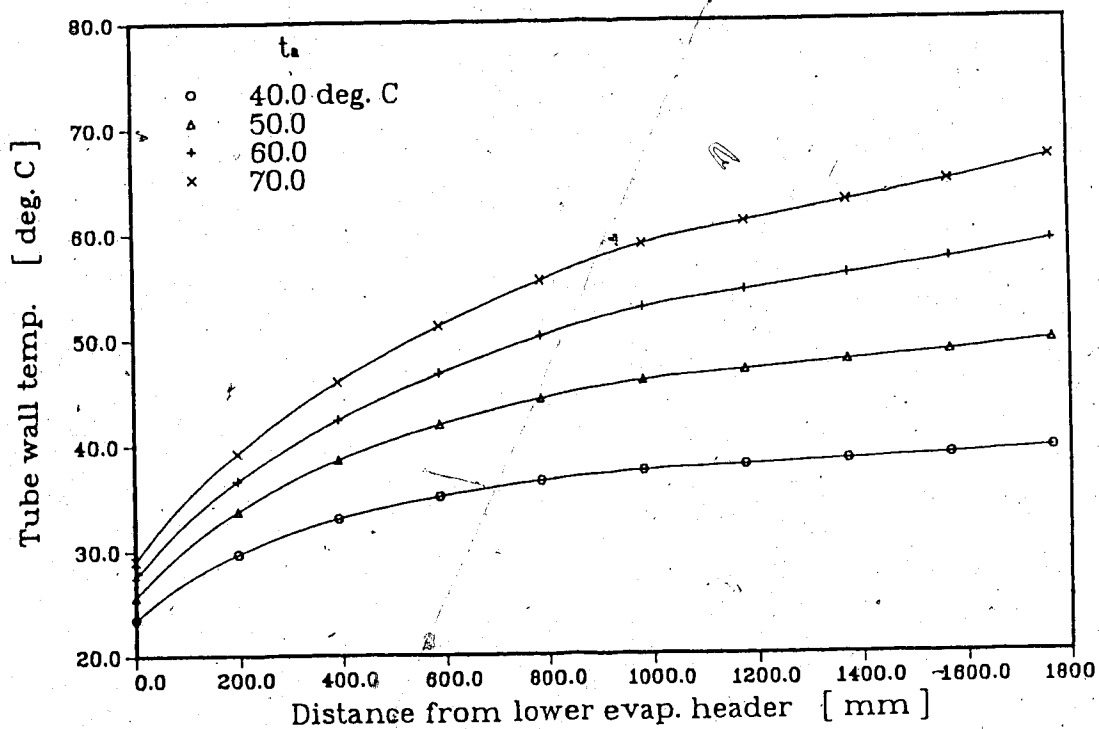


Fig. 2.33 Wall temp. distribution for evap. tube no. 4 of panel 3 as a function of air temp., air flow rate=0.44m³/s, w.fl. flow rate=10 g/s

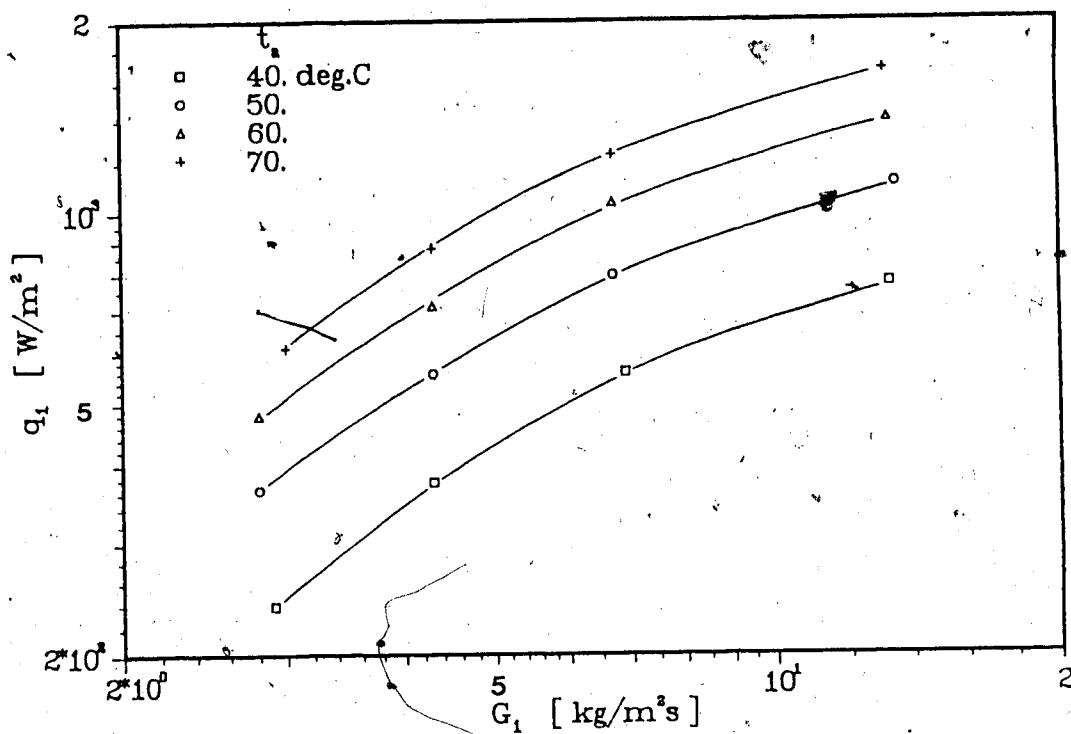


Fig. 2.34 Wall heat flux for working fluid side of evaporator vs. inlet mass flux for one evaporator tube

20 g/s. It is seen from these two figures that the heat transfer coefficient for the working fluid side of the evaporator decreased with increasing air volume flow rate. This is the same result which is obtained from Fig. 2.19, and it is believed to be the result of increased heat loss from the air to the surroundings across the evaporator. The heat loss increased with increasing air flow rates as shown in Figs. 2.9 and 2.10.

Nusselt number versus Reynolds number, Re , is plotted in Fig. 2.37. The results approximated the thermosyphon results, Fig. 2.20, over the same Reynolds number range. The small discrepancies are believed to be caused by the different heating air temperatures used for the two systems (40 - 70°C for forced flow and 75 - 96°C for thermosyphonic flow).

Nusselt number versus inverse Graetz number is plotted in Fig. 2.38. Prandtl number is one of the independent variables used to calculate Graetz number, Eqs. (2.20) and (2.21), and it decreased with increased working fluid (and air) temperature, hence Graetz number increased as well. It is this effect which is seen in Fig. 2.38 where inverse Graetz number is shown to increase as the air temperature increased.

2.7.3 Condenser results

The overall heat transfer coefficient and cooling water wall heat flux are shown in Fig. 2.39. This heat transfer

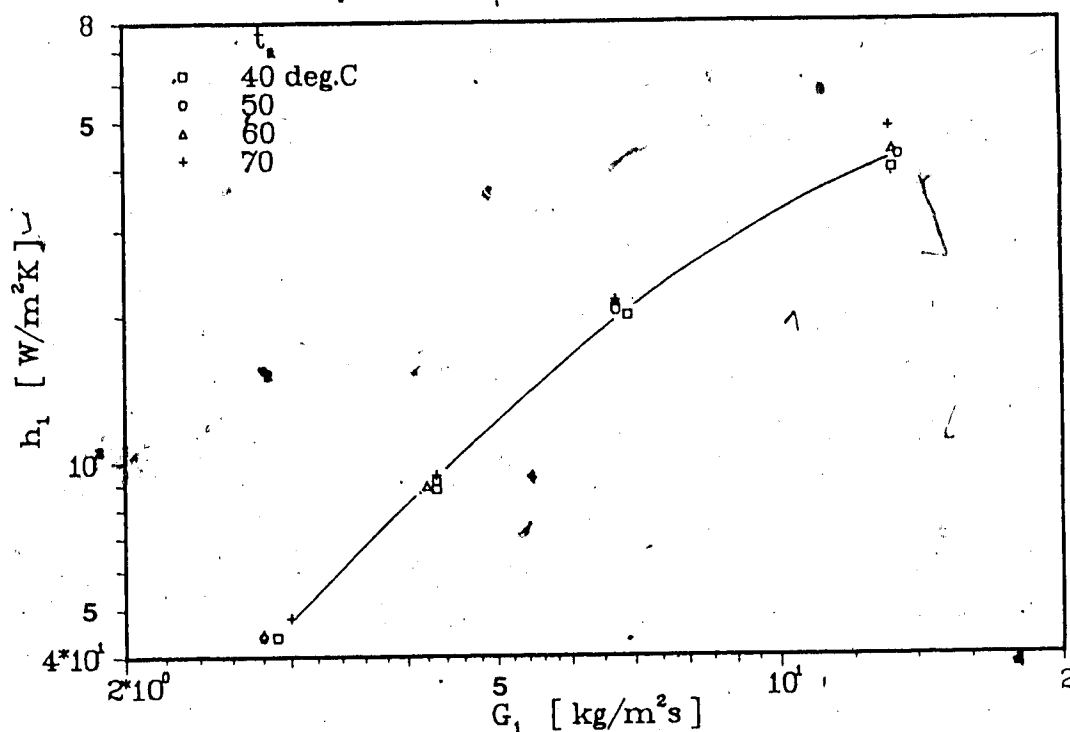


Fig. 2.35 Heat transfer coefficient for working fluid side of evap. vs. mass flux for working fluid flow thru one evap. tube, air flow rate is $0.44 \text{ m}^2/\text{s}$

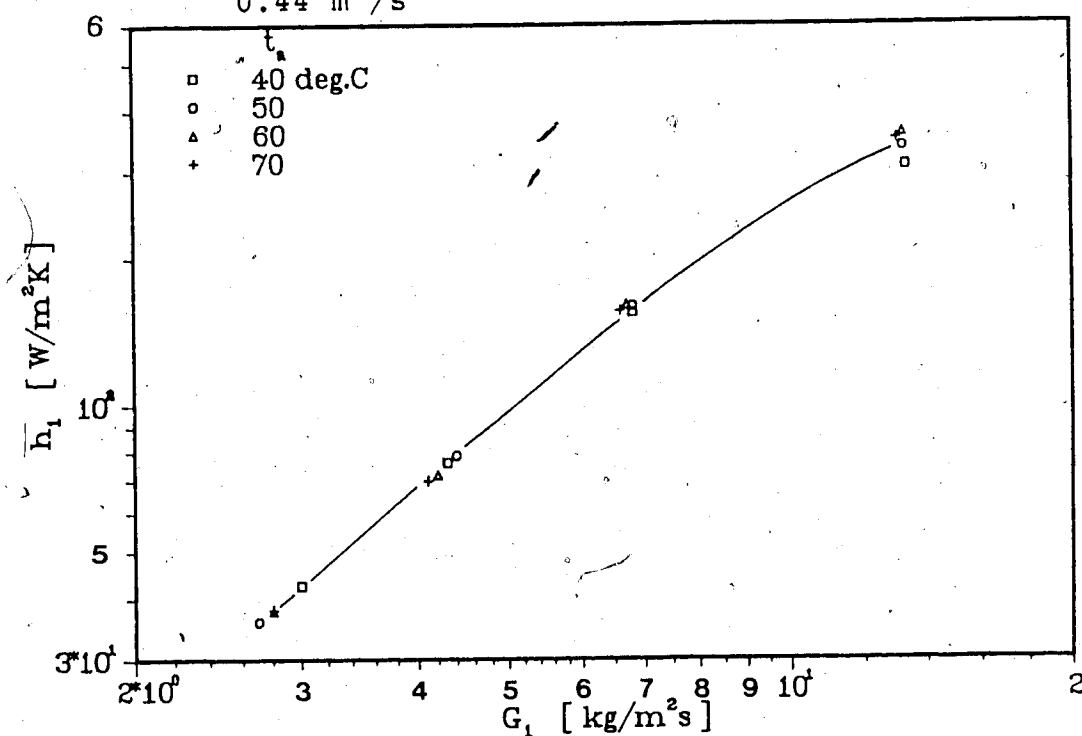


Fig. 2.36 Heat transfer coefficient for working fluid side of evap. vs. mass flux for working fluid flow thru one evap. tube, air flow rate is $72 \text{ m}^2/\text{s}$

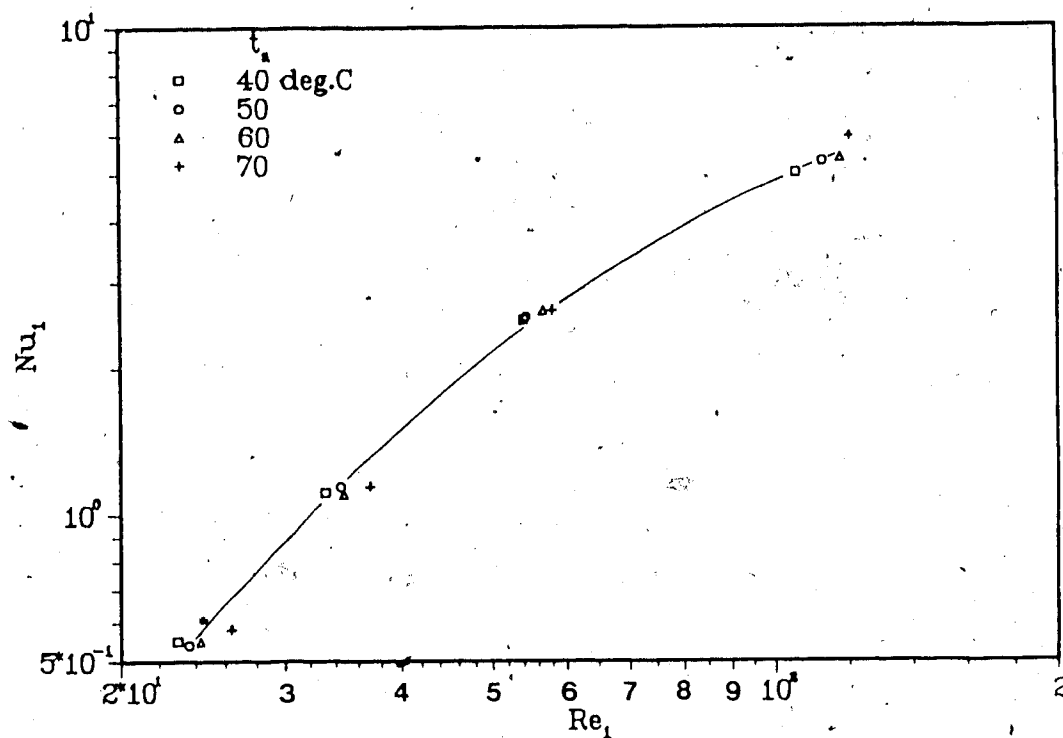


Fig. 2.37 Nusselt number for evap. working fluid side vs. Reynolds number for one evap. tube

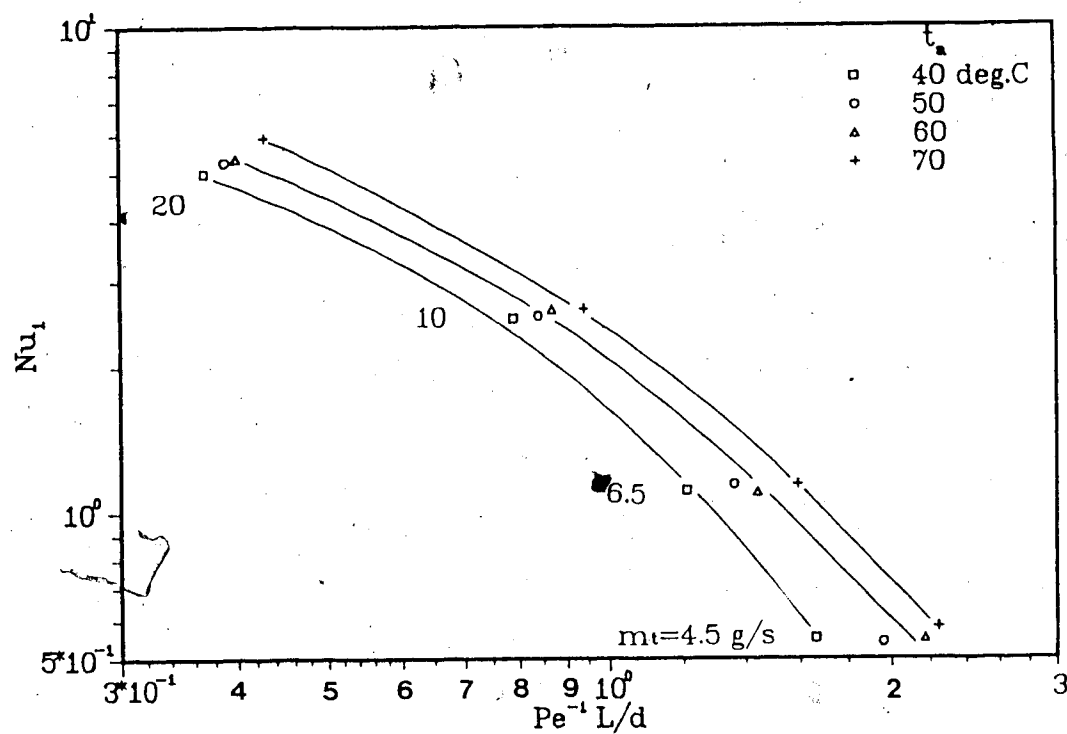


Fig. 2.38 Nusselt number for evap. working fluid side vs. inverse Graetz number for working fluid of evap.

coefficient shows only small changes, less than 5% of the heat transfer coefficient values as the air temperature is increased from 40 to 60°C. This is caused by the increasing temperature difference between average working fluid and average cooling water through the condenser, shown in Table 2.11. The increasing cooling water heat recovery rate, or wall heat flux, is not sufficient to increase the overall heat transfer coefficient over this temperature range (40 - 60°C). However, as the temperature is altered from 60 to 70°C, the heat rate transferred to the cooling water is high enough to increase the heat transfer coefficient. It is only the highest air temperature (70°C) which transfers enough heat to increase the heat transfer coefficient. For a certain wall heat flux the overall heat transfer coefficient was lower than what was experienced for the thermosyphon flow result shown in Fig. 2.23. This is due to the lower heating temperatures used during the forced flow tests. It is noticeable however, that the results shown in Fig. 2.39 for the highest air temperature and the two lowest working fluid flow rates (4.5 and 6.5 g/s) are nearly the same as the thermosyphon results. The overall heat-transfer coefficient is fundamentally dependent on the working fluid flow rate, Eqs.(2.1) and (2.6). It is this dependency which results in the improved heat transfer coefficient with increasing working fluid mass flow rate, shown in Fig. 2.39.

Fig. 2.40 shows the estimated working fluid heat transfer coefficient for the condenser versus the working

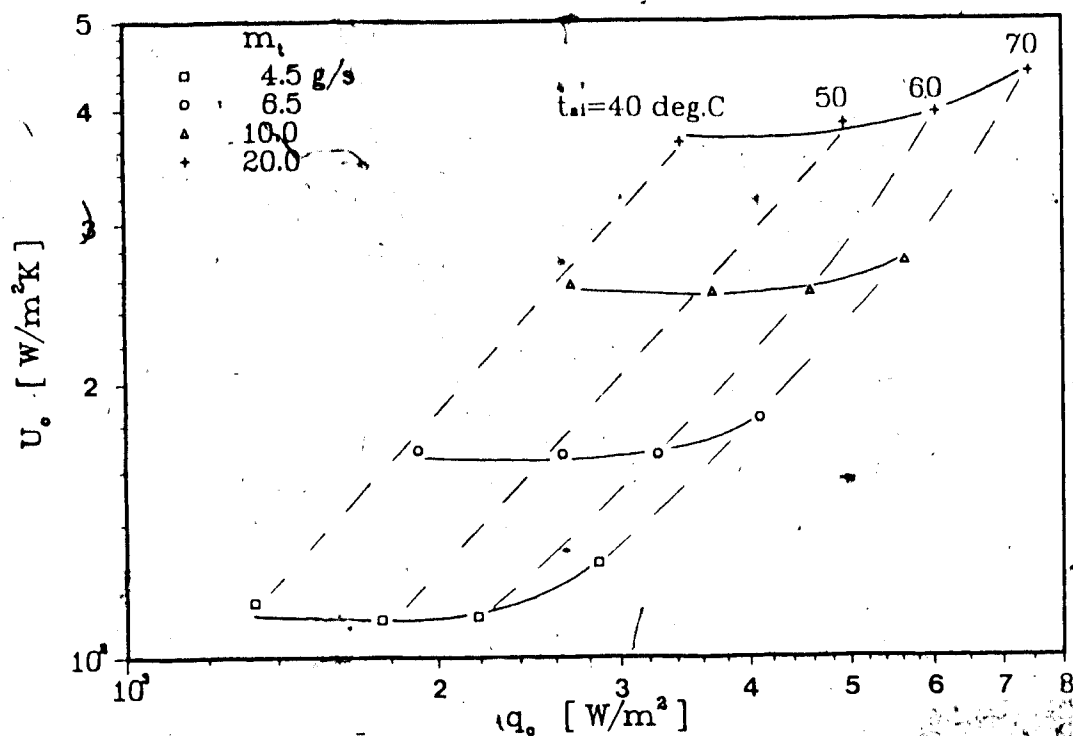


Fig. 2.39 Arithmetic mean overall heat transfer coefficient for cond. vs. wall heat flux for the cooling water

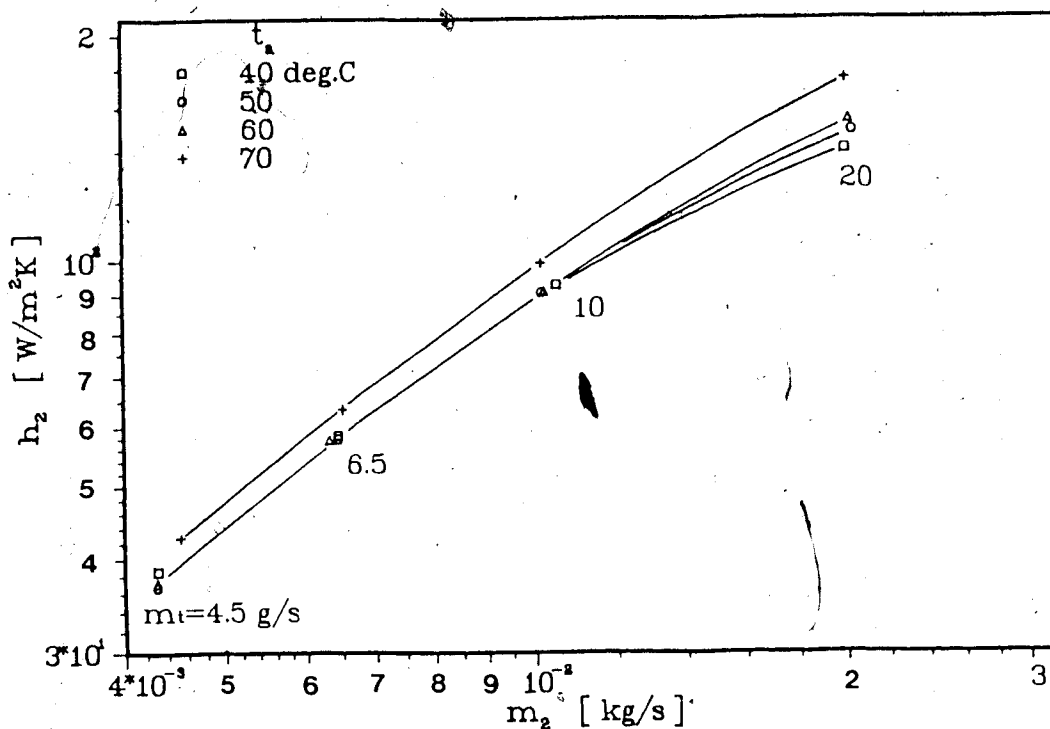


Fig. 2.40 Estimated outside heat transfer coefficient for cond. coil vs. mass flow rate of working fluid flow thru évap.

TABLE 2.11: WORKING FLUID AND COOLING WATER TEMPS., HEAT RECOVERY RATE AND OVERALL HEAT-TRANSFER COEFFICIENT FOR THE CONDENSER

m_t [g/s]	$t_{a,i}$ [°C]	t_3 [°C]	t_a [°C]	$t_{c,i}$ [°C]	$t_{c,o}$ [°C]	$\Delta T'$ [°C]	Q_c [W]	U_c [W/(m ² K)]
4.5	40	36.1	13.2	11.9	14.3	11.6	404.	115.
	50	45.5	13.6	12.0	15.0	13.1	536.	110.
	60	53.8	14.3	12.3	16.4	19.7	665.	111.
	70	61.7	15.5	13.4	18.6	22.6	869.	127.
6.5	40	35.9	14.0	11.9	15.4	11.3	582.	169.
	50	45.6	14.9	12.1	16.9	15.8	803.	167.
	60	54.2	15.8	12.5	18.5	19.5	991.	167.
	70	62.2	16.9	13.4	20.9	22.4	1242.	183.
10.0	40	34.4	15.9	12.2	17.1	10.5	818.	257.
	50	43.5	17.0	12.2	18.9	14.7	1121.	252.
	60	51.9	18.3	12.8	21.2	18.1	1391.	252.
	70	59.3	19.3	13.4	23.7	20.7	1716.	272.
20.0	40	34.3	18.7	12.5	18.7	9.4	1044.	367.
	50	38.3	20.5	12.3	21.2	12.6	1480.	384.
	60	45.4	22.6	13.1	24.2	15.3	1840.	395.
	70	51.0	23.8	13.5	27.2	17.0	2262.	437.

$$\Delta T = 0.5(t_3 + t_a) - 0.5(t_{c,i} + t_{c,o})$$

fluid mass flow rate. For the same working fluid flow rate changes (4.5 to 6.5 g/s), the results for the outside heat transfer coefficient of the condenser coil show only small differences compared to data resulted from the thermosyphon analyses, Fig. 2.25.

2.8 Concluding Remarks

The purposes of these single phase tests were to obtain a general understanding of the system behaviour and to acquire characteristic system operating parameters which

will be applicable to the two-phase working fluid test analyses.

The thermosyphon tests were conducted with four heating air flow rates ($0.27 - 0.72 \text{ m}^3/\text{s}$) and the air temperatures were in the range of $75 - 96^\circ\text{C}$. The cooling water operating parameters were not changed: the flow rate was 40 g/s and the condenser entrance temperature was 13°C . Working fluid pressure was 110 kPa abs. when the tests commenced.

The thermosyphonic flow test results showed system heat recovery rates in the range $650 - 1800 \text{ W}$, condenser cooling water exit temperatures from 18 to 25.5°C and working fluid flow rates between 3.4 and 6.6 g/s .

The same air volume flow rates ($0.27 - 0.72 \text{ m}^3/\text{s}$) were used for the forced circulation tests, while the heat source temperatures were varied between 40 and 70°C . Four working fluid flow rates ($4.5 - 20.0 \text{ g/s}$) were used with the same condenser cooling water inlet operating conditions as the thermosyphon tests.

The forced circulation tests resulted in cooling water heat recovery rates between $350 - 2400 \text{ W}$, while the cooling water exit temperature ranged between $14.5 - 28.7^\circ\text{C}$.

The system efficiencies were $2 - 6.5\%$ for the thermosyphon tests and $2 - 11\%$ for the forced flow tests. The maximum evaporator efficiency, (35%) for both thermosyphonic and forced flow, indicated that the major cause for the low system efficiencies was the evaporator design.

The total heat loss to the surroundings across the working fluid loop, evaporator excluded, was generally between 40 and 80 W and never as much as 100 W. This heat loss was normally less than 4% of the heat recovery rate by the cooling water. Hence, the heat losses across the condenser can be neglected in later analyses, since it was less than 2% of the heat recovery. This will be done for the two-phase working fluid analyses.

The heat loss from the air to the surroundings across the evaporator, 250 - 970 W, will be used as the standard heat loss for two-phase flow for the particular air flow rate.

The natural and forced circulation tests show similar results for the same working fluid flow rates, and the results from both experimental methods indicate the necessity for system modification for use with single phase water as a working fluid.

3. A Closed-Loop Two-Phase Thermosyphon System Using Water under Partial Vacuum as Working Fluid

Summary

The steady state operation characteristics were studied for a two-phase closed-loop thermosyphon system which used water under partial vacuum as the working fluid.

The tests were conducted with air as the heating fluid. The air flow rate was constant, $0.44 \text{ m}^3/\text{s}$ and the temperature entering the evaporator was controlled ranging from 55 to 78°C . The results are discussed for the highest primary loop vacuum (21 kPa abs. pressure) and four different working fluid charge levels, as well as the effect of open and closed liquid-vapour separator. The cooling water conditions were not changed. The mass flow rate was 40 g/s and the temperature entering the condenser was approximately 15°C .

The system efficiency ranged from 6 to 11% . The heat rate recovered by the cooling water varied from 900 to 2300 W and the cooling water exiting from the condenser was in the range $20 - 30^\circ\text{C}$.

The experimental results are compared with both single phase thermosyphon results and empirical equations developed for heat transfer with two-phase fluid flow.

3.1 Introduction

A two-phase closed-loop thermosyphon is studied with water under partial vacuum as the working fluid. If reasonable system performance is obtained, further research with such a system would be in order, as water has numerous advantages as working fluid (mentioned in Chapter 2). The results from these tests are compared with the single phase test results discussed with water as the working fluid in Chapter 2.

A two-phase heat recovery system is assumed to have superiority over a single phase system, especially during low grade heat transfer. Because of the latent heat transfer process occurring for a two-phase system, more heat can be transported between the heat source and the working fluid before the difference between the two temperatures of the fluids vanishes. Generally, the differences between the heat sink and heat source are between 15 - 60°C for low grade heat recovery.

If the wall heat flux from the heat source is large, it is advantageous for the system performance to use a working fluid with high latent heat capacity, like water. Because large heat rates can be transferred from the the heat source to the working fluid without superheating the latter fluid.

The experiments were conducted varying the following system parameters; air temperature (55 - 78°C), absolute working fluid pressure (21 - 47 kPa), working fluid liquid level (41 - 100% of the distance between the lower

evaporator header and the horizontal centre line of the condenser) and downcomer line of the liquid-vapour separator (open - closed). Other system operating parameters such as, heating air flow rate ($0.44 \text{ m}^3/\text{s}$), cooling water flow rate (40 g/s) and cooling water temperature (approximately 15°C) were not changed for any of the tests.

3.2 Experimental Apparatus, Instrumentation and Calibration

Only minor modifications were made to the primary loop described in Chapter 2, Section 2.2. The rotameter was replaced by a turbine flow meter and another turbine flow meter was installed in the downcomer line from the liquid-vapour separator. The water expansion tank was replaced by a storage tank, which acted as a reservoir for the working fluid as the liquid level in the primary loop was altered. A schematic diagram of the two-phase thermosyphon system is shown in Fig. 3.1.

Except for the two turbine flow meters no instruments were attached to or detached from the thermosyphon system. These two flow meters were connected to the HP-3497A data acquisition/control unit and recorded in the same manner as the cooling water turbine flow meter.

All liquid flow meters, pressure transducers and sheathed thermocouples were recalibrated according to the calibration procedures explained in Section 2.3. The new calibration curves showed minimal deviations, less than 0.3%, from the old calibration curves. However, the new

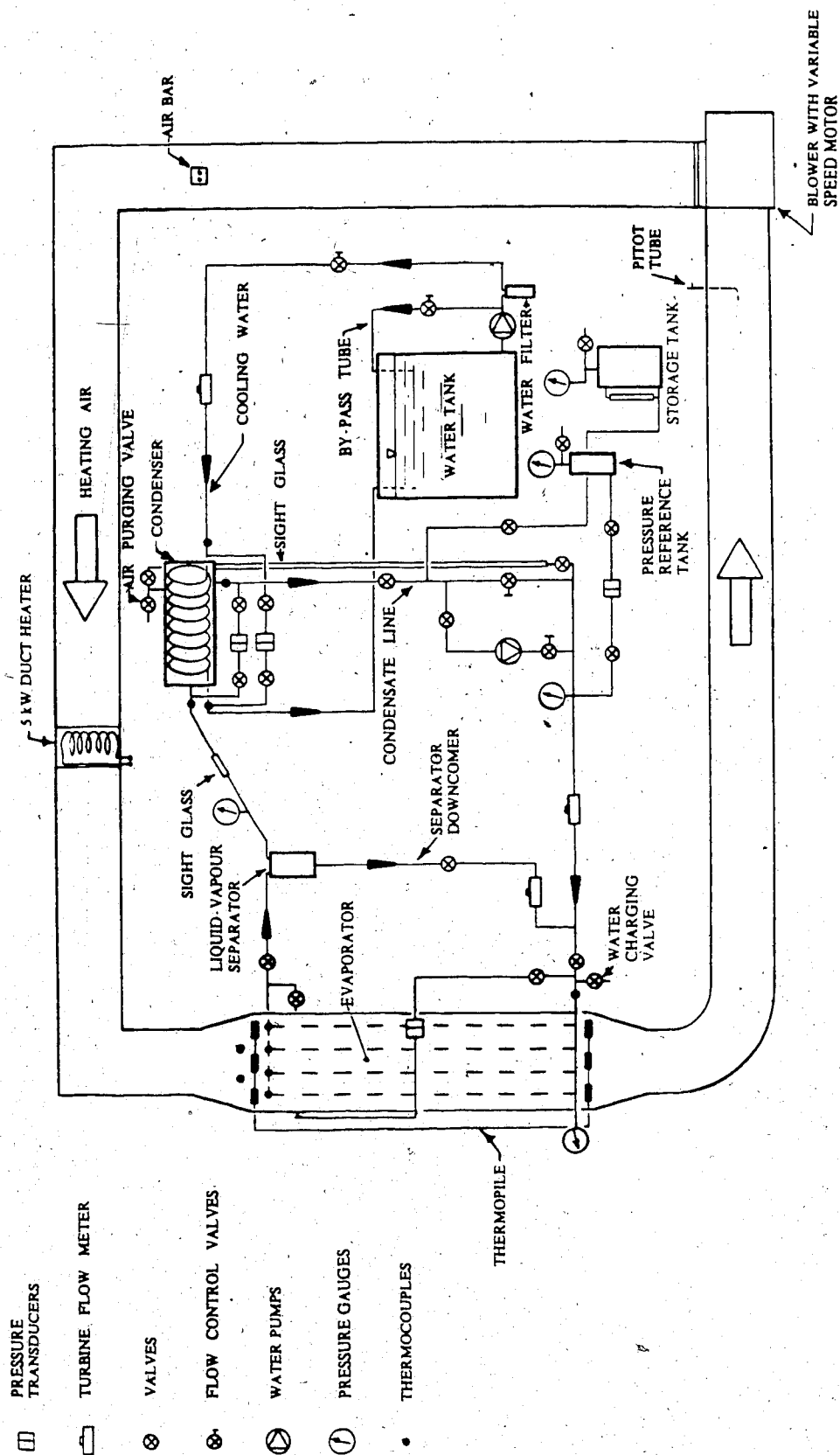


Fig. 3.1 Schematic diagram of two-phase closed-loop thermosyphon

calibrations were employed during the data execution.

3.3 Experimental Procedure

The primary loop was tested for both pressure and vacuum leaks. It was pressurized with dry air (300 kPa) and evacuated with a vacuum pump (12 kPa absolute pressure, 26.5 inHg vacuum) during the leak tests. Each test period lasting 48 hours was conducted using the same procedure as explained in Section 2.4. If leaks were indicated by the primary loop pressure transducer during a vacuum test, the system was pressurized and Snoop was used to find the faults. When no significant pressure change (less than 7.0 Pa) was detected the system was assumed leak free.

The working fluid loop was charged with the treated water using the same procedure described in Section 2.4. When all the air was removed from the working fluid, the desired liquid level was charged into the primary loop. This was done by sucking excessive working fluid into the storage tank whose absolute pressure was lower than that of the primary loop. The primary loop was charged with additional working fluid as the fluid was drawn back to the loop from the storage tank. During this charging process the pressure in the storage tank was higher than the pressure in the working fluid loop.

A venturi with a static pressure tap was used to create partial vacuum in the working fluid loop. A vacuum hose connected the static pressure tap to the air purging valve

on the condenser shell, and the desired vacuums (21, 26, 35 and 47 kPa abs. pressure) were created. Tests were conducted with 6 initial charge levels (100, 96, 83, 76, 59, and 41% of the distance between the lower evaporator header and the horizontal centre line of the condenser)¹. The initial charge levels are referred to as such, since the heating of the working fluid caused the levels to increase somewhat during the tests. The schematic diagram in Fig. 3.2 indicates the different initial charge levels. The working fluid was exposed to the same vacuum for all 6 charge levels before the vacuum was altered. Sets of experiments with charge levels 1 to 4 were performed with the liquid downcomer from the liquid-vapour separator alternately open and closed. The line was always open during tests done with the two lowest liquid levels.

Experiments were conducted with 4 different heating air temperatures per charge level and initial working fluid vacuum. The tests were always done with the maximum obtainable air temperature for a particular vacuum. Because of low working fluid flow rates for lower heating air temperatures, the experiments were done with temperatures 3 to 7°C below the previous air temperature depending on charge level and system vacuum. Tests with closed downcomer were done for the two highest air temperatures only.

¹These initial liquid levels of the working fluid will for convenience be referred to as charge level (Ch.L.) 1, 2, 3, 4, 5 or 6 in this chapter and in Chapter 4.

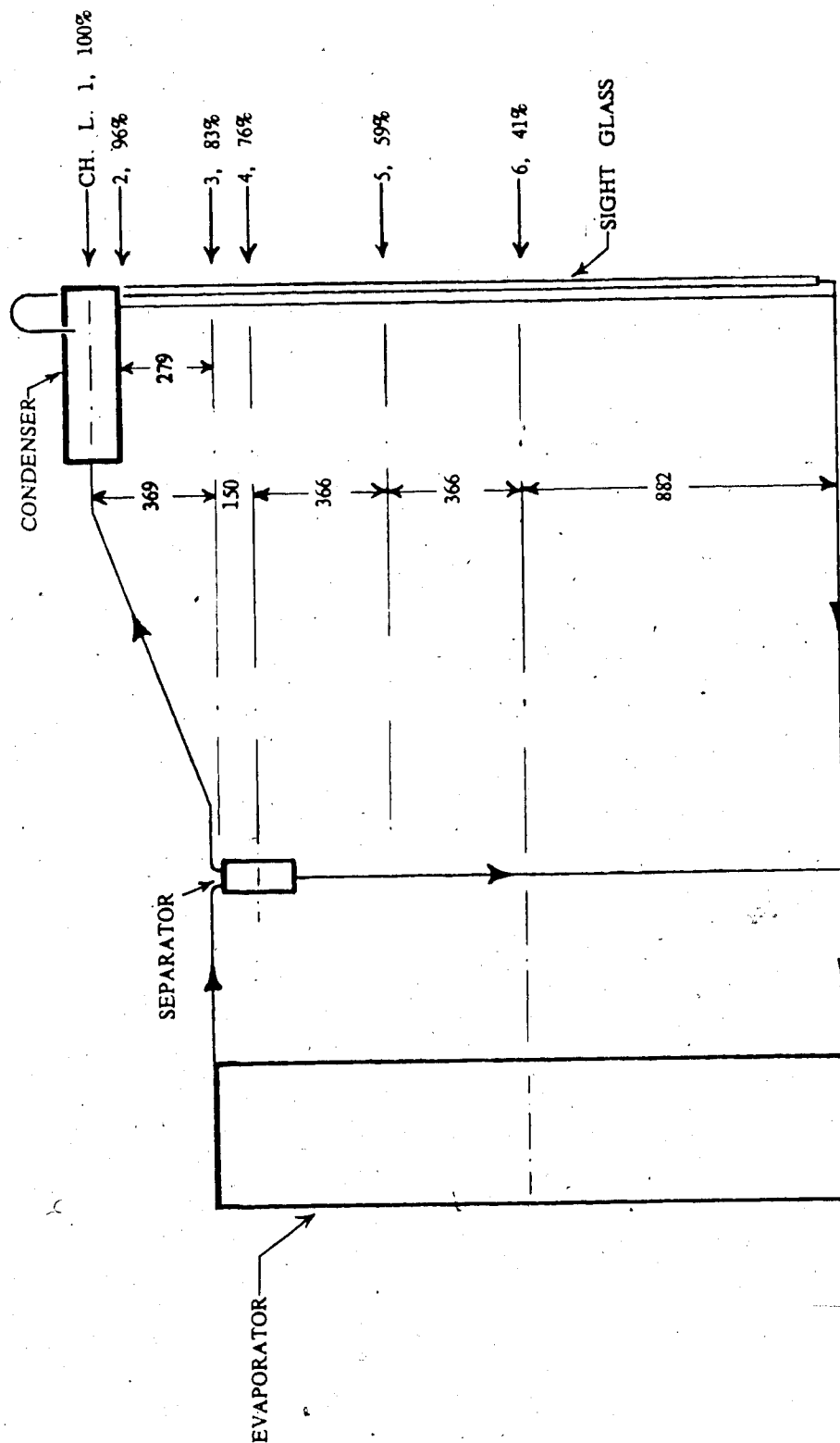


Fig. 3.2 Schematic diagram defining the six initial working fluid charge levels (dim. in mm)

The experimental operating temperatures for the four highest charge levels, 21 kPa absolute working fluid pressure and open separator downcomer are shown in Table 3.1. For charge levels 5 and 6 only the maximum heating air temperature and maximum obtainable vacuum (21 kPa) were used as operating air temperature and working fluid vacuum. This was done in an attempt to reach superheated vapour.

Hewlett Packard chart recorders were used to record the working fluid flow rates and the system pressure continuously during each experiment. The experimental testing procedure was similar to the single phase tests.

The fluid properties for boiling flow are known to have inherent instabilities [28]. Because of these instabilities, the system was assumed steady when the working fluid vacuum and flow rates fluctuated around the same mean value for at least 30 minutes and the air temperature changed less than 0.1°C over the same period. When steady state was reached, two recording sets were done 5 minutes apart. The data were stored on tape and printed as explained in Section 2.3.

3.4 Basic Equations for Data Analysis

Definition of system variables

Many variables encountered in the heat transfer theory have the same definition for single and two-phase flow analyses. Those variables whose derivation is not changed from the single phase theory discussed in Section 2.5 will not be repeated, while new or modified definitions are

TABLE 3.1: OPERATING WORKING FLUID CHARGE LEVELS AND AIR TEMPERATURES

WORKING FLUID CHARGE LEVEL [# , %]	HEATING AIR TEMPERATURE [°C]
1 , 100	55.4
	60.7
	68.8
	76.6
2 , 96	64.3
	67.2
	70.8
	75.5
3 , 83	60.4
	65.0
	69.1
	74.3
4 , 76	69.0
	71.2
	74.6
	76.3

Notes: Abs. pressure in primary loop is 21 kPa
Downcomer is open from separator

mentioned here.

The heat rate recovered by the working fluid in the evaporator, Q_1 , is obtained using

$$Q_1 = Q_a - Q_{al} \quad (3.1)$$

where, Q_{al} , is the heat rate lost by the air to the surroundings across the evaporator and is assumed to be the same as for single phase flow tests. These heat losses are

determined by comparing similar heating air conditions for the two systems (the heat losses for air temperatures above 80, below 70 and between 70 and 80°C were 550, 500 and 450 W respectively). In Chapter 2 the heat loss from the working fluid to the surroundings across the condenser is found to be less than 4% of the heat rate released by the working fluid and is neglected in this analysis. Hence, the heat rate released by the working fluid, Q_2 , is assumed to equal the heat rate recovered by the cooling water, Q_c , through the condenser.

When Q_1 is known the vapour quality of the working fluid exiting the evaporator, x_1 , can be determined from

$$x_1 = \left[\frac{Q_1}{m_1} - c_{pl}(t_{\text{sat}} - t_1) \right] / i_{fg} \quad (3.2a)$$

where i_{fg} is the latent heat of vaporization of the working fluid at the particular temperature. The vapour quality of the working fluid entering the condenser, x_2 , is defined as

$$x_2 = \left[\frac{Q_2}{m_2} - c_{pl}(t_{\text{sat}} - t_4) \right] / i_{fg} \quad (3.2b)$$

These equations are only valid when the working fluid exits the evaporator or enters the condenser in the saturated vapour-liquid state. The working fluid exit temperature, t_2 , is the same as the saturation temperature, t_{sat} ,

corresponding to the exit pressure recorded with the

¹¹The ratio of vapour mass flow rate to total mass flow rate of the of the working fluid

pressure gauge in the vapour line between the evaporator and the condenser, shown in Fig. 3.1. If t_2 is higher than the saturation temperature superheating occurs and the following equation applies

$$Q_1 = m_1 [c_{pl}(t_{\text{sat}} - t_1) + i_{fg} + c_{pv}(t_2 - t_{\text{sat}})] \quad (3.3)$$

where c_{pl} is the specific heat of the liquid and c_{pv} is the specific heat of the vapour.

All thermodynamic properties for air, cooling water and liquid working fluid are calculated using the average temperature of the fluid entering and exiting the heat exchanger. The exception is Reynolds number which is calculated using the entering fluid conditions. If superheated vapour is encountered, the thermodynamic properties of the liquid are calculated using the average temperature of the liquid fluid and the saturated fluid. The saturation temperature is obtained by assuming the recorded gauge pressure in the vapour line is the saturation pressure. The thermodynamic properties of the vapour are calculated based on the saturation temperature and recorded vapour pressure.

Heat transfer correlation

Different two-phase heat transfer correlations employ Dittus-Boelter equation [29,30] to estimate a single phase heat transfer coefficient, which is used to predict a two-phase heat transfer coefficient. The original Dittus-Boelter equation often quoted [30,31] defines the

single phase heat transfer coefficient h_s , as

$$h_s = 0.023 \text{ Re}^{0.8} \text{ Pr}^{0.4} \frac{k_l}{d} \quad (3.4)$$

where Reynolds number is calculated for one evaporator tube.

To incorporate the effects of different vapour exit qualities, Eq. (3.4) has been modified when used with recent two-phase heat transfer correlations (for example in the method employed by Kandlikar [32]). This modified Dittus-Boelter equation defines the heat transfer coefficient, which in this work will be referred to as liquid-only heat transfer coefficient (h_l), as

$$h_l = 0.023 [\text{Re}(1 - x)]^{0.8} \text{ Pr}^{0.4} \frac{k_l}{d}$$

where the Reynolds number term, $\text{Re}(1-x)$, represents the part of the working fluid entering one evaporator tube and exits the evaporator as liquid.

Nusselt numbers, Eq. (2.19), which are calculated using the heat transfer coefficients h_s , Eq. (3.4), and h_l , Eq. (3.5), are referred to as Nu_s and Nu_l respectively.

Boiling number, Bo , as well as Lockhart-Martinelli parameter, X_{tt} , are commonly associated with two-phase heat transfer correlations [30-33]. These two parameters are defined as

$$Bo = \frac{q x_1}{G i_{fg}} \quad (3.6)$$

and

$$x_{tt} = \left(\frac{1-x}{x} \right)^{0.9} \left(\frac{\rho_v}{\rho_l} \right)^{0.5} \left(\frac{\mu_l}{\mu_v} \right)^{0.1} \quad (3.7)$$

where the subscript l indicates the liquid component and v indicates the vapour component of the fluid.

Shah modified the Lockhart-Martinelli parameter in his CHART correlation [34] by developing the Convection number, Co , defined as

$$Co = \left(\frac{1-x}{x} \right)^{0.8} \left(\frac{\rho_v}{\rho_l} \right)^{0.5} \quad (3.8)$$

Due to the successful results Shah obtained with this dimensionless number, Kandlikar used the Convection number in the convection term of his empirical two-phase heat transfer correlation [32].

The experimental results in this work are compared with the computed results from the following four empirical equations

$$\frac{Nu_{tp}}{Nu_l} = 7390. (Bo + 1.5 \times 10^{-4} x_{tt}^{-2/3}) \quad (3.9)$$

$$\frac{Nu_{tp}}{Nu_l} = 230. Bo^{1/2} \quad (3.10)$$

$$h_{tp} = D1 (Co)^{D2} h_l + D3 (Bo)^{D4} h_l F_{fl} \quad (3.11)$$

$$h_{tp} = 3.5 Nu_s \left(\frac{k_l}{d} \right) X_{tt}^{-1/2} \quad (3.12)$$

where Eqs. (3.9), (3.10), (3.11) and (3.12) were proposed by Schrock-Grossman [31], Shah [33], Kandlikar [32] and Ref. [30] respectively. The constants D1, D2, D3, D4 and F suggested by Kandlikar in Eq. (3.11) are dependent on flow orientation and fluid. These values corresponding to boiling water with vertical flow direction and with a Convection number smaller than 0.65 are found in Table 3.2.

TABLE 3.2: CONSTANTS USED IN THE KANDLIKAR CORRELATION FOR VERTICAL WATER FLOW

D1	D2	D3	D5	F
1.091	-0.948	887.46	0.726	1.0

Note: The constants are valid for $Co < 0.65$

Empirical heat transfer coefficient equations similar to Eq. (3.12) are proposed in [35].

3.5 Results and Discussion

A summary of the operating characteristics for the tests are shown in Table 3.3. The system performance was lower as the initial vacuum in the primary loop was decreased. Since low performance is encountered even for the highest working fluid vacuum (21 kPa abs. pressure), only test results with this vacuum level are discussed in this chapter. The effect of open and closed downcomer from the liquid-vapour separator is shown in the graphs discussed in this section.

The two lowest liquid charge levels, 5 and 6, are excluded from this discussion as the condensate^{1,2} flow rates were too low (less than 3 g/s) to be registered by the flow meter.

Only the second of the two recording sets are used for the system analyses. This is done because the working fluid flow fluctuated rapidly over a wide range (as will be discussed later in this section). This caused a wide scatter of the recorded data for the same stable condition, and it is believed that a display of two data points for the same stable condition in the graphs, will make the graphs more difficult to read.

^{1,2} The return line from the condenser to the evaporator will be referred to as the condensate downcomer and the condensed working fluid flowing through this tube is the condensate

TABLE 3.3: SUMMARY OF THE OPERATING CHARACTERISTICS
FOR 2-PHASE WATER TESTS

VARIABLES	EVAPORATOR	CONDENSER
Air volume flow rate [m^3/s]	0.44	1
Air temperature [$^{\circ}\text{C}$]	55-78	
Liquid mass flow rate [g/s]	6.3-21.2	40
Outlet minus inlet water temp. [K]		6.0-13.4
Maximum outlet water temp. [$^{\circ}\text{C}$]		30.8
Heat supply (air) [W]	1300-3000	
Heat recovery [W]		900-2300
Wall heat flux [W/m^2]	700-1800 ²	3000-7500
Heat transfer coefficient [$\text{W}/(\text{m}^2\text{K})$]	60-300 ²	100-350
Overall heat transfer coefficient [$\text{W}/(\text{m}^2\text{K})$]	32-60 ³	300-750
Vapour quality [%]	0.2-25	2-25
Nusselt number	0.8-3.4 ^{2,3}	
Reynolds number	19-115 ⁴	
Reynolds number	200-1300 ⁵	3500
Dean number		1200
Graetz number	0.4-2.8	47
Boiling number	0.000003-0.0003	
Lockhart-Martinelli parameter	0.025-2.5	
$h_{\text{ex}}/h_{\text{i}}$	0.6-3.0	
$h_{\text{ex}}/h_{\text{i}}$	0.65-4.0	
$h_{\text{ex}}/h_{\text{tp}}$ (S.G.)	0.15-1.0	
$h_{\text{ex}}/h_{\text{tp}}$ (Shah)	0.35-1.6	
$h_{\text{ex}}/h_{\text{tp}}$ (Kandl.)	0.05-0.45	
$h_{\text{ex}}/h_{\text{tp}}$ ([30])	0.09-0.3	
System efficiency:	6-11% ⁶	

Notes:

- ¹ Cooling water
- ² Working fluid
- ³ Based on ΔMTD .
- ⁴ W.fl. flow (1 evap.tube)
- ⁵ Total w.fl. flow
- ⁶ Overall system

The overall system performance, the evaporator and the condenser results are discussed in separate subsections.

The heat rates recovered by the cooling water are higher for two-phase than for single phase thermosyphon. This is easily seen when Figs. 3.3 and 2.5 are compared.

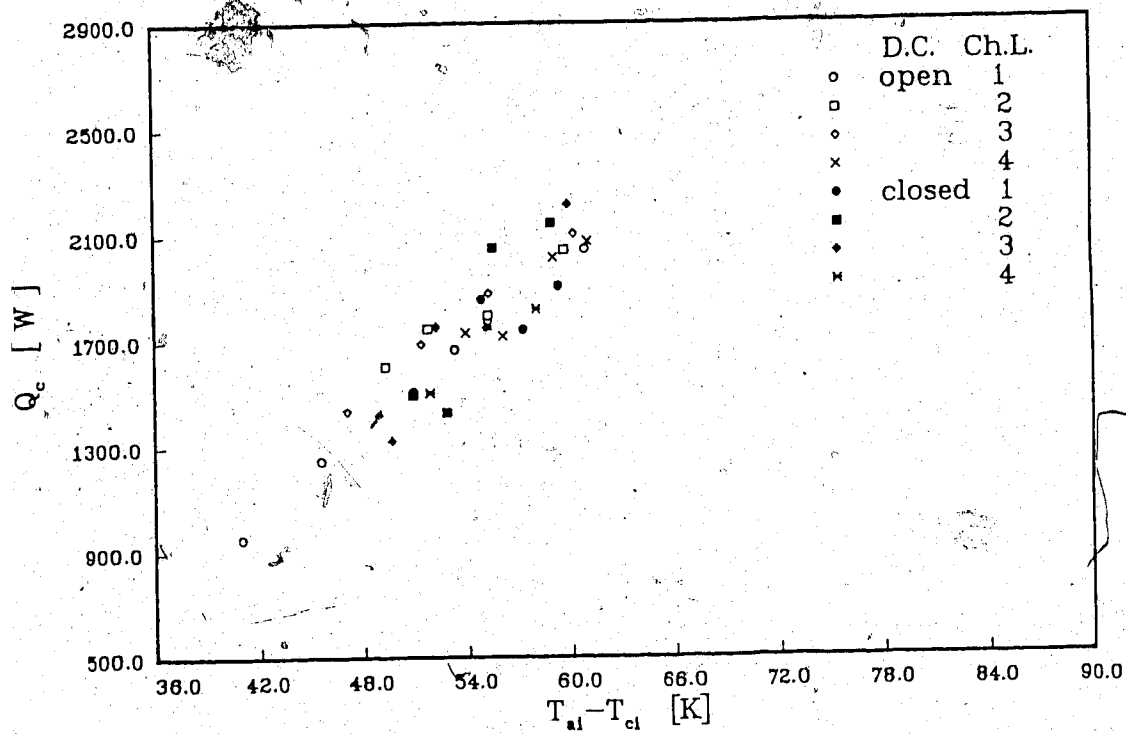


Fig. 3.3 Heat recovered by cooling water vs. extreme system temperature difference

These figures display the relationship between Q_c and $t_{a,i}$ minus $t_{a,o}$. The heat recovery rates are higher for the two-phase system even though the heating air is lower for this thermosyphon. This indicates increased system efficiency (Eq. 2.27), this is confirmed when Figs. 3.4 and 2.6 are compared.

Any apparent differences between the open and closed downcomer test results are not obvious in either Fig. 3.3, 3.4 or 3.5. The system efficiency versus the average wall heat flux from the evaporator wall to the working fluid is displayed in Fig. 3.4, and the system efficiency versus Reynolds number based on the working fluid conditions at the entrance of one evaporator tube is shown in Fig. 3.5. Even though the two-phase thermosyphon is more efficient than the single phase system as seen from Figs. 3.4 and 2.6, the two-phase test results are still low (maximum 11%).

Typical recordings of condensate and downcomer mass flow rates and system pressure are shown in Fig. 3.6. These system parameters undergo innate fluctuations as discussed in Section 3.4. Therefore, the figure indicates the mean values and the amplitude of the fluctuations. The recordings were taken during steady state with charge level 2, initial 21 kPa absolute pressure and 75°C air temperature. When the charge level decreased the flow fluctuations became more unstable as the mean values decrease towards unmeasurable flow rates.

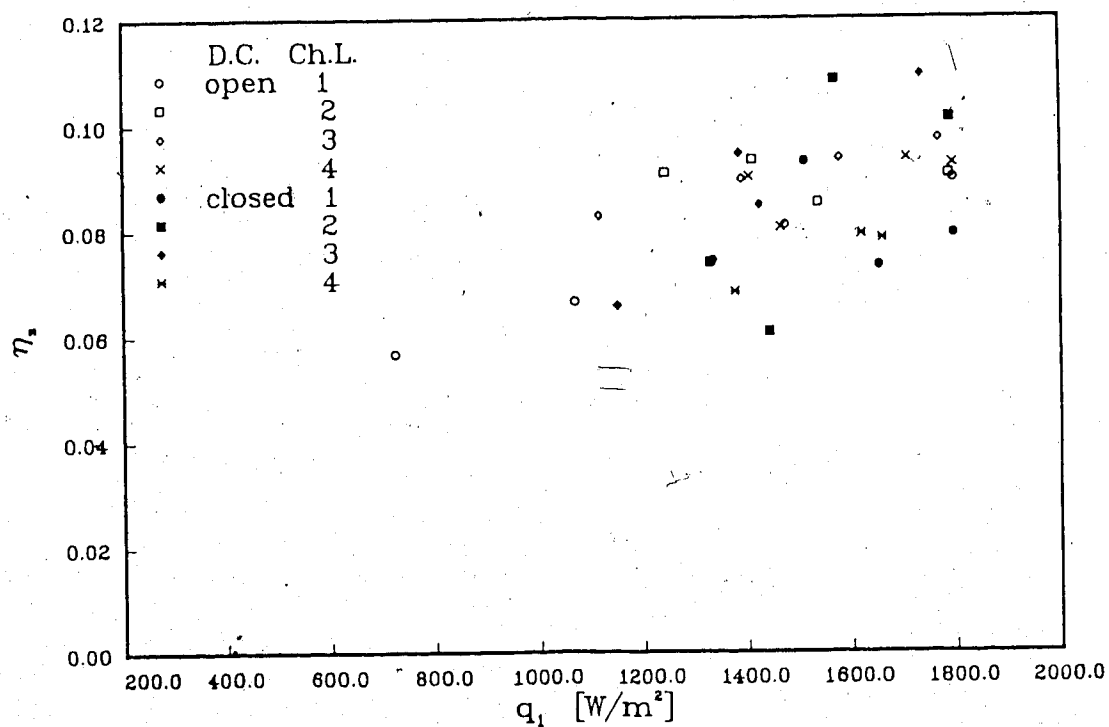


Fig. 3.4 System efficiency vs. wall heat flux from evap. tube wall to working fluid

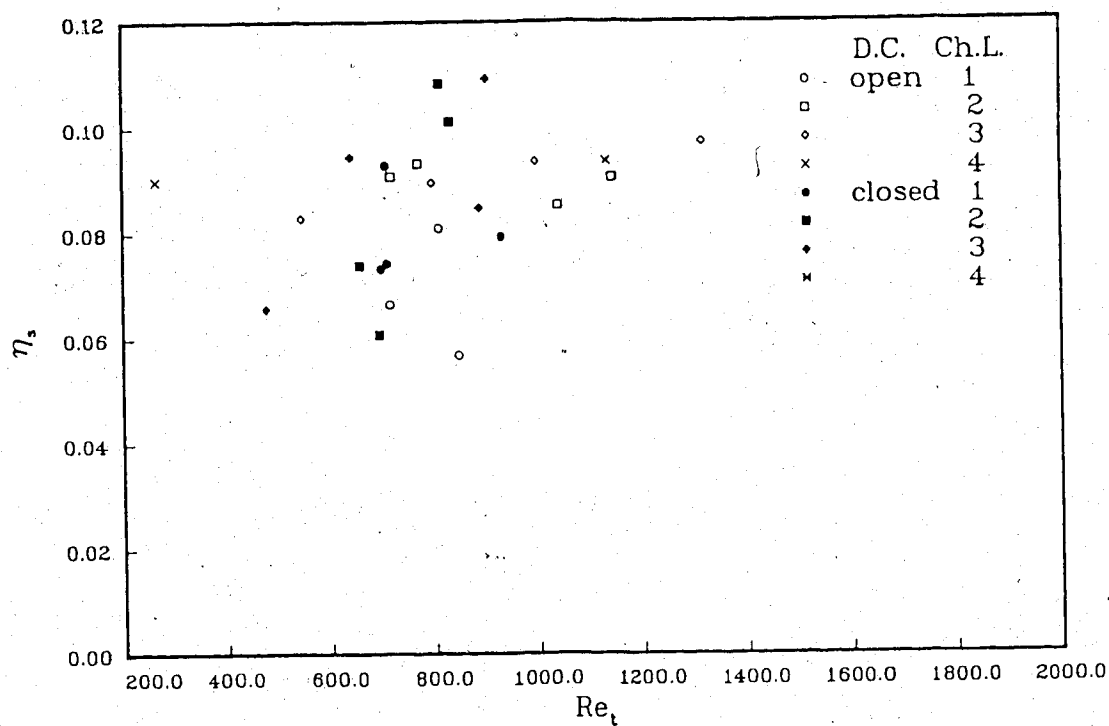


Fig. 3.5 System efficiency vs. Reynolds number based on the inlet fluid conditions for one evaporator tube

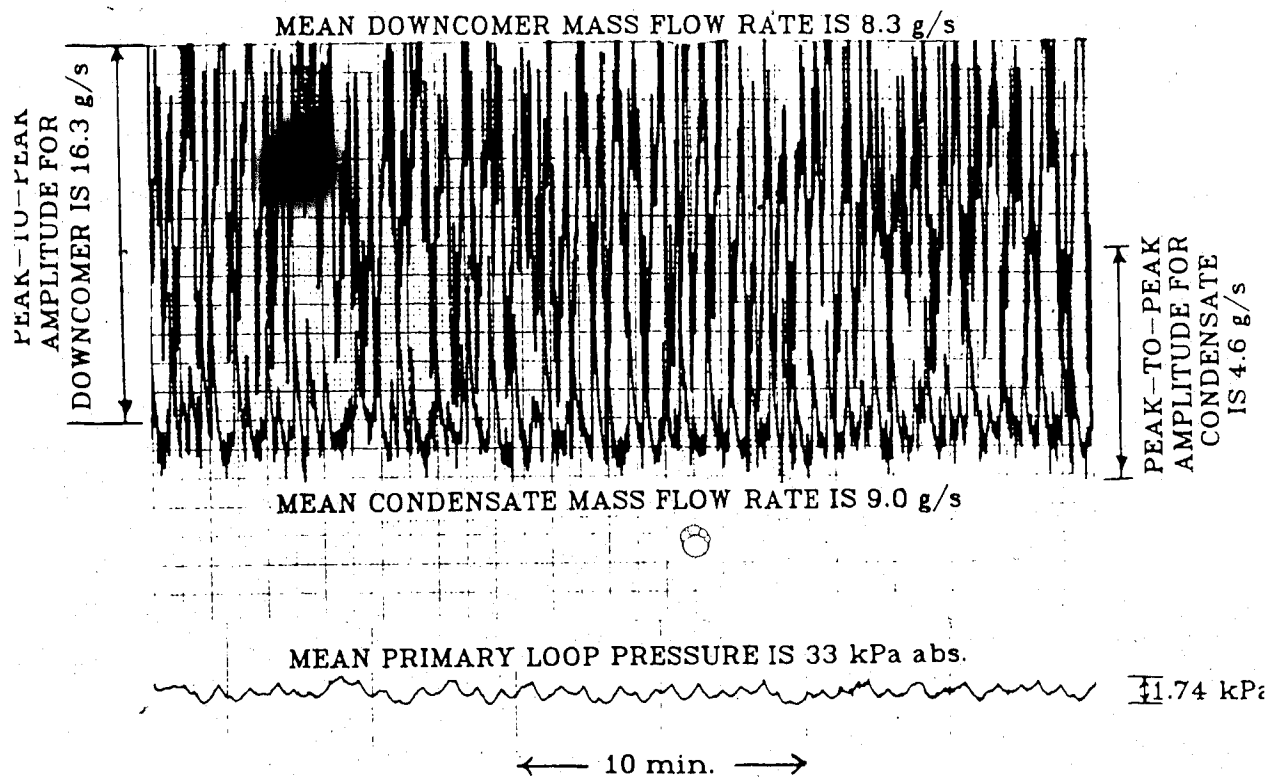


Fig. 3.6 Downcomer and condensate mass flow rates and system pressure recorded by chart recorders during steady state for Ch.L. 2, 21 kPa abs. pressure and 75°C air temperature

3.5.1 Evaporator results

Simultaneous temperature distributions along evaporator tube #4 on panel 1 and 3 are shown in Figs. 3.7 and 3.8. The two figures correspond to the same instantaneous recordings. These recordings were taken for charge level 4, the initial vacuum was 21 kPa and the downcomer tube was open. The evaporator tube wall temperature increases as the subcooled working fluid in the evaporator tube approaches saturation temperature. This temperature is reached in the upper half of the evaporator tube. The low quality working fluid flow is exposed to pressure drops, which causes decreasing saturation and working fluid temperatures, hence, the wall temperature decreases for the upper part of the evaporator tube. It is obvious from the two graphs that the working fluid flowed through the two evaporator tubes with a different flow condition at the same instant. This is believed to be caused by the system fluctuations during the boiling flow and by the heat and mass transfer characteristics being different for each evaporator tube as discussed in Section 2.6.

The overall heat transfer coefficient of the evaporator relative to the average wall heat flux from the evaporator tube to the working fluid is shown in Fig. 3.9. The overall heat transfer coefficient is based on the arithmetic mean difference of the inlet and outlet temperatures of the two fluids. Both overall heat transfer coefficient and the wall heat flux have increased compared to the single phase

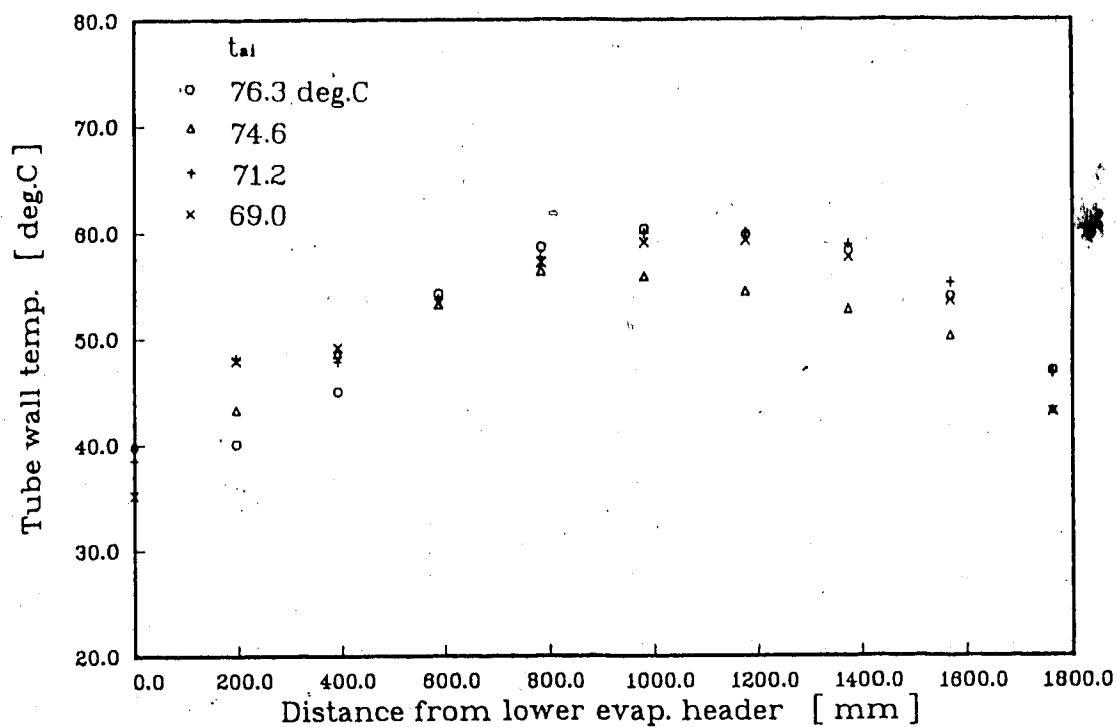


Fig. 3.7 Temperature distribution along the wall of evap. tube #4 on panel 1 at steady state (Ch.L. 4, 21 kPa abs. pressure, open downcomer)

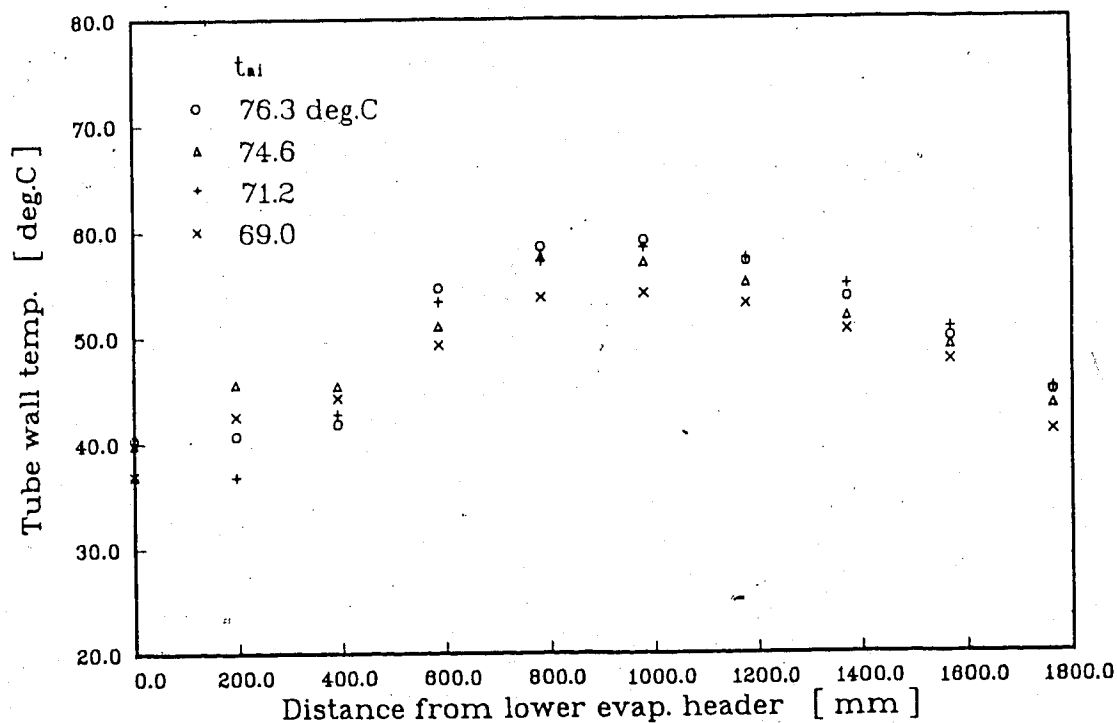


Fig. 3.8 Temperature distribution along the wall of evap. tube #4 on panel 3 at steady state (Ch.L. 4, 21 kPa abs. pressure, open downcomer)

thermosyphon results, Fig. 2.14. The range of the two-phase data points for different operating conditions seen in Fig. 3.9 (compare Ch.L. 1 and open D.C. towards Ch.L. 2 and closed D.C.) are caused by uneven air temperature difference between each test condition. These different system operating temperatures were necessary in order to obtain recordable working fluid flow rates as discussed earlier in Section 3.4. For some of the conducted tests working fluid flow rates were not obtainable for Ch.L.'s 3 and 4 either as can be seen in some graphs.

The overall heat transfer coefficient versus mass flux of the working fluid for one evaporator tube is shown in Fig. 3.10. A few data points for Ch.L.s 3 and 4 do not appear in the graph due to low working fluid flow rates.

The heat transfer coefficients for the air side of the evaporator, the combined convection and radiation (Fig. 3.11) and radiation (Fig. 3.12), agree closely (± 2 W/m²K) with those obtained during single phase thermosyphon tests, Figs. 2.16 and 2.17. The radiation component is somewhat smaller for the two-phase case, which is believed to be caused by the lower heating air temperatures.

The heat transfer coefficient for the working fluid side of the evaporator is plotted versus the mass flux of the working fluid for one evaporator tube in Fig. 3.13. The maximum two-phase heat transfer coefficient is almost three times higher than the single phase heat transfer coefficient shown in Fig. 2.18. The mass flux and the heat transfer

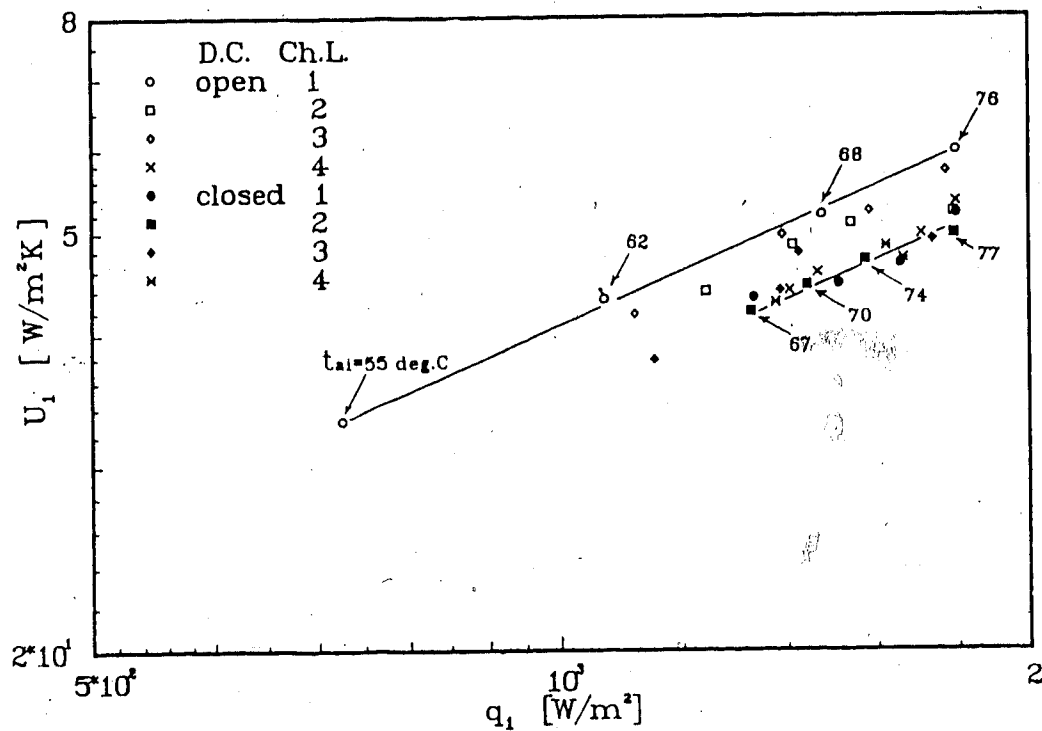


Fig. 3.9 Overall heat transfer coefficient of the evaporator vs. average wall heat flux from the evap. tube wall to the working fluid

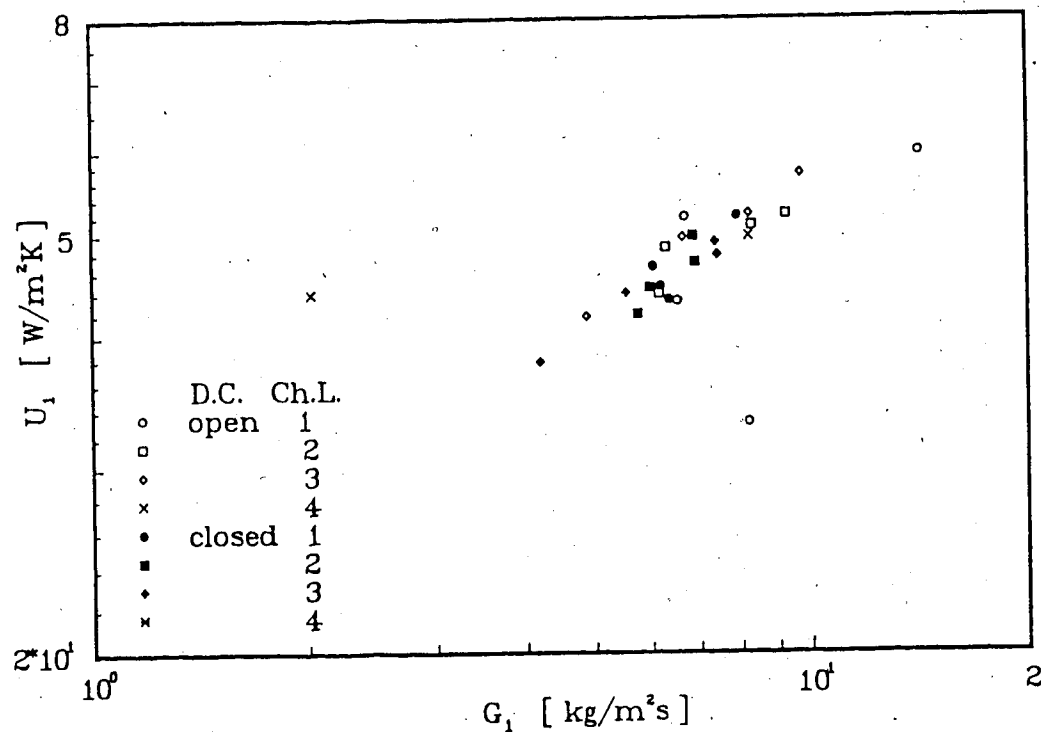


Fig. 3.10 Overall heat transfer coefficient of the evaporator vs. mass flux through one evaporator tube

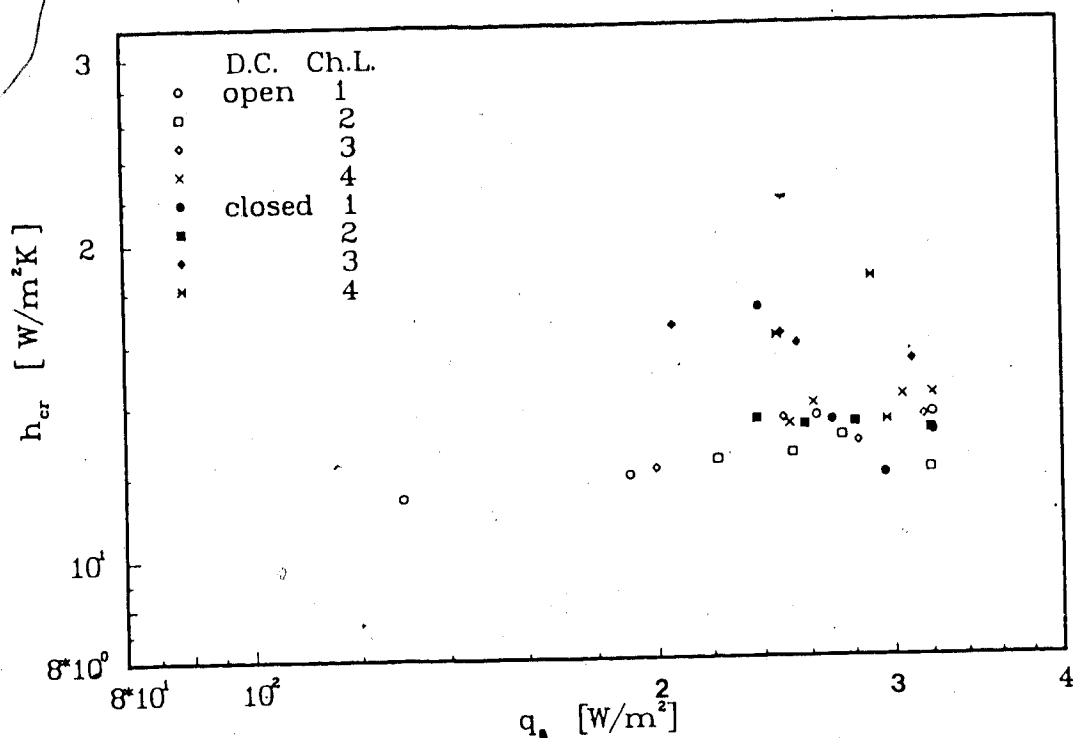


Fig. 3.11 Combined radiation and convection heat transfer coefficient vs. wall heat flux from air to evap. wall

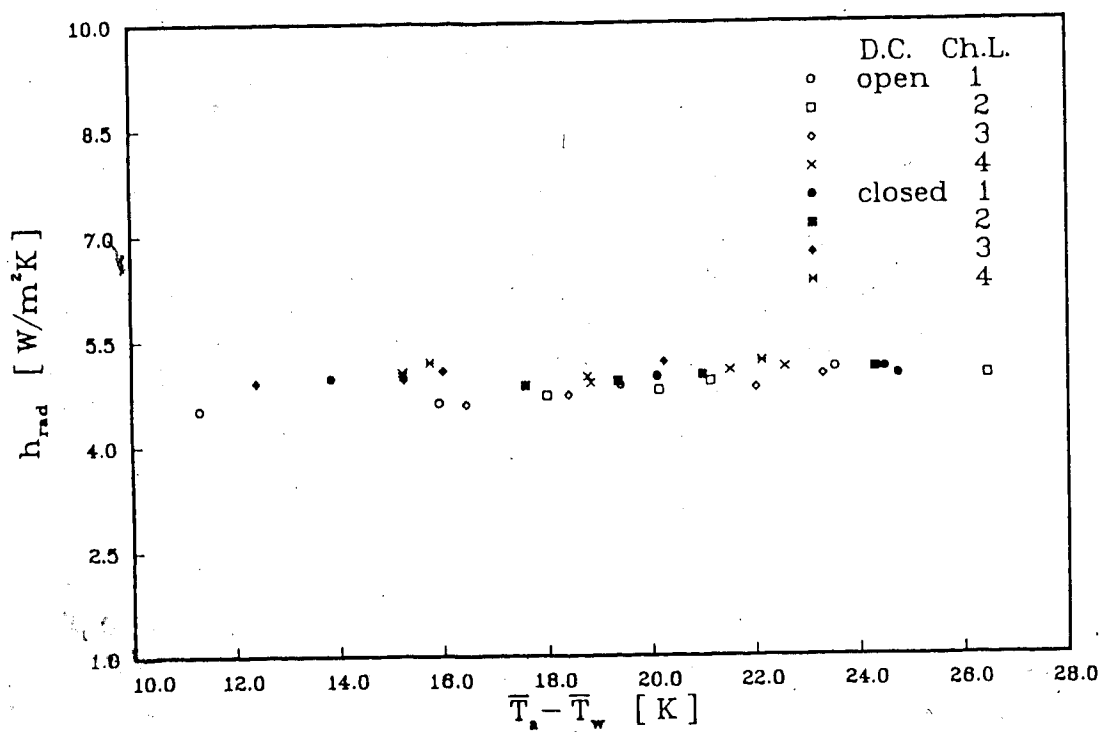


Fig. 3.12 Radiation heat transfer coefficient vs. difference between mean air and mean wall temperatures

coefficient data show a reasonable relationship for some test results (e.g. Ch.L. 3, open and closed D.C.), whereas for other operating conditions (Ch.L. 1, open D.C.) there is no apparent relationship. This is believed to be partly caused by the inherent fluctuations of the working fluid properties, and that some data were recorded during time periods when the flow rates had large deviations from the mean flow.

The strong functional relationship between the mass flux of the working fluid for one evaporator tube and the average wall heat flux from the evaporator wall to the working fluid observed for the single phase tests in Fig. 2.19 is not evident for the two-phase tests shown in Fig. 3.14. The reasons are believed to be the same as discussed in the text above.

The vapour quality exiting the evaporator versus the average wall heat flux from the evaporator tube wall to the working fluid is seen in Fig. 3.15. The vapour quality never exceeded 25%, therefore, Eq. (3.2) is applied to calculate all these data. One of the reasons for the low vapour qualities is the limited wall heat flux from the heating air to the evaporator panels (less than 2000 W/m^2). Most of the energy released by the air in the evaporator is used to heat the subcooled water to saturated liquid. When the working fluid is saturated, the high latent heat of vaporization of the water allows only low vapour qualities to exit the evaporator. This means that water is an impractical working

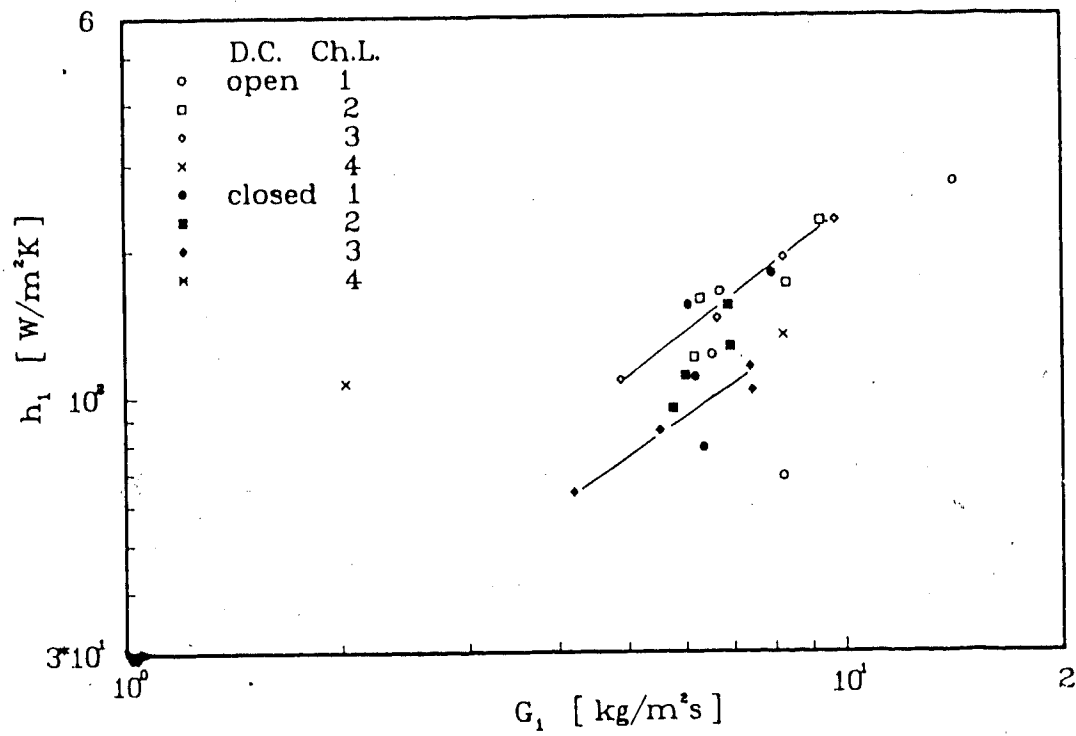


Fig. 3.13 Inside heat transfer coefficient of evaporator vs. inlet working fluid mass flux for one evap. tube

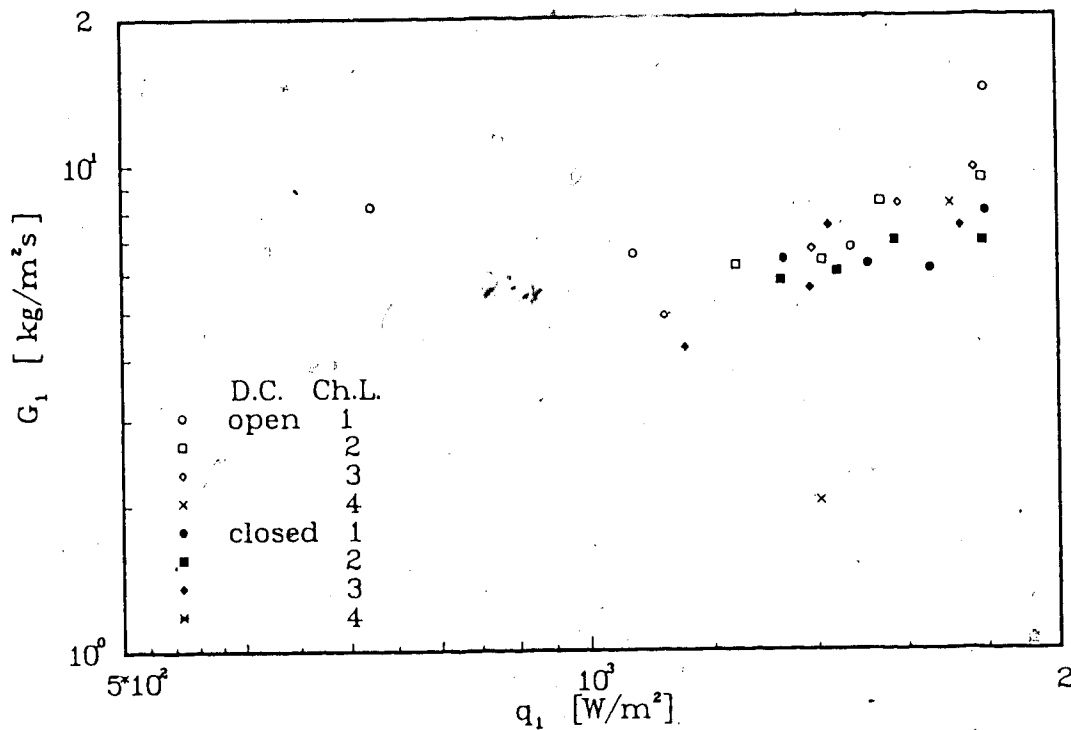


Fig. 3.14 Mass flux of the working fluid per evap. tube vs. average wall heat flux from evap. wall to working fluid

fluid for these test conditions. The low vapour quality exiting the evaporator explains why many of the obtained results for the two-phase thermosyphon tests compare favourably with the single phase test results.

Nusselt number for the working fluid in the evaporator is plotted as a function of inverse Graetz number in Fig. 3.16. Graetz number is calculated based the working fluid flow through one evaporator tube. The two-phase test results appears to be a continuation of the single phase results shown in Fig. 2.21. All the Nusselt numbers are still below 3.66 which is known as the minimum value for single phase test results conducted with constant wall temperature. These low results are believed to be partially caused by uneven flow distribution through the evaporator tubes. The low working fluid flow rates ($Re_1 = 19 - 115$), and the assumptions of equal heat and mass distribution for the working fluid through the evaporator do somewhat explain the the low Nusselt numbers.

3.5.2 The condenser results

The overall heat transfer coefficient for the condenser versus the average inside wall heat flux and entrance vapour quality of the working fluid are shown in Figs. 3.17 and 3.18 respectively. The overall heat transfer coefficient is based on the arithmetic difference of the entrance and exit temperatures of the two fluids. The wall heat flux results are basically the same as those obtained for the single

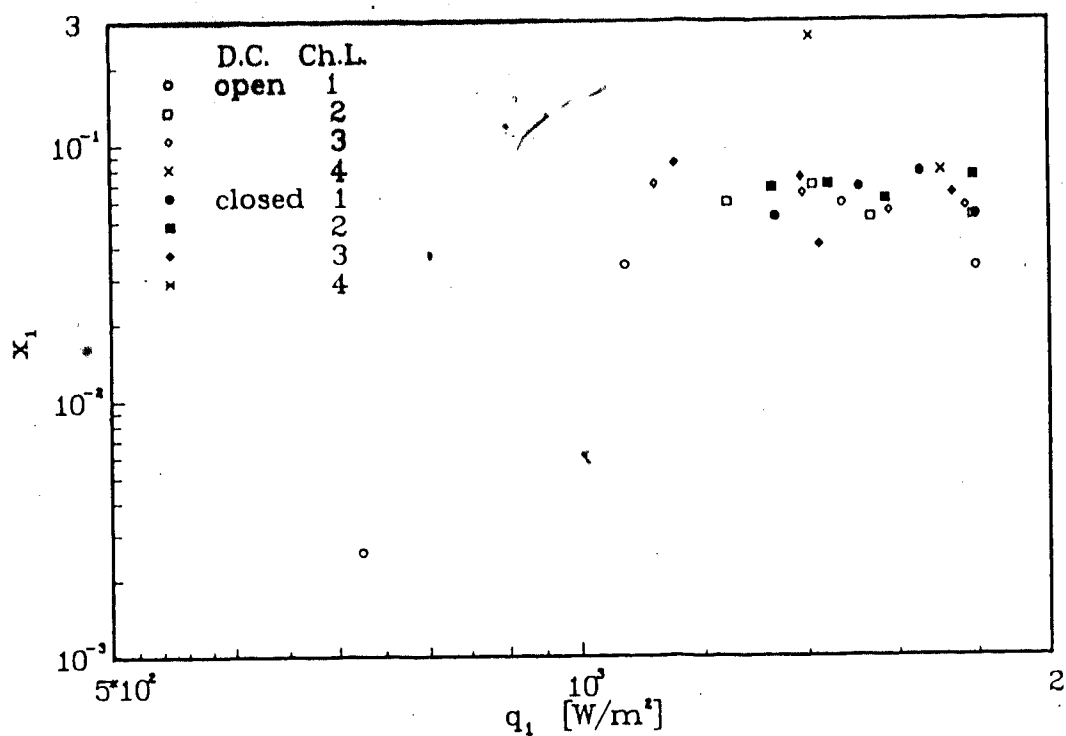


Fig. 3.15 Vapour quality exiting the evap. vs. average wall heat flux from evap. wall to working fluid

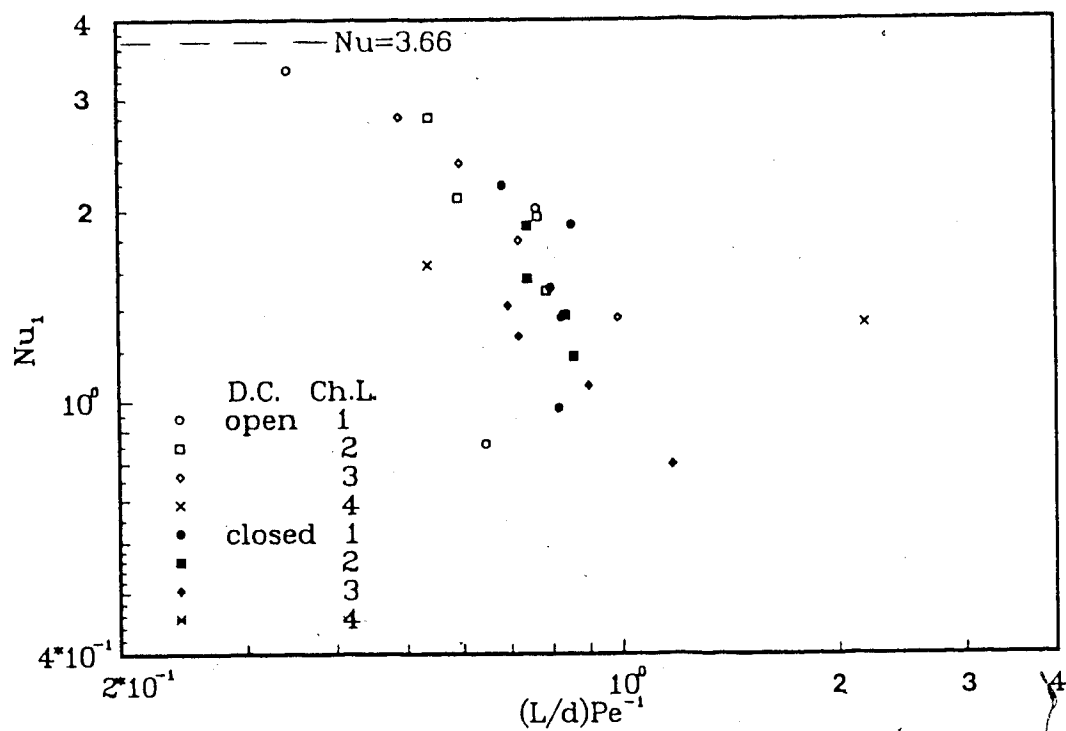


Fig. 3.16 Nusselt number for the working fluid vs. inverse Graetz number per evap. tube

phase tests, while the overall heat transfer coefficient has doubled in value, as shown in Fig. 2.23. This increase is caused by the lower temperature difference between the recorded mean working fluid bulk temperature and the average cooling water temperature through the condenser.

Opening the separator downcomer line increased the vapour qualities entering the condenser for charge level 3, whereas the effect of the separator is not obvious for the two highest charge levels 1 and 2, as seen in Fig. 3.18. These observations are reasonable, since the liquid levels for both Ch.L.s 1 and 2 are above the liquid-vapour separator.

The heat transfer coefficient of the fin side of the condenser coil, h_2 , for the two-phase working fluid is obtained using the same Eqs. (2.13) and (2.18) as employed during single phase heat transfer analyses. This heat transfer coefficient is shown versus average wall heat flux from working fluid to the condenser coil in Fig. 3.19 and versus vapour quality entering the condenser in Fig. 3.20. The heat transfer coefficient is increased compared to the single phase results in Fig. 2.25. This is caused by the overall heat transfer coefficient whose values has increased compared to the single phase test results as mentioned above.

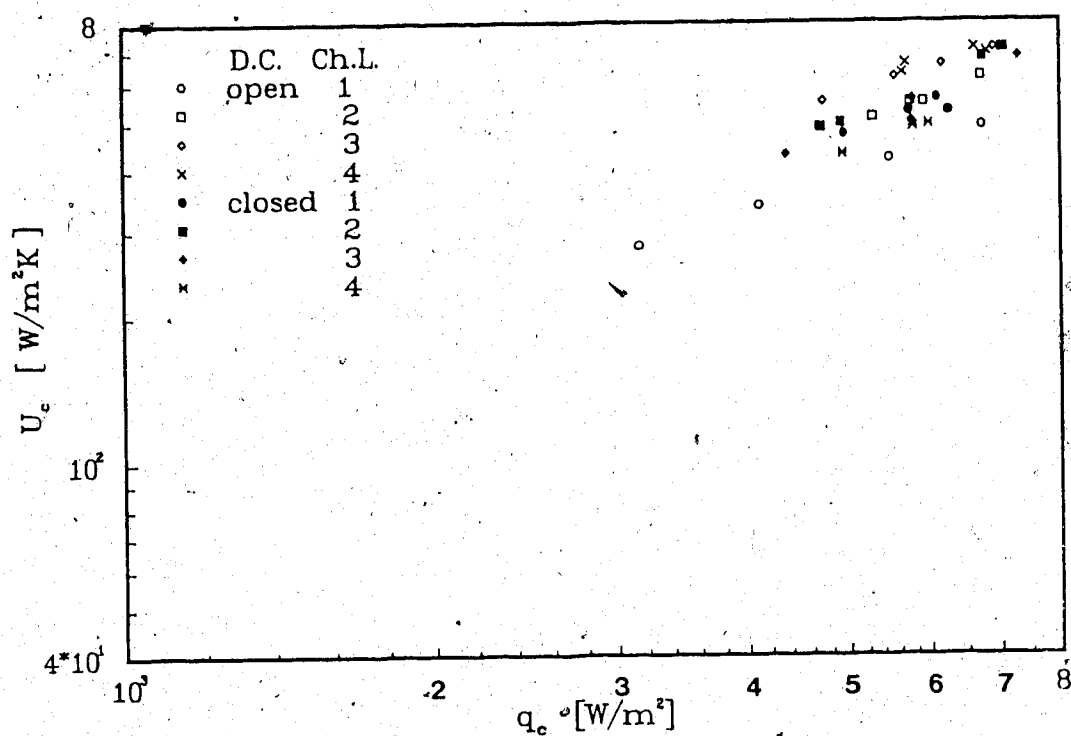


Fig. 3.17 Overall heat transfer coefficient of the condenser vs. average wall heat flux from wall to cooling water

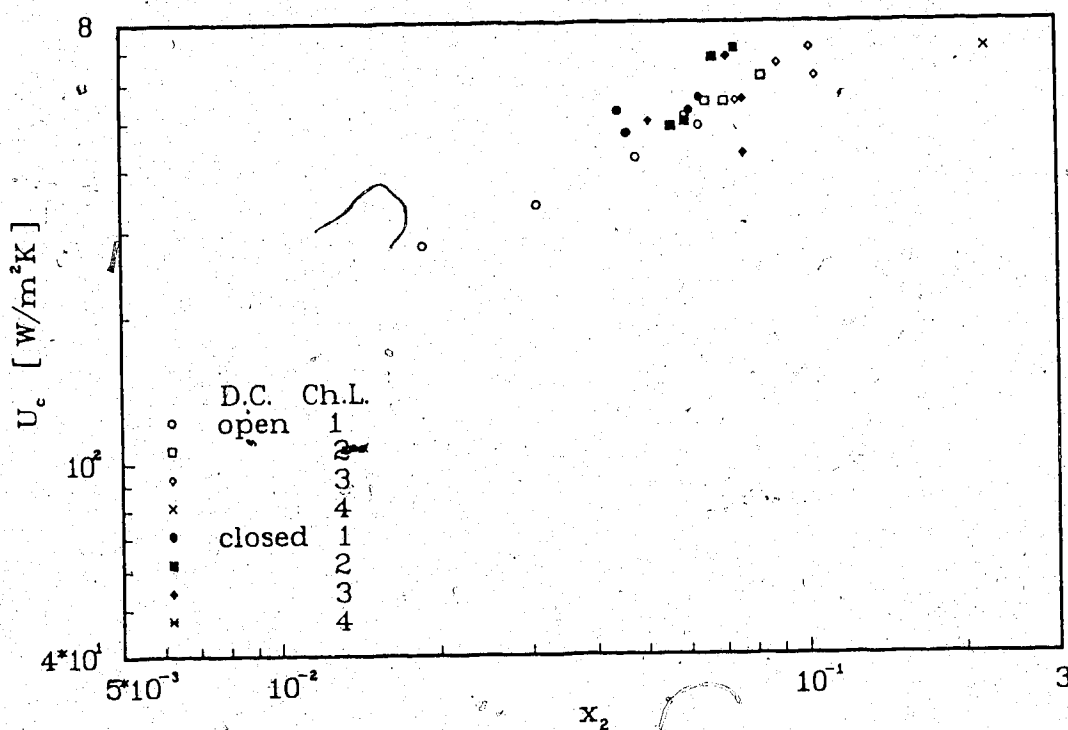


Fig. 3.18 Overall heat transfer coefficient of the condenser vs. vapour quality entering the condenser

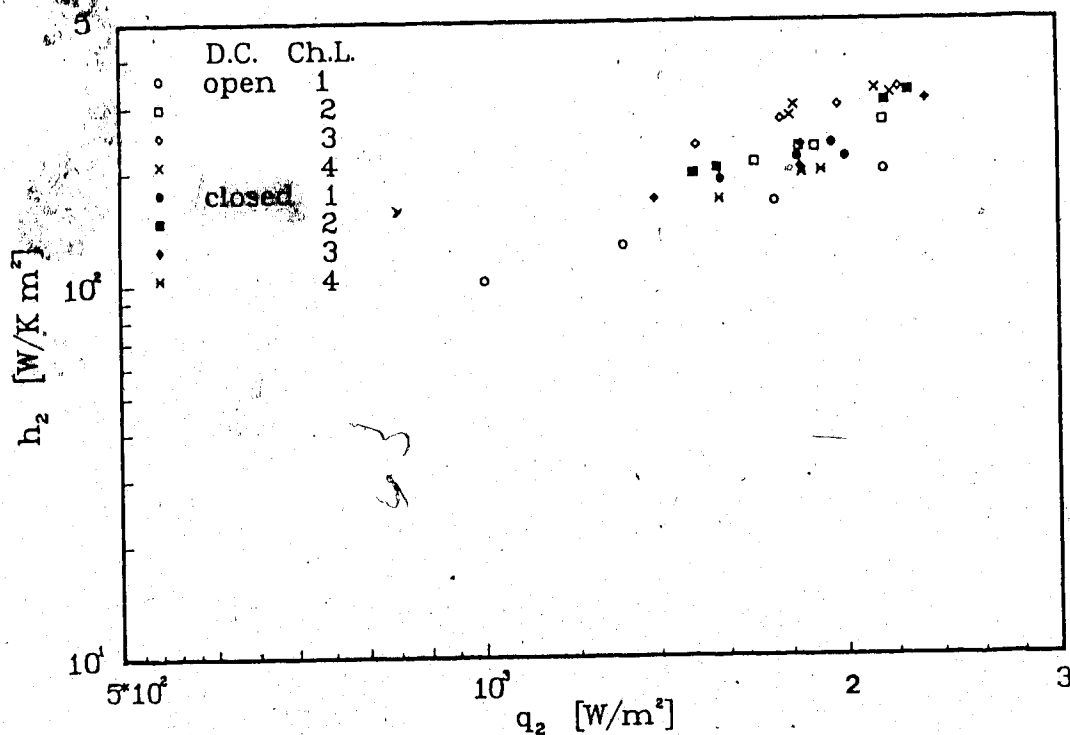


Fig. 3.19 Estimated heat transfer coefficient of fin side of condenser coil vs. average wall heat flux from working fluid to condenser coil

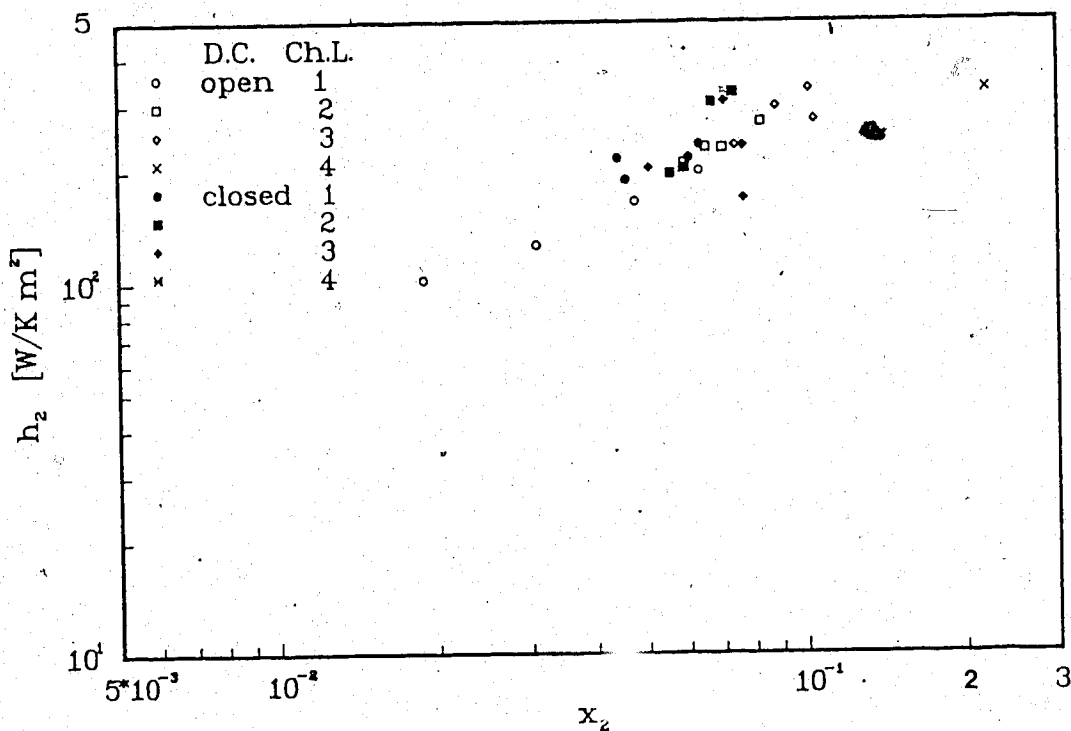


Fig. 3.20 Estimated heat transfer coefficient of the fin side of the condenser coil vs. entering vapour quality

3.5.3 Heat transfer correlations

The heat transfer coefficient results for the working fluid side of the evaporator, $h_{e,p}$ ¹³ is correlated with several empirical single phase and two-phase heat transfer coefficients.

The ratio of experimental to single phase Dittus-Boelter heat transfer coefficient, h , eq.(3.4), versus Boiling number and inverse Lockhart-Martinelli parameter are shown in Figs. 3.21 and 3.22 respectively. The ratio of experimentally obtained heat transfer coefficient to the liquid-only heat transfer coefficient based on the modified Dittus-Boelter equation, h , Eq. (3.5), is plotted versus Boiling number in Fig. 3.23. The reasonable heat transfer coefficient ratios between 1.0 and 2.0 for both the empirical liquid-only and single phase heat transfer coefficient indicates the low quality of the working fluid flow through the evaporator. One reason for the good agreement between the empirical values themselves and the reasonable agreement between the empirical values and the experimental values is the low vapour qualities obtained during these tests. Therefore the two-phase system results approach single phase heat transfer results.

Both Boiling number and the inverse Lockhart-Martinelli parameter are scattered over a relative narrow range, which is believed to be caused by the small changes of the vapour

¹³When this heat transfer coefficient is referred to in this subsection the experimental value is called $h_{e,p}$ rather than h_1 .

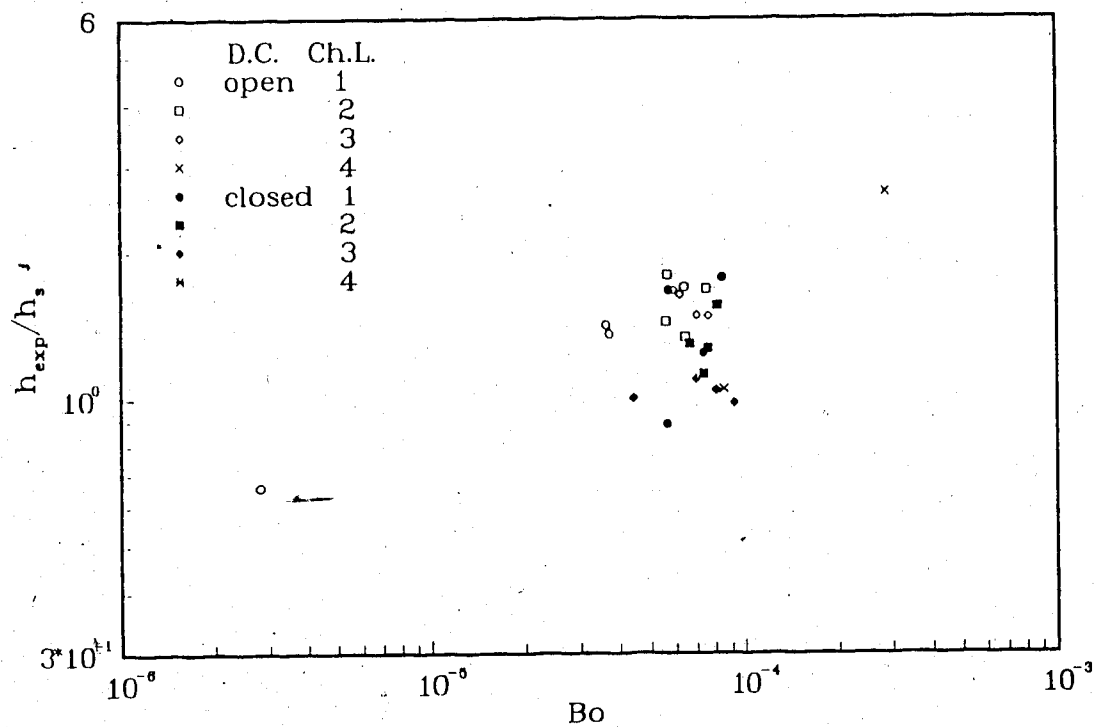


Fig. 3.21 Ratio of exp. to single phase Dittus-Boelter heat transfer coefficient vs. Boiling number

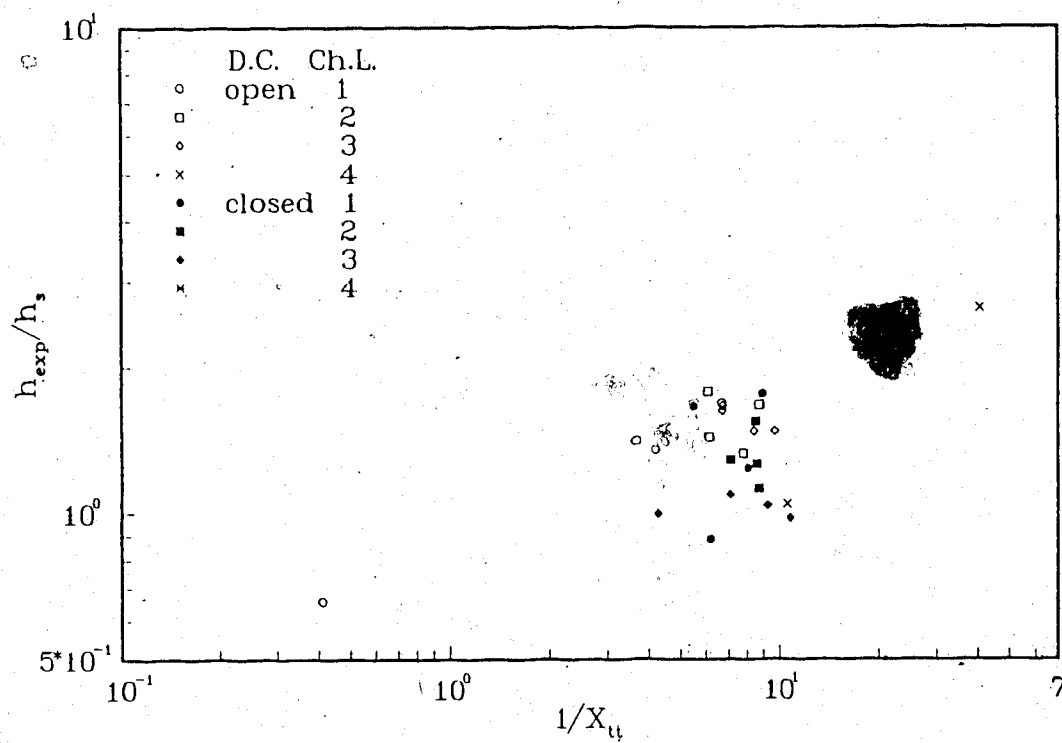


Fig. 3.22 Ratio of exp. to single phase Dittus-Boelter heat transfer coefficient vs. inverse Lockhart-Martinelli parameter

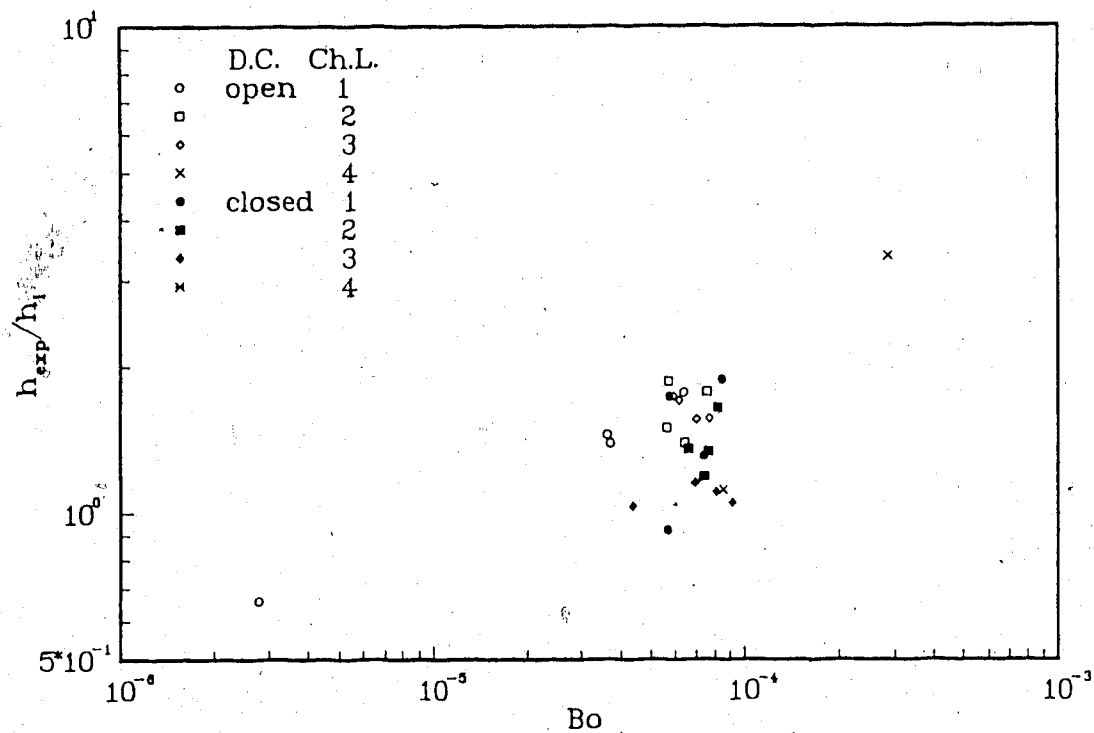


Fig. 3.23 Ratio of exp. to liquid-only Dittus-Boelter heat transfer coefficient vs. Boiling number

qualities.

The experimental heat transfer coefficient has lower values than the heat transfer coefficients obtained from the two-phase heat transfer correlations as shown in Figs. 3.24 - 3.27. In these figures the ratio of the experimental to the empirical heat transfer ratios are plotted versus Boiling number.

The experimental heat transfer coefficient is within the same order of magnitude as the heat transfer coefficients predicted with the empirical Schrock-Grossman and Shah equations. The Shah correlation shows the best agreement with the experimental results.

The experimental heat transfer coefficient is an order of magnitude lower than the heat transfer coefficients estimated with Kandlikar and Ref. [30] correlations as shown in Figs. 3.26 and 3.27.

3.6 Concluding Remarks

Water subjected to partial vacuum was used as working fluid in a two-phase closed-loop thermosyphon system. Four different initial working fluid pressures were investigated (21, 26, 35 and 47 kPa abs. pressure) with the liquid-vapour separator downcomer in both open and closed position. Each system condition was examined for four different charge levels, 1 to 4 (100, 96, 83 and 76% of the distance between the lower header of the evaporator and the horizontal centre line of the condenser). Tests were conducted for working

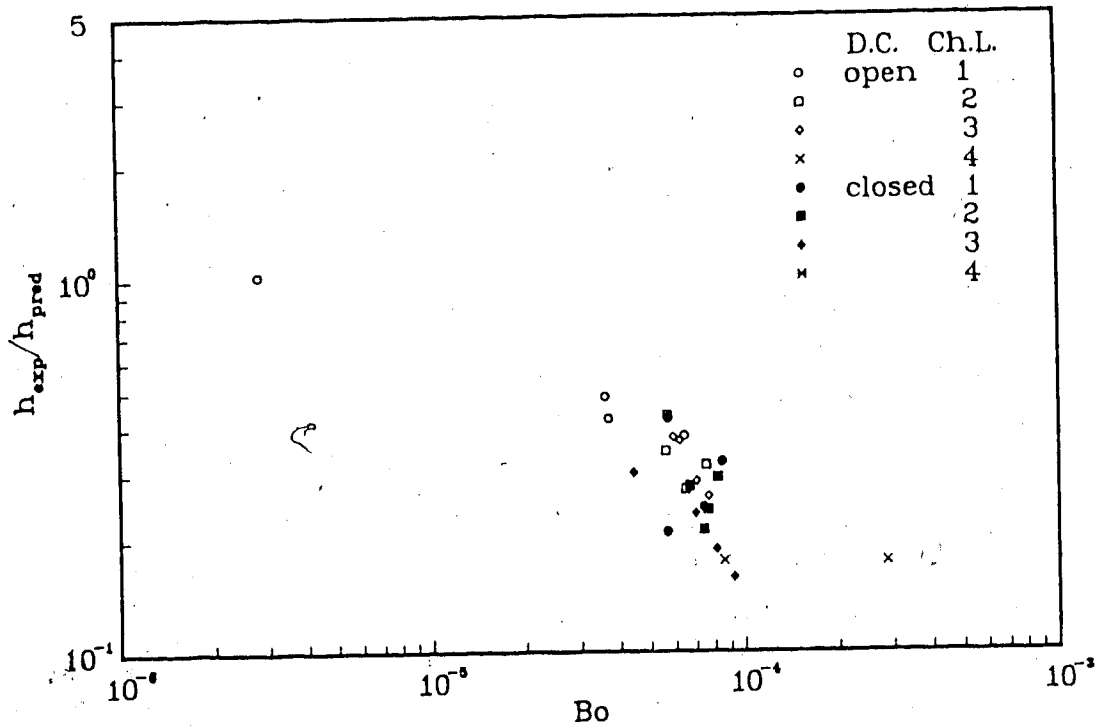


Fig. 3.24 Ratio of experimental heat transfer coefficient to Schrock-Grossman prediction vs. Boiling number

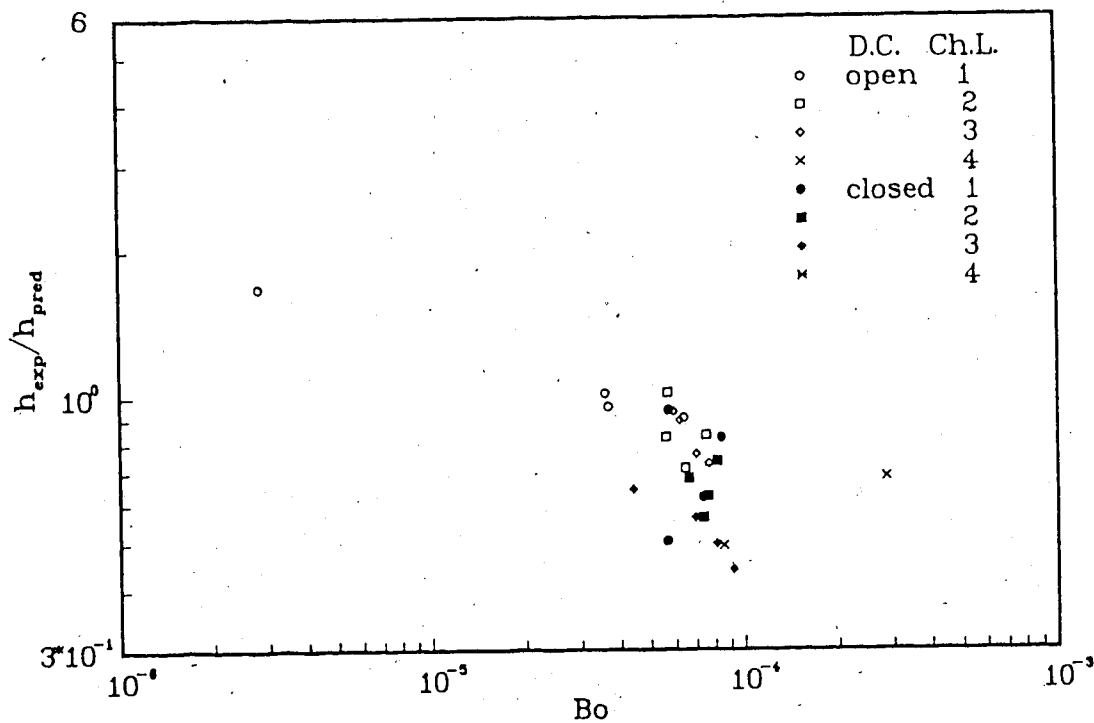


Fig. 3.25 Ratio of experimental heat transfer coefficient to Shah prediction vs. Boiling number

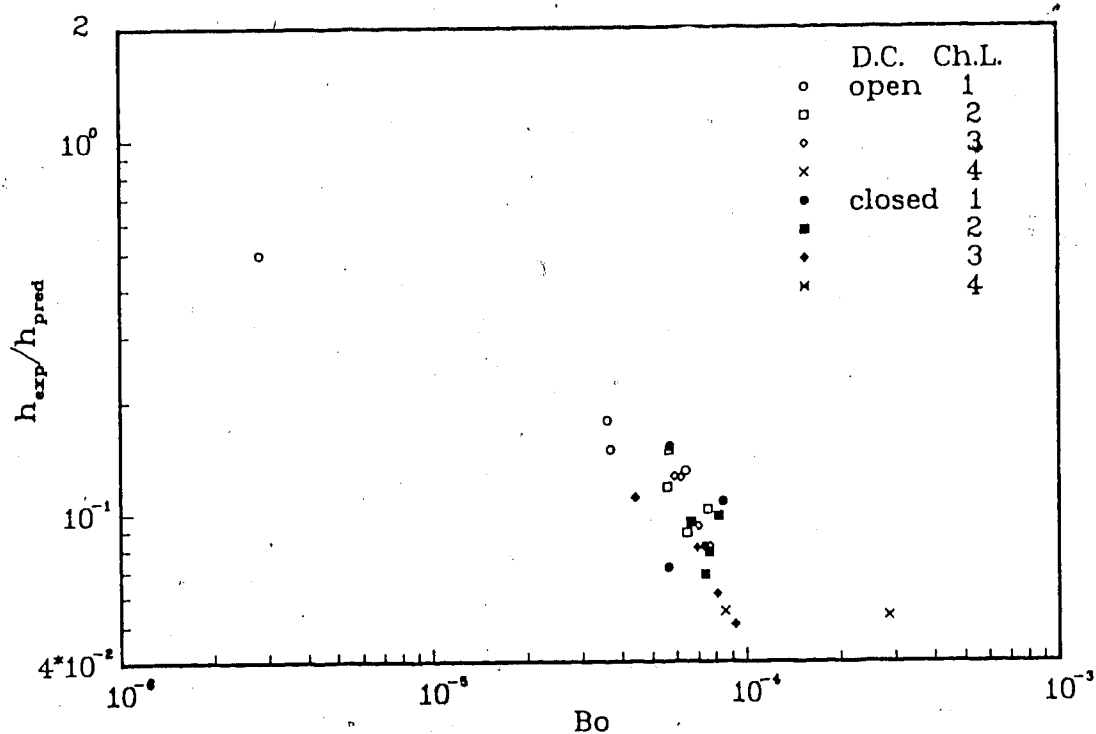


Fig. 3.26 Ratio of experimental heat transfer coefficient to Kandlikar prediction vs. Boiling number

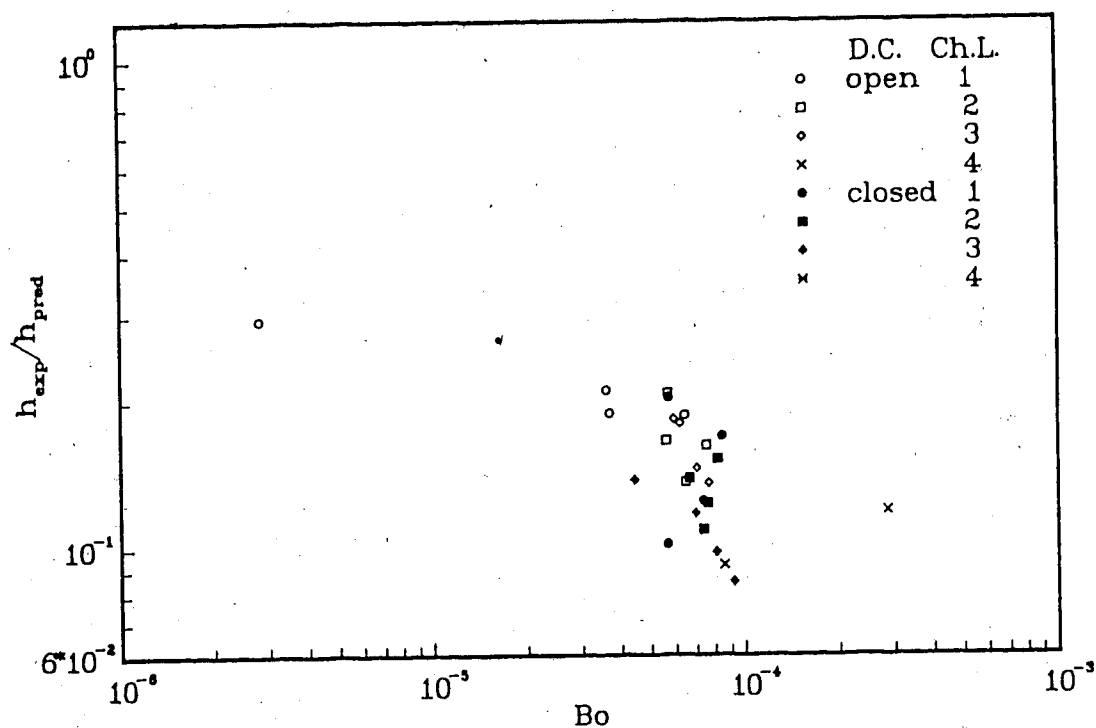


Fig. 3.27 Ratio of experimental heat transfer coefficient to prediction in [30] vs. Boiling number

fluid charge levels, 5 and 6 (59 and 41%). These data were not investigated, because recordable working fluid flow rates were not acquired.

Four heating air temperatures were studied for each system parameter when the downcomer line was open. Only two air temperatures were investigated when this line was closed. The highest obtainable air temperature was always studied for each charge level and working fluid vacuum as well as with the downcomer open and closed. The experiments were not always done with the same air temperature difference between consecutive tests. Problems with the system performance at lower air temperatures made it necessary to vary this temperature interval from 2 - 7°C depending upon the operating conditions.

Due to low working fluid flow rates, some data from working fluid charge levels 3 and 4 had to be discarded.

The system performance for the two-phase thermosyphon tests was comparable with the single phase thermosyphon results. The lower two-phase results were often seen to overlap the higher single phase test results. However, these two-phase water test results cannot be given too much emphasis, because the large working fluid property fluctuations encountered caused somewhat arbitrary data recordings over the relative short recording interval (less than 1 minute). It might have been better to record the data over half an hour period and used the average recording for the analyses.

The heat recovery rates of the system varied between 900 and 2300 W, the overall system efficiency was in the range of 6 - 11%, while the exiting cooling water temperature varied from 17 - 28°C. The saturation temperature of the working fluid was between 40 and 75°C depending upon the partial vacuum of the working fluid and the air temperature.

The low system efficiency is believed to be caused by inefficient system design or that water is an impractical working fluid for this application or a combination of both.

The inherent fluctuation of the working fluid flow rates and the pressure in the primary loop caused by flow boiling was continuously monitored on chart recorders as shown in Fig. 3.6. At higher working fluid charge levels and higher heat source temperatures, the fluctuations decreased in magnitude simultaneously as the mean values increased.

Both working fluid downcomer and condensate mean flow rates decreased towards zero as the liquid charge level was lowered (3 - 6) and the air temperature was decreased more than 2 - 6°C below maximum temperature for the particular system parameters, while the peak-to-peak amplitude of the fluctuation became more unpredictable until the flow rates became negligible. This caused some of the scattered data, since the recorded values occasionally varied considerably from the mean. It also explains why the results for some parameters did not always follow the expected relationship.

The experimental heat transfer coefficient agreed favourably with that predicted by the original and the modified Dittus-Boelter equations, as their ratio was mostly between 1.0 and 2.0. However, the experimental heat transfer coefficient values were from 4 to 50 times smaller than the predicted values obtained with four different correlation methods. This is believed to be caused by the low working fluid vapour qualities obtained during the experiments. Hence, the working fluid conditions were closer to single phase flow than two-phase flow.

It must be concluded from these tests that water was an impractical working fluid for this two-phase closed-loop thermosyphon system, particularly because of operating limitations of the system. The advantageous high latent heat of vapourization, which water has, was not utilized, particularly because of the low wall heat flux from the air to the evaporator wall.

4. A Closed-Loop Two-Phase Thermosyphon System Using Freon R-11 as Working Fluid

Summary

Freon R-11 is used as the working fluid in a closed-loop two-phase thermosyphon. The absolute working fluid pressure is 122 kPa. Six working fluid liquid levels 100, 96, 83, 76, 59 and 41% (1 to 6)¹ are studied and the liquid-separator downcomer tube is always open. The thermosyphon loop recovers heat from hot air whose volume flow rate is 0.44 m³/s and temperature ranges from 40 to 68°C. This heat is transported to cooling water with flow rate 40 g/s and initial temperature 12 - 13°C.

The heat rates recovered by the cooling water ranged from 800 to 2800 W and the temperatures of the cooling water exiting the the condenser varied between 17 and 31°C. The vapour qualities exiting the evaporator ranges from 20 to 100% and superheated vapour was obtained for three test runs. The system efficiency, 9 - 17%, showed improvements compared with the efficiency for the two phase water test, 6 - 11%. Reasonable correlations were found when the experimentally obtained heat transfer coefficient was compared with the empirical heat transfer coefficients [30,32].

¹ Defined as a fraction of the vertical distance between the lower evaporator header and the horizontal centre line of the condenser.

4.1 Introduction

The final part of this study is to investigate the performance of the system using Freon R-11 as the working fluid of the primary loop. Even though the specific heat and latent heat of vaporization of R-11 are almost five and thirteen times lower than that of water respectively, the refrigerant still has high latent heat of vaporization (relative to most refrigerants [36]) and low boiling point (23.7°C at std. atm. pressure). The low boiling point and the relatively low latent heat of vaporization are both advantageous when heat recovery from low temperature heat sources (below 100°C) is desired and the wall heat flux is low.

The tests were conducted with various heating air temperatures and wall heat flux. Other operating parameters like air flow rate, cooling water flow rates and cooling water temperature are not changed for these tests. The downcomer of the liquid-vapour separator was always open for all the tests performed.

The experimentally obtained heat transfer results are correlated with empirical methods.

4.2 Experimental Apparatus, Instrumentation and Calibration

The system and the instruments used are the same as shown in Fig. 3.1 in Section 3.2. The only exception is a refrigerant filter-drier installed in parallel with the condensate line of the primary loop.

All the turbine flow meters, pressure transducers and sheathed thermocouples were calibrated according to the procedure in Section 2.3. The differences between the old and the new calibrations were small, less than 0.5%. However, the new calibrations were used during the experiments.

4.3 Experimental Procedure

The system was leak tested under pressure (300 kPa) for 48 hours and partial vacuum (27 inHg) for 48 hours, before it was charged with Freon R-11. The leak-testing procedure is explained in Section 3.3. When no leaks were detected the system was charged completely via the storage tank. All the air was evacuated from the working fluid loop. Then the desired liquid level was obtained according to the procedure explained in Section 3.3.

Six charge levels 100, 83, 76, 59 and 41% (generally referred to as levels 1, 2, 3, 4, 5 and 6 as shown in Fig. 3.2 in the previous chapter) were studied with the downcomer open. At each charge level, the system was tested with four air temperatures (40, 50, 60 and 68°C), where 68°C was the highest obtainable air temperature. The initial pressure in the primary loop (122 kPa), the air volume flow rate (0.44 m³/s), the cooling water mass flow rate (40 g/s) and the temperature of the cooling water at the condenser inlet (12-13°C) were constant for all experiments.

After each charge level change, the system was allowed a 24 hour stabilizing period before a new set of tests were commenced. The testing and data recording procedures are explained in Sections 2.4 and 3.3.

4.4 Basic Equations for Data Analysis

The methods and equations employed for this system analysis are the same as used for two-phase water tests in Chapter 3. The only new variable introduced in this chapter is the working fluid, Freon R-11. The thermodynamic properties of R-11 are calculated using empirical equations, developed by Fujii, Nozu and Honda [37]; listings of Fortran routines are given in Appendix IV.

The equations employed in the calculations and data analyses in this chapter are the same as used in Chapters 2 and 3. Therefore, these previously defined equations will be referred to rather than redefining the equations in this section.

The fluid and flow dependent constants used in the two-phase correlation proposed by Kandlikar, Eq. 3.11, are shown in Table 4.1.

4.5 Results and Discussion

Two data sets were recorded when the system had reached steady state. The results from these two readings compared well, as seen in the graphs, where data points from both readings are plotted.

TABLE 4.1: CONSTANTS USED IN THE KANDLIKAR CORRELATION
FOR VERTICAL FREON R-11 FLOW

D1	D2	D3	D5	F
1.091	-0.948	887.46	0.726	1.35

Note: The constants are valid for $Co < 0.65$

The overall system, evaporator and condenser results and the the heat transfer correlations are discussed in different subsections.

4.5.1 The overall system results

A summary of the operating characteristics is shown in Table 4.2.

For the majority of the tests the difference between the highest working fluid temperature and the ambient temperature ranged between 7 and 10°C, and for no experiment did this temperature difference exceed 18°C. For the single phase water tests similar temperature differences ranged from 40 to 60°C. The heat rates lost across the connecting tubes and ~~and~~ condenser insulation varied between 25 and 91 W, as shown in Table 2.6. Since the temperature differences are much lower for the two-phase experiments discussed in this chapter, it is assumed that these heat losses can be neglected.

The heat rate recovered by the working fluid in the evaporator versus the heat rate recovered by the cooling water is shown in Fig. 4.1. The heat rates lost by the R-11 to the surroundings can be found in this figure. The losses

TABLE 4.2: SUMMARY OF THE OPERATING CHARACTERISTICS
FOR FREON R-11 TESTS

VARIABLES	EVAPORATOR	CONDENSER ¹
Air volume flow rate [m^3/s]	0.44	
Air temperature [$^{\circ}\text{C}$]	40-68	
Liquid mass flow rate [g/s]	12-65	40
Outlet minus inlet water temp. [K]		6-16
Maximum outlet water temp. [$^{\circ}\text{C}$]		30.1
Heat supply (air) [W]	1200-3400	
Heat recovery [W]		900-2850
Wall heat flux [W/m^2]	600-2200 ²	2800-9000
Heat transfer coefficient [$\text{W}/(\text{m}^2\text{K})$]	150-1600 ²	140-550
Overall heat transfer coefficient [$\text{W}/(\text{m}^2\text{K})$]	48-87 ³	370-1000
Vapour quality [%]	8.5-100	20-100
Nusselt number	14-150 ^{2, 3}	
Reynolds number	19-115 ⁴	
Reynolds number	200-1300 ⁵	3500
Dean number		1200
Graetz number	1.5-2.5	47
Boiling number	0.00008-0.001	
Lockhart-Martinelli parameter	0.8 $\rightarrow\infty$	
$h_{e, x_p}/h_s$	2-50	
$h_{e, x_p}/h_i$	5 $\rightarrow\infty$	
$h_{e, x_p}/h_{t, p}$ (Kandl.)	0.6-4.5	
$h_{e, x_p}/h_{t, p}$ ([30])	0.45-3.	
Efficiency:	8.5-17% ⁶	

Notes:

- ¹ Cooling water
- ² Working fluid
- ³ Based on AMTD.
- ⁴ W.fl. flow (1 evap.tube)
- ⁵ Total w.fl. flow
- ⁶ Overall system

are small, normally less than 5%, which verifies that the used assumption is reasonable.

The heat rate recovered by the cooling water is shown against the extreme temperature difference of the system in Fig. 4.2. The heat recovery rate increases with increasing air temperature, as one would expect. Smaller temperature

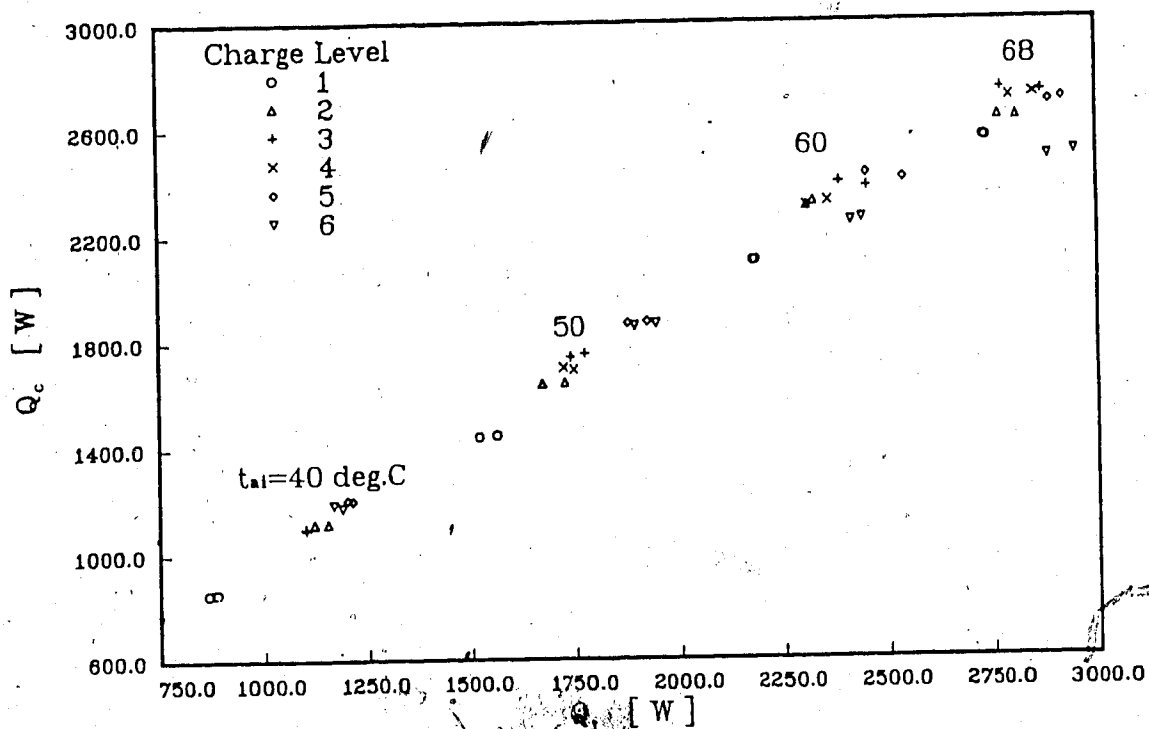


Fig. 4.1 Heat recovered by cooling water vs. heat recovered by working fluid in evap.

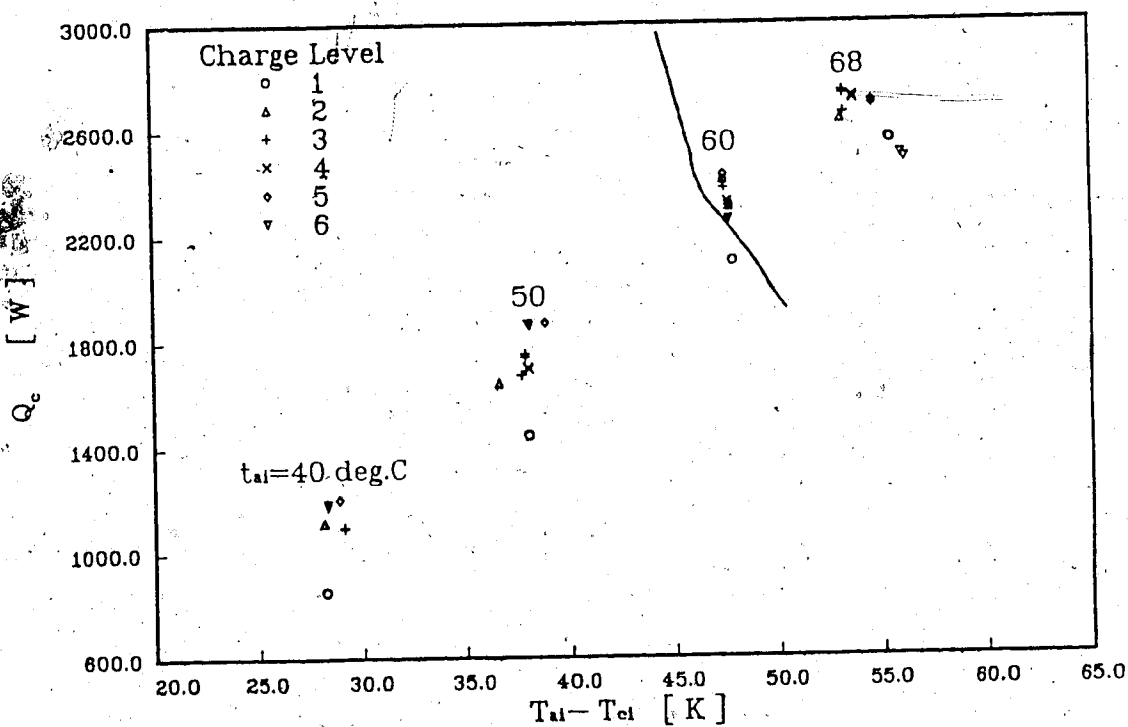


Fig. 4.2 Heat recovered by cooling water vs. heating air temperature minus entrance cooling water temperature

differences causes higher heat recovery rates (max. 2800 W) compared with the two-phase water results (max. 2300 W) shown in Fig. 3.3.

Flow visualization studies were performed for a similar condenser used in a closed-loop two-phase thermosyphon system employing Freon R-113 as the working fluid [38,39]. This investigation showed that the liquid level of the working fluid in the condenser increased as the heat source temperature increased. Tests conducted with a charge level as low as 20% and a heat source temperature of 85°C had condensate in the condenser covering half the heat transfer area of the condenser coil. It was observed that when the condenser coil was mainly covered with liquid, most of the refrigerant vapour condensed in the liquid before reaching the condenser. Furthermore, the study showed that the higher the initial charge level was, the lower heating source temperature was needed to cover the condenser coil with condensate. For the highest charge level (identical to Ch.L. 1 in the present study) the condenser coil was almost covered with working fluid for the lowest heating source temperature (45°C). The liquid covering the surface area of the condenser coil increases the resistance to heat transfer from the working fluid to the copper coil compared to a liquid-vapour film covering the coil. In the present study the condensate is believed to collect in the condenser in a similar manner, hence, being one cause for the low system performance encountered.

The system efficiency, Eq. (2.27), versus the average wall heat flux for the working fluid side of the evaporator is shown in Fig. 4.3. The system efficiency has increased compared with the water results shown in Figs. 2.6 and 3.4. However, a maximum system efficiency of 17% indicates that either the system design has to be improved or that Freon R-11 is not suitable as working fluid for this system.

The system efficiency increases with increasing air temperature for charge level 1 (from 9 to 15%) as seen in Fig. 4.3. For charge levels 2, 3 and 4 the efficiency changes little (from 13 to 17%) over the operating range of the air temperature (40 - 68°C), while the efficiencies decrease as maximum air temperature is approached for the two lowest charge levels. The probable cause for these results will be discussed later in this section.

Representative fluctuations of the working fluid flow rates, temperature and pressure caused by the flow boiling are shown in Fig. 4.4. The results are recorded with a chart recorder at steady state conditions for an air temperature of 68°C and for charge level 2. The mean mass flow rates are 15.0 g/s for the condensate and 47.6 g/s for the downcomer flow. These results are higher than the recorded mass flow rates for two-phase water (9.0 g/s for the condensate and 8.3 g/s for the downcomer) shown in Fig. 3.6. The fluctuations recorded for the R-11 tests have much lower peak-to-peak amplitudes (condensate flow=1.1 g/s and separator downcomer flow=4.5 g/s) than what are recorded for

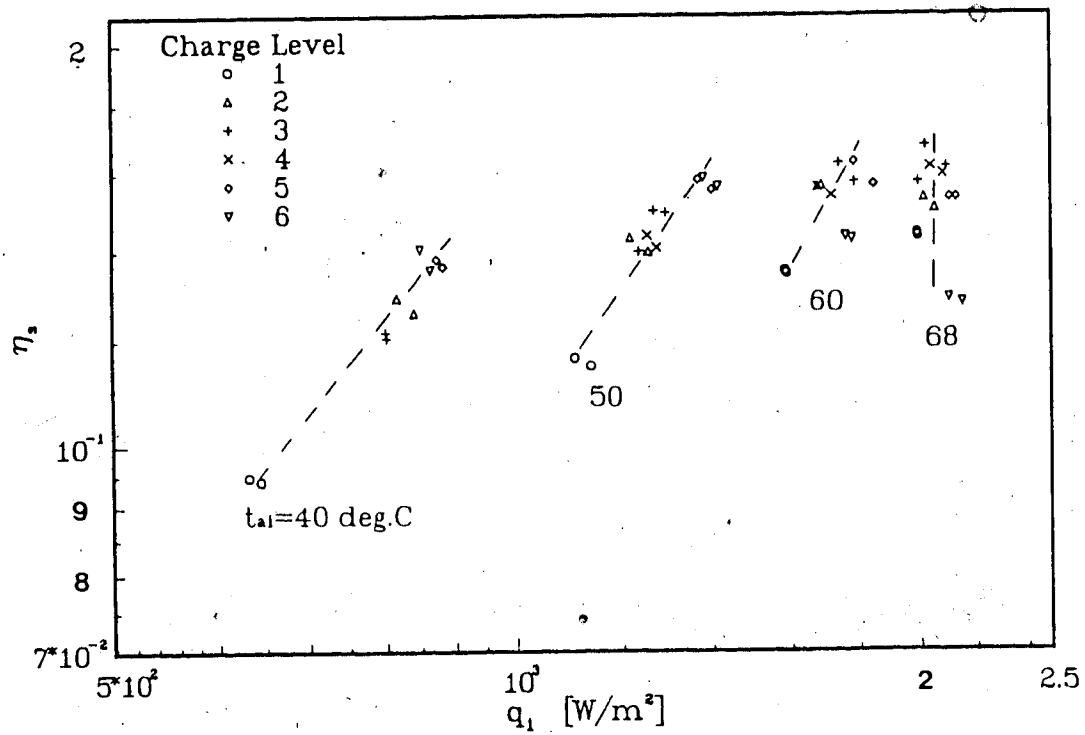


Fig. 4.3 System efficiency vs. average wall heat flux for the working fluid side of the evaporator

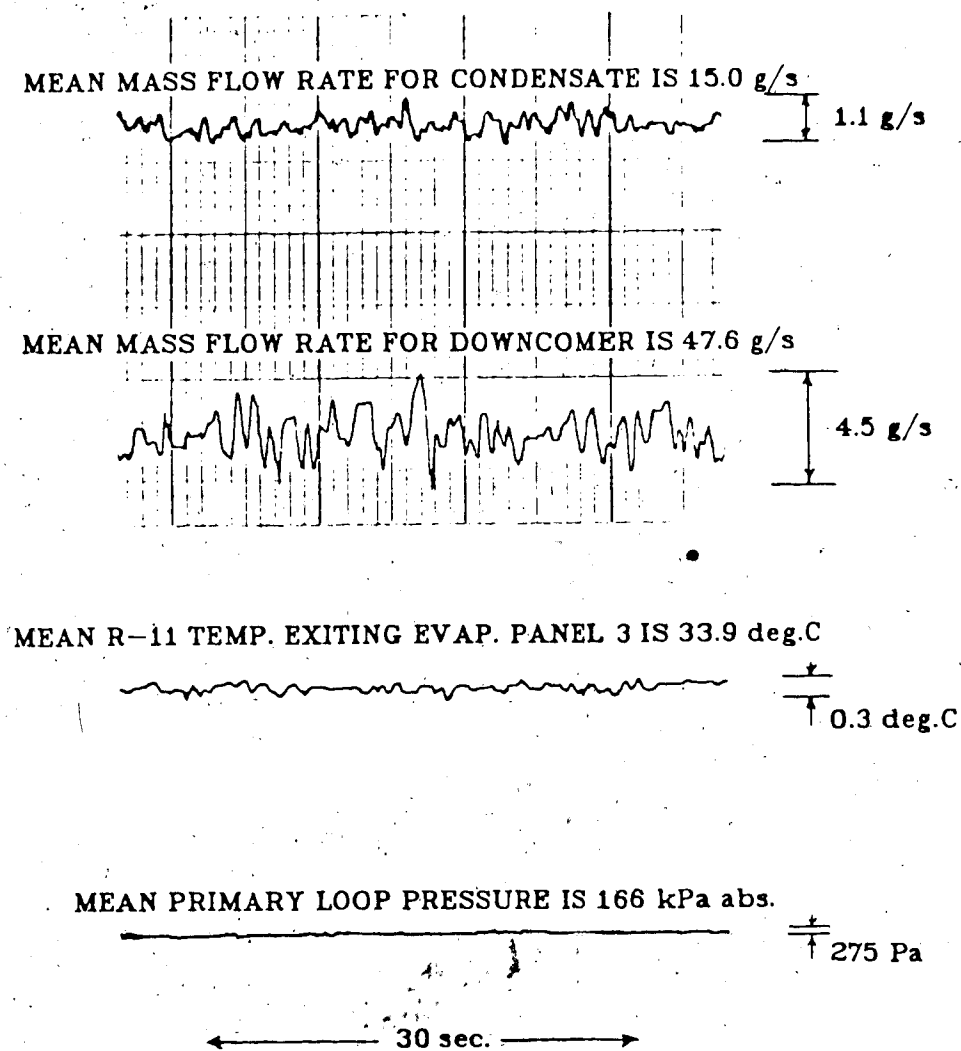


Fig. 4.4 Fluctuations of working fluid properties due to flow boiling (air temperature=68°C, Ch.L. 2)

the two-phase water tests (condensate flow=4.6 g/s and separator downcomer flow=16.3 g/s) for the same working fluid charge level. This is indicative of the improved system performance caused by the change of working fluid from water to R-11.

4.5.2 The evaporator results

The wall temperature distribution for evaporator tube #4 of panel 3 (this evaporator tube is indicated in Fig. 2.2b) is shown in Figs. 4.5, 4.6 and 4.7, where temperature distributions for charge level 1 (Fig. 4.5), charge level 3 (Fig. 4.6) and charge level 6 (Fig. 4.7) are shown. Results from the two data sets for the steady system are shown in the figures, and only small deviations are observed.

The sensible heating and subcooled boiling of the working fluid can be observed in the figures as the wall temperature is seen increasing for the lower part of the evaporator tube. When saturated boiling occurs, the wall temperature becomes constant. Higher heating air temperature increases the vapour pressure of the Freon and causes higher saturation temperatures. Tests done with the two highest air temperatures and charge level 6 caused the temperature of the upper part of the tube wall to increase as shown in Fig. 4.7. This occurs when the working fluid reaches dry-out and superheating [40]. This occurred for the two mentioned system conditions and for the highest air temperature with

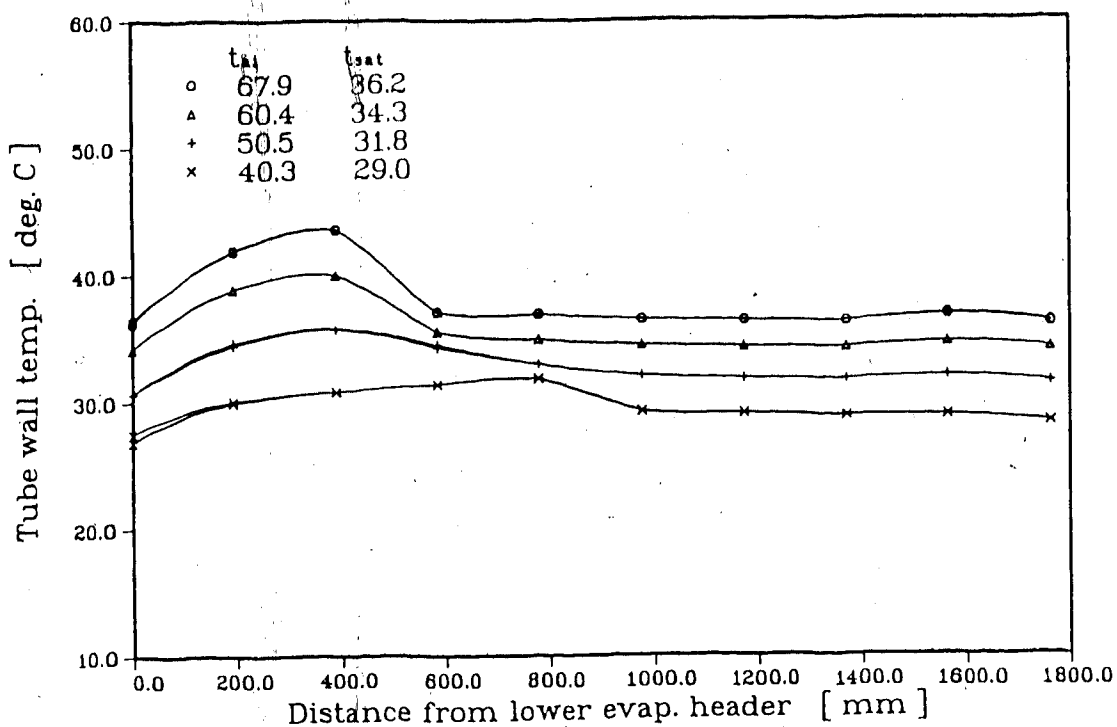


Fig. 4.5 Wall temperature distribution for evaporator tube #4 on panel 3 (air volume flow rate is 0.44 m³/s, Ch.L. 1)

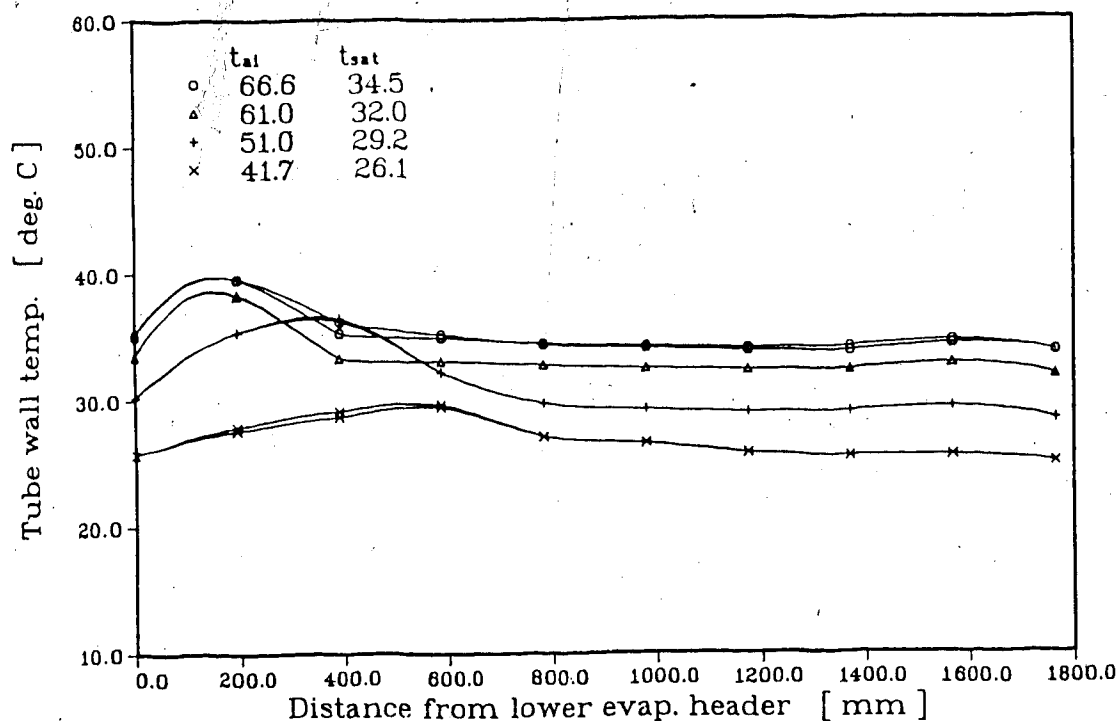


Fig. 4.6 Wall temperature distribution for evaporator tube #4 on panel 3 (air volume flow rate is 0.44 m³/s, Ch.L. 3)

charge level 5. The onset of boiling is seen to occur lower in the evaporator tubes with higher air temperatures and lower charge levels.

The overall heat transfer coefficient of the evaporator, based on the arithmetic mean difference of the entrance and exit fluid temperatures is shown in Fig. 4.8, plotted against the average wall heat flux for the working fluid side of the evaporator. The maximum overall heat transfer coefficient is more than 15% higher than the water test results as shown by comparison of Fig. 4.8 with Fig. 3.9. The similar dependency of the overall heat transfer coefficient on wall heat flux for both the refrigerant and water tests is expected, given the definition of the overall heat transfer coefficient, Eqs. (2.6) and (2.8)

The combined convection and radiation heat transfer coefficient for the air side, of the evaporator is plotted versus the average air side wall heat flux in Fig. 4.9. Heat transfer coefficient results between 11 and 15 W/(m² K) are almost the same as the results shown in Figs. 2.16 (10.5 - 19 W/m² K) and 3.11 (11 - 18 W/m² K). This is as expected since the wall heat fluxes and the air temperatures are within $\pm 25^{\circ}\text{C}$.

The radiation heat transfer coefficient, calculated using (Eq. 2.12), is plotted against the difference between the mean air temperature and the mean wall temperature for the evaporator in Fig. 4.10. The radiation heat transfer

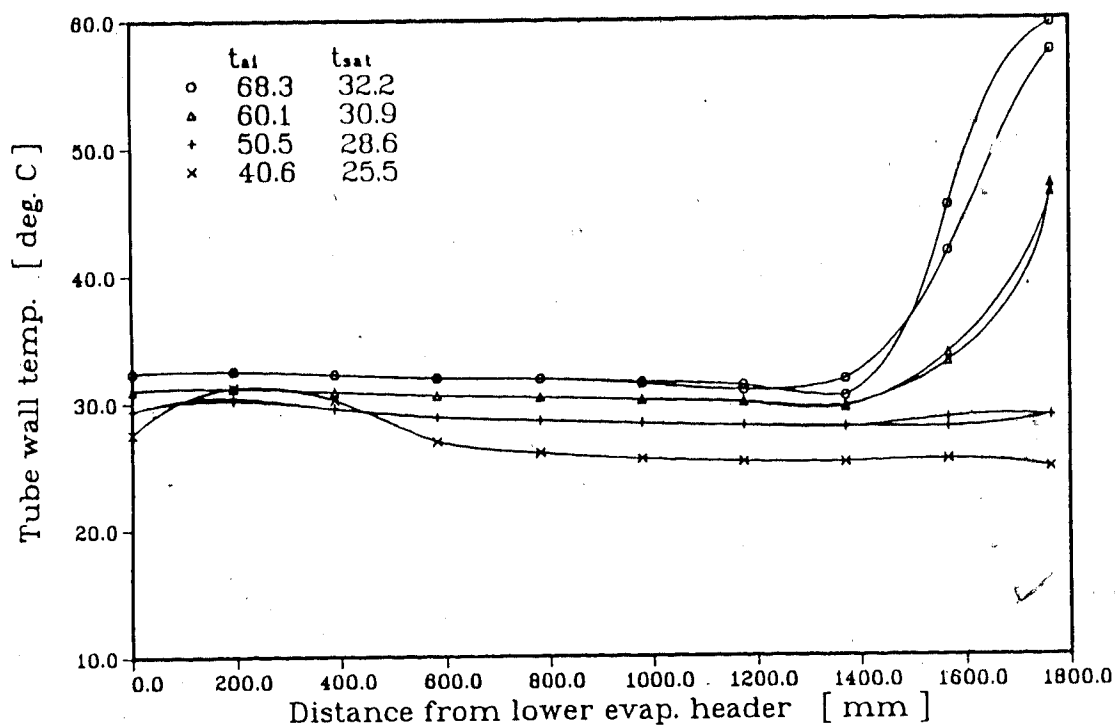


Fig. 4.7 Wall temperature distribution for evaporator tube #4 on panel 3 (air volume flow rate is $0.44 \text{ m}^3/\text{s}$, Ch.L. 6)

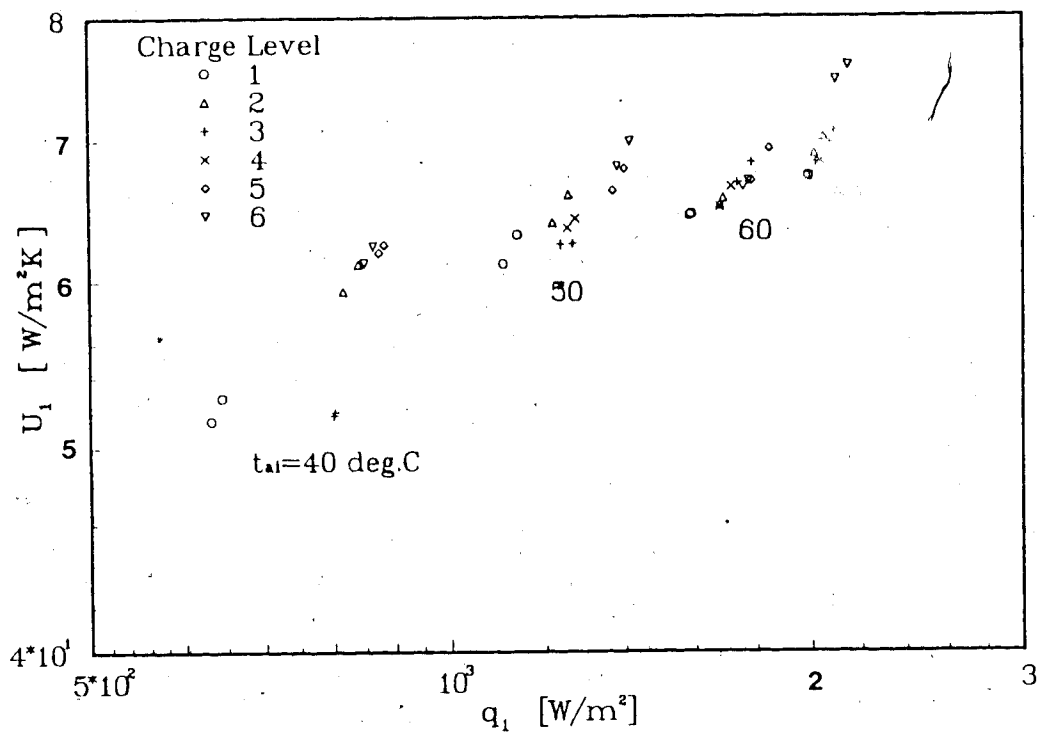


Fig. 4.8 Overall heat transfer coefficient for evap. vs. wall heat flux for Freon

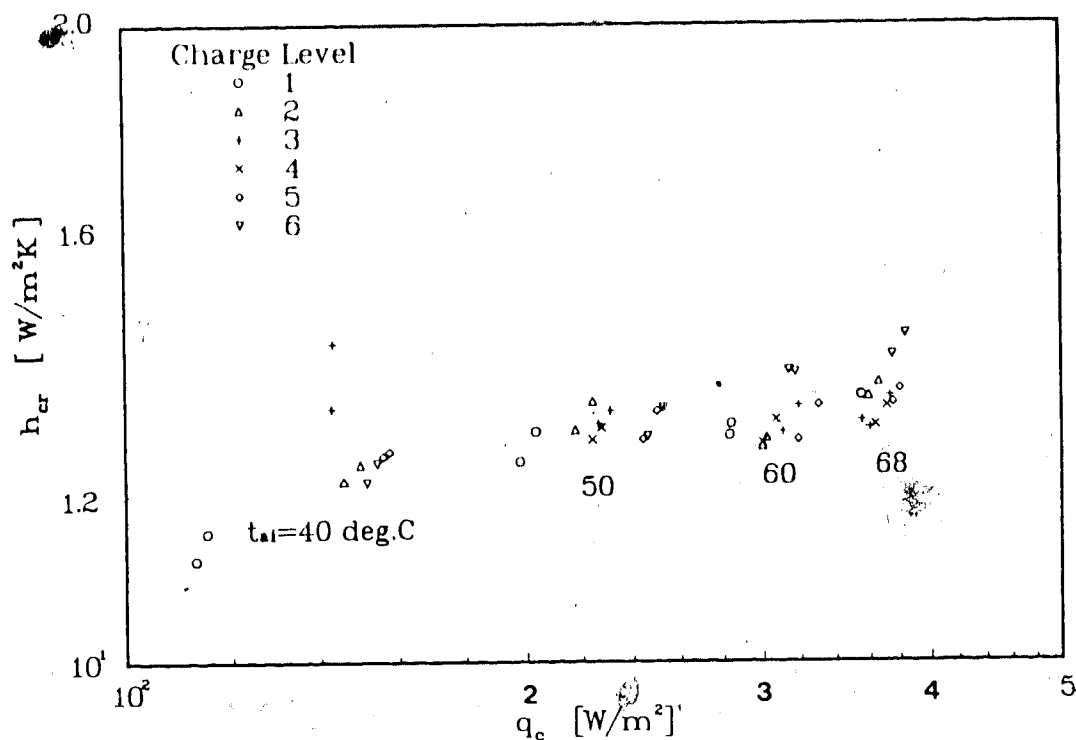


Fig. 4.9 Combined convection and radiation heat transfer coefficient for air side vs. average air side wall heat flux

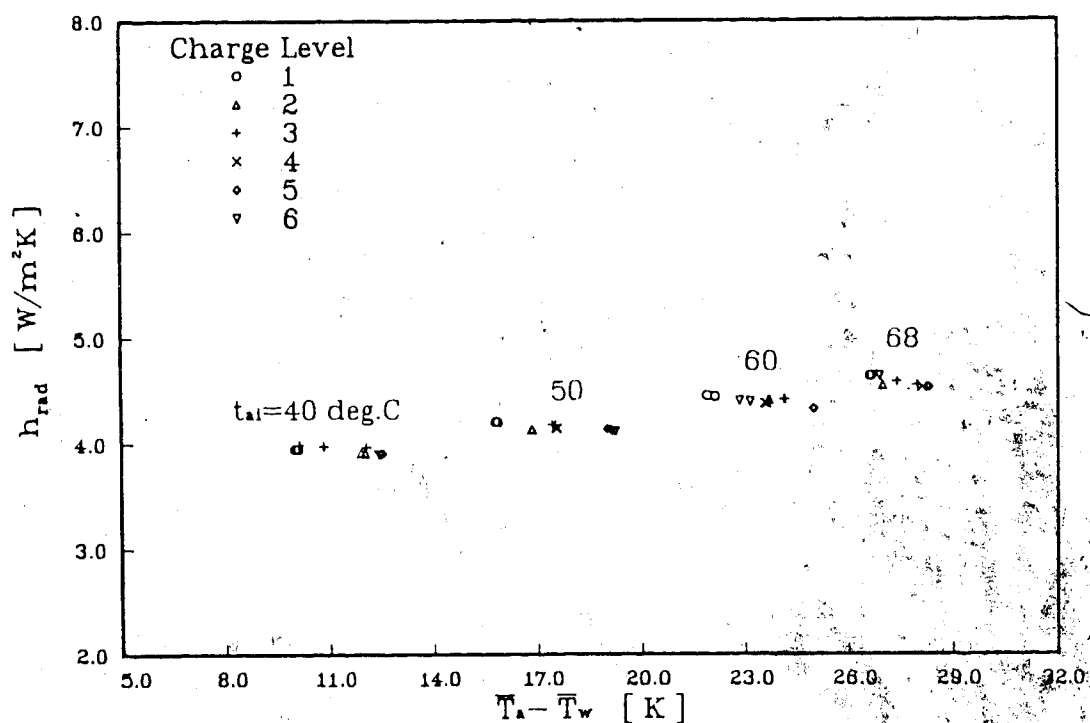


Fig. 4.10 Radiation heat transfer coefficient for air vs. difference between mean air and mean evap. wall temperatures

coefficients (4.0 to $4.5 \text{ W/m}^2 \text{ K}$) are similar to the results shown for two-phase water tests (4.5 to $5.2 \text{ W/m}^2 \text{ K}$). in Fig. 3.12 and for single phase thermosyphon tests shown in Fig. 2.17 (5.5 to $6.0 \text{ W/m}^2 \text{ K}$). The differences are likely a result of the higher operating air temperatures: $55 - 78^\circ\text{C}$ was used for the two-phase thermosyphon tests and 75 to 96°C was used for the single phase thermosyphon tests.

The working fluid mass flux per evaporator tube versus the average wall heat flux for the working fluid side of the evaporator is shown in Fig. 4.11. The mass flux is approximately constant ($\pm 2\%$) for the two highest charge levels for any wall heat flux. The only exception is the lowest wall heat flux ($640 \text{ W/m}^2\text{K}$) for charge level one for which the mass flux is 15% lower than other mass flux results for this charge level. For charge levels 3 and 4, the mass flux falls slightly (10% and 25% respectively) for the highest heat flux ($2100 \text{ W/m}^2\text{K}$); while for charge levels 5 and 6, there is a dramatic decrease in mass flux with increasing wall heat flux (from $30 \text{ kg/m}^2\text{s}$ at 850 W/m^2 to $8 \text{ kg/m}^2\text{s}$ at 2100 W/m^2 for charge level 6). The decrease in mass flux with increasing wall heat flux may be due to higher vapour qualities produced in the evaporator. That the vapour quality increased with increasing wall heat flux is seen in Fig. 4.12, and the increase is most pronounced for the two lowest charge levels (Ch. L. 5 and 6). The data points which show basically the same vapour qualities in Fig. 4.12, show close to the same mass fluxes in Fig. 4.11.

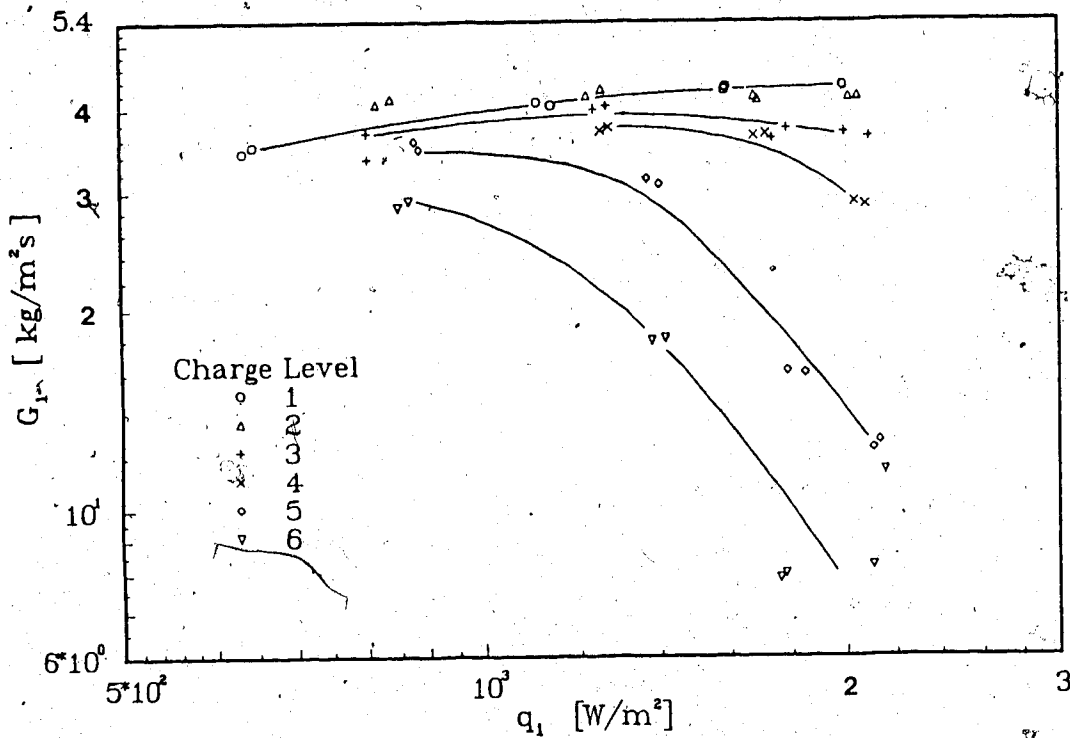


Fig. 4.11 Average mass flux for one evap. tube vs. average inside wall heat flux for evap.

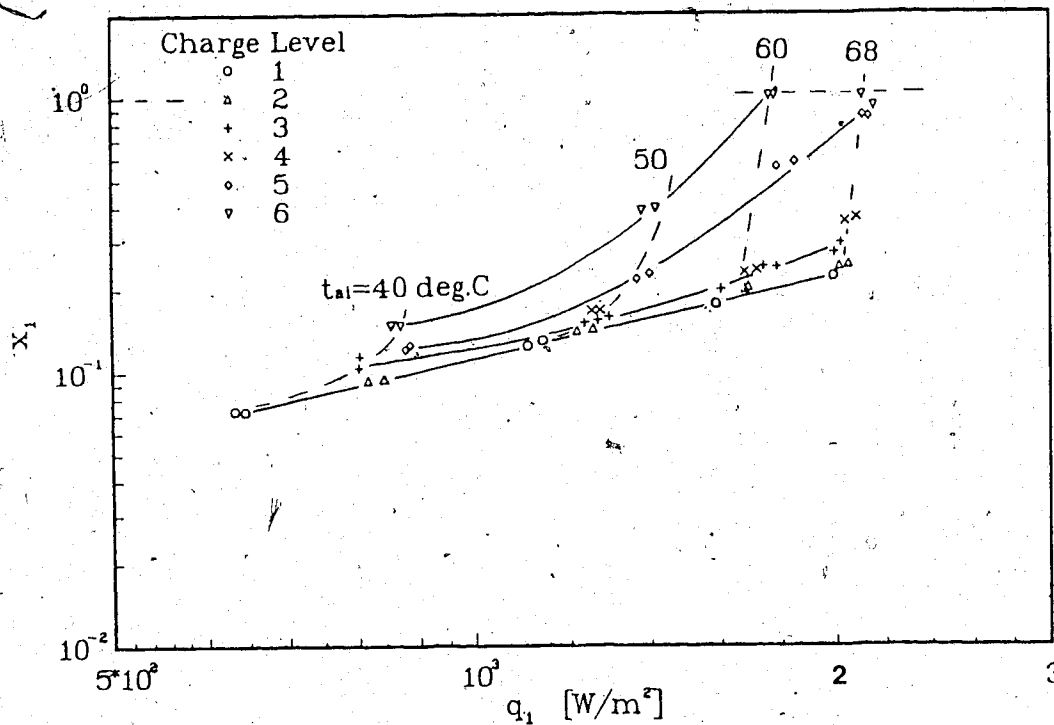


Fig. 4.12 Vapour quality at evap. exit vs. average inside wall heat flux for evap

The 100% vapour quality results shown for charge level 6 in Fig 4.12 correspond with the increasing wall temperatures shown in Fig. 4.7. This indicates that superheated vapour exited the evaporator for these test conditions.

The decreasing mass flux at higher qualities is believed to be caused by the limited available wall heat flux from the heating air. Because of the almost constant wall heat flux and therefore constant heat rate transferred to the working fluid, it is seen from Eq. (3.2a) that the mass flow rate and mass flux has to decrease with increasing vapour quality.

It is known from the literature [41], that the heat transfer coefficient for boiling increases with increasing working fluid vapour quality until dry-out occurs; from dry-out until the vapour is superheated the heat transfer coefficient decreases. These phenomena are also seen in Fig. 4.13, which shows heat transfer coefficient of the working fluid based on the arithmetic mean temperature difference plotted versus the evaporator exit quality.

Nusselt number versus inverse Graetz number for the working fluid per evaporator tube is shown in Fig. 4.14. Nusselt number is more than an order of magnitude higher than the results from the water tests in Chapters 2 and 3. Nusselt number increases until dry-out is reached, or; then it levels off and decreases as shown for charge levels 5 and 6. These results are similar to the heat transfer coefficient results shown in Fig. 4.13. This is as expected

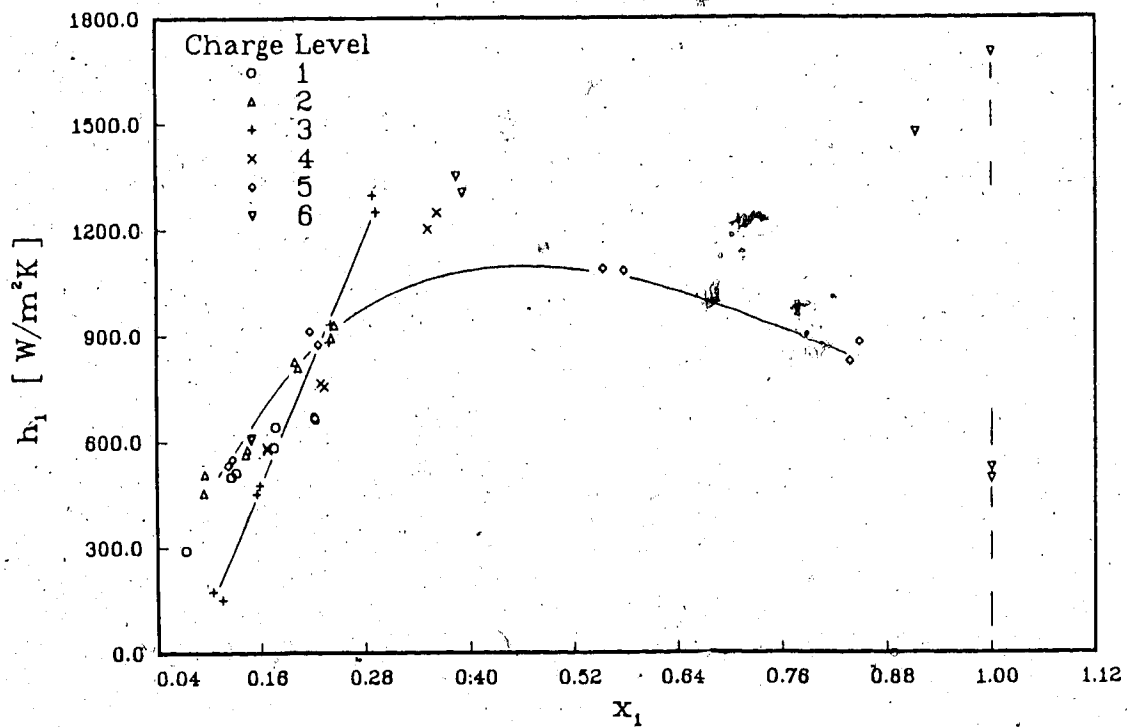


Fig. 4.13 Heat transfer coefficient for working fluid side of evap. vs. exit vapour quality

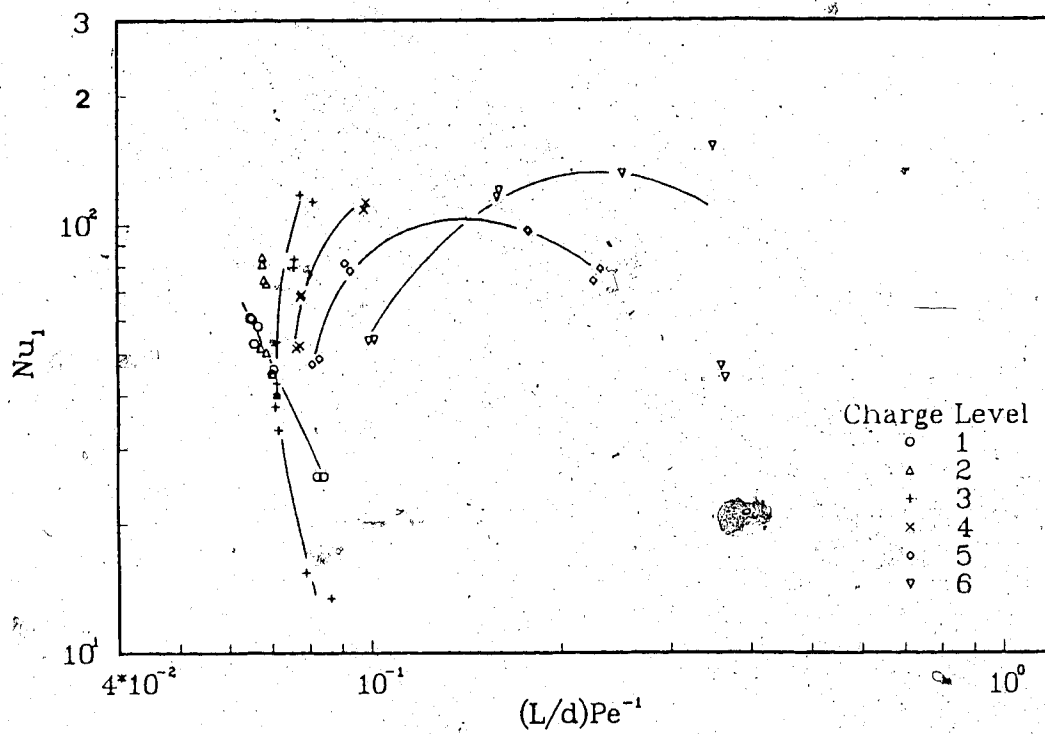


Fig. 4.14 Nusselt number for working fluid side of evap. vs. inverse Graetz number for working fluid per evap. tube

since Nusselt number is the dimensionless heat transfer coefficient for the working fluid side of the evaporator. Due to the narrow mean temperature range of the working fluid (20 - 27°C), Prandtl number is almost constant (less than 5% variation). The L/d -ratio is constant for the evaporator, hence, Graetz number, Eq. (2.21), for the liquid is mainly a function of Reynolds number. Therefore, corresponding to the mass flux in Fig. 4.11, the inverse Graetz number is approximately constant for liquid charge levels 1 to 3, while it increases as the working fluid level decreases with increasing air temperature for charge levels 4 to 6.

The vapour quality at the condenser entrance versus exit vapour quality for the evaporator is shown in Fig. 4.15. This figure shows the effect of the liquid-vapour separator whose downcomer is open. The lower the charge level, the more liquid is separated for the liquid-vapour flow entering the separator. Even at 100% charge level, the vapour quality doubled after the working fluid passed through the separator (e.g. from 8.5 to 20%).

4.5.3 The condenser results

The heat rate recovered by the cooling water versus the Freon vapour quality at the condenser entrance is shown in Fig. 4.16. The results in this figure show that increasing vapour quality did not increase the heat recovery rate significantly unless the air temperature was increased.

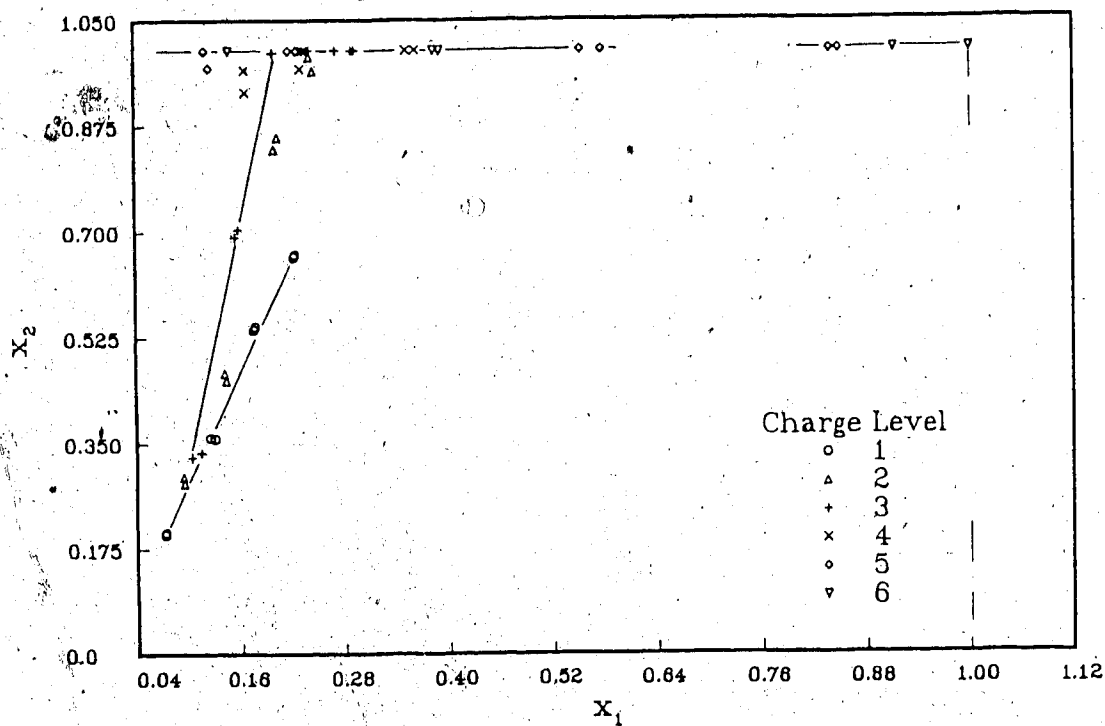


Fig. 4.15 Vapour quality at cond. entrance vs. vapour quality at evap. exit

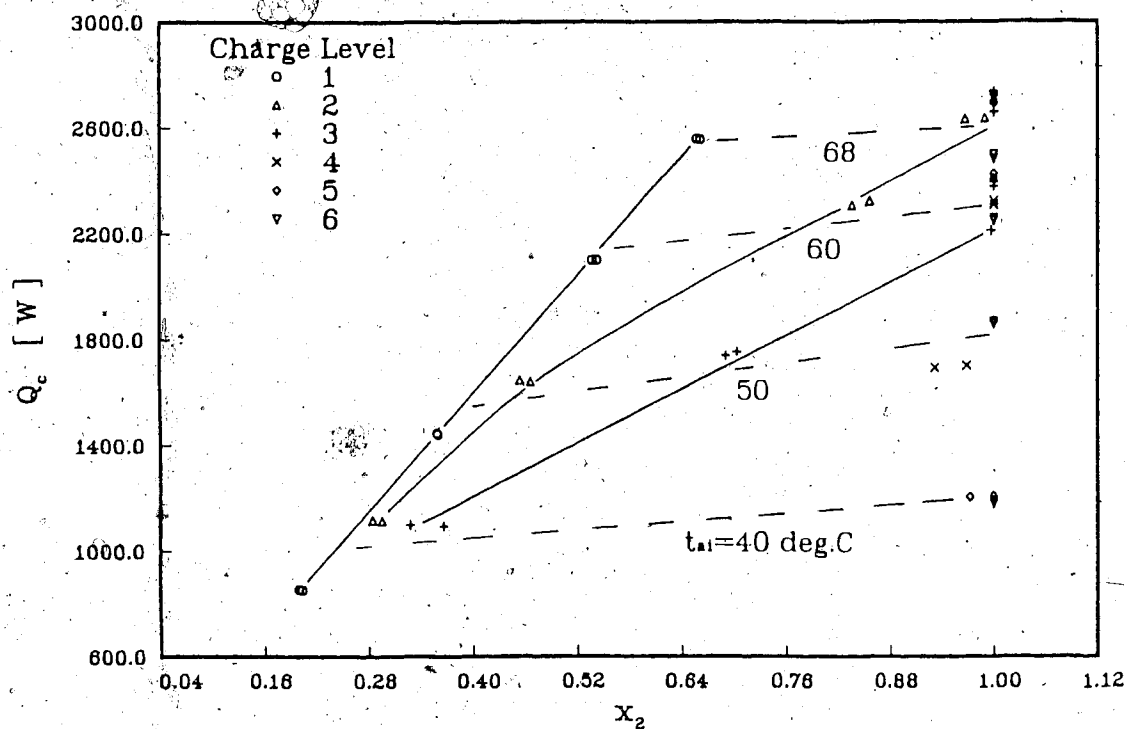


Fig. 4.16 Heat recovered by cooling water vs. vapour quality at cond. entrance

The overall heat transfer coefficient for the condenser is plotted against the wall heat flux for the cooling water side of the condenser in Fig. 4.17, and the estimated heat transfer coefficient for the fin side of the condenser coil (Eqs. (2.13) and (2.18)) versus the wall heat flux for the fin side is plotted in Fig. 4.18. Both heat transfer coefficients increased with increasing wall heat flux, the only exceptions were the tests done with the highest air temperature and charge levels 5 and 6, for which the tests resulted in decreasing heat transfer coefficients. The decreasing heat transfer coefficient results calculated for these tests are believed to be a result of superheated vapour.

The heat transfer coefficients are lower for charge level 1 than for the other charge levels for the same heating air temperature. As discussed in Subsection 4.5.1 more condensate covered the condenser coil for tests done with the highest charge level. This could have caused a reduction in the heat transfer coefficient similar to that shown in Figs. 4.17 and 4.18.

4.5.4 Heat transfer correlation

The heat transfer coefficient for the working fluid in the evaporator, h_1 , will in this section be referred to as h_{exp} . The ratio of this variable to the empirical heat transfer coefficients calculated using the single phase Dittus-Boelter equation, h , Eq. (3.4), is plotted versus

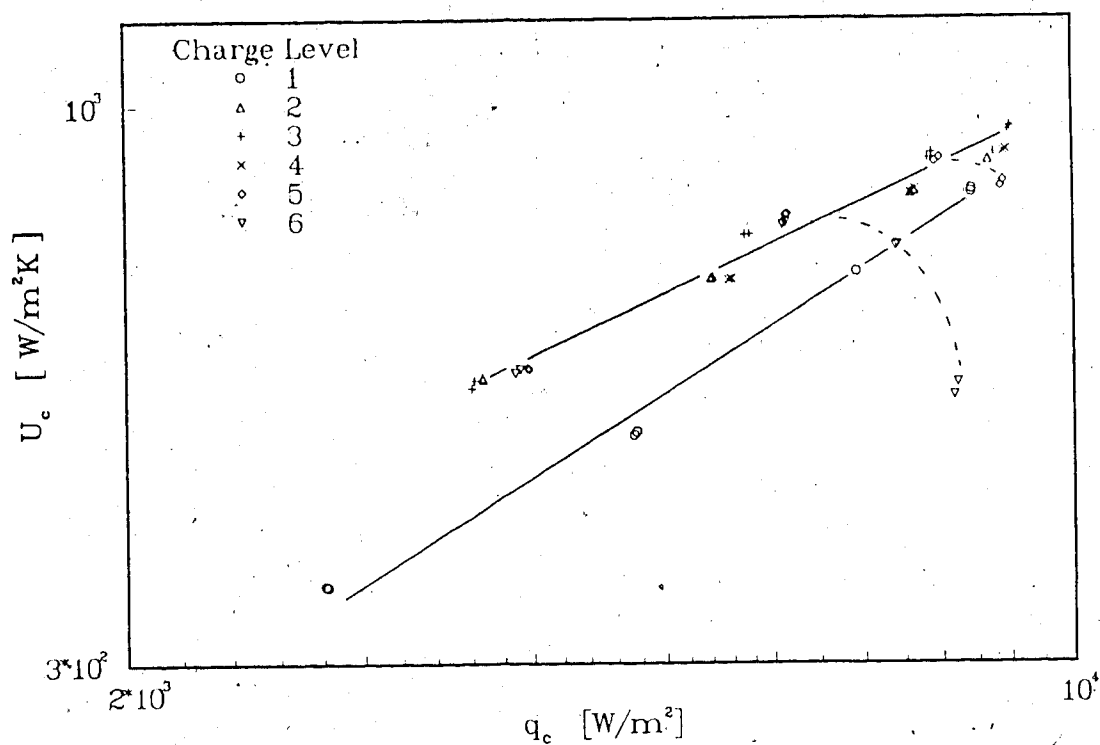


Fig. 4.17 Overall heat transfer coefficient for cond. vs. cooling water wall heat flux

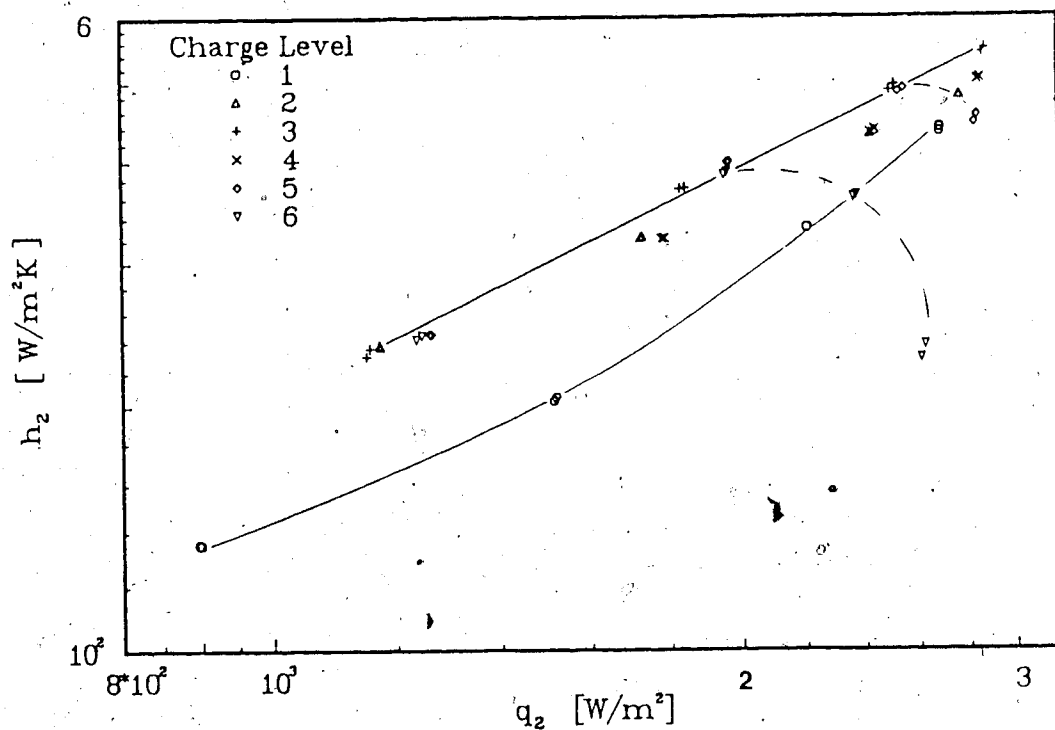


Fig. 4.18 Predicted fin side heat transfer coefficient of cond. vs. fin side wall heat flux of cond.

Boiling number, Eq. (3.6), in Fig. 4.19. The ratio between the experimental heat transfer coefficient and empirical liquid-only heat transfer coefficient, h , Eq. (3.5), versus Boiling number is shown in Fig. 4.20.

The major difference between the two Dittus-Boelter definitions is seen for higher Boiling number, i.e. higher vapour generation in the evaporator, as indicated by the comparison of Figs. 4.19 and 4.20. The liquid-only heat transfer coefficient, h_l , goes to zero as the vapour quality approaches 100% according to Eq. (3.5). Therefore, the ratio of experimental to empirical heat transfer coefficient approaches infinity as seen in Fig. 4.20. The single phase Dittus-Boelter heat transfer coefficient, h , is indirectly dependent on the vapour quality. Indirectly, because it is dependent on Reynolds number, Re , as seen in Eq. (3.4). Reynolds number is dependent on the mass flux, G , Eq. (2.16), and the mass flux decreased as the vapour quality increased as shown in Fig. 4.11. Hence, the heat transfer coefficient calculated from the single phase Dittus-Boelter equation will also decrease as the vapour quality increases. The heat transfer coefficient calculated from the experimental data is dependent on the mass flow rate (mass flux) as well, Eqs. (2.9), (2.2) and (2.1). However, the experimental heat transfer coefficient appears to decrease more than the empirical heat transfer coefficient as the vapour quality approaches 100%, according to Fig. 4.19. This figure shows that the heat transfer

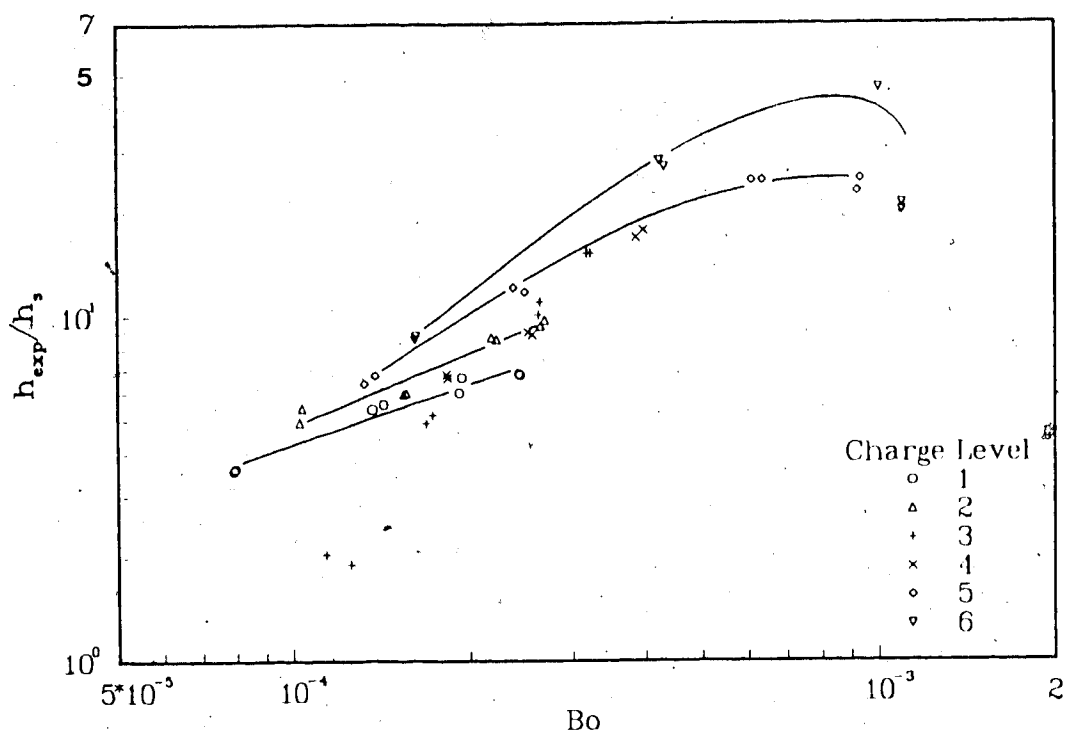


Fig. 4.19 Ratio of exp. heat transfer coefficient to Dittus-Boelter single phase prediction vs. Boiling number

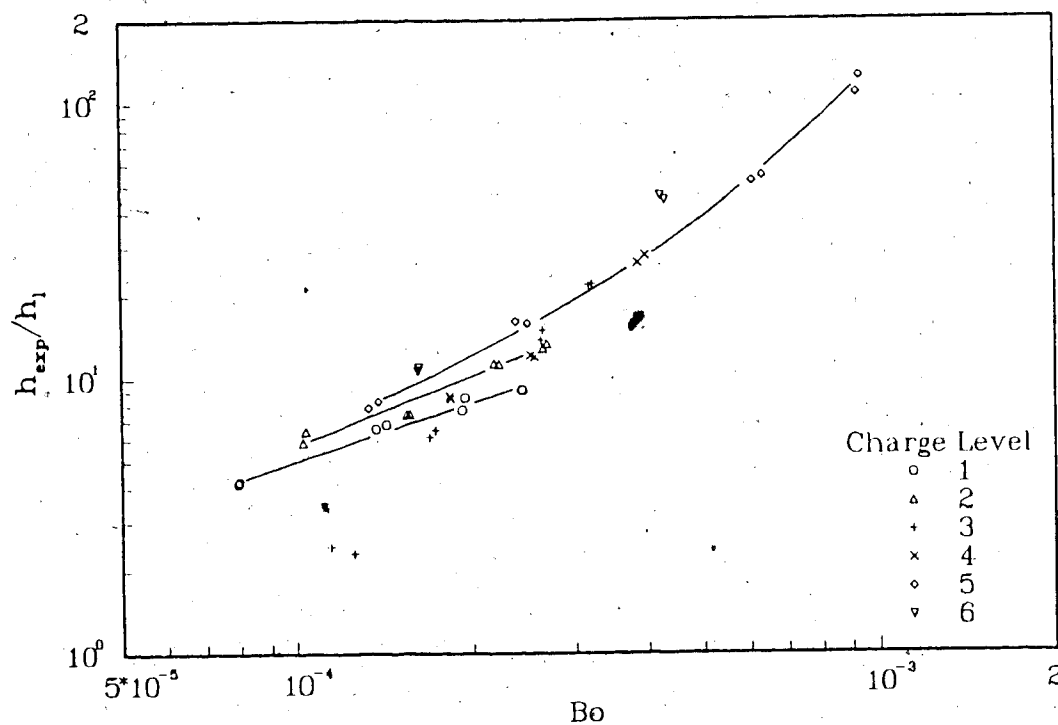


Fig. 4.20 Ratio of exp. heat transfer coefficient to Dittus-Boelter liquid-only prediction vs. Boiling number

coefficient ratio (experimental to single phase Dittus-Boelter prediction) decreases as the working fluid approaches superheated vapour. When these test results are compared with the two-phase water results in Section 3.5, Figs. 3.21 and 3.23, the same heat transfer coefficient ratios are 2 to 10 times higher for the Freon tests.

The Boiling number ranged from 0.00008 to 0.001 for the Freon tests. The lowest values obtained from these tests are in the same range as the two-phase water results, shown in Fig. 3.27.

The same heat transfer ratios, $h_{e,xp}/h$, and $h_{e,xp}/h_f$, are plotted versus Lockhart-Martinelli parameter, Eq. (3.7), as well. The empirical single phase heat transfer coefficient is used in Fig. 4.21, and the liquid-only Dittus-Boelter equation is used to calculate the heat transfer ratio shown in Fig. 4.22. Lockhart-Martinelli parameter goes to zero as the vapour quality approaches 100%, Eq. (3.7). Therefore, the inverse Lockhart-Martinelli parameter approaches infinity as the vapour quality becomes 100%. The ratio of the experimental to the Dittus-Boelter single-phase prediction increased as long as the vapour qualities exiting were less than 60%, but appeared to reach a maximum value as superheated vapour was approached, as shown for charge levels 5 and 6 in Fig. 4.19. The heat transfer coefficient ratio levels out as the inverse Lockhart-Martinelli parameter approaches infinity in Fig. 4.21.

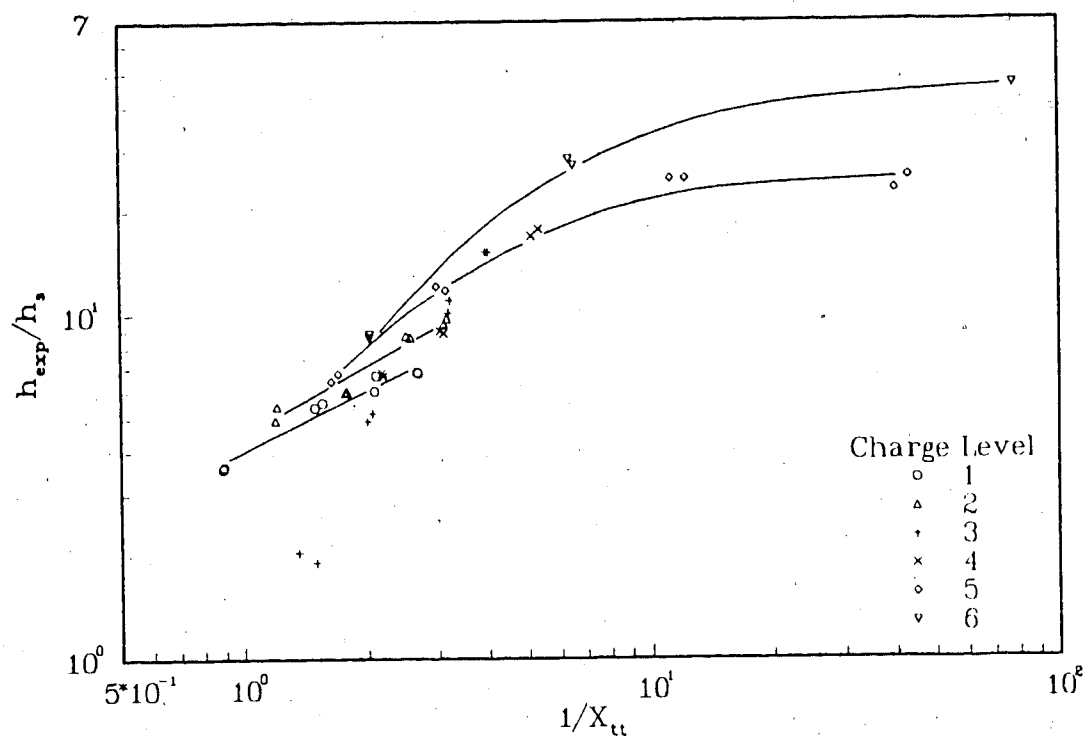


Fig. 4.21 Ratio of exp. heat transfer coefficient to Dittus-Boelter single phase prediction vs. inverse Lockhart-Martinelli parameter

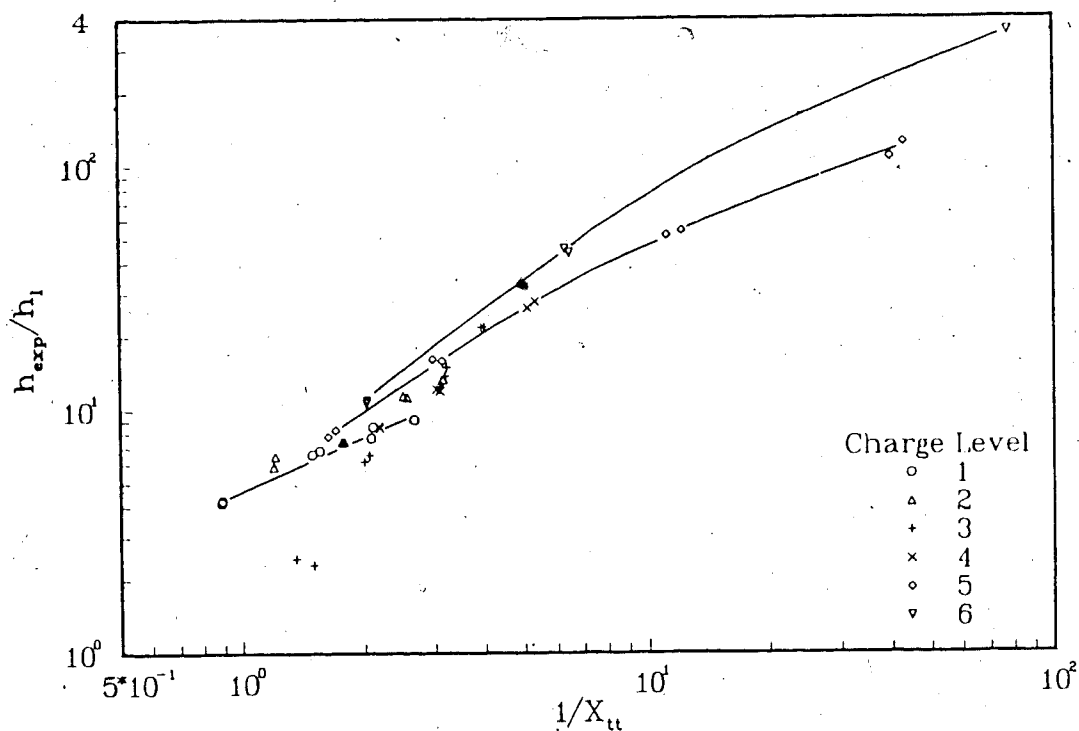


Fig. 4.22 Ratio of exp. heat transfer coefficient to Dittus-Boelter liquid-only prediction vs. inverse Lockhart-Martinelli parameter

The ratio of the experimental heat transfer coefficient to the liquid-only prediction is not seen to reach any maximum value in Fig. 4.22 as the inverse Lockhart-Martinelli parameter approaches infinity.

The experimental heat transfer coefficient does not correlate well with the two-phase heat transfer coefficients predicted by the Schrock-Grossman method, Eq. 3.9, and the Shah method, Eq. 3.10. The experimental value were close to two magnitudes higher than the predicted empirical values. Hence, these two correlation methods did not give representative predictions for the tested operating conditions.

The ratio of the experimental heat transfer coefficient to the empirical result from the Kandlikar coefficient is plotted versus Boiling number in the graph shown in Fig. 4.23. The experimental heat transfer coefficient was 1 to 5 times higher than the two-phase heat transfer coefficient calculated with the Kandlikar equation, Eq. (3.11).

The two-phase heat transfer coefficient calculated with Eq. (3.12), Ref. [12], is plotted versus Boiling number in Fig. 4.24. The experimental results were normally 1 to 3 times higher than the empirical results from Eq. (3.12).

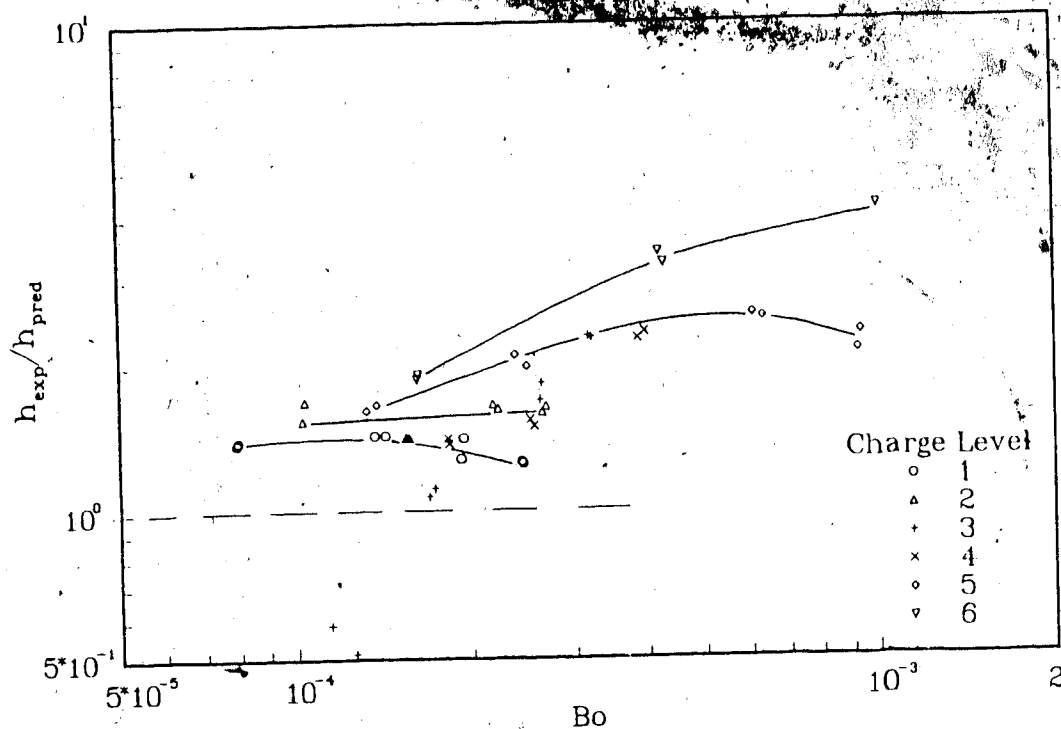


Fig. 4.23 Ratio of experimental heat transfer coefficient to Kandlikar prediction vs. Boiling number

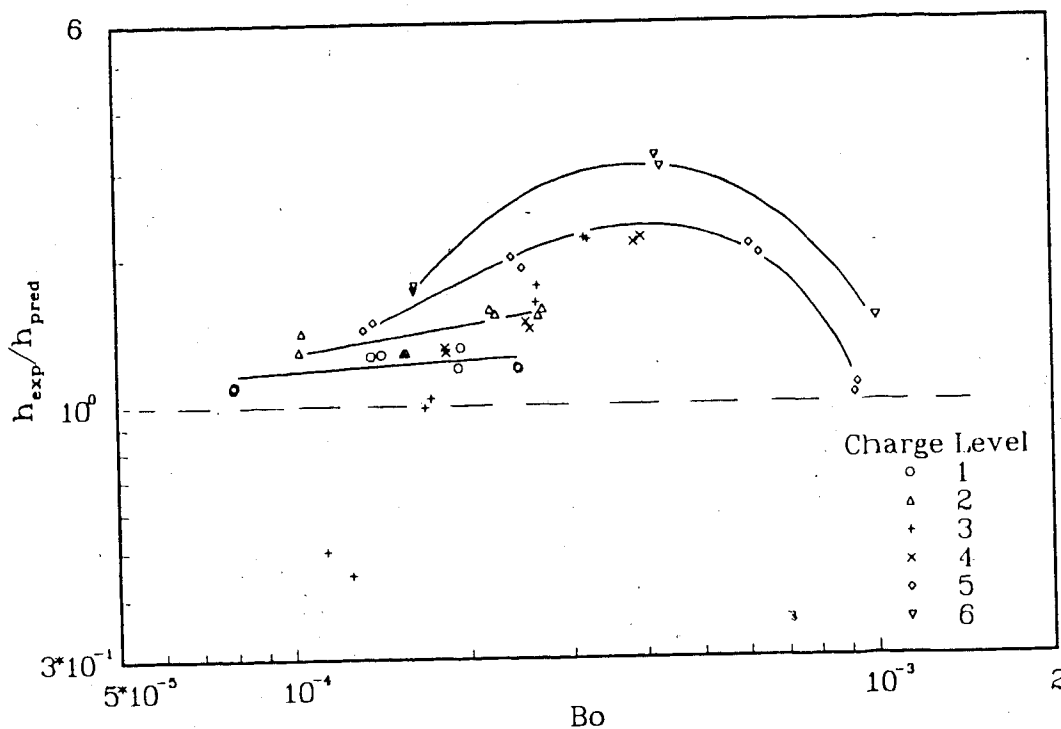


Fig. 4.24 Ratio of experimental heat transfer coefficient to prediction with Ref. [30] vs. Boiling number

4.6 Concluding Remarks

A closed two-phase thermosyphon loop with Freon R-11 as the working fluid has been used to transport heat from hot air to a cold water heat sink.

Experiments were performed with four air temperatures (40, 50, 60 and 68°C) and six working fluid charge levels, 100, 96, 83, 76, 59 and 41% of the vertical distance between evaporator inlet and the horizontal centre line through the condenser. The air volume flow rate (0.44 m³/s), cooling water mass flow rate (40 g/s), cooling water inlet temperature (12 - 13°C), initial working fluid vapour pressure (122 kPa abs. pressure) and the downcomer from the liquid-vapour separator (open) were system operating parameters which were not changed for any of the experiments.

The heat recovery of the cooling water varied from 800 to 2800 W, while the condenser cooling water exit temperature was between 17 and 31°C.

The total system efficiency was 9 to 17% and the vapour qualities exiting the evaporator ranged between 8.5 and 100% with superheating occurring for the highest air temperature for charge level 5 and 6. The effect of the liquid-vapour separator was clearly seen as, depending upon liquid charge level, it increased the vapour quality from an evaporator exit quality of 15% to a condenser entrance quality of 100% (air temp.=40°C for Ch.L. 5).

The system performance was marginally improved compared to two-phase thermosyphon performance with water as the working fluid. Nevertheless, the system performance was not satisfactory. The low system efficiency and heat recovery rates are caused by the system design. A modified system design, like improved connecting tube and evaporator design would most likely increase the system performance.

5. Conclusions

The purpose of this study is to explore the possibility of using a two-phase closed-loop thermosyphon to transfer heat from a low grade heat source (air) to a heat sink (water). The temperature difference between the heat source and the heat sink was normally between 30 and 75°C for the tests conducted. Both single phase and two-phase thermosyphon tests were performed with water as the working fluid, while only two-phase tests were conducted with Freon R-11 as the working fluid.

The primary loop had a built on-site evaporator, a liquid-vapour separator and a commercially made condenser as the main components. The evaporator consisted of 4 solar collector panels mounted in parallel, 0.07 m apart. The heating air stream flowed parallel to the collector panels and in counter flow with the working fluid.

The studies were conducted in four parts, namely:

1. single phase thermosyphon using water as the working fluid.
2. forced circulation with water as the working fluid.
3. two-phase thermosyphon with water as the working fluid.
4. two-phase thermosyphon with Freon R-11 as the working fluid.

Since each of the three main chapters (2-4) are written with their own concluding remarks, only the most important overall experimental observations are discussed in this chapter.

The single phase water tests were conducted to acquire a general understanding of the system performance. Thermosyphon and forced flow tests showed that the performance of the system was highly dependent on the mass flow rate of the working fluid. Higher air volume flow rates improved the heat transfer from heat source to heat sink. The thermosyphon tests resulted in low system efficiency (max. 6%) and low heat recovery rates (max. 1850 W). The natural and forced circulation tests showed similar results for the same working fluid flow rate range.

Many tube reductions, bends and inefficiently designed manifolds (evaporator headers), as well as flow meters and wire meshes caused significant pressure drops in the primary loop. The resulting low working fluid flow rates caused by the restrictions inhibited system performance and contributed to poor efficiency.

The test results indicated clearly a need for a different working fluid or different system operating condition, e.g. two-phase flow rather than single phase.

During the two-phase thermosyphon tests with water as the working fluid, the primary loop was exposed to partial vacuum, hence lowering the boiling point of the water. These tests revealed that the limited energy supply of the heating

source and the poor evaporator design resulted in low wall heat flux. Due to large working fluid fluctuation over the relative short data collection collection time (45 seconds), the results are believed to be somewhat misleading. For further work with two-phase water under similar conditions, which is not recommended, the data should be average over a longer collection peride (e.g. 30 minutes). The heat recovery rates (max. 2300 W) and the system efficiency (max 11%) improved somewhat compared to the single phase thermosyphon tests. However, the limited wall heat flux and the high latent heat of vaporization and specific heat of water caused low evaporator exit qualities (max. 25%). Hence, the boiling occured in the subcooled region through most of the evaporator. This caused the heat transfer results to correspond better with theoretical single phase flow results rather than with two-phase empirical predictions.

The effect of the liquid-vapour separator on the heat transfer performance could not be determined from the two-phase water test results.

Best system performance was obtained with Freon as the working fluid. The latent heat of vaporization is twelve times less and the specific heat is almost five times less than that of water. This resulted in much higher vapour quality flow in the evaporator and superheated vapour was produced for some test conditions.

The working fluid property fluctuations were less for these R-11 tests than for the two-phase water tests. The data are believed to be reasonable, which is verified by the results from the two recordings per steady state. These two results are almost identical as seen in most of the graphs in Chapter 4. However, for future work, it could be advantageous to sample the data over a 30 minutes period as well as a 45 second period.

The maximum heat rate recovered by the cooling water (2800 W) was 20% higher than that of two-phase water tests. Maximum system efficiency for the Freon tests was 17%.

The experimental heat transfer coefficient results were higher than those predicted by two-phase correlation equations used [30,32], but were still within the same order of magnitude.

The experiments showed that a closed-loop thermosyphon was able to transport heat from a low grade heat source to a cold liquid sink, even when the temperature difference between the source and the sink was as low as 30°C. This indicates the possibility of utilizing such a system for practical applications. However, the poor design of the system tested made it difficult to obtain encouraging results. Using the knowledge gained in this work, a more efficient system could be constructed for further investigation in low grade heat recovery research. This includes better evaporator design and reduction of flow restrictions in the primary loop.

In particular, Freon appeared to be well suited as working fluid, due to the low latent heat of vaporization and low specific heat capacity. This allows the working fluid to reach the saturated liquid state in the entering part of the evaporator tubes, and to attain higher working fluid vapour qualities exiting the evaporator. Hence, the heat transfer coefficients and heat transfer between heat source and heat sink improve as long as dry out and superheat are avoided.

References

1. McDonald, T.W., Hwang, K.S. and DiCiccio, R., "Thermosiphon Loop Performance Characteristics: Part 1. Experimental Study", ASHRAE Trans. 83(2), 1977, pp. 151-170.
2. Mochida, Y., Kawano, S., Takahata, T. and Miyoshi, M., "Performance of the Heat Exchangers of a 100-kW (Gross) OTEC Plant", Journal of Solar Energy Engineering, Vol.106, May 1984, pp. 187-192.
3. Lock, G.S.H. and Maezawa, S., "The Aerosyphon: An Exploratory Study", Int. J. Heat Mass Transfer, Vol. 18, Pergamon Press 1975, pp. 219-225.
4. De Marchi Desenzani, P. "Geothermal Energy and Biofuel Production in Agriculture", Nejat Veziroglu, T., ed., Alternative Energy Heat Sources II, Geothermal Power/Energy Program Vol. 5, McGraw-Hill International Book Company 1981, pp 2023-2032.
5. Larkin, B.S., "An Experimental Study of the Two-phase Thermosyphon Tube" CSME Trans., Vol.14, 1971, pp. 208-215.
6. Cheng, K.C., Morioka, I., Ichimiya, K., and Sadler G.W., "Experimental Study of a Two-phase Thermosyphon System", Alternative Energy Sources IV, Vol.1, 1982 pp. 151-170.
7. Al-Tamimi, A.I., Performance of Flat-Plate Solar Collector in a Closed-Loop Thermosiphon using Refrigerant-11, Ph. D. Thesis, The Univ. of Michigan, 1982.
8. Peace-Athabasca Delta Project Report, Intergovernmental Study Group, Dept. of the Environment, Queens Printer, Edmonton, 1972.
9. Schreyer, J.M., "Residential Application of Refrigerant-Charged Solar Collectors", Solar Energy, Vol.26, pp. 307-312., 1981.
10. Bottum, E.W., "Refrigerant Charged Phase Change Solar Water and Space Heating Systems", ASHRAE Trans., Vol. 87(2), 1981, pp. 397-404.
11. Lee, C.A., An Experimental Study of Refrigerant Charge Two-Phase Solar Collector Systems, M. Sc. Thesis, University of Alberta, 1983.

12. Cheng, K.C., Application of Boiling and Condensation Heat Transfer to Flat Plate Solar Collectors in Cold Region, Final Report, Alberta/Canada Energy Resources Research Fund, Contract U-79-9, 1982.
13. ASHRAE Handbook, 1981 Fundamentals, American Society of Heating, Refrigeration and Air-Conditioning Engineering, Inc., pp 13.15 -13.16.
14. Fujii, T., Kato, Y. and Mihara, K., "Expressions of Transport and Thermodynamic Properties of Air, Steam and Water", Report No. 66, Institute of Industrial Science, Kyushu University, Japan, 1972.
15. Ozisik, M.N., Basic Heat Transfer, McGraw-Hill, Inc., 1977, p. 10.
16. Gebhart, B., Heat Transfer 2.ed., McGraw-Hill Book Company, 1971, p. 164.
17. General Electric Corporate Research and Development: Heat Transfer and Fluid Flow Data Books, Forced Convection, Dec. 1980, p. 21.
18. Kreith, F., Principles of Heat Transfer, 3rd ed., Harper & Row, Publishers, New York, N.Y., 1973, p. 43.
19. ASHRAE Handbook 1981 Fundamentals, American Society of Heating, Refrigerating and Air-Conditioning Engineers, Inc., Table 3, p. 39.3.
20. Ozisik, M.N. Basic Heat Transfer, McGraw-Hill, Inc., 1977, p. 455-456.
21. Pippard, A.B., The Elements of Classical Thermodynamics, 4th. edition, Cambridge University Press, 1981, p. 100.
22. Callen, H.B., Thermodynamics, John Wiley & Sons, Inc., 1976, p. 55.
23. Moran, M.J., Availability Analysis: A Guide to Efficient Energy Use, Prentice-Hall 1982, pp. 44-76 and 86.
24. Ozisik, M.N. Basic Heat Transfer, McGraw-Hill, Inc., 1977, p. 451.
25. Kreith, F., Principles of Heat Transfer, 3rd ed., Harper & Row, Publishers, New York, N.Y., 1973, p. 438-444.
26. McAdams, W.H., Heat Transmission, McGraw-Hill, 3rd. edition, 1954, pp. 230-235 1977, p. 10.
27. Ozisik, M.N. Basic Heat Transfer, McGraw-Hill, Inc., 1977, p. 196-198.

28. Kakac., S., and Veziroglu, T.N., "A Review of Two-Phase Flow Instabilities", Advances in Two-Phase Flow and Heat Transfer, Vol. II, Martinus Nijhoff Publishers, 1983, pp. 577-667.
29. Dittus, F.W. and Boelter, L.M.K., "Heat Transfer in Automobile Radiators of the Turbular Type", Univ. of California Publications in Engineering, Vol. 2, No. 13, 1930, pp. 443-461.
30. Cheng, K.C., Private Library, Mech. Eng., Univ. of Alberta.
31. Schrock, V.E. and Grossman, L.M., "Forced Convection Boiling in Tubes", Nuclear Science and Engineering, Vol. 12, 1962, pp. 474-481.
32. Kandlikar, S.G., "An Improved Correlation for Predicting Two-Phase Flow Boiling Heat Transfer Coefficient in Horizontal and Vertical Tubes", Paper presented at the 21st National Heat Transfer Conference, Seattle, Wash. July 24-28, 1984.
33. Shah, M.M., "Chart Correlation for Saturated Boiling Heat Transfer: Equations and Further Study", ASHRAE Trans., Vol. 88(1), 1982, pp. 185-196.
34. Shah, M.M., "A new Correlation for Heat Transfer During Boiling Flow Through Pipes", ASHRAE Trans., Vol. 82, Part 1, 1976, pp. 66-86.
35. Rohsenow, W.M. & Harnett, J.P., editors, Handbook of Heat Transfer, McGraw-Hill Book Company, 1973, Table 4, p. 13.44.
36. Dupont of Canada, "Freon Refrigerants", Physical Properties Pamphlet, R11-371, FR-82.
37. Fujii, T., Nozu, S. and Honda, H., "Expressions of Transport and Thermodynamic Properties of R-11, R-12, R-22 and R-113", Report No. 66, Institute of Industrial Science, Kyushu University, Japan, 1977.
38. Cheng, K.C. and Rovang, G.W., "Heat Transfer Characteristics of a Closed-Loop Two-Phase Thermosyphon System for Low Grade Waste Heat Recovery from Liquid Heat Sources", Paper presented at ASME Nat. Heat Transfer Conference, Denver, Colorado, Aug. 4-7 1985.
39. Rovang, G.W., An Experimental Investigation of a Closed-Loop Two-Phase Thermosyphon System for Low Grade Heat Recovery from Liquid Heat Sources, M. Sc. Thesis, University of Alberta, 1985.

40. ASHRAE Handbook, 1981 Fundamentals, American Society of Heating, Refrigeration and Air-Conditioning Engineering, Inc., pp 2.20-2.21.
41. Collier, J.G., Convective Boiling and Condensation, 2nd edition, McGraw-Hill International Book Company, 1981, pp. 133-141.

Appendix I

Sample Data Acquisition Program
Basic Computer Language is Used

10 REM RECOVERY OF WASTE HEAT USING 2-PHASE THERMOSYPHON
WITH FREON R-11 AS THE WORKING FLUID.

20 REM AUTHOR:BJORN YSTAD, M.Sc. STUDENT, U.A. 1982-85

30 REM DECEMBER 11 - 1984

40

50 OPTION BASE 0

60 PRINTER IS 704,132

70 PRINT CHR\$(27)&"[4w"

80 ON KEY# 1,"START" GOTO 760

90 ON KEY# 2," GO " GOTO 1080

100 ON KEY# 3,"TCHECK" GOTO 2800

110 ON KEY# 4,"TEMP " GOTO 3920

120 DIM C1\$[10],C2\$[95],D\$[10]

124 DIM S\$[300],S1\$[400],S2\$[400],S3\$[400],S4\$[400],
S5\$[400],S6\$[400],S7\$[400],S8\$[400],S9\$[400]

130 SHORT A1(20),A2(10),A3(5),A4(9),A5(35),B(96),
B1(20),B2(10),B3(5),F(10),P(10),PO(10),S(74)

134 SHORT T(74),B0(96)

140 ON ERROR GOTO 1110

150 R\$=CHR\$(13)

160 C\$=","

170 REM

180 REM DATA ROUTINE

190 REM THERMOCOUPLE DATA TC#0 TO TC#63 + TC#78

200 REM T.C.Equation : $A1() \cdot \text{volt} + B1() = \text{Temp}$

210 REM A1(0) - A1(16)

220 DATA 18641.192,18863.738,18800.354,18918.651,
18958.755,18636.461,18939.017

230 DATA 18983.361,19355.458,19552.46,18946.779,
18644.492,1.013,19591.142

240 DATA -19609.725,18485.543,19034.819

250 REM B1(0) - B1(16)

260 DATA 30.495,30.087,30.076,30.089,30.091,
30.469,30.065,30.073

270 DATA 29.859,29.932,30.061,30.459,1.96,28.899,
28.88,27.969,27.509

280 REM PRESSURE TRANSD. $A2() \cdot \text{volt} + B2() = \text{psi}(1,4), \text{inH}_2\text{O}(5,6)$

290 DATA .1,.111,1.009,.504,.077,.081

300 DATA -.003,-.007,-.03,-.037,.002,-.004

310 REM FL.METER $A3() \cdot \text{record} + B3() = \text{g/sec}$

320 DATA 6.715,-.174,6.464,-.236,11.18,2.334,11.837,2.231

330 REM DENSITY OF AIR [kg/m3]; A4(1)-A4(7)

[0,20,40,60,80,100,127 deg.C]

340 DATA 1.29,1.21,1.12,1.06,.99,.94,.88

350 REM DENSITY R11[kg/m3]; A(1)-A(35) [2,7,10,17,22,27,
29,31,....,75,77,82,87,92,97]

360 DATA 1529.5,1518.2,1506.8,1495.3,1483.6,1471.8,
1467,1462.2,1457.4,1452.6,1447.7

370 DATA 1442.8,1437.9,1433,1428,1423,1417.9,1412.9,
1407.8,1402.6,1397.5,1392.3,1387

380 DATA 1381.8,1376.5,1371.1,1365.7,1360.3,1354.8,
1349.3,1343.8,1329.7,1315.3,1300.5,1285.5

390 REM

400 FOR I=0 TO 16


```

410 READ A1(I)
420 NEXT I
430 FOR I=0 TO 16
440 READ B1(I)
450 NEXT I
460 FOR I=1 TO 6
470 READ A2(I)
480 NEXT I
490 FOR I=1 TO 6
500 READ B2(I)
510 NEXT I
520 FOR I=1 TO 4
530 READ A3(I)
540 READ B3(I)
550 NEXT I
560 FOR I=1 TO 7
570 READ A4(I)
580 NEXT I
590 FOR I=1 TO 35
600 READ A5(I)
610 NEXT I
620 REM
630 REM STARTING
640 A1=0 B1=0 W1=0 P(10)=0
650 CLEAR DISP USING 660
660 IMAGE "INPUT DATE; SEC.SINCE MIDNIGHT; BAROM.PRESSURE;
SYSTEM PRESSURE;LAST TAPE STORAGE #"
670 INPUT D$,T0,P1,P0,J9
680 SETTIME T0,0
690 REM INITIALIZING THE ACQUISITION VECTOR ARRAY
700 FOR I=0 TO 96
710 B(I)=0 B0(I)=0
720 NEXT I
730 CLEAR KEY LABEL DISP USING 740
740 IMAGE "FOR INITIAL RECORDINGS; HIT K1"
750 GOTO 750
760 CLEAR DISP USING 770
770 IMAGE " DATA ACQUISITION IN PROGRESS ",//
" DO NOT ENTER ANY KEY NOW REM"
780 S0=0 S1=63 N=2 N1=1 A1=0 F1=0 A0=0
790 T1=IP(TIME/3600) REM Hours
800 T2=IP(TIME/60-T1*60) REM Minutes
810 GOSUB 3530
820 S0=64 S1=96 N=24 N1=1
830 GOSUB 3530
840 B0(70)=B0(95)
850 FOR I=0 TO 73
860 B(I)=B0(I)
870 NEXT I
880 FOR I=1 TO 6
890 P0(I)=B(63+I)*A2(I)+B2(I) REM INITIAL PRESS. REC.
900 NEXT I
910 P0(3)=0
920 GOTO 1600

```

```

930 REM
940 CLEAR KEY LABEL: DISP USING 950
950 IMAGE "START UP THE SYSTEM",/,,"COOLING H2O ON",/,
"FAN ON",/,,"HEATER ON"
960 CLEAR DISP USING 970
970 IMAGE " INPUT THE FAN SPEED"
980 INPUT F1
990 DISP USING 1000
1000 IMAGE "IF YOU WANT TO COMPARE TEMP.
MEASUREMENTS; - HIT K3 "
1010 BEEP 50,300 WAIT 15000
1020 DISP USING 1030
1030 IMAGE ///,"WHEN YOU ARE FINISHED, HIT K2"
1040 GOTO 1040
1050 DISP USING 1060
1060 IMAGE "FOR CRITICAL TEMP.RECORDING
HIT K4 ELSE HIT K2"
1070 GOTO 1070
1080 CLEAR DISP USING 1090
1090 IMAGE "INPUT IF:",/,,"NO FAN; 1",/,,"15 MIN.RUN;
2",/,,"ROTAMETER ; 3",/,,"TURBINE METER; 4"
1100 INPUT Z0
1110 CLEAR DISP USING 1120
1120 IMAGE "DO YOU WANT A COMMENT TO EACH
RECORDING; HIT [ 1 ] ELSE [ 0 ]"
1130 INPUT Z1
1140 CLEAR DISP USING 1150
1150 IMAGE "DO YOU WANT TO STORE ONTO TAPE;
HIT [ 1 ] ELSE [ 0 ]"
1160 INPUT Z2
1170 REM
1180 A1=A1+1
1190 REM ELECTRONIC (AND MANUAL) DATA RECORDING
1200 W1=0
1210 IF Z0=3 THEN 1220 ELSE 1260
1220 CLEAR DISP USING 1230
1230 IMAGE "INPUT:WORKING H2O"
1240 INPUT W1
1250 REM INITIALIZING THE ACQUISITION VECTOR ARRAY
1260 FOR I=0 TO 74
1270 B(I)=0
1280 NEXT I
1290 N1=0
1300 CLEAR DISP USING 770
1310 S0=0 S1=63 N=2 N1=N1+1
1320 FOR I=0 TO 96
1330 B0(I)=0
1340 NEXT I
1350 T1=IP(TIME/3600) REM Hours
1360 T2=IP(TIME/60-T1*60) REM Minutes
1370 GOSUB 3530
1380 S0=64 S1=67 N=10
1390 GOSUB 3530
1400 S0=71 S1=73 N=10

```

```

1410 GOSUB 3530
1420 S0=95 S1=95 N=10
1430 GOSUB 3530
1440 S0=68 S1=69 N=25
1450 GOSUB 3530
1460 B0(70)=B0(95)
1470 FOR I=0 TO 73
1480 B(I)=B(I)+B0(I)
1490 NEXT I
1500 IF Z0=2 THEN 1510 ELSE 1530
1510 IF N1=25 THEN 1520 ELSE 1310
1520 BEEP 200,500
1530 BEEP 100,200
1540 IF Z1=0 THEN 1560 ELSE 1550
1550 IF Z0=3 THEN 1560 ELSE 1600
1560 CLEAR DISP USING 1230
1570 INPUT W3
1580 W1=(W1+W3)/2
1590 REM
1600 CLEAR DISP USING 1610
1610 IMAGE "INPUT SOME CHARACTERISTIC COMMENTS"
1620 INPUT C2$
1625 CLEAR DISP USING 1630
1630 IMAGE "INPUT SYSTEM REF. PRESSURE"
1640 INPUT P0
1650 REM
1660 REM CONVERTING THE RECORDINGS TO PROPER UNITS
1670 FOR I=0 TO 73
1680 B(I)=B(I)/N1
1690 NEXT I
1700 REM TEMP. DATA FROM Volts TO deg.C
1710 FOR I=0 TO 11
1720 T(I)=B(I)*A1(I)+B1(I)
1730 NEXT I
1740 T(12)=B(12)*18290*A1(12)/9 REM THERMOPILE
1750 FOR I=13 TO 61
1760 T(I)=B(I)*A1(15)+B1(15)
1770 NEXT I
1780 T(62)=B(62)*A1(13)+B1(13)
1790 T(63)=B(63)*A1(14)+B1(14)
1800 REM AVERAGE TUBE WALL TEMP. PER COLLECTOR PANEL
1810 T3=T(20)+T(21)+T(22)+T(24)+T(25)+T(26)+
T(28)+T(29)+T(31)+T(32)
1820 T3=T3/10 REM [deg.C]
1830 T4=T(43)+T(44)+T(45)+T(47)+T(48)+T(49)+
T(51)+T(52)+T(54)+T(55)
1840 T4=T4/10 REM [deg.C]
1850 REM T4 & T3 ARE FOR PANEL #1 & #3 RESPECTIVELY
1860 REM PRESSURE FROM Volts TO Pa
1870 FOR I=1 TO 4
1880 P(I)=(B(63+I)*A2(I)+B2(I)-P0(I))*6.89476 REM [kPa]
1885 IF I=3 THEN P(I)=(B(63+I)*A2(I)+B2(I)+P0)
*6.89476+101.3 REM [kPa]
1890 NEXT I

```

```

1900 FOR I=5 TO 6
1910 P(I)=(B(63+I)*A2(I)+B2(I)-P0(I))*
997.13/999.89 REM/[inH2O]
1920 NEXT I
1930 IF A1=0 THEN GOTO 2100
1940 REM FLOW RATES
1950 F(1)=0 ROTOMETER [g/sec]
1960 F(2)=(B(70)*A3(2)+B3(2))*FND(T(8))/998.48
REM MAIN FL.METER [g/s]; CAL.WITH H2O t=16.3 deg.C
1970 F(3)=(B(71)*A3(3)+B3(3))*FND(T(6))/998.48
REM DOWCOMER [g/s]; CAL.WITH H2O t=16.3 deg.C
1980 F(4)=(B(72)*A3(4)+B3(4))*FND(T(62))/999.34
REM COOL.WATER [g/s]; CAL.WITH H2O t=10.35deg.C
1990 IF B(70)<.05 THEN F(2)=0
2000 IF B(71)<.05 THEN F(3)=0
2010 V1=1096.5*SQR(ABS(P(6)/FNA(T(13)-T(12))))
*0.3048/60 REM AIR VEL. - USING C.L.RECORDING
2020 B1=1 V9=1096.5*.5713*SQR(P(5)/FNA(T(13)
-T(12)))*0.3048/60 REM AIR VEL - USING AIR BAR
2030 B1=0
2040 F(5)=V1*1.045*PI/4*(13*.0254)2 REM VOLUME
FLOW RATE [m3/sec]
2050 F(6)=V9*1*.30482 REM VOLUME FLOW
RATE [m3/sec] - AIR BAR
2060 P(10)=B(73)*1000
2070 Q1=F(2)*((-T(1)+(T(2)+T(3)+T(4)+T(10))/4)*
FNB((T(1)+T(2))/2)
2080 Q2=F(2)*(T(7)-T(8))*FNB((T(7)+T(8))/2)
2090 Q3=F(4)*(T(63)-T(62))*FNB((T(62)+T(63))/2)
2100 REM PRINTING
2110 REM HEADING
2120 PRINT USING 2140 ; D$,T1,T2,F1
2130 REM TEMPERATURES
2140 IMAGE ////"DATE:" ,10A,2X,3D,"/ HOURS " ,3D,
" MINUTES FAN SPEED: " ,3D
2150 PRINT USING 2160 ; C2$
2160 IMAGE 100A
2170 REM TEMPERATURES
2180 PRINT USING 2190
2190 IMAGE "WORKING FLUID AND AIR TEMPERATURES [deg.C] :"
2200 PRINT USING 2210 ; T(1),T(2),T(3),T(4),T(10),
T(6),T(7),T(8)
2210 IMAGE 8(7D.2D)
2220 PRINT USING 2210 ; T(12),T(13),T(14),T(62),T(63),
T(9),T4,T3
2230 PRINT USING 2210 ; T(0),T(5),T(11)
2240 PRINT USING 2250
2250 IMAGE /,"TEMPERATURES PANEL#1 [deg.C] :"
2260 PRINT USING 2270 ; T(38),T(43),T(56)
2270 IMAGE 10X,7D.2D,10X,7D.2D,20X,7D.2D
2280 PRINT USING 2290 ; T(44)
2290 IMAGE 30X,7D.2D
2300 PRINT USING 2270 ; T(39),T(45),T(57)
2310 PRINT USING 2320 ; T(46)

```

```

2320 IMAGE 35X,7D.2D
2330 PRINT USING 2290 ; T(47)
2340 PRINT USING 2270 ; T(40),T(48),T(58)
2350 PRINT USING 2290 ; T(49)
2360 PRINT USING 2320 ; T(50)
2370 PRINT USING 2270 ; T(41),T(51),T(61)
2380 PRINT USING 2290 ; T(52)
2390 PRINT USING 2320 ; T(53)
2400 PRINT USING 2290 ; T(54)
2410 PRINT USING 2270 ; T(42),T(55),T(60)
2420 PRINT USING 2430
2430 IMAGE "TEMPERATURES PANEL#3 [deg.C] :"
2440 PRINT USING 2270 ; T(15),T(20),T(33)
2450 PRINT USING 2290 ; T(21)
2460 PRINT USING 2270 ; T(16),T(22),T(34)
2470 PRINT USING 2320 ; T(23)
2480 PRINT USING 2290 ; T(24)
2490 PRINT USING 2270 ; T(17),T(25),T(35)
2500 PRINT USING 2290 ; T(26)
2510 PRINT USING 2320 ; T(27)
2520 PRINT USING 2270 ; T(18),T(28),T(36)
2530 PRINT USING 2290 ; T(29)
2540 PRINT USING 2320 ; T(30)
2550 PRINT USING 2290 ; T(31)
2560 PRINT USING 2270 ; T(19),T(32),T(37)
2570 IF A1=0 THEN 2630
2580 REM FLOW RATES
2590 PRINT USING 2600
2600 IMAGE "FLOW RATES:"
2610 PRINT USING 2620 ; F(1),F(2),F(3),F(4),F(5),F(6)
2620 IMAGE 4(4D.2D," g/sec"),2(4D.3D," m3/sec")
2630 REM PRESSURE DROPS & SYSTEM PRESSURE
2640 PRINT USING 2650
2650 IMAGE "PRESSURES (1:EVP - 2:COND -
3:SYST.PR. - 4:COOLING H2O) "
2660 PRINT USING 2670 ; P(1),P(2),P(3),P(4)
2670 IMAGE " 1: ",4D.4D,"[kPa] 2: ",4D.4D,"[kPa]
3: ",6D.4D,"[kPa] 4: ",6D.4D,"[kPa]"
2680 IF A1=0 THEN GOTO 940
2690 PRINT USING 2700 ; P(10),Q1,Q2,Q3
2700 IMAGE "OUTPUT EL.HEATER & SENSIBLE HEATS: ",
5D.D," Watt",3((5D.D)," Watt ")
2710 IF Z2=1 THEN GOSUB 2970
2720 IF Z1=0 THEN 1180 ELSE 2730
2730 CLEAR DISP USING 2740
2740 IMAGE " DO YOU WANT MORE RECORDINGS, YES OR NO?"
2750 INPUT C1$[1,3]
2760 IF C1$[1,1]="Y" THEN 1050
2770 CLEAR DISP USING 2780
2780 IMAGE " THIS IS IT REM"
2790 END
2800 REM
2810 CLEAR DISP USING 770
2820 B0(13)=0 B0(14)=0 B0(78)=0

```

```

2830 S0=13 S1=14 N=4
2840 GOSUB 3530
2850 S0=78 S1=78 N=4
2860 GOSUB 3530
2870 T(13)=B0(13)*A1(15)+B1(15)
2880 T(14)=B0(14)*A1(15)+B1(15)
2890 T(64)=B0(78)*A1(16)+B1(16)
2900 PRINT USING 2910 ; T(13),T(14),T(64)
2910 IMAGE //,3(4D.3D," deg.C ")
2920 DISP USING 2930
2930 IMAGE "HIT K2 TO END TEMP. COMPARISON"
2940 BEEP 10,1000 WAIT 5000
2950 GOTO 2810
2960 REM
2970 REM SUBROUTINE FOR STORING DATA ONTO TAPE
2980 REM CREATING DATA FILE - THIS IS DONE ONCE
2990 REM CREATE "R11.D",90,2100
3000 FOR I=64 TO 67
3010 T(I)=P(I-63)
3020 NEXT I
3030 FOR I=68 TO 73
3040 T(I)=F(I-67)
3050 NEXT I
3060 T(74)=P(10)
3070 J9=J9+1
3080 S$=""
3090 S1$=""
3100 S2$=""
3110 S3$=""
3120 S4$=""
3130 S5$=""
3140 S6$=""
3150 S7$=""
3160 S8$=""
3170 S9$=""
3180 REM PUTTING ESSENTIAL DATA INTO THE "S.$()-ARRAYS"
3190 S$=VAL$(J9)&C$&D$&C$&VAL$(T1)&C$&VAL$(T2)&C$&C2$&C$&R$
3200 FOR I=0 TO 8
3210 I1=I
3220 I2=9+I
3230 I3=18+I
3240 I4=27+I
3250 I5=36+I
3260 I6=45+I
3270 I7=54+I
3280 I8=63+I
3290 S1$=S1$&VAL$(T(I1))&C$
3300 S2$=S2$&VAL$(T(I2))&C$
3310 S3$=S3$&VAL$(T(I3))&C$
3320 S4$=S4$&VAL$(T(I4))&C$
3330 S5$=S5$&VAL$(T(I5))&C$
3340 S6$=S6$&VAL$(T(I6))&C$
3350 S7$=S7$&VAL$(T(I7))&C$
3360 S8$=S8$&VAL$(T(I8))&C$.

```

```

3370 NEXT I
3380 S9$=VAL$(T(72))&C$&VAL$(T(73))&C$&VAL$(T(74))&C$&R$
3390 S1$=S1$&R$
3400 S2$=S2$&R$
3410 S3$=S3$&R$
3420 S4$=S4$&R$
3430 S5$=S5$&R$
3440 S6$=S6$&R$
3450 S7$=S7$&R$
3460 S8$=S8$&R$
3470 ASSIGN# 1 TO "R11.D"
3480 PRINT# 1,J9 ; S$,S1$,S2$,S3$,S4$,S5$,S6$,S7$,S8$,S9$
3490 ASSIGN# 1 TO *
3500 C2$=""
3510 RETURN
3520 REM
3530 REM SUBROUTINE FOR DATA AQUISITION
3540 CLEAR 709
3550 OUTPUT 709 ; "VR5VT4SO1"
3560 FOR J=1 TO N
3570 FOR I=S0 TO S1
3580 OUTPUT 709 ; "AC"&VAL$(I); "VT3"
3590 ENTER 709 ; A
3600 REM SUMMING B0(I)
3610 B0(I)=B0(I)+A
3620 NEXT I
3630 NEXT J
3640 FOR I=S0 TO S1
3650 B0(I)=B0(I)/N
3660 NEXT I
3670 RETURN
3680 REM
3690 REM FUNCTION DEFINITIONS
3700 REM AIR DENSITY FNA
3710 DEF FNA(X)
3720 IF F1=0 THEN P3=0
3730 IF F1=80 THEN P3=-.01 [psig]
3740 IF F1=120 THEN P3=-.022 [psig]
3750 IF F1=160 THEN P3=-.037 [psig]
3760 IF F1=200 THEN P3=-.054 [psig]
3770 P2=P1*70.5269/144+P3 [psia] STATIC PRESS.
IN THE DUCT AT PITOT-STATIC TUBE LOCATION
3780 IF B1=1 THEN P2=P1*70.5269/144-P3 [psia]
STATIC PRESS. IN THE DUCT AT AIR BAR.
3790 C1=0
3800 FOR I=1 TO 7
3810 C1=C1+1
3820 IF I<7 THEN Y=20*I-20
3830 IF I=7 THEN Y=127
3840 IF X<=Y THEN 3870
3850 NEXT I
3860 IF X>Y THEN D1=A4(7)/.4536*.30483 GOTO 3900
3870 IF C1=1 THEN D1=A4(1)/.4536*.30483 GOTO 3900
3880 IF C1>=2 THEN D1=(A4(C1)-(A4(C1)-A4(C1-1)))/

```

```

20*(Y-X))/ .4536*.30483 GOTO 3900
3890 IF C1=7 THEN D1=(A4(7)-(A4(7)-A4(6))/27*(Y-X))/
.4536*.30483 REM [lb/ft3]
3900 FNA=D1*P2/14.73*520/(460+(X*1.8+32)) REM CORRECTED
AIR DENSITY [lb/ft3]
3910 FN END
3920 REM
3930 REM SPECIFIC HEAT OF WATER [J/(g K)]
3940 DEF FNB(X)
3950 FNB=4.179+.000079*(X-10)2.9
3960 FN END
3970 REM
3980 REM SPECIFIC DENSITY OF WATER [kg/m3], FNC
3990 DEF FNC(X)
4000 Y=(1+.0000087*X1.85)/1000
4010 FNC=1/Y
4020 FN END
4030 REM
4040 REM DENSITY OF R11 [kg/m3], FND
SOURCE: ASHRAE FUND.1981
4050 DEF FND(X)
4060 N1=2
4070 IF X<27 THEN N1=5
4080 IF X>=77 THEN N1=5
4090 Y=-3
4100 C1=0
4110 FOR I=1 TO 35
4120 C1=C1+1
4130 IF X<27 THEN Y=Y+5 GOTO 4160
4140 IF X>77 THEN Y=Y+5 GOTO 4160
4150 Y=Y+2
4160 IF Y>X THEN 4180
4170 NEXT I
4180 FND=A5(C1)-(A5(C1)-A5(C1-1))/N1*(Y-X)
4190 FN END
4200 REM
4210 CLEAR DISP USING 770
4220 B0(1)=0 B0(3)=0 B0(5)=0
4230 S0=1 S1=5 N=2
4240 GOSUB 3530
4250 T(1)=B0(1)*A1(1)+B1(1)
4260 T(3)=B0(3)*A1(3)+B1(3)
4270 T(5)=B0(5)*A1(5)+B1(5)
4280 PRINT USING 4290 T(1),T(3),T(5)
4290 IMAGE //,3(4D.3D," deg.C ")
4300 GOTO 1050

```


Appendix II

Fortran Routines for Thermodynamic
Properties of Liquid Water

C THERMODYNAMIC PROPERTIES OF SATURATED WATER AND STEAM

C THE EMPIRICAL EQUATIONS ARE DEVELOPED BY:
C T.FUJII, Y.KATO AND K.MIHARA ; [14]

C ALL THE TEMPERATURES USED IN THE EQS. HAVE
C UNITS [deg.C] UNLESS OTHERWISE IS SPECIFIED.

C *****

C THERMAL CONDUCTIVITY OF WATER, WK [W/(m K)]
C FUNCTION WK(T)
C IF (T.LE.0.) T=10.
C WK=.6881-4.E-6*(135.-T)**2.1
C RETURN
C END

C VOLUMETRIC COEFFICIENT OF THERMAL EXPANSION
C OF WATER, WBETA [1/K]
C FUNCTION WBETA(T)
C IF (T.LE.0.) T=10.
C A1=-.06427E-3
C A2=8.5053E-6
C A3=-6.79E-8
C B1=A1+2.*A2*T+3.*A3*T**2.
C B2=1.+A1*T+A2*T**2.+A3*T**3.
C WBETA=B1*B2
C RETURN
C END

C VISCOSITY OF WATER, WMJU [kg/(m s)]
C FUNCTION WMJU(T)
C IF (T.LE.0.) T=10.
C A=251./(T+135.)
C WMJU=2.4E-5*10.**A
C RETURN
C END

C DYNAMIC VISCOSITY OF SATURATED STEAM
C VAPOUR, "WMJUV"
C FUNCTION WMJUV(T)
C WMJUV=(8.02+0.04*T)*1E-6
C RETURN
C END

C SPECIFIC HEAT CAPACITY OF WATER, WCP [J/(kg K)].
C FUNCTION WCP(T)
C IF (T.LE.10.) GOTO 50
C WCP=4179.+(7.9*1.E-5)*(T-10.):**2.9
C GOTO 60
50 WCP=4179.
60 RETURN
C END

C
C

```
DENSITY OF WATER, WDENS [kg/cu.m].  
FUNCTION WDENS(T)  
IF (T.LE.0.) T=10.  
Y=(1.+(8.7*1.E-6)*T**1.85)*1.E-3  
WDENS=1./Y  
RETURN  
END
```

Appendix III

Flow Distribution Tests Through Modified Evaporator

After all the two-phase thermosyphon tests were finished, the upper evaporator header was detached from the heat exchanger.

The inlet of the evaporator and the cold water storage tank was connected with a plastic hose

as shown in the

schematic diagram in Fig. A1.

Cold water (13°C) was pumped from the water tank through the evaporator panels.

Plastic hoses attached to the outlet of each evaporator panel distributed the water to buckets whose tare weight was found before the tests commenced.

Two separate test sets were performed 24 hours apart and the results are shown in Tables A1 and A2.

TABLE A1: FLOW DISTRIBUTION THROUGH EVAP. PANELS
TEST #1

TOTAL FLOW		PANEL #1		PANEL #2		PANEL #3		PANEL #4	
[g/s]	[%]	[g/s]	[%]	[g/s]	[%]	[g/s]	[%]	[g/s]	[%]
55	100	11.2	20.4	20.4	37.1	13.5	24.5	9.9	18.0
45	100	8.2	18.2	18.9	42.0	10.9	24.2	7.0	15.6
35	100	5.8	16.5	17.0	48.6	7.9	22.6	4.3	12.3
25	100	3.45	13.8	13.8	55.2	5.6	22.4	2.15	8.6
15	100	1.30	8.7	10.38	69.2	3.06	20.4	0.26	1.7

TABLE A1: FLOW DISTRIBUTION THROUGH EVAP. PANELS
TEST #2

TOTAL FLOW		PANEL #1		PANEL #2		PANEL #3		PANEL #4	
[g/s]	[%]	[g/s]	[%]	[g/s]	[%]	[g/s]	[%]	[g/s]	[%]
55	100	10.9	19.8	19.6	35.6	14.0	25.5	10.5	19.1
45	100	8.3	18.4	18.0	40.0	11.2	24.9	7.5	16.7
35	100	6.0	17.1	15.7	44.9	8.5	24.3	4.8	13.7
25	100	3.6	14.4	13.3	53.2	6.0	24.0	2.1	8.4
15	100	1.32	8.8	10.25	68.3	3.21	21.4	0.22	1.5

Five water flow rates (55, 45, 35, 25 and 15 g/s), recorded by a turbine flow meter, were tested per data set. The results for the two test sets gave good agreement. However, the flow distribution through the different evaporator panels for one test showed large deviations. The lower the total mass flow rate, the less uniform was the flow rate through the four evaporator panels. Even though the test conditions are different, it is reasonable to assume that uniform flow distribution through the evaporator did not exist for the thermosyphonic tests either.

Appendix IV

Fortran Routines for Thermodynamic
Properties of Freon R-11

THERMODYNAMICAL PROPERTIES OF SATURATED LIQUID
AND VAPOUR FREON R-11.

THE EMPIRICAL EQUATIONS ARE DEVELOPED BY
T.FUJII, S.NOZU AND H.HONDA, [37]

ALL THE TEMPERATURES USED IN THE EQS. HAVE
UNITS [deg.C] UNLESS OTHERWISE IS SPECIFIED.

ALL THE PRESSURES USED IN THE EQS. HAVE
UNITS [Pa] UNLESS OTHERWISE IS SPECIFIED.

THIS FUNCTION "RDENSV" CALCULATES THE DENSITY OF
OF SATURATED R11-VAPOUR, [kg/cu.m].

FUNCTION RDENSV(P,T)

WM=137.38

R=8314.

PC=4377.024

PRS=P/PC

TS=T+273.15

ZS=1./((1+.63*(PRS**.726+PRS**2.71)))

RDENSV=WM*P*1000./(R*ZS*TS)

RETURN

END

THIS FUNCTION "RDENSL" CALCULATES THE DENSITY OF
OF SATURATED R11-LIQUID, [kg/cu.m].

FUNCTION RDENSL(T)

Y=(.652+7.52E-4*T**1.1)/1000.

RDENSL=1./Y

RETURN

END

THIS FUNCTION "RLHEAT" CALCULATES THE LATENT HEAT
OF VAPORIZATION FOR R11, [J/kg].

FUNCTION RLHEAT(T)

RLHEAT=(1.898-3.94E-3*T)*100000.

RETURN

END

THIS FUNCTION "RCPV" CALC. SPECIFIC HEAT, Cp,
OF SATURATED R11-VAPOUR, [J/(kg K)].

FUNCTION RCPV(P,T)

PC=4377.024

PRS=P/PC

TS=T+273.15

CP0=(.545+8.13E-4*T)*1000.

RCPV=(.76*PRS**.61+4.46*PRS**3.24)*TS+CP0

RETURN

END


```
C
C   THIS FUNCTION "RCPL" CALC. SPECIFIC HEAT, Cp,
C   OF SATURATED R11-LIQUID, [J/(kg K)].
C   FUNCTION RCPL(T)
C   RCPL=(.867+8.1E-4*T+1.8E-9*T**3.6)*1000.
C   RETURN
C   END

C
C   THIS FUNCTION "RMJUV" CALC. DYNAMIC VISCOSITY
C   OF SATURATED R11-VAPOR, [kg/(m s)].
C   FUNCTION RMJUV(T)
C   RMJUV=(.99+4.E-3*T+8.E-14*T**5.4)/100000.
C   RETURN
C   END

C
C   THIS FUNCTION "RMJUL" CALC. DYNAMIC VISCOSITY
C   OF SATURATED R11-LIQUID, [kg/(m s)].
C   FUNCTION RMJUL(T)
C   Y=385./(T+281.)
C   RMJUL=2.29E-5*10.**Y
C   RETURN
C   END

C
C   THIS FUNCTION "RKV" CALC. THERMAL CONDUCTIVITY
C   OF R11-VAPOR, [W/(m K)].
C   FUNCTION RKV(T)
C   RKV=(6.542+4.77E-2*T)/1000.
C   RETURN
C   END

C
C   THIS FUNCTION "RKL" CALC. THERMAL CONDUCTIVITY
C   OF R11-LIQUID, [W/(m K)].
C   FUNCTION RKL(T)
C   RKL=.0943-2.75E-4*T
C   RETURN
C   END
```